Study on Mitigation Measures against Debris Flow Disasters with Driftwood(Dissertation_全文)

AUTHOR(S):

SHRESTHA, Badri Bhakta

Study on Mitigation Measures against Debris Flow Disasters with Driftwood

By

SHRESTHA Badri Bhakta

2009

Abstract

Debris flows are common in mountainous areas throughout the world, which contain varying amounts of mud, sand, gravel, boulders, and water. In addition to causing significant morphological changes along riverbeds and mountain slopes, these flows are frequently reported to have brought about extensive property damage and loss of life. Therefore, the understanding of behavior and mechanism of debris flow and the study of preventive measures are very important in order to manage the sediment disasters in the river basin and prevent the downstream hazards. To reduce the debris flow hazards, it is common to couple structural and non-structural preventive measures. Preventive measures require the consideration of the various scenarios and involve the evaluation of hydrological, hydraulic, sediment size distribution, topographical and other parameters.

Check dams are one of the effective structural countermeasures for debris flow control. Check dams can effectively store the debris flow as long as there is an adequate storage capacity, when check dam loses such storage capacity, the check dam can not capture enough sediment to reduce the debris flow. Check dams can be distinguished as closed and open types. In closed type check dam, it is difficult to prevent from losing its trapping capacity unless sediments are continuously removed, whereas open type dams may keep their trapping capacity without any need of artificially removing the sediment. To evaluate the effectiveness of check dams against debris flow, it is necessary to investigate the debris flow deposition and erosion processes upstream of a check dam, in order to reduce the debris flow disasters.

In recent years much driftwood has combined with debris flow, due to heavy downpours over mountainous rivers, which results in damage of properties and loss of lives in the lower reaches of rivers. Generally the catchment area of mountainous rivers is covered by forest. In these areas, debris flow flows down along the river with driftwood. Such driftwood clogs narrows in the river course or bridge or culvert sites giving rise to flooding, bridge/piers or embankments damage or destruction. Therefore, the studies on debris flow with driftwood, scattering process of driftwood in low land areas, and structural and non-structural countermeasures are very important in order to reduce the extensive property damage and loss of life due to debris flow disasters with driftwood. It is also necessary to understand the mechanism of debris flow with driftwood behavior to clarify the nature of debris flow disasters with driftwood. In this context, the main aim of this study is to develop a numerical model to investigate the most effective and reliable mitigation measures of debris flow disasters with driftwood.

A numerical model is developed to reproduce the debris flow deposition process upstream of check dams. The constitutive equations of Takahashi et al. (1997) and those of Egashira et al. (1997) are chosen for the study on deposition process upstream of a check dam. The deposition velocity models proposed by many authors are proportional to the flow velocity. The debris flow deposition upstream of a check dam by such velocity models can not be calculated when the flow velocity becomes zero, and also the calculated deposition upstream of a check dam is too small. Therefore, a new deposition velocity equation to calculate the deposition upstream of a check dam is also developed. The numerical simulations and experiments are performed for closed type and open (grid or slit) type check dams. The simulated results of debris flow deposition upstream of check dams and reduction in outflow discharge agree well with the experimental results. The proposed deposition velocity model of upstream of a check dam and both the constitutive equations could calculate the debris flow deposition phenomenon upstream of check dams. The erosion process of deposited sediment upstream of a check dam by a normal scale flood flow is investigated by using a one-dimensional riverbed erosion model under unsaturated bed condition. The simulated results of erosion of deposited sediment upstream of check dams are also agreeable with the experimental results.

A two-dimensional numerical model is developed for computing the behavior of debris flow with driftwood. Equations of the rotational motion and the translational motion of driftwood are evaluated dynamically in the Lagrangian form. A numerical model has been developed with an interacting combination of Eulerian expression of the debris flow and Lagrangian expression of the driftwood, in which the fluctuation components of the position and the rotational angular velocity of the driftwood are dealt with stochastically as random variables based on the results of a statistical analysis of experimental values. The position and rotational angular velocity of the driftwood fluctuate due to the collision of driftwood with boulders and disturbances on the flow surface during the collision of the sediment particles, which are considered in the diffusion coefficients. The scattering process of driftwood is described as a diffusion process and the diffusion coefficients are defined by the hydraulic experiments. The simulated results of outflow discharge, sediment concentration and the percentage of driftwood outflow at the downstream end of the flume are in good agreement with the experimental results.

Open type check dams such as grid type or slit type check dams are commonly used for debris flow control and capturing driftwood because they are preferable over closed type check dams for conserving the natural environment and landscape of mountain torrents as much as possible. In the debris flow section where driftwood is assumed to flow down with a debris flow, both of

them are captured together by the open type check dam. The capturing process of debris flow with driftwood is investigated numerically and experimentally. A numerical model is developed for computing the debris flow with driftwood capturing by open type check dams such as grid or slit dam. The jamming of driftwood on open type check dams is evaluated based on the geometric conditions and probabilistic approaches. A deposition velocity model is also presented to calculate the debris flow deposition due to driftwood jamming on open type check dams. To simulate the debris flow with driftwood capturing by open type check dams, a driftwood jamming model and a model of sediment deposition behind check dam, are incorporated in a two-dimensional flow model of the debris flow with driftwood. The flow and sediment discharge passing through a grid or slit dam are reduced due to driftwood jamming. The results of flow discharge, sediment discharge and the percentage of driftwood passed through a grid or slit dam are in good agreement with the experimental results. The simulated results of debris flow deposition upstream of check dams are also agreeable with the experimental results.

Numerical analysis and experimental studies are carried out to investigate the deposition of debris flows with driftwood on the fan. A two-dimensional integrated numerical model is developed for computing the characteristics of debris flow with driftwood, which can simulate all stages of debris flow from initiation, transportation and deposition stages. A capturing model of debris flow with driftwood by open type check dams is also incorporated into an integrated numerical model. The calculated results of the shapes and thicknesses of a debris flow fan and the positions and rotational angles of deposited driftwood in a debris flow fan are in good agreement with the experimental results. The effects of check dams in a debris flow fan formation are also investigated.

Key Words: *debris flow, driftwood, mitigation measures, check dams, erosion/deposition, capturing process, fan deposition, integrated model*

Acknowledgements

I would like to express my sincere gratitude and appreciation to many people who made this thesis possible.

I would like to express my deepest and sincere gratitude to my academic supervisor, Professor Dr. Hajime Nakagawa, Disaster Prevention Research Institute, Kyoto University, for his continuous guidance, encouragement and support throughout the whole period of my study.

I am deeply grateful to my thesis reviewers, Professor Hideo Sekiguchi and Professor Masaharu Fujita, Disaster Prevention Research Institute, Kyoto University, for their valuable comments and suggestions to refine the thesis.

I wish to express my sincere gratitude to Dr. Kenji Kawaike, Dr. Yasuyuki Baba and Dr. Hao Zhang, for their valuable guidance and suggestions during my study. I would also like to express my gratitude to Dr. Yasunori Muto for his support in many aspects. I appreciate Professor Yoshifumi Satofuka (Ritsumeikan University) for providing the values of numerical constants of grid dam blockage model. I would like to express my sincere thank to Dr. Ripendra Awal for his valuable suggestions and friendly help.

I am indebted to my all colleagues of River Disaster Prevention System, Disaster Prevention Research Institute, Kyoto University for their kind cooperation, helps and unforgettable friendship. I am especially grateful to Mr. Hiroshi Teraguchi, Mr. Dong-Keun Lee, Mr. Ram Krishna Regmi, Mr. Hideaki Mizutani, Mr. Daizaburo Touchi, Mr. Takaharu Utsumi, Mr. Yasunori Nanbu, Mr. Yasutaka Saito, Mr. Toshimasa Mataga, Mr. Satoshi Kohda, Mr. Atsushi Shimizu, Mr. Sohshi Yoneda, Mr. Makoto Ano, Ms. Akiko Takao and Mr. Shiro Nakanishi.

I would like to thank all the professors and friends in the Research Center for Fluvial and Costal Disaster, Disaster Prevention Research Institute of Kyoto University, who have made my academic experience rich and memorable. I would like to thank Mr. Seiji Fujihara, Mr. Kazuhiro Nishimura, Mrs. Natsuyo Sugimura and all the staffs in Ujigawa Open Laboratory, Disaster Prevention Research Institute of Kyoto University for their support in routine administrative process and experiments.

I gratefully acknowledge the financial support of the Monbukagakusho (Ministry of Education,

Culture, Sports, Science and Technology, Japan).

I would like to thank all my family members and relatives for their encouragement and loving support. Finally, I am deeply grateful to my wife Durga Shrestha and daughters Anima Shrestha and Sanima Shrestha, for their understanding, contribution and support throughout my study period.

Table of Contents

Chapter 1

Introduction

1.1 General

Debris flow, slope failure and landslide are the most common mass movements in mountainous areas throughout the world and important as far as the sediment hazards are concerned. They frequently cause extensive damage of properties and loss of lives (Takahashi, 1991, 2007; Nakagawa et al., 2002a). The risk of sediment hazards has been increasing tremendously by urbanization and rapid development activities in mountainous areas. In mountainous areas, intense and localized storms may cause flash floods with important erosion, mass movement and sediment transport. Generally sediment movement tends to occur in steep slope and weak geology area caused by heavy rainfall or strong tremor. Furthermore, the mass of earth debris and other materials are transported by flood toward downstream and sediment disaster spreads in wide area. Sediment disasters are classified into direct and indirect disaster in the meaning of mass movement attacks house and properties directly or not. Mass movements occur basically in the motion of gravity and water (Parise and Calcaterra, 2000). The typical mass movements such as debris flow, slope failure and landslide in mountainous areas are shown in Figure 1.1. Figure 1.2 shows photograph of the debris flow occurred at Tahoma Creek, USA. The photographs of slope failure and landslide disasters occurred in Japan are shown in Figure 1.3. Figure 1.4 shows the number of occurrence of debris flow, landslide and slope failure disasters from 1982 to 2008 in Japan.

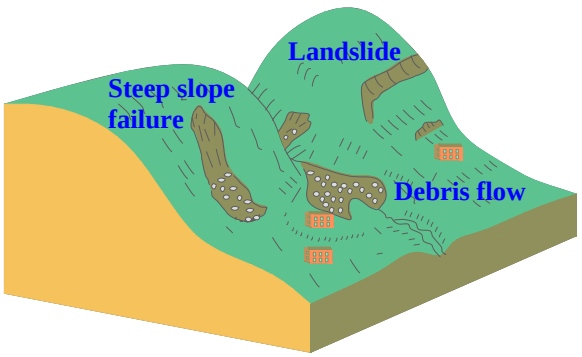

Figure 1.1 Sediment disasters in mountainous areas

Figure 1.2 Debris flow at Tahoma Creek, USA, July 26, 1988
(*Photo Courtesy: USGS)*

Figure 1.3 (a) Slope failure disaster on September 6, 2005 at Takeda, Oita Prefecture, Japan, (b) Landslide at Kitauebaru, Nakagusuku, Okinawa Prefecture, Japan, June 2006 (*Photo Courtesy: (a) Sabo Department, MLIT, Japan, (b) Arial photographs by Geographical Survey Institute, Japan)*

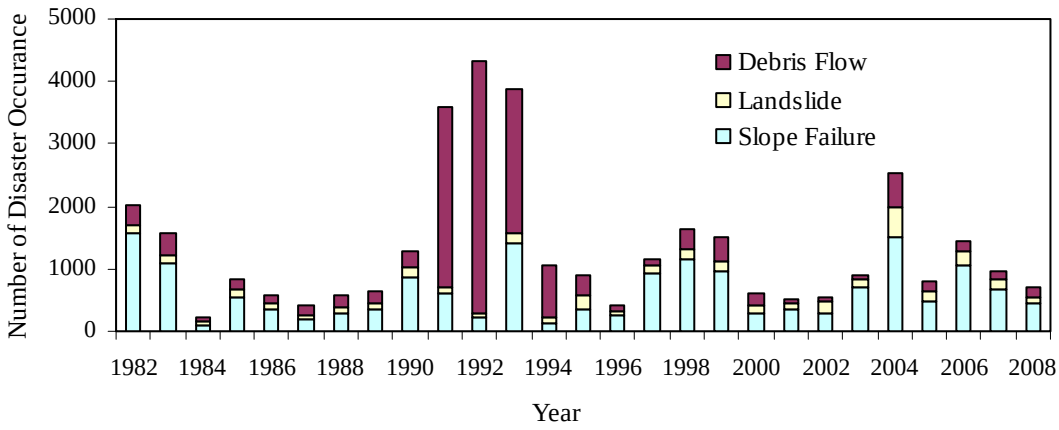

Figure 1.4 The number of debris flow, landslide and slope failure disasters occurrence in Japan *(Data of debris flow from 1991 to 1993 include pyroclastic flow caused by the eruption of Mt. Unzen Fugendake in Nagasaki Prefecture) (Source: Sabo Department, MLIT, Japan)*

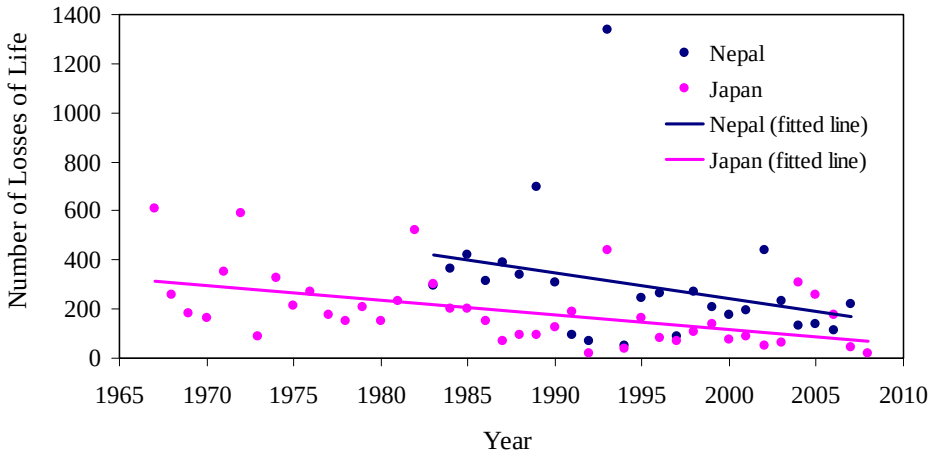

Figure 1.5 Trend of number of losses of life due to sediment disasters in Nepal and Japan *(Source: Sabo Department, MLIT, Japan and Department of Water-Induced Disaster Prevention, Nepal)*

Debris flow is a phenomenon that stones and soil on the hillside or in the riverbed are carried downstream in a rush by a long-continuing or localized torrential rainfall. Because a debris flow is capable of transporting huge boulders measuring several meters in diameter and its velocity can reach some ten meters per a second, the destructive force of it is surprisingly high. Thus damages by debris flow are very severe and sometimes tragic. In addition to causing significant morphological changes along riverbeds and mountain slopes, debris flows are frequently reported to have brought about extensive property damage and loss of life (Takahashi, 1991; Hunt, 1994; Huang and Garcia, 1997; Nakagawa et al., 2002a; Shrestha et al., 2007, 2008a, 2008c). Debris flow stops at the mouth of the gully and buries houses and farms and destroys

roads. The thickness of the accumulation sometimes reaches 10m. The thick layer of large boulders often obstruct restoration and in some cases forces abandonment. The phenomenon of debris flow is usually so abrupt that it makes difficult to take refuge after realizing its outbreak. Debris flow is generated not only by heavy rainstorms, but also by earthquakes, volcanic eruptions and quick melting of glaciers (Takahashi, 2000; Armanini and Gregoretti, 2000; Chen and Ling, 2000; Nakagawa et al., 2002a). Therefore, the understanding of behavior and mechanism of debris flow and the study of preventive measures are very important in order to manage the sediment disasters in the river basin and prevent the downstream hazards. To reduce the debris flow hazards, it is common to couple structural and non-structural preventive measures. Preventive measures require the consideration of the various scenarios and involve the evaluation of hydrological, hydraulic, sediment size distribution, topographical and other parameters (Brufau et al., 2000; Shrestha, 2004; Shrestha et al., 2008b). Figure 1.5 shows the historical trend line of number of losses of life due to sediment disasters such as debris flow/landslide, slope failure and floods in Nepal and Japan. There is decreasing trend of loss of life due to the development of countermeasures against sediment hazards.

In recent years much driftwood has combined with debris flow, due to heavy downpours over mountainous rivers, which results in damage of properties and loss of lives in the lower reaches of rivers. Generally the catchment area of mountainous rivers is covered by forest. In these areas, debris flow flows down along a river with driftwood. Such driftwood clogs narrows in the river course or bridge or culvert sites giving rise to flooding, bridge/piers and embankments damage or destruction (Shrestha et al., 2009). Therefore, recent attention is required to focus on behavior

Figure 1.6 The debris flow flowing with driftwood, down the Aratani River at Saeki Ward, Hiroshima Prefecture, Japan, June 1999 *(Photo Courtesy: Sabo Department, MLIT, Japan)*

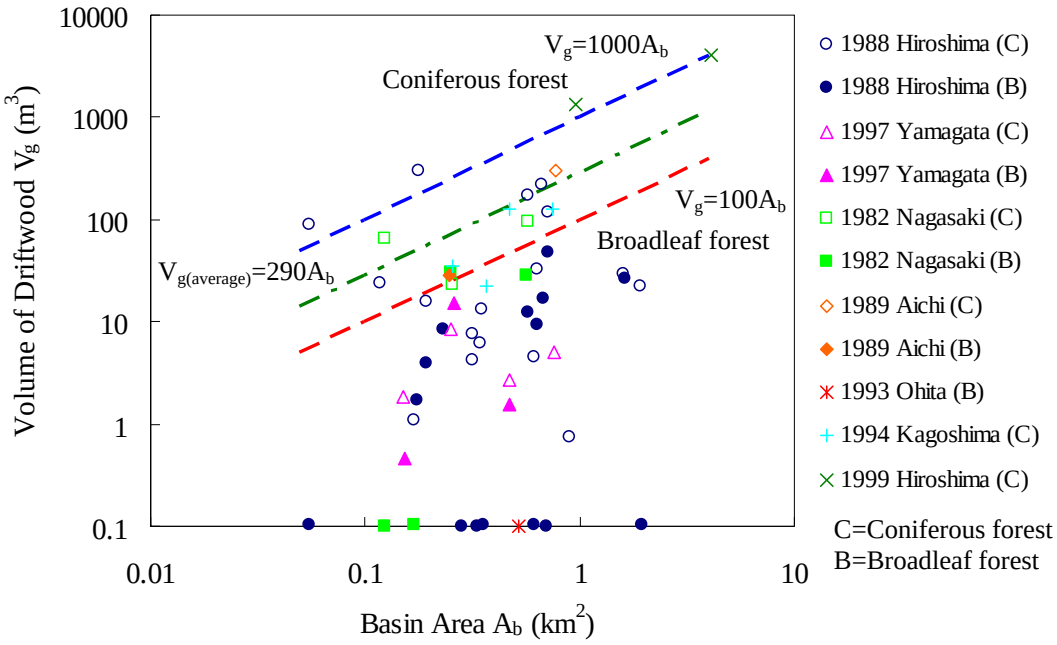

Figure 1.7 Basin area and volume of driftwood carried by debris flow in Japan

(Source: Sabo Department, Ministry of Construction, Japan, 2000)

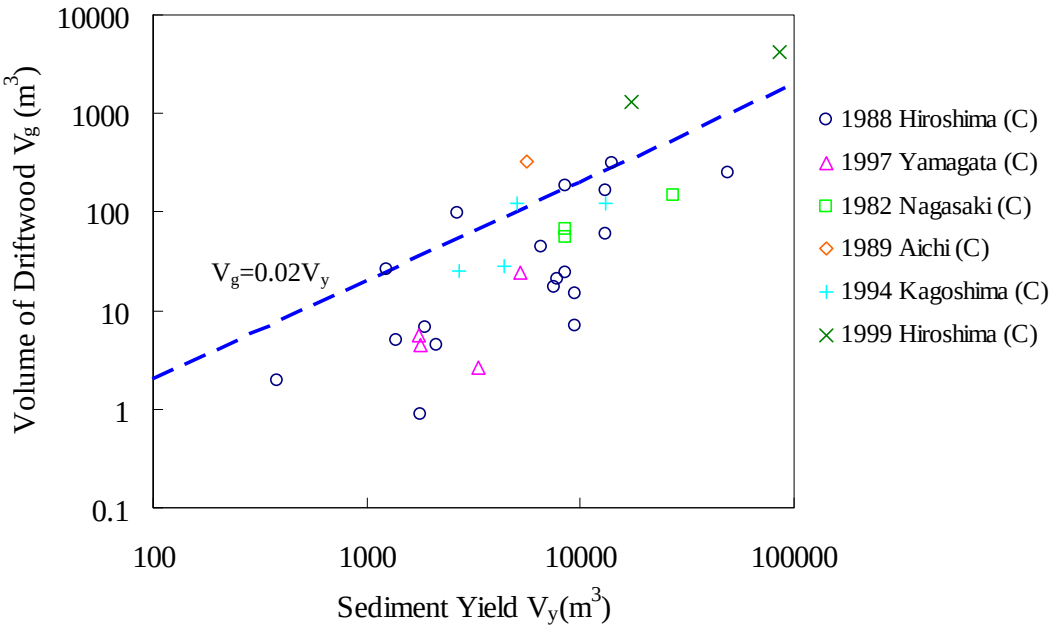

Figure 1.8 Sediment yield and volume of driftwood carried by debris flow in Japan

(Source: Sabo Department, Ministry of Construction, Japan, 2000)

of debris flow with driftwood and countermeasures against debris flow disasters with driftwood. Figure 1.6 shows the debris flow flowing with driftwood at the Aratani River, Hiroshima, Japan in June 1999. Figure 1.7 shows the observed yield quantities of driftwood carried by debris flow in both coniferous and broadleaf forests of Japan. The relationship between the yield quantities of driftwood and sediment is shown in Figure 1.8.

The main aim of this study is to develop a most effective and reliable method to reduce the debris flow disasters with driftwood through laboratory experiments and numerical simulation models. In that aim, this study focuses on debris flow deposition and erosion processes upstream of check dams, debris flow with driftwood characteristics, capturing process of debris flow with driftwood by open type check dams such as grid or slit type check dams and the deposition of debris flows with driftwood on the fan.

1. 2 Types of debris flows

Debris flows occur in a variety of forms depending on the conditions of the site and the factors contributing to their occurrence. A number of types by contributing factors have been published by Daido (1971), Ikeya (1989), Nakagawa et al. (2002a), Takahashi (2007) and so on. Debris flows can be divided into five types by the contributing factors. Riverbed sediment movement type debris flow occurs due to triggering mass discharge of sediment when the sediment accumulated on the riverbed exceeds the gradient made by the bed load transport of sediment and the balance between them is lost. Slope failure type debris flow occurs due to directly changing slope failure into debris flow. Natural dam collapse type debris flow occurs due to the collapse of a natural dam which is formed by landslide or slope failure. Landslide type debris flow occurs as the last stage phenomenon of a landslide, because the soil is almost liquefied due to extremely clayey alteration. Volcanic activity type debris flow occurs by a volcanic eruption or an earthquake.

The flow mode and flow characteristics of debris flows differ largely depending on the type, size, and concentration of stony grains included in them. If a large amount of coarse gravel and a relatively small amount of fine grain finer than silt are contained, it is called the gravel type debris flow. In contrast, if a small amount of coarse gravel and a large amount of fine grain are contained, it is called the mudflow type debris flow. If the amount of clay and silt is especially large, it is called the viscous type debris flow.

1.3 Debris flow disasters and their countermeasures in practice

Hazardous events and disasters strike without warning. Therefore, the protection systems that guarantee complete safety from these events are almost impossible. However, there are measures that, if planned and implemented effectively, can reduce the extent of damage (Mainali and Rajartnam, 1991). Debris flows are among the most dangerous natural hazards that affect humans and properties, which are common in mountainous areas throughout the world (Takahashi, 1991). Figure 1.9 shows the debris flow disaster occurred on July 10, 1997 at the

Figure 1.9 Debris flow disaster at the Harihara River, Sakai-machi, Izumi City, Kagoshima Prefecture, Japan, July 10, 1997 *(About 29 houses were damaged by the debris flow disaster, 21 people were killed and 13 people were injured in this debris flow disaster) (Photo Courtesy: MLIT and Infrastructure Development Institute-Japan, 2004)*

Figure 1.10 Debris flow disaster (a) at Odaizawa stream, Okaya, Nagano Prefecture, Japan, July 19, 2006, (b) at Miyama, Fukui Prefecture, Japan, July 18, 2004 *(Photo Courtesy: Sabo department, MLIT, Japan)*

Figure 1.11 Debris flow disaster at Churia hill, Butwal, Nepal, 1998 *(About 35 houses were collapsed by the debris flow, one people was killed and two people were injured by the debris flow)*
(Photo Courtesy: MLIT and Infrastructure Development Institute-Japan, 2004)

Figure 1.12 Debris flows occurred at Songhe, Taichung County, Taiwan, caused by Typhoon Mindulle on July 3, 2004 *(About 40 houses were buried or severely damaged by the debris flows, but fortunately, only two people were killed by the debris flows due to successful warning and evacuation)*
(Photo Courtesy: Jan, 2005)

Harihara River, Izumi, Kagoshima Prefecture, Japan. Figure 1.10 shows the other examples of debris flow disasters that occurred at Odaizawa stream of Nagano Prefecture and at Miyama town of Fukui Prefecture, Japan. Figures 1.11 and 1.12 show the debris flow disasters occurred at Churia hill of Nepal and Songhe of Taiwan, respectively. Figure 1.13 shows the debris flow with driftwood deposited at the Camuri Grande fan, Venezuela and houses destroyed by the driftwood transported by sediment flow at the Kono River, Hiroshima Prefecture, Japan. Thus, it is very important to control and mitigate driftwood as well as a debris flow in order to reduce the debris flow disasters with driftwood.

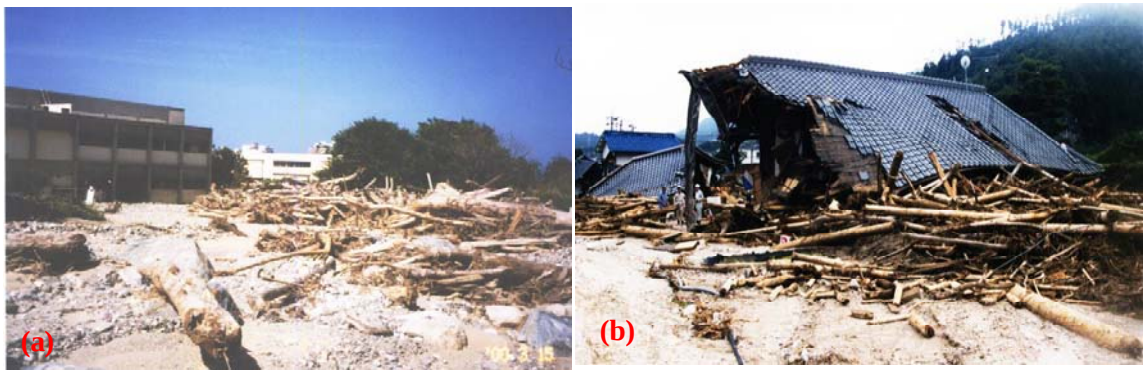

Figure 1.13 (a) Sediment and driftwood deposited at the Camuri Grande fan, Venezuela in 1999, (b) Houses destroyed by the driftwood transported by sediment flows at the Kono River, Hiroshima Prefecture, Japan in 1998 *(Source: Nakagawa et al., 2002a)*

(a) Grid dam constructed to prevent downstream sediment disaster due to debris flow at the Hirayu River, Gifu Prefecture, Japan (*Source: Shrestha et al., 2008b*)

(b) Slit dam constructed at the Rerukomabetsu River, Hokkaido Prefecture, Japan (*Source: Nakagawa et al., 2002a*)

(c) Closed dam constructed at Khahare Khola stream in Muglin-Narayanghat Highway, Nepal (*Source: Department of Water-Induced Disaster Prevention, Nepal*)

Figure 1.14 Different types of check dam constructed to prevent debris flow disasters

Figure 1.15 (a) Debris flow and driftwood captured by grid dam at the Mae Tanikawa River, Fukui Prefecture, Japan, 18 July, 2004, (b) Sabo dam trapped about 6000m^3 debris flow and driftwood at the Kawabegawa River, Kumamoto Prefecture, Japan, 24 July, 2006 (*Photo Courtesy: Sabo Department, MLIT, Japan)*

Countermeasures designed to reduce the debris flow disasters can be classified as structural or non-structural measures. Structural measures include check dams, levees and channel works, while non-structural measures include hazard mapping, warning and evacuation systems, emergency communication systems, proper land use, and improvement of buildings (Sharma, 2006; Mizuyama, 2008; Shrestha et al., 2008b). The combination of structural and non-structural countermeasures is commonly used to reduce the debris flow disasters effectively. Figure 1.14 shows the different types of check dam such as grid dam, slit dam and closed dam constructed for debris flow control. Figure 1.15 shows the debris flow and driftwood captured by grid dam and sabo dam in Japan. Check dams are one of the effective structural countermeasures for debris flow control. Open type check dams such as grid or slit type check dams are being adopted more often for debris flow control because they are preferable over the conventional closed type check dams for conserving the natural environment and landscape (Mizuyama and Mizuno, 1997). Systematic analyses of comprehensive structural and non-structural countermeasures to prevent from debris flow disasters are very important, which can be done effectively by numerical simulation model.

1.4 Objectives of the research

The aim of this study is to develop a numerical model to investigate the most effective and reliable mitigation measures of debris flow disasters with driftwood. The main objectives of this study are summarized as follows.

(a) to develop a numerical model for computing the debris flow deposition upstream of a check dam and flushing out of deposited sediment upstream of a check dam due to erosion process by a normal flow discharge,
(b) to develop a numerical model for computing the characteristics of debris flow with driftwood,
(c) to develop a numerical model of capturing process of debris flow with driftwood by open type check dams such as grid or slit dam,
(d) to develop an integrated numerical model to compute the behavior of debris flow with driftwood and their capturing process by open type check dams into an integrated system, which can simulate all stages of debris flow with driftwood from initiation, transportation and deposition stages, capturing by check dams and driftwood deposition in a debris flow fan,
(e) to investigate the effectiveness of check dams to reduce the debris flow disasters with driftwood.

1.5 Previous researches: a brief overview

1.5.1 Debris flow control by check dams

Check dams are commonly used for debris flow control, which can effectively reduce and prevent debris flow disasters. Many open type or closed type check dams are constructed in mountainous areas where debris torrents might have catastrophic and dramatic impacts. These dams can reduce the energy of a debris flow, thereby controlling the surface erosion that usually occurs in upstream areas. In recent years open type check dams such as grid type or slit type check dams have become increasingly popular than closed type check dams from the viewpoint of the comprehensive sediment management in the river basin and river environment. These dams have the merits that a debris flow is captured by blocking of open spaces and the sediment during small or medium flood passes through the dam. The experimental and numerical studies

on debris flow control by check dams are reported in many literatures (Ashida and Takahashi, 1980; Mizuyama et al., 1984, 1995; Ashida et al., 1987; Honda and Egashira, 1997; Mizuno et al., 2000; Wang, 2001; Takahashi et al., 2001a, b, 2002; Miyazawa et al., 2003; Shrestha, 2004; Satofuka and Mizuyama, 2005, 2006; Gotoh et al., 2006; Osti and Egashira, 2008). The locations of check dams in a river channel are also very important for effective debris flow control. From the numerical studies of Wang (2001) have revealed that the optimum positions of grid dam installation is where debris flow arrives at its most developed stage.

Ashida and Takahashi (1980) obtained a suitable spacing between columns from the experimental studies as L_g/d_{max}=1.5 ~ 2 (L_g=span of open space and d_{max} =maximum diameter of particle) for effective capturing of debris flow by a grid type check dam. Ashida et al. (1987) tried to clarify the relation among pass rates of sediment through grid dam, sediment sizes and opening length of grids. Mizuyama et al. (1995) considered that the trap efficiency of the grid dam should not only depend on L_g/d_{max} but also on the sediment concentration and the velocity of forefront of the debris flow. An empirical equation was developed from the experiments in order to predict the instantaneous trapped rates of debris flow front by grid dam. Mizuno et al. (2000), Miyazawa et al. (2003) and Gotoh et al. (2006) tried to do the debris flow trap simulation by using the distinct element method. Mizuyama et al. (1995), Mizuno et al. (2000), Miyazawa et al. (2003) and Gotoh et al. (2006) intended to define the trap efficiency of grid dam deterministically by giving the debris flow conditions and the properties of dam. Takahashi et al. (2001b) considered that a small difference in the arrival time of individual boulders would markedly affect the blocking rate of grid dam, and therefore, the phenomena should be intrinsically stochastic, and proposed stochastic model of blocking caused by formation of an arch composed of several boulders. Based on this blocking model, Satofuka and Mizuyama (2006) developed growing rate formula to calculate debris flow capturing by a grid dam.

The sediment control function of the slit type check dam has been mainly discussed with reference to its use in the case of bed load transport (Mizuyama et al., 1990; Okubo et al., 1997; Fujita et al., 1998, 2001; Armanini and Larcher, 2001; Busnelli et al., 2001; Masuda et al., 2002). Mizuno et al. (2001) presented mudflow control function of slit or conduit type check dams. Previous research works have not been focused on sediment control function of the slit type check dam in the case of debris flow. However, Nakatani et al. (2008) tried to do the simulation of debris flow trap by slit dam in some extent as the narrowing river width between upstream and downstream calculation points. Thus, further studies on debris flow control function of slit type check dam are very important.

Many researchers also investigated the debris flow control by closed type check dams (Honda and Egashira, 1997; Takahashi et al., 2001a; Nakagawa et al., 2002b; Shrestha, 2004; Satofuka and Mizuyama, 2005; Osti and Egashira, 2008). Takahashi et al. (2001a) proposed a method to take into account the effect of a closed type check dam. This method uses the relationship between dam height and riverbed height at the upstream of dam to determine whether materials will pass over a closed dam. This method was used by Nakagawa et al. (2002b), Shrestha (2004), and Satofuka and Mizuyama (2005) for the evaluation of the effectiveness of closed dam by using a one-dimensional model in order to reduce the debris flow disasters.

Most of the above models can analyze to some level of debris flow control function of check dams. However, the investigation of debris flow deposition process in upstream area of check dams have not yet been focused by previous researchers. In the upstream area of a check dam, sediment concentration of debris flow becomes maximum sediment concentration due to existence of the check dam, and we can not ignore the effect of static pressures in a numerical model. The constitutive equations and deposition velocity equation are very important to calculate the debris flow deposition in upstream area of a check dam. Therefore, it is necessary to study on deposition process of debris flow in upstream area of a check dam in order to reduce the sediment disasters in the river basin. It is also necessary to study on erosion process of deposited sediment upstream of a check dam to investigate the flushing out of deposited sediment upstream of check dams by a normal scale flood flow.

1.5.2 Model of debris flow with driftwood

Numerical models of debris flow based on the conservation of mass and momentum of the flow have been proposed by several researchers (Takahashi and Kuang, 1986; Takahashi et al., 1988, 1992; Egashira, 1993a, b; Nakagawa et al., 1996; Honda and Egashira, 1997; Brufau et al., 2000; Iverson, 2003). Only some of them include erosion and deposition processes and the various behaviors of different classes of sediments within the flow. Erosion and deposition are directly related to both the variation of debris flow density and the temporal evolution of the channel bed. Models that account for these processes simulate phase separation; therefore the sediments may settle even when the interstitial fluid continues to flow downstream. The flow is considered as a one-phase constant-density fluid (Johnson and Rodine, 1984; O'Brien et al., 1993; Jan, 1997; Jin and Fread, 1997; Laigle and Coussot, 1997; Locat, 1997) or a two-phase variable-density mixture composed by granular material immersed in an interstitial fluid (Takahashi, 1991; Takahashi et al., 1992; Takahashi and Nakagawa, 1994; Shieh et al., 1996;

Egashira et al., 1997; Iverson, 2003). This assumption strongly influences the choice of the rheological model; the typical situation of a debris flow stopping where the channel slope decreases may be simulated either with a constant density fluid or with a variable density mixture; but in the former case, the debris flow stops only if the rheological model allows for a yield stress. On the other hand, in a variable density mixture, the sediments settle even though the interstitial fluid continues to flow downstream (Brufau et al., 2000). The one-phase fluid approach is usually used for the simulation of muddy debris flow whereas the two-phase mixture approach is used for the simulation of granular or clay-poor debris flow.

All of the above models consider debris flow as a mixture of sediment and water only. The previous researchers have not yet considered the behavior of debris flow with driftwood in their numerical models. However, some numerical studies to compute the behavior of driftwood only with clear water flow have been carried out by some researchers (Nakagawa et al., 1991, 1992, 1994, 1995; Gotoh et al., 2002; Ikari et al., 2006; Yabe and Watanabe, 2008; Shimizu and Osada, 2008). Nakagawa et al. (1992, 1994, 1995) performed the numerical simulation of the driftwood behavior in a horizontally two-dimensional flow field evaluated dynamically in the Lagrangian form, based on equations of the rotational motion and the translational motion of the driftwood. They estimated the time-dependent change of the driftwood distribution in an inundated area and compared them with the results obtained from the hydraulic model experiments. Furthermore, Nakagawa et al. (1995) clarified the damming up process of driftwood caused by driftwood caught between and / or in front of buildings. Gotoh et al. (2002) conducted the Lagrangian simulation of the drift-timbers motion, induced flood by using moving particle semi-implicit method originally proposed by Koshizuka et al. (1998). They clarified damming-up and flooding process due to accumulation of drift-timbers at a small bridge in the vertical two dimensional fields. Ikari et al. (2006) investigated the blocking phenomena by driftwood at the bottom outlet of the river bed. Yabe and Watanabe (2008) clarified the relationship between discharge and the locations of driftwood accumulation on a sandbar. Shimizu and Osada (2008) performed numerical simulation of the behavior of driftwood motion by using distinct element method. They also simulated the temporal changes of distribution of driftwood in channel flow with piers and the bar covered with riparian trees. All of the above researchers and others have not focused on computing the behavior of driftwood with debris flow or sediment water mixture flow. Therefore, it is very necessary to study on the mechanism of debris flow with driftwood in order to reduce the debris flow disasters with driftwood and prevent the downstream hazards.

1.5.3 Debris flow with driftwood capturing by check dams

Many researchers have investigated debris flow capturing by check dams considering sediments of the flow only. Debris flow with driftwood capturing by check dams are reported in very few experimental and field studies (Ozaki et al., 1998; Yamada et al., 1999; Doi et al., 2000; Katatani and Yamada, 2006). Ozaki et al. (1998) investigated on debris flow with woody debris trapped by a steel-pipe gridded sabo dam through flume experiments and field observations. They found that the sediment in the frontal part of debris flow as well as the successive trains of debris flow was trapped by the woody debris that occluded the opening sections of the dam. Based on the field data and flume experiments, Yamada et al. (1999) and Doi et al. (2000) have reported about woody debris trapping rate by impermeable type sabo dam, already filled with sediment. They also classified woody debris trapped by impermeable type sabo dams in patterns such as trapped on the sediment before reached the spillway, trapped by spillway clogging, trapped by the mixing of the debris flow in the sediment and trapped by friction in the sediment trapping zone. Katatani and Yamada (2006) investigated the driftwood trapping by slit dams through hydraulic model experiments. They proposed a new convexity shaped type slit sabo dam for reduction of slit blockade by driftwood.

The above discussed studies are limited to the experimental studies and field observations only. A numerical model to investigate the capturing process of debris flow with driftwood by check dams has not yet been developed. Debris flow may be captured due to jamming of driftwood on an open type check dam such as grid or slit type check dam. Therefore, recent attention is required to focus on capturing process of debris flow with driftwood by open type check dams.

1.5.4 Debris flow fan deposition

To establish the soft countermeasures for debris flow hazards, it is essential to delineate the hazardous zone at the debouchment of a ravine due to a potential debris flow (Takahashi and Tsujimoto, 1984). Thus, the investigation on process of deposition of debris flow on the fan is very important for the prediction of hazards zone. The two-dimensional depth average models that can simulate three-dimensional debris flow approximately are reported in many literatures (Takahashi and Tsujimoto, 1984; Savage and Hutter, 1991; Takahashi et al., 1992; O'Brien et al., 1993; Shieh et al., 1996; Hirano et al., 1997; Jan, 1997; Nakagawa et al., 2000; Iverson and Denlinger, 2001; Ghilardi et al., 2001; Pudasaini et al., 2005; Rickenmann et al., 2006; Egashira,

2007; Tsai, 2007; Wada et al., 2008). Some of these models did not incorporate erosion and deposition mechanism; only the models by Takahashi et al. (1992), Shieh et al. (1996), Nakagawa et al. (2000), Ghilardi et al. (2001), Egashira (2007), Tsai (2007) and Wada et al. (2008) incorporated the possibility of erosion and deposition.

Takahashi and Tsujimoto (1984) presented a two-dimensional debris flow model based on a dilatant-fluid model and modified the model to include turbulence (Takahashi et al., 1992). The model proposed by Takahashi et al. (1992) can calculate the topography of a debris fan formed by a debris flow, as well as the three-dimensional sediment-size distribution in the debris fan.

Savage and Hutter (1991) described a model to predict the flow of an initially stationary mass of cohesionless material down rough curved beds based on the assumptions of material incompressibility and Coulomb-like constitutive behavior. O'Brien et al. (1993) developed a two-dimensional flooding model that is a valuable tool for delineating flood hazards and simulating flood-wave attenuation, mudflow, and debris flow. Shieh et al. (1996) presented a two-dimensional numerical model to describe debris flow with deposition process. The local non-equilibrium sediment concentration in the reach of the abrupt variation of bed inclination was roughly estimated under a particular combination of two equilibrium sediment concentrations. Hirano et al. (1997) used an empirical discharge formula of high-concentrated flow on the basis of a wide range of experimental data in the model. Jan (1997) used Bingham model to express the rheological behavior of debris flow. Nakagawa and Takahashi (1997) proposed numerical model for the prediction and assessment of debris flow hazards. Flooding was analyzed by assigning an arbitrary rainfall to an arbitrary, very steep basin. They also presented a simulation method for evacuation based on a refuge network. Nakagawa et al. (2000) proposed a numerical model that can simulate the behavior and depositional process of a debris flow and applied to analysis of the debris flow disaster occurred at Harihara River, Japan. Chau et al. (2000) summarized an experimental investigation on shape of deposition fan and debris flow runout as functions of the particle size distribution of the debris material and of the water content. Liu and Lai (2000) developed a numerical method for vertical two-dimensional debris flow using the rheological model proposed by Julien and Lan (1991).

Iverson and Denlinger (2001) developed a generalization of the depth-averaged, two-dimensional grain-fluid mixture model that describes finite masses of variably fluidized grain-fluid mixtures that move unsteadily across three-dimensional terrain. Bouchut and Westdickenberg (2004) developed a multidimensional shallow water model for arbitrary

topography. Chau and Lo (2004) presented an approach to estimate the potential hazards of debris flow by incorporating the results of numerical simulations of debris flow and Geographical Information Systems (GIS) technology. They used flow model proposed by Takahashi et al. (1992) with appropriate modifications incorporated. Pudasaini et al. (2005) presented a two-dimensional depth-integrated theory for the gravity-driven free-surface flow of a granular avalanche over an arbitrarily but gently curved and twisted topography which is an important extension of the original Savage and Hutter (1991) theory. Rickenmann et al. (2006) compared three two-dimensional debris flow simulation models with field events, and these models are based on a Voellmy fluid rheology reflecting turbulent-like and basal frictional stresses, a quadratic rheologic formulation including Bingham, collision and turbulent stresses, and a Herschel-Bulkley rheology representing a viscoplastic fluid.

Egashira (2007) described two-dimensional depth-integrated models to predict the spreading of the flow on flat area such as alluvial fans. Tsai (2007) proposed a numerical model to describe debris flow covering both erosion and deposition processes. The numerical model was employed to simulate the debris flow by the Hebo typhoon on the Shen-Mu Stream, Taiwan. Wang et al. (2008) presented a two-dimensional numerical model using Navier-stokes equations. Wada et al. (2008) described integrated model for debris flow simulation. They used one-dimensional models in gullies and two-dimensional models in alluvial fans.

The above discussed numerical models were proposed considering debris flow as a mixture of sediment and water. In recent years, numerical model to compute the deposition of debris flows with driftwood on the fan is necessary. A numerical model to investigate the scattering and deposition processes of driftwood in a debris flow fan is also important. Furthermore, most of the study is focused on assessing specific stages of debris flow. Nevertheless, there is a pressing need for more advanced models that can seamlessly all stages of movement initiation, transportation and deposition of debris flow with driftwood and thereby improve forecasting ability. The investigation of effect of check dams in the process of debris flow fan formation is also necessary to combine the structural and non-structural countermeasures.

1.6 Outlines of the dissertation

The dissertation concerns the most effectives and reliable methods to reduce the debris flow disasters with driftwood. It is organized in six chapters.

Chapter 1 presents brief background of the work, objectives of the study and previous literature reviews.

Chapter 2 presents a numerical model to calculate the debris flow deposition upstream of check dams. A numerical model to investigate the erosion of deposited sediment upstream of check dams by a normal flow discharge is also presented. The proposed models are verified with different cases of experimental results.

Chapter 3 presents a two-dimensional numerical model for computing the behavior of debris flow with driftwood. A numerical model has been developed with an interacting combination of Eulerian expression of the debris flow and Lagrangian expression of the driftwood, in which the fluctuation components of the position and the rotational angular velocity of the driftwood are dealt with stochastically as random variables based on the results of a statistical analysis of experimental values. The motion of driftwood is restricted near the flow surface. The simulated results are compared with those obtained from the hydraulic model experiments.

Chapter 4 presents a numerical simulation model of debris flow with driftwood capturing by open type check dams such as grid or slit type check dams. The jamming of driftwood on open type check dams is evaluated based on the geometric conditions and probabilistic approaches. A deposition velocity model is also presented to evaluate the debris flow capturing due to driftwood jamming on open type check dams.

Chapter 5 describes the deposition process of debris flow with driftwood in a fan area. A two-dimensional integrated numerical model for computing the deposition of debris flow with driftwood on the fan is presented, which can simulate all stages of debris flow from initiation to deposition stages. A capturing model of debris flow with driftwood by open type check dams is also incorporated into an integrated numerical model. A numerical model to compute the scattering and deposition processes of driftwood in a debris flow fan is also presented. The effects of driftwood and check dams on debris flow fan formation are also investigated numerically and experimentally.

Chapter 6 summarizes the conclusions of the study and recommendations for the future researches.

Chapter 2

Debris Flow Deposition and Erosion Upstream of a Check Dam

2.1 Introduction

Debris flow is a rapidly moving mass of a dense mixture of sediment and water that occurs in a wide variety of environments throughout the world. It is among the most dangerous natural hazard that affects humans and properties (Takahashi, 1991). Therefore, the understanding of behavior and mechanism of debris flow and the study of preventive measures are very important in order to manage the sediment disasters in the river basin and reduce the downstream hazards.

Check dams are one of the effective structural countermeasures for debris flow control. Check dams can effectively store the debris flow as long as there is an adequate storage capacity, when check dam loses such storage capacity, the check dam can not capture enough sediment to reduce the debris flow (Mizuyama et al., 1998). In closed type check dam, it is difficult to prevent from losing its trapping capacity unless sediments are continuously removed, whereas open type dams may keep their trapping capacity without any need of artificially removing the sediment (Bovolin and Mizuno, 2000). It is necessary to investigate the debris flow deposition and erosion processes upstream of a check dam for effective sediment disaster prevention.

A numerical model is presented to investigate the debris flow deposition upstream of a check dam and flushing out of deposited sediment due to erosion process by a normal flow discharge. The constitutive equations of Takahashi et al. (1997) and those of Egashira et al. (1997) are chosen for the study on deposition process upstream of a check dam. A new deposition velocity equation to calculate the debris flow deposition upstream of a check dam is also presented. To simulate the debris flow deposition upstream of a closed or an open type check dam, a deposition model and a blockage model of open spaces by large sediment particles in the case of an open type check dam, are incorporated in a flow model of the debris flow. A riverbed erosion model under unsaturated bed condition is used to simulate the erosion process of deposited

sediment upstream of a check dam. The simulated and experimental results of closed type and open type check dams are presented.

2.2 Debris flow deposition upstream of a check dam

2.2.1 Basic governing equations

Transport and bed surface elevation equations

The stony type debris flow is considered to move as continuous fluid. The flow of the solid-liquid mixture is described using one-dimensional depth averaged equations for the momentum conservation of the flow mixture, the mass conservation of sediment-water mixture and the mass conservation of sediment as following equations.

Momentum equation of sediment and water flow mixture:

$$\frac{\partial M}{\partial t} + \beta \frac{\partial (uM)}{\partial x} = gh\sin\theta - gh\cos\theta \frac{\partial h}{\partial x} - \frac{\tau_b}{\rho_T} \tag{2.1}$$

Continuity equation of flow mixture:

$$\frac{\partial h}{\partial t} + \frac{\partial M}{\partial x} = i_b \tag{2.2}$$

Continuity equation of sediment particles:

$$\frac{\partial (Ch)}{\partial t} + \frac{\partial (CM)}{\partial x} = i_b C_* \tag{2.3}$$

where $M\,(=uh)$ is the flow flux in x direction, u is the mean velocity, h is the flow depth, t is time, i_b is the erosion (≥ 0) or deposition (<0) velocity, C is the sediment concentration in the flow, C_* is the sediment concentration in the bed, β is the momentum correction factor equal to 1.25 for a stony debris flow (Takahashi et al., 1992) and to 1.0 for both an immature debris flow and a turbulent flow, g is the acceleration due to gravity, θ is the bed slope, τ_b is the bottom shear stress, ρ_T is the mixture density $(\rho_T = \sigma C + (1-C)\rho)$, σ is the density of the sediment particle and ρ is the density of the water.

When the cross section of the channel is rectangular with fixed walls and loose bottom, the movement of the bed due to erosion or deposition that takes place in presence of given sediment

concentration is represented by the following equation.

$$\frac{\partial z_b}{\partial t} + i_b = 0 \tag{2.4}$$

where z_b is erosion or deposition thickness of the bed measured from the original bed surface elevation.

Erosion and deposition velocity equations

The bed erosion or deposition velocity i_b is source term. The dependence of this quantity with the basic set of dependent variables has to be modeled which can be done using model proposed by Takahashi et al. (1992). The erosion and deposition velocity that have been given by Takahashi et al. (1992) are described as follows.

Erosion velocity, if $C \le C_\infty$;

$$i_b = \delta_e \frac{C_\infty - C}{C_* - C_\infty} \frac{M}{d_m} \tag{2.5}$$

Deposition velocity, if $C > C_\infty$;

$$i_b = \delta_d \frac{C_\infty - C}{C_*} \frac{M}{d_m} \tag{2.6}$$

where δ_e is erosion coefficient, δ_d is deposition coefficient, d_m is mean diameter of sediment and C_∞ is the equilibrium sediment concentration described as follows (Nakagawa et al., 2003).

If $\tan\theta_w > 0.138$, a stony type debris flow occurs, and

$$C_\infty = \frac{\rho_m \tan\theta_w}{(\sigma - \rho_m)(\tan\phi - \tan\theta_w)} \tag{2.7}$$

If $0.03 < \tan\theta_w \le 0.138$, an immature type debris flow occurs, and

$$C_\infty = 6.7\left\{\frac{\rho_m \tan\theta_w}{(\sigma - \rho_m)(\tan\phi - \tan\theta_w)}\right\}^2 \tag{2.8}$$

If $\tan\theta_w \le 0.03$, a turbulent water flow with bed load transport occurs, and

$$C_\infty = \frac{(1+5\tan\theta_w)\tan\theta_w}{\sigma/\rho_m - 1}\left(1 - \alpha_0^2 \frac{\tau_{*c}}{\tau_*}\right)\left(1 - \alpha_0^2 \sqrt{\frac{\tau_{*c}}{\tau_*}}\right) \tag{2.9}$$

where θ_w is water surface gradient, ρ_m is density of the interstitial muddy fluid, ϕ is internal friction angle of the sediment, and

$$\alpha_0^2 = \frac{2\{0.425 - (\sigma/\rho_T)\tan\theta_w/(\sigma/\rho_T - 1)\}}{1 - (\sigma/\rho_T)\tan\theta_w/(\sigma/\rho_T - 1)} \tag{2.10}$$

$$\tau_{*c} = 0.04 \times 10^{1.72\tan\theta_w} \tag{2.11}$$

$$\tau_* = \frac{h\tan\theta_w}{(\sigma/\rho_T - 1)d_m} \tag{2.12}$$

in which τ_{*c} is the non-dimensional critical shear stress and τ_* is the non-dimensional shear stress.

2.2.2 Deposition model upstream of a check dam

In the upstream region of a check dam, sediment concentration is higher than that of equilibrium state and becomes maximum concentration due to existence of the check dam, and the yield stress exceeds the driving force, then debris flow stops and deposition occurs, before filling up upstream of the dam. This mechanism of deposition is incorporated in momentum equation of the flow mixture as considering yield stress in the bottom shear stress. The bottom shear stress is evaluated as follows:

$$\tau_b = \tau_y + \rho f_b |u| u \tag{2.13}$$

where τ_y is the yield stress and f_b is the coefficient of resistance.

Constitutive equations

Several constitutive equations for debris flows have been proposed (Takahashi, 1977, 1980, 1991; Ackermann and Shen, 1982; Tsubaki et al., 1982; Miyamoto, 1985; Chen, 1988; O'Brien and Julien, 1988; Egashira et al., 1989, 1997; Takahashi et al., 1992, 1997; Egashira and Ashida, 1992; Hunt, 1994). The equations for yield stress as the static pressure due to particle-particle contacts have been proposed by Takahashi et al. (1997) and Egashira et al. (1997). They incorporated the yield stress with their formerly developed constitutive equations for water-grain mixtures flow or debris flow. Thus, the constitutive equations of Takahashi et al. (1997) and those of Egashira et al. (1997) have been chosen for the study on debris flow deposition process upstream of a check dam.

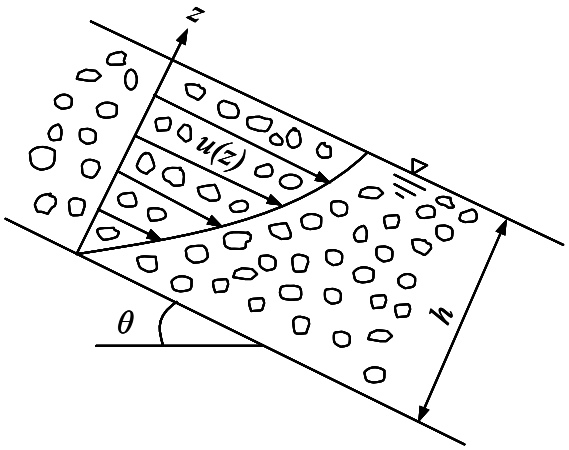

Figure 2.1 Coordinate of two-dimensional uniform debris flow

Takahashi et al.'s constitutive equations and bottom shear stress

The constitutive equations of Takahashi et al. (1997) for a fully stony debris flow are described as follows. The expression for the shear stress is as

$$\tau = \tau_y + a_i \sin\alpha_i \left\{ \left(\frac{C_*}{C} \right)^{1/3} - 1 \right\}^{-2} \sigma d_m^2 \left(\frac{\partial u}{\partial z} \right)^2 \tag{2.14}$$

$$\tau_y = p_s \tan\phi \tag{2.15}$$

where a_i is experiment constant, α_i is the collisions angle of the particle ($a_i \sin\alpha_i$ =0.02) (Takahashi et al., 1992), z is the coordinate perpendicular to the bed and positive upward in the normal direction of flow (Figure 2.1) and p_s is static pressure which can be expressed as follows (Takahashi et al., 1997).

$$p_s = f(C)(\sigma - \rho)Cg(h - z)\cos\theta \tag{2.16}$$

in which $f(C)$ is described as

$$f(C) = \begin{cases} \dfrac{C - C_3}{C_* - C_3} & ; \quad C > C_3 \\ 0 & ; \quad C \le C_3 \end{cases} \tag{2.17}$$

where C_3 is the limitative sediment concentration.

The bottom shear stress for a stony debris flow is derived by substituting the constitutive equations into the momentum conservation equation under a steady and uniform flow

conditions. The momentum conservation equation is descried as follows:

$$\tau(z) = \rho_T g(h-z)\sin\theta \tag{2.18}$$

where $\tau(z)$ is shear stress at any distance from the bed along the z-axis. By substituting constitutive equations of Takahashi et al. (1997) in momentum equation, the following equation is obtained

$$\frac{\partial u}{\partial z} = \frac{du}{dz} = \left[\frac{\rho_T g(h-z)\sin\theta - f(C)(\sigma-\rho)cg(h-z)\cos\theta\tan\phi}{a_i \sin\alpha_i \left\{ \left(\frac{c_*}{c} \right)^{1/3} - 1 \right\}^{-2} \sigma d_m{}^2} \right]^{1/2} \tag{2.19}$$

By introducing dimensionless quantities as $\tilde{u} = u/\sqrt{gh}$ and $\tilde{z} = z/h$, above equation is modified as

$$\frac{d\tilde{u}}{d\tilde{z}} = K_T \sqrt{\sin\theta}\, \frac{h}{d_m} (1-\tilde{z})^{1/2} \tag{2.20}$$

$$\frac{u(\tilde{z})}{u_*} = \frac{2}{3} K_T \frac{h}{d_m} \left\{ 1 - (1-\tilde{z})^{3/2} \right\} \tag{2.21}$$

$$\frac{u}{u_*} = \frac{2}{5} K_T \frac{h}{d_m} \tag{2.22}$$

$$K_T = \left\{ \frac{\rho_T - f(C)(\sigma-\rho)c\dfrac{\tan\phi}{\tan\theta}}{a_i \sin\alpha_i \sigma \left\{ \left(\dfrac{c_*}{c} \right)^{1/3} - 1 \right\}^{-2}} \right\}^{1/2} \tag{2.23}$$

in which u_* is friction velocity defined as $u_* = \sqrt{gh\sin\theta}$. The evaluation method of shear stress of momentum equation of debris flow is fundamentally equal to the case of the water. In the evaluation of the shear stress at the bed (τ_b), Equation (2.13) is used. The yield stress is written as

$$\tau_y = p_s \tan\phi = f(C)(\sigma-\rho)Cgh\cos\theta\tan\phi \tag{2.24}$$

The coefficient of resistance f_b is calculated by assuming an equilibrium state as

$$\rho_T gh\sin\theta = f(C)(\sigma-\rho)cgh\cos\theta\tan\phi + \rho f_b |u| u \tag{2.25}$$

The following equation is obtained by solving above equation

$$f_b = \frac{gh\sin\theta\left(\rho_T - f(C)(\sigma-\rho)C\dfrac{\tan\phi}{\tan\theta}\right)}{\rho u^2} \tag{2.26}$$

By using Equations (2.22) and (2.23), Equation (2.26) can be described as

$$f_b = \frac{1}{8}\frac{(\sigma/\rho)}{\left\{(C_*/C)^{1/3}-1\right\}^2}\left(\frac{d_m}{h}\right)^2 \tag{2.27}$$

The bottom shear stress for stony debris flow is derived as

$$\tau_b = \tau_y + \frac{1}{8}\rho\frac{(\sigma/\rho)}{\left\{(C_*/C)^{1/3}-1\right\}^2}\left(\frac{d_m}{h}\right)^2 |u|u \tag{2.28}$$

An immature debris flow occurs when C is less than $0.4C_*$ and the bottom shear stress is described as follows (Takahashi et al., 1992):

$$\tau_b = \frac{\rho_T}{0.49}\left(\frac{d_m}{h}\right)^2 u|u| \tag{2.29}$$

The Manning's equation is used to determine the bottom shear stress in the case of a turbulent flow when C is less than 0.02 as follows (Takahashi et al., 1992):

$$\tau_b = \frac{\rho g n^2 u|u|}{h^{1/3}} \tag{2.30}$$

Egashira et al.'s constitutive equations and bottom shear stress

The constitutive equations of Egashira et al. (1997) are described as follows. The shear stress is described as

$$\tau = \tau_y + \sigma k_d\left(1-e^2\right)C^{1/3}d_m^2\left(\frac{\partial u}{\partial z}\right)^2 + \rho k_f\left(1-C\right)^{5/3}/C^{2/3}\,d_m^2\left(\frac{\partial u}{\partial z}\right)^2 \tag{2.31}$$

$$\tau_y = p_s\tan\phi \tag{2.32}$$

where e is the restitution of sediment particles, k_d and k_f are empirical constants, $k_d = 0.0828$ and $k_f = 0.16$. The static pressure is described as follows:

$$p_s = f(C)(\sigma-\rho)Cg(h-z)\cos\theta \tag{2.33}$$

in which $f(C)$ is described as

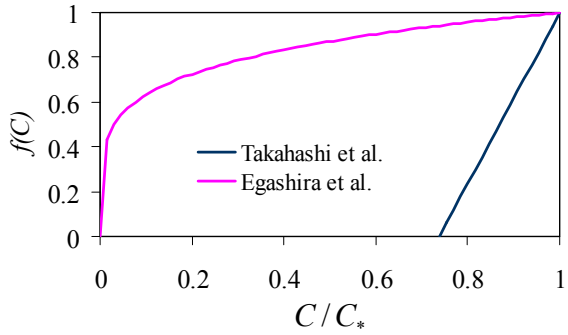

Figure 2.2 Plots of *f(C)* according to Takahashi et al. (1997) and Egashira et al. (1997), $C_* = 0.65,\ C_3 = 0.48$

$$f(C) = \left(\frac{C}{C_*}\right)^{1/5} \tag{2.34}$$

By substituting the constitutive equations of Egashira et al. (1997) in momentum equation, the following equations are obtained

$$\frac{d\tilde{u}}{d\tilde{z}} = K_H \sqrt{\sin\theta}\,\frac{h}{d_m}\left(1-\tilde{z}\right)^{1/2} \tag{2.35}$$

$$\frac{u(\tilde{z})}{u_*} = \frac{2}{3}K_E\,\frac{h}{d}\left\{1-\left(1-\tilde{z}\right)^{3/2}\right\} \tag{2.36}$$

$$\frac{v}{u_*} = \frac{2}{5}K_E\,\frac{h}{d} \tag{2.37}$$

$$K_E = \left\{\frac{(\sigma/\rho-1)C+1-(\sigma/\rho-1)Cf(C)\dfrac{\tan\phi}{\tan\theta}}{k_f(1-C)^{5/3}/C^{2/3}+k_g(\sigma/\rho)(1-e^2)C^{1/3}}\right\}^{1/2} \tag{2.38}$$

Equation (2.13) is used to evaluate the shear stress at the bed (τ_b) and the yield stress is described as

$$\tau_y = p_s \tan\phi = f(C)(\sigma-\rho)Cgh\cos\theta\tan\phi \tag{2.39}$$

Similarly as above, the coefficient of resistance f_b is derived as

$$f_b = \frac{25}{4}\left\{k_f(1-C)^{5/3}/C^{2/3}+k_g(\sigma/\rho)(1-e^2)C^{1/3}\right\}\left(\frac{d_m}{h}\right)^2 \tag{2.40}$$

The bottom shear stress is derived as

$$\tau_b = \tau_y + \rho\frac{25}{4}\left\{k_d(\sigma/\rho)(1-e^2)C^{1/3}+k_f(1-C)^{5/3}/C^{2/3}\right\}\left(\frac{d_m}{h}\right)^2|u|u \tag{2.41}$$

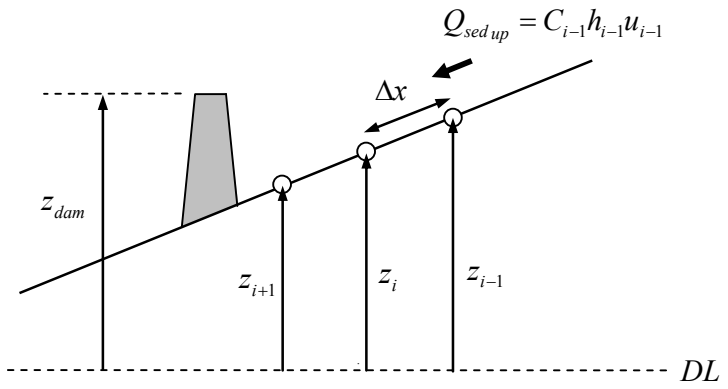

Figure 2.3 Definition sketch of deposition upstream of a check dam

Equations (2.17) and (2.34) are represented in Figure 2.2, from which the role of the both constitutive equations assigned to static pressures or yield stresses are evident. The static pressures in Equation (2.16) are influential when sediment concentration is higher than C_3, while in Equation (2.33) they are predominant even for lower sediment concentrations.

Deposition velocity equation upstream of a check dam

The deposition velocity models given by previous researchers such as Takahashi et al. (1992), Egashira et al. (2001) and others are proportional to the flow velocity, and deposition upstream of a check dam can not be calculated, when the flow velocity becomes zero, also the calculated deposition upstream of check dam is too small. Debris flow deposition upstream of a check dam is very rapid deposition phenomenon, which can not be calculated by such available deposition velocity equations. Therefore, new deposition velocity equation for upstream of a check dam is derived. Upstream of a check dam, deposition usually takes place when yield stress exceeds the equilibrium shear stress, before filling up the sediment storage capacity. In the upstream area of a check dam, if bed elevation z_i is less than elevation of the dam crown z_{dam} at the calculation point i (Figure 2.3), the sediment discharge from the upstream will deposit in the distance increment of the calculating point Δx when yield stress exceeds the equilibrium shear stress. The sediment discharge per unit width from upstream is described as

$$Q_{sed\,up} = C_{i-1}h_{i-1}u_{i-1} \tag{2.42}$$

Effective non-dimensional shear stress on the bed responsible for the deposition should be $\tau_{*e}-\tau_{*y}$ and deposition velocity is written as

$$i_{dep} \propto (\tau_{*e}-\tau_{*y}) \tag{2.43}$$

$$i_{dep} = K_{dep}(\tau_{*e} - \tau_{*y})\frac{C_{i-1}h_{i-1}u_{i-1}}{C_*\Delta x} \tag{2.44}$$

where i_{dep} is the deposition velocity upstream of a check dam (if $z_i < z_{dam}$ or $z_i < z_{i+1}$ and $\tau_{*y} > \tau_{*e}$), K_{dep} is constant, τ_{*e} is the non-dimensional equilibrium shear stress and τ_{*y} is the non-dimensional yield stress. These non-dimensional stresses are described as follows.

$$\tau_{*e} = \frac{\rho_T g h \sin\theta}{(\sigma - \rho) g d_m} \tag{2.45}$$

$$\tau_{*y} = \frac{Cgh\cos\theta\tan\phi}{gd_m} \tag{2.46}$$

2.2.3 Conditions of check dams

Closed type check dam

Takahashi et al. (2001a) have proposed a method to take into account the effect of a closed type check dam. The closed dam position is set at the calculation point of flow discharge per unit width, M_i (Figure 2.4). The effective flow depth, h', at the dam point to calculate the outflow flux and the flow surface gradient, θ_e, are described as follows:

$$h' = \begin{cases} h_i + z_i - z_{dam} & ;(h_i + z_i - z_{dam} > 0) \\ 0 & ;(h_i + z_i - z_{dam} \le 0) \\ h_i & ;(z_i > z_{dam}) \end{cases} \tag{2.47}$$

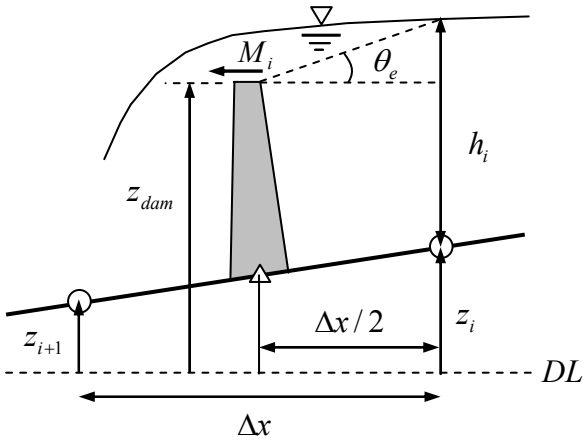

Figure 2.4 Definition of the variables and flow surface gradient at closed dam

$$\theta_e = \tan^{-1}\left\{\frac{[z_i + h_i - z_{dam}]}{(\Delta x/2)}\right\} \tag{2.48}$$

The gradient, $\theta_e^{'}$, needed to calculate the equilibrium sediment concentration, C_∞, is described as

$$\theta_e^{'} = \tan^{-1}\left\{\frac{[z_i - z_{dam}]}{(\Delta x/2)}\right\} \tag{2.49}$$

Grid type check dam

In grid type check dam, when debris flow occurs, the opening of a grid dam is blockaded by large sediment particles in the debris flow. This blockade phenomenon is influenced by the width of dam opening, the maximum particle diameter of sediment, and the sediment concentration of debris flow (Ashida and Takahashi, 1980; Ashida et al., 1987; Mizuyama et al., 1995; Mizuno et al., 2000; Takahashi et al., 2001b, 2002; Miyazawa et al., 2003; Satofuka and Mizuyama, 2006). Takahashi et al. (2001b) proposed stochastic model of blocking caused by formation of an arch composed of several boulders. They clarified the relationship between the probability of blockage of grid and parameters such as boulder's diameter, sediment concentration and clear spacing of dam. Based on this probability of blockage model, deposition velocity of grid dam blockage developed by Satofuka and Mizuyama (2006) is used as follows.

$$i_b^{'} = i_b - a_2 \frac{Chu}{C_* \Delta x} \tag{2.50}$$

where a_2 coefficient parameter depends on the instantaneous blockade probability of grid and influence of horizontal beam. If z_L^j and z_H^j are the elevations of the undersurface and the upper surface of the j -th beam, respectively (Figure 2.5). In the case where the bed is between the j -th beam and the $j+1$-th beam, the influence of beams changes by whether the gap between the undersurface of the $j+1$ -th beam and the bed is larger or smaller than the boulder's diameter. If the gap under the beam is smaller than the boulder's diameter, a fraction of debris flow is deposited from the bed to the upper surface of the beam. In such situation, a_2 is calculated as

$$a_2 = a_1 + (z_H^{j+1} - z_d)/h \tag{2.51}$$

where z_d is bed elevation immediately upstream of the dam.

In contrast, if the gap under the beam is larger than the boulder's diameter, the beam's influence

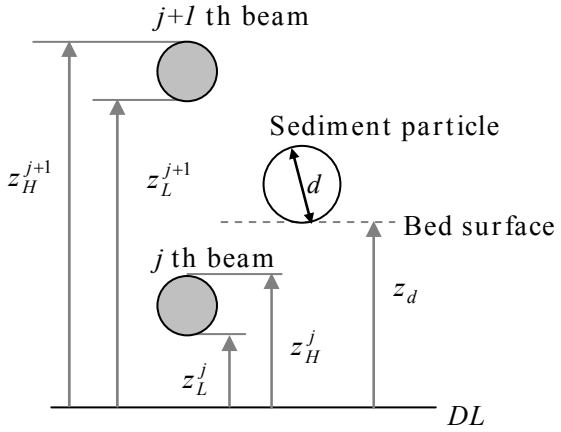

Figure 2.5 Side view of the grid dam with definition of variables

can be neglected. Thus, a_2 is described as

$$a_2 = a_1 \tag{2.52}$$

where a_1 is an approximation using parameters such as boulder concentration and opening width, which is described as

$$a_1 = \zeta_5 + \zeta_6 \log_{10} C \tag{2.53}$$

If $D/d > 1$;

$$\zeta_5 = \xi_8 + \xi_9 \frac{l-d}{d} \tag{2.54}$$

$$\zeta_6 = \xi_{10} + \xi_{11} \frac{l-d}{d} \tag{2.55}$$

If $D/d \le 1$;

$$\zeta_5 = \xi_8 + \xi_9 \frac{l-D}{d} \tag{2.56}$$

$$\zeta_6 = \xi_{10} + \xi_{11} \frac{l-D}{d} \tag{2.57}$$

where l is distance between centers of columns of grid dam, D is diameter of column, d is diameter of large sediment particle, and ξ_8, ξ_9, ξ_{10} and ξ_{11} are constants.

Slit type check dam

In the case of slit dam, previous researchers such as Mizuyama et al. (1990), Okubo et al. (1997), Armanini and Larcher (2001), Fujita et al. (2001) and others have investigated sediment

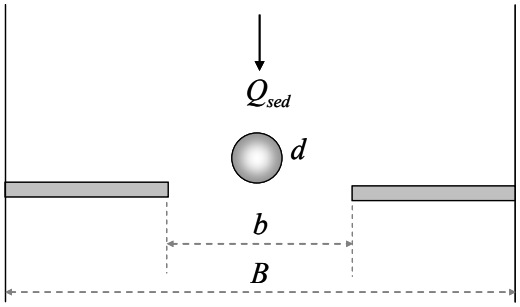

Figure 2.6 Definition of variables of sediment passing through slit dam

control function of slit dam only to its use in the case of bed load transport. If the slit type check dam is used for the debris flow control, debris flow is deposited behind a slit dam by clogging of open space of slit dam due to simultaneous arrival of two or more particles and sudden reduction in flow width. A new deposition velocity equation is derived to calculate the sediment deposition behind a slit type check dam based on diameter of sediment particle, width of slit opening, sediment discharge and channel width of the flow (Figure 2.6). The sediment passing rate, P_{sd} , through slit dam and the deposition velocity, i_{dep} , behind a slit dam caused by clogging of open space due to simultaneous arrival of two or more particles are expressed as

$$P_{sd} = (b - d)/b \tag{2.58}$$

$$i_{dep} = -K_{sd}(1 - P_{sd})\frac{Q_{sed}}{C_* \Delta x} \tag{2.59}$$

where b is width of slit opening, K_{sd} is numerical constant and Q_{sed} is sediment discharge per unit width. By considering the influence of sudden reduction in flow width with n number of slit opening of same width, b , the deposition velocity Equation (2.59) is described as follows:

$$i_{dep} = -K_{sd}(1 - P_{sd})\frac{B}{nb}\frac{Q_{sed}}{C_* \Delta x} \tag{2.60}$$

where B is channel width and nb is total width of open spaces of slit dam.

2.3 Erosion of deposited sediment upstream of a check dam

The large boulders deposited upstream of a check dam can not be transported by a normal scale of flood flow (Takahashi, 2007; Shrestha et al., 2008a). If we remove large boulders deposited upstream of a grid dam or blockaded large boulders at open spaces of grid, deposited sediment upstream of grid dam may be transported to the downstream of grid dam by a normal scale

Figure 2.7 Deposited sediment upstream of grid dam at the Hirayu River, Gifu Prefecture, Japan *(Source: River Disaster Prevention System, DPRI)*

flood flow due to the erosion process (Shrestha et al., 2008a) (Figure 2.7). Thus, the grid dams will have debris flow storage capacity to control the next debris flow event in monsoon season. Hence, a one-dimensional mathematical riverbed erosion equation proposed by Takahashi et al. (1992) is used to simulate the erosion process of deposited sediment upstream of a grid dam as follows.

$$\frac{i_b}{\sqrt{gh}} = K \sin^{3/2}\theta \left\{ 1 - \frac{\sigma - \rho_T}{\rho_T} C \left(\frac{\tan\phi}{\tan\theta} - 1 \right) \right\}^{1/2} \left(\frac{\tan\phi}{\tan\theta} - 1 \right) (C_\infty - C) \frac{h}{d_m} \tag{2.61}$$

where K is a numerical constant.

2.4 Solution methods

The domain where the variables are going to be calculated is divided in a temporal and spatial computational mesh. Each point is represented by the pair (x_i, t^n), where x_i represents the position in the space and t^n the time level. Figure 2.8 shows the definition of arrangement of variables with the finite difference mesh. The partial differential equations are solved by leap frog scheme, which needs three-time-level variables, i.e., n, $n+1$, and $n+2$ to get a value at $t = (n+3)\Delta t$. For example, scalar value h^{n+3} is obtained by using h^{n+1} and M^{n+2}. Vector value M^{n+2} is obtained by using h^{n+1} and M^n. So that, each time level of h and M is different. The

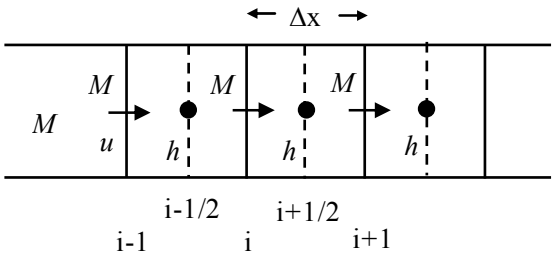

Figure 2.8 Arrangement of variables on meshes

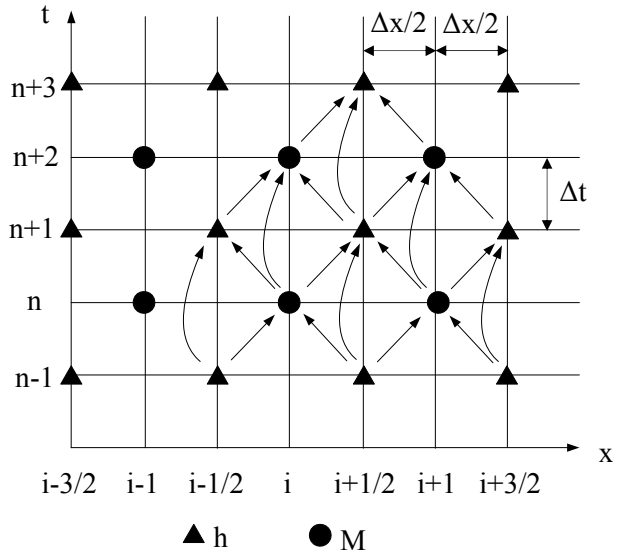

Figure 2.9 The way of advancing the calculation

scalar values such as h, C and z_b are set in the middle of the cell and the vector value M is set on the grid. Thus this is a staggered cell. This computational cell acts as control volume for the dependent variables associated with the basic equations. Referring Figure 2.9 which shows the way to proceed with calculation, the finite differential equations can be obtained by using the method of Nakagawa (1989), in which upwind scheme is adopted in the advection term and implicit scheme is introduced in the friction term.

Calculation method of conservation of momentum

The value of vector M_i^{n+2} in Figure 2.9 can be obtained from following finite differential equation.

$$\frac{M_i^{n+2}-M_i^n}{2\Delta t}+\beta(XDX)=g\frac{h_{i+1/2}^{n+1}+h_{i-1/2}^{n+1}}{2}\sin\theta_m^{n+1}$$
$$-gh\frac{h_{i+1/2}^{n+1}+h_{i-1/2}^{n+1}}{2}\cos\theta_m^{n+1}\frac{h_{i+1/2}^{n+1}-h_{i-1/2}^{n+1}}{\Delta x}-\frac{1}{\overline{\rho_{\mathrm{T}}}}\left(\tau_y+\rho f_b\frac{M_i^{n+2}+M_i^n}{2\bar{h}}\left|\frac{M_i^n}{\bar{h}}\right|\right) \tag{2.62}$$

where,

$$u_i^n=2M_i^n/(h_{i+1/2}^{n+1}+h_{i-1/2}^{n+1}) \tag{2.63}$$

$$XDX=\begin{cases}\dfrac{u_i^nM_i^n-u_{i-1}^nM_{i-1}^n}{\Delta x} & :\ u_i^n\ge 0,\quad u_{i-1}^n\ge 0\\ \dfrac{u_i^nM_i^n-0}{\Delta x} & :\ u_i^n\ge 0,\quad u_{i-1}^n<0\\ \dfrac{u_{i+1}^nM_{i+1}^n-u_1^nM_i^n}{\Delta x} & :\ u_i^n<0,\quad u_{i-1}^n<0\\ \dfrac{0-u_1^nM_i^n}{\Delta x} & :\ u_i^n<0,\quad u_{i-1}^n\ge 0\end{cases} \tag{2.64}$$

The calculation of the above gives M_i^{n+2} in the following equation.

$$M_i^{n+2}=\frac{\left\{\begin{array}{l}g\bar{h}\sin\theta_m^{n+1}-g\bar{h}\cos\theta_m^{n+1}\dfrac{h_{i+1/2}^{n+1}-h_{i-1/2}^{n+1}}{\Delta x}\\ -\beta(XDX)-\dfrac{\tau_y}{\overline{\rho_T}}+\left(\dfrac{1}{2\Delta t}-\dfrac{\rho}{\overline{\rho_T}}f_b\dfrac{1}{2\bar{h}}\left|\dfrac{M_i^n}{\bar{h}}\right|\right)M_i^n\end{array}\right\}}{\dfrac{1}{2\Delta t}+\dfrac{\rho}{\overline{\rho_T}}f_b\dfrac{1}{2\bar{h}}\left|\dfrac{M_i^n}{\bar{h}}\right|} \tag{2.65}$$

in which,

$$\bar{h}=\frac{h_{i-1/2}^{n+1}+h_{i+1/2}^{n+1}}{2} \tag{2.66}$$

$$\overline{\rho_T}=(\sigma-\rho)\overline{C}+\rho \tag{2.67}$$

$$\overline{C}=\frac{C_{i-1/2}^{n+1}+C_{i+1/2}^{n+1}}{2} \tag{2.68}$$

$$\sin\theta_m^{n+1}=\frac{\sin\theta_{i+1/2}^{n+1}+\sin\theta_{i-1/2}^{n+1}}{2} \tag{2.69}$$

$$\cos\theta_m^{n+1}=\frac{\cos\theta_{i+1/2}^{n+1}+\cos\theta_{i-1/2}^{n+1}}{2} \tag{2.70}$$

$$\theta_{i+1/2}^{n+1}=-\arctan\left(\frac{z_{i+1/2}^{n+1}-z_{i-1/2}^{n+1}}{\Delta x}\right) \tag{2.71}$$

$$\tau_y = f(\overline{C})(\sigma-\rho)\overline{C}g\overline{h}\cos\theta_m^{n+1}\tan\phi \tag{2.72}$$

for Takahashi et al.'s (1997) constitutive equations

$$f(\overline{C}) = \begin{cases} \dfrac{\overline{C}-C_3}{C_*-C_3} & ;\quad \overline{C} > C_3 \\ 0 & ;\quad \overline{C} \le C_3 \end{cases} \tag{2.73}$$

$$f_b = \frac{1}{8}\frac{(\sigma/\rho)}{\left(\left\{\left(C_*/\overline{C}\right)^{1/3}-1\right\}^2\right)}\left(\frac{d_m}{\overline{h}}\right)^2 \tag{2.74}$$

for Egashira et al.'s (1997) constitutive equations

$$f(\overline{C}) = \left(\frac{\overline{C}}{C_*}\right)^{1/5} \tag{2.75}$$

$$f_b = \frac{25}{4}\left\{k_f\left(1-\overline{C}\right)^{5/3}/\overline{C}^{2/3} + k_g(\sigma/\rho)\left(1-e^2\right)\overline{C}^{1/3}\right\}\left(\frac{d_m}{\overline{h}}\right)^2 \tag{2.76}$$

Calculation method of conservation of mass and river bed variation

When the values of vector properties M are given or obtained from the beginning to step $n+2$ ($t=(n+2)\Delta t$), and the values of scalar quantities such as h, C and z_b are given or obtained to step $n+1$, the value of scalar $z_{b\,i+1/2}^{\,n+3}$, $h_{i+1/2}^{n+3}$, and $C_{i+1/2}^{n+3}$ in Figure 2.9 can be obtained from following finite differential equations.

$$\frac{h_{i+1/2}^{n+3}-h_{i+1/2}^{n+1}}{2\Delta t} + \frac{M_{i+1}^{n+2}-M_i^{n+2}}{\Delta x} = i_{b1+1/2}^{\,n+1} \tag{2.77}$$

$$\frac{(Ch)_{i+1/2}^{n+3}-(Ch)_{i+1/2}^{n+1}}{2\Delta t} + CXDX = i_{b\,i+1/2}^{\,n+1}C_* \tag{2.78}$$

in which,

$$CXDX = \begin{cases} \dfrac{C_{1+1/2}^{n+1}M_{i+1}^{n+2}-C_{i-1/2}^{n+1}M_i^{n+2}}{\Delta x} & ;\left(M_i^{n+2}\ge 0,\ M_{i+1}^{n+2}\ge 0\right) \\ \dfrac{C_{1+1/2}^{n+1}M_{i+1}^{n+2}-C_{i+1/2}^{n+1}M_i^{n+2}}{\Delta x} & ;\left(M_i^{n+2}< 0,\ M_{i+1}^{n+2}\ge 0\right) \\ \dfrac{C_{1+3/2}^{n+1}M_{i+1}^{n+2}-C_{i-1/2}^{n+1}M_i^{n+2}}{\Delta x} & ;\left(M_i^{n+2}\ge 0,\ M_{i+1}^{n+2}< 0\right) \\ \dfrac{C_{1+3/2}^{n+1}M_{i+1}^{n+2}-C_{i+1/2}^{n+1}M_i^{n+2}}{\Delta x} & ;\left(M_i^{n+2}< 0,\ M_{i+1}^{n+2}< 0\right) \end{cases} \tag{2.79}$$

$$\frac{z_{i+1/2}^{n+3} - z_{i+1/2}^{n+1}}{2\Delta t} + i_{b1+1/2}^{n+1} = 0 \tag{2.80}$$

2.5 Laboratory experiments

2.5.1 Experiments of debris flow deposition upstream of a check dam

A rectangular flume of 5m long, 10cm wide and 13cm deep was used for the experiments. The experiments were carried out with flume slope of 18 degrees and 20 degrees. The details of the experimental setup and photograph of the flume are shown in Figure 2.10 and Figure 2.11, respectively. A sediment bed of silica sand and gravel mixtures 1.9m long and 7cm deep was positioned from 2.8m to 4.7m upstream measured from the outlet of the flume. This laid sediment bed was retained by installing a partition of 7cm in height at 2.8m upstream from the outlet of the flume and saturated by water as seepage flow. Sediment materials with mean diameter $d_m = 2.53$mm, maximum diameter $d_{\max} = 15$mm, $\tan\phi = 0.7$ and sediment density $\sigma =$ 2.65g/cm^3 were used. The particle size distribution of the sediment bed is shown in Figure 2.12.

Check dams were set at 20cm upstream from the downstream end of the flume. The closed type check dam, grid type check dams and slit type check dams were used for the study. The details of check dams are shown in Figure 2.13. To determine a suitable spacing between columns of grid dam the following design criterion obtained by Ashida and Takahashi (1980) was used as

$$L_g / d_{\max} = 1.5 \sim 2.0 \tag{2.81}$$

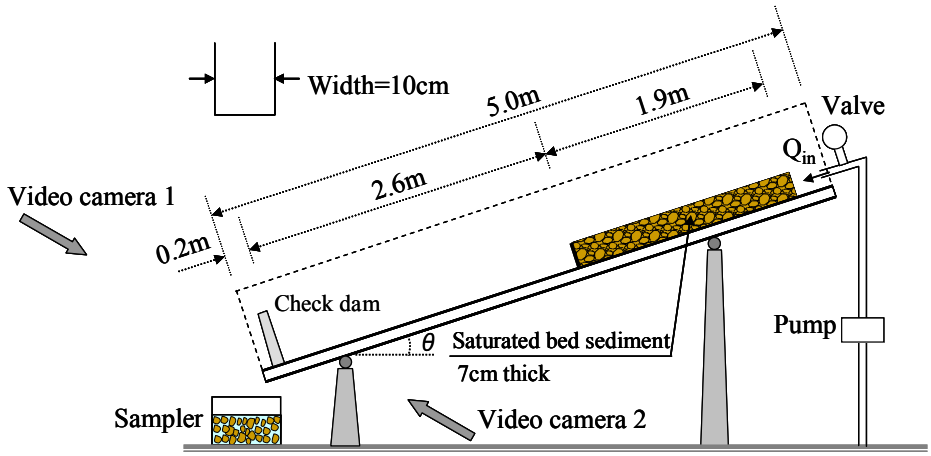

Figure 2.10 Experimental flume setup

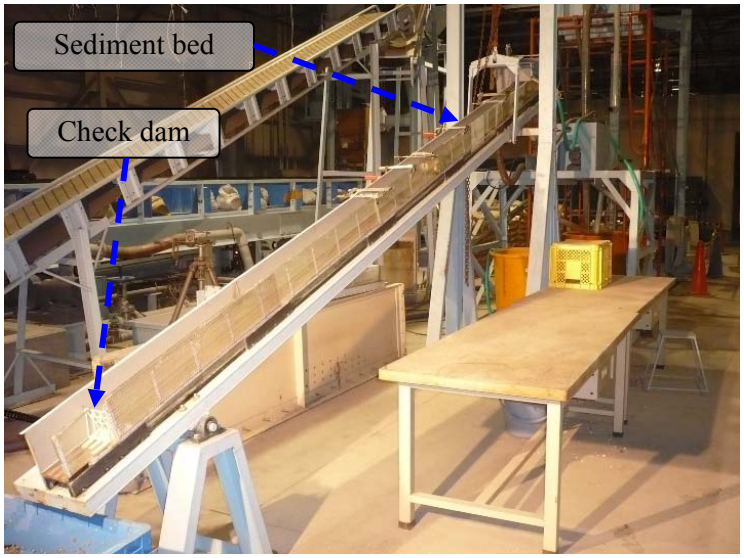

Figure 2.11 Photo of the flume in Ujigawa Open Laboratory, Kyoto University, Japan

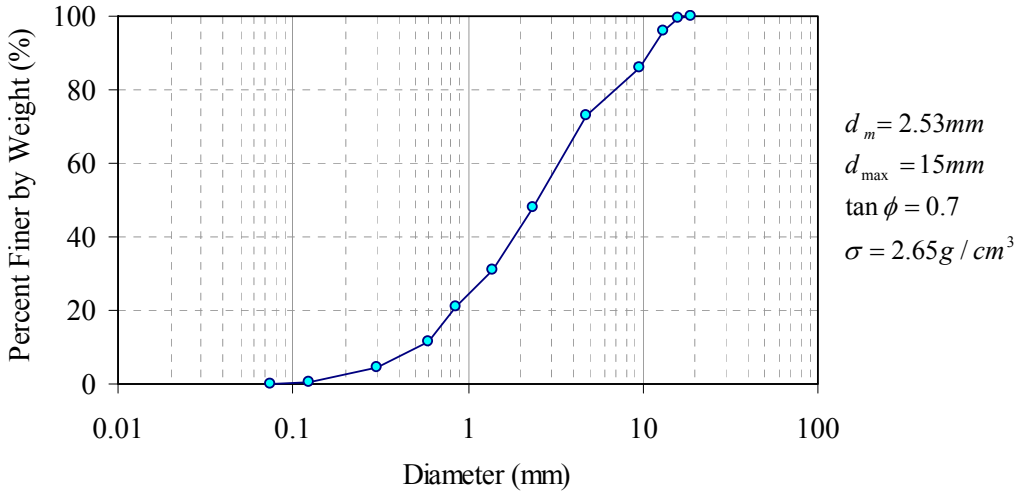

Figure 2.12 Particle size distribution of the sediment bed

where L_g is clear spacing between columns of grid dam.

Debris flow was generated by supplying a constant water discharge 260cm^3/sec for 10sec from the upstream end of the flume. Debris flow produced in the experiments was the fully stony type debris flow and the largest particles were accumulated in the forefront of debris flow. The details of the experimental conditions are shown in Table 2.1. Because the sediment composition and degree of saturation might not be uniform throughout the sediment layer, the

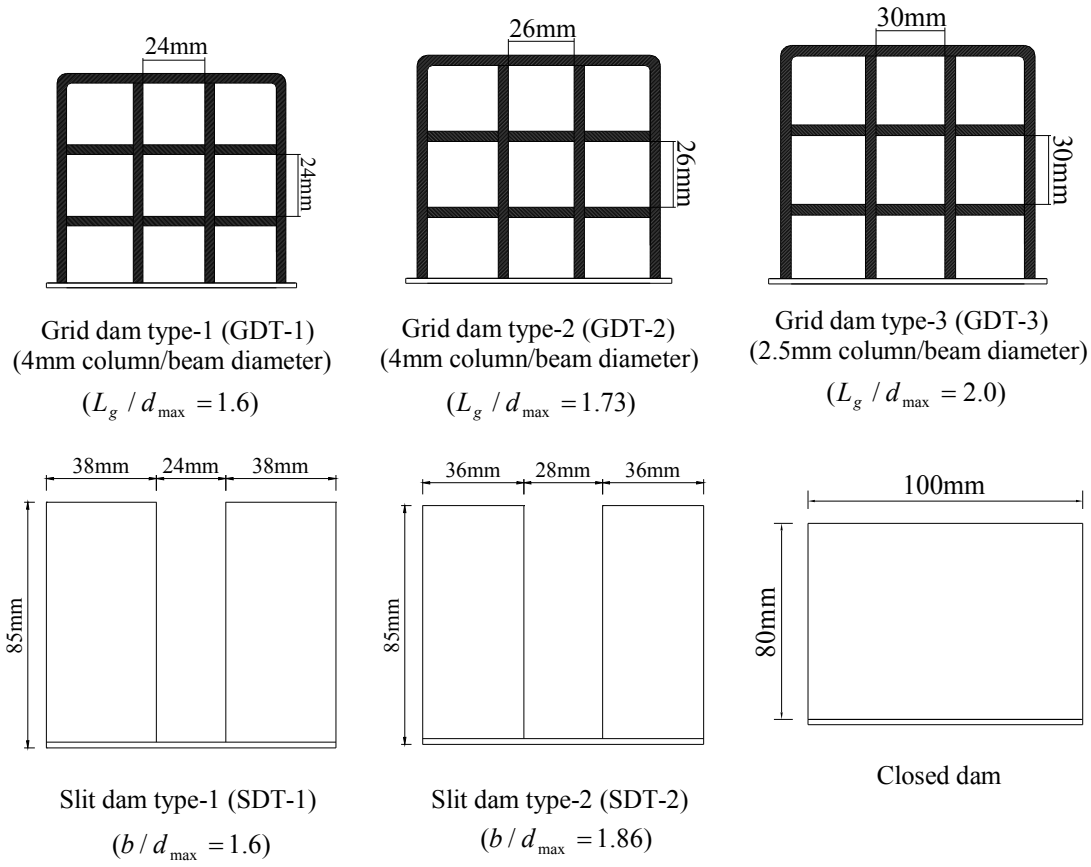

Figure 2.13 Details of check dams

Table 2.1 Conditions of the experiments for deposition upstream of check dams

S. No.	Exp. Ref.	Supply water discharge (cm^3/sec)	Flume slope θ (deg)	Check dam type	Remarks
1	Exp1	260	18	Without dam	
2	Exp3	260	18	Closed dam	
3	Exp15	260	18	Grid dam type-1	GDT-1
4	Exp6	260	18	Grid dam type -2	GDT-2
5	Exp16	260	18	Grid dam type -3	GDT-3
6	Exp7	260	18	Slit dam type -1	SDT-1
7	Exp8	260	18	Slit dam type -2	SDT-2
8	Exp9	260	20	Without dam	
9	Exp11	260	20	Closed dam	
10	Exp12	260	20	Grid dam type-1	GDT-1
11	Exp17	260	20	Grid dam type -2	GDT-2
12	Exp18	260	20	Grid dam type -3	GDT-3
13	Exp13	260	20	Slit dam type -1	SDT-1

experiments were repeated three times under the same identical conditions. Debris flow deposition patterns upstream of check dams were captured by two standard video cameras located at side and above the flume end. The outflow discharge at downstream end of the flume was also collected using manually movable sampler boxes. Total flow discharge and sediment discharge were calculated on the basis of the residence time of each box under the flume mouth which was determined by analyzing the images shot by a video camera located above the flume end and using following relations.

$$W_T = W_s + W_w = \sigma V_s + \rho V_w \tag{2.82}$$

$$V_T = V_s + V_w \tag{2.83}$$

$$C = \frac{V_s}{V_T} \tag{2.84}$$

where W_T is the total weight of collected discharge in each sampler box, W_s is the weight of the sediment, W_w is the weight of the water, V_T is the total volume of collected discharge in each sampler box, V_s is the volume of the sediment and V_w is the volume of the water.

2.5.2 Experiments of erosion of deposited sediment

Debris flow was deposited at upstream of a check dam in the flume of 5m long, 10cm wide and 13cm deep at 18 degrees of slope. Check dams were set at 20cm upstream from the downstream end of the flume. The debris flow was generated with the same conditions and properties of sediment bed and supplying inflow discharge as of experiment for debris flow deposition (section 2.5.1). Then, after removing the remain sediment in the initial laid sediment bed and installed partition to retain the sediment, a prescribed rate of water flow was supplied via the upstream end of the flume onto the deposited sediment upstream of a check dam to erode it freely with following two cases, with removing and without removing some large boulders from the upstream of the check dam. In CASE-I: clear water discharge at a rate of 260cm^3/sec was supplied for 15sec after removing some large boulders deposited upstream of the check dam. In CASE-II: clear water discharge at a rate of 260cm^3/sec was supplied for 15sec without removing any large boulders deposited from the upstream of the check dam, the deposited sediment could not be effectively transported to the downstream, after that some deposited large boulders were removed, then again clear water discharge at a rate of 260cm^3/sec was supplied for 15sec to check the flushing out of deposited sediment. The erosion process of deposited sediment was analyzed from the images shot by video cameras.

2.6 Results and discussions

The numerical simulations and experiments were performed to investigate the debris flow deposition and erosion processes upstream of the check dams with different hydraulic conditions. The parameters of the numerical simulation are as follows; the grid size Δx =5cm, the time interval $\Delta t = 0.001$sec, $\rho = 1.0$g/cm^3 for water, $\rho_m = 1.15$g/cm^3 for interstitial muddy fluid, $g =$ 980cm/sec^2, $\delta_e =$ 0.0007, $\delta_d =$ 0.01, $C_* =$ 0.65, $C_3 =$ 0.48, n =0.04, $e =$ 0.85, $K_{dep} = 1.0$, $\xi_8 = 1.4954$, $\xi_9 =$ -0.4350, $\xi_{10} = 0.7431$, $\xi_{11} =$ -0.0804, $K_{sd} = 0.6$ and $K =$ 0.1. The outflow condition of the downstream end of the flume was used the drop flow equation $M = h\sqrt{2gh}$.

2.6.1 Debris flow deposition upstream of check dams

To simulate the debris flow deposition upstream of check dams, a proposed deposition model upstream of check dams and conditions of check dams for each type of check dam described in section 2.2.3 were incorporated in a flow model of the debris flow. The numerical simulations were carried out to investigate the debris flow deposition process upstream of a check dam. The outflow discharge and sediment concentration at the downstream end of the flume without check dam for flume slope 18 degrees using the constitutive equations of Takahashi et al. (1997) and Egashira et al. (1997) are shown in Figure 2.14 and Figure 2.15, respectively.

Figure 2.16 shows the simulated results using proposed deposition velocity model of upstream of a check dam and the constitutive equations of Takahashi et al. (1997), and experimental results of debris flow deposition upstream of check dams such as closed type, grid type and slit type check dams for flume slope 18 degrees. The calculated results of the debris flow deposition upstream of a check dam using the constitutive equations of Egashira et al. (1997) are shown in Figure 2.17. From the both figures, the simulated results of deposition depth upstream of a check dam are quite consistent with the experimental results at the front and near the check dam parts. However, some discrepancies can be found in the shape of deposition between the simulated and experimental results at the most upstream part of the deposition, which may be due to the effect of the air entrapped in the fluid, which results from churning up the flow, when a debris flow from the upstream collides with the check dam or the deposited surface, and high turbulence is generated at upstream end of the deposition in the experiments.

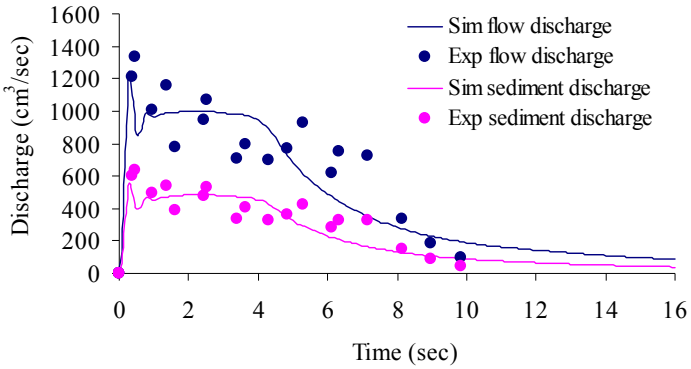

(a)

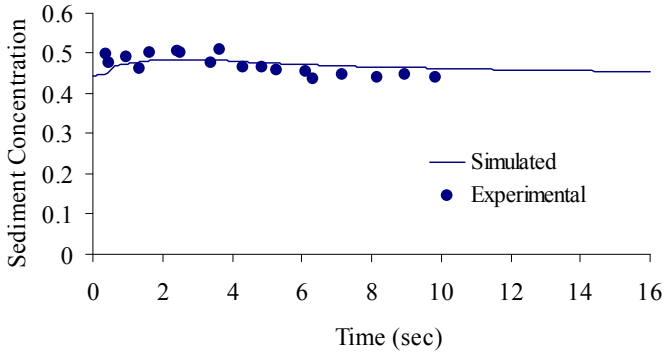

(b)

Figure 2.14 (a) Flow and sediment discharge, (b) sediment concentration at downstream end, without check dam, $\theta = 18^o$, using constitutive equations of Takahashi et al.

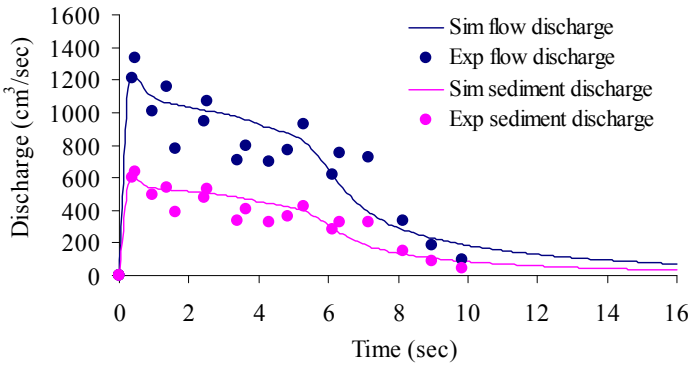

(a)

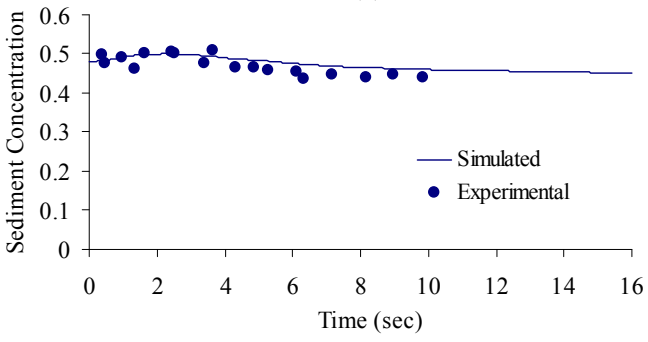

(b)

Figure 2.15 (a) Flow and sediment discharge, (b) sediment concentration at downstream end, without check dam, $\theta = 18^o$, using constitutive equations of Egashira et al.

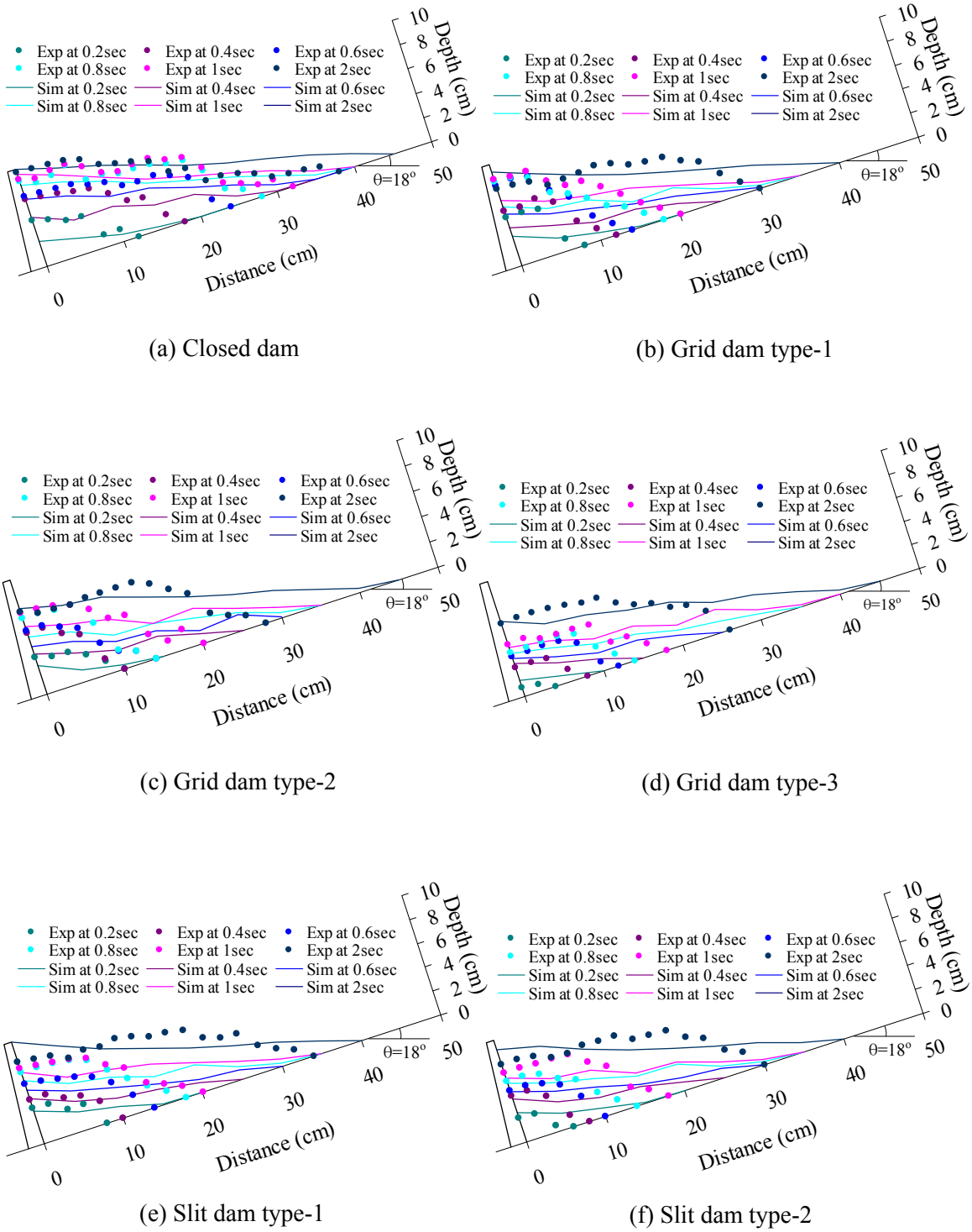

(a) Closed dam

(b) Grid dam type-1

(c) Grid dam type-2

(d) Grid dam type-3

(e) Slit dam type-1

(f) Slit dam type-2

Figure 2.16 Debris flow deposition upstream of check dams (using proposed deposition velocity model of upstream of check dam and the constitutive equations of Takahashi et al.), flume slope $\theta = 18^o$

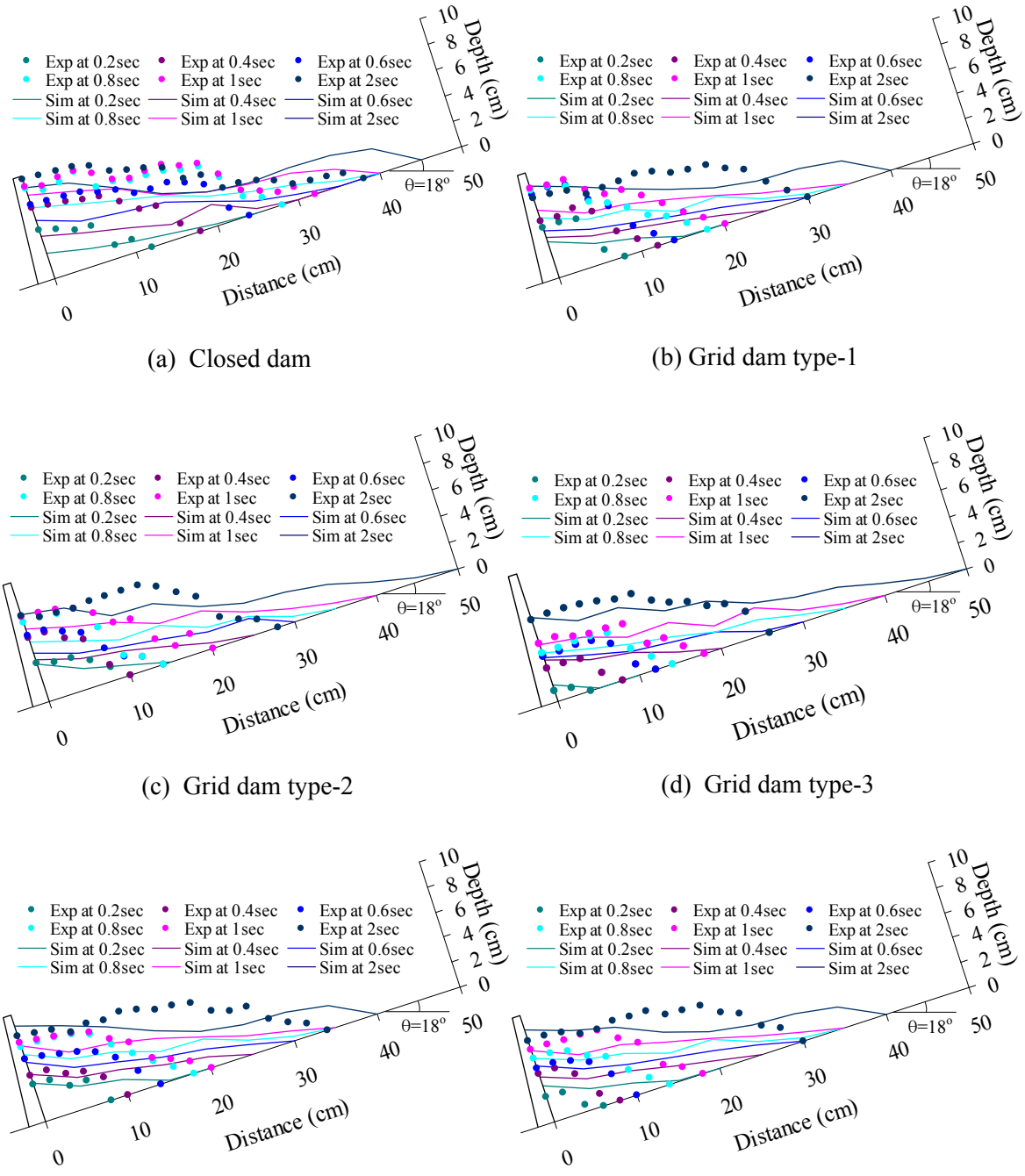

Figure 2.17 Debris flow deposition upstream of check dams (using proposed deposition velocity model of upstream of check dam and the constitutive equations of Egashira et al.), flume slope $\theta = 18^o$

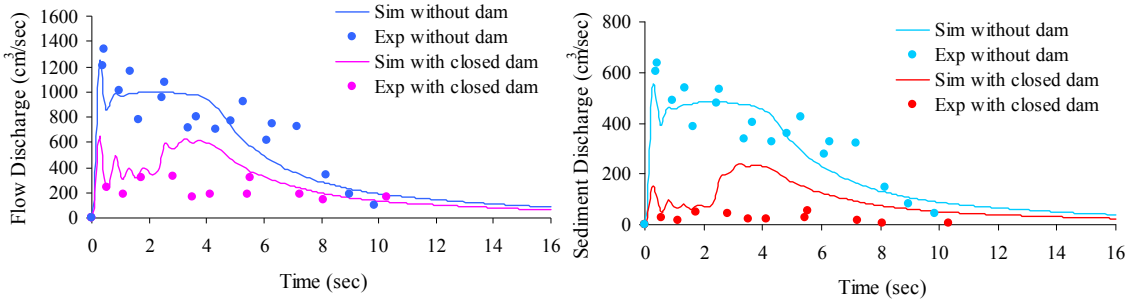

Closed dam

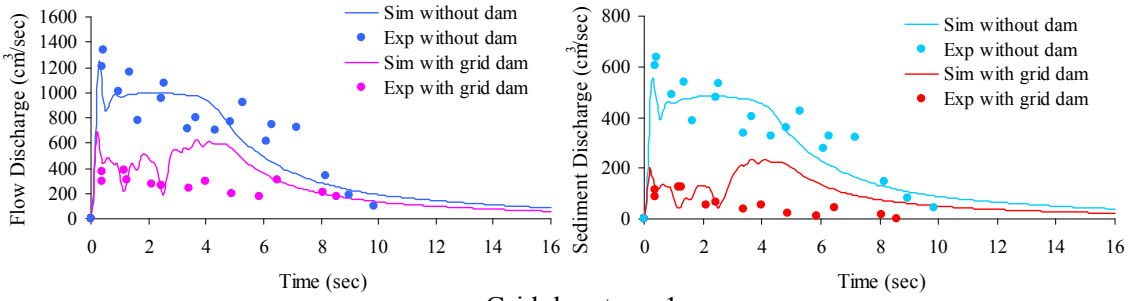

Grid dam type-1

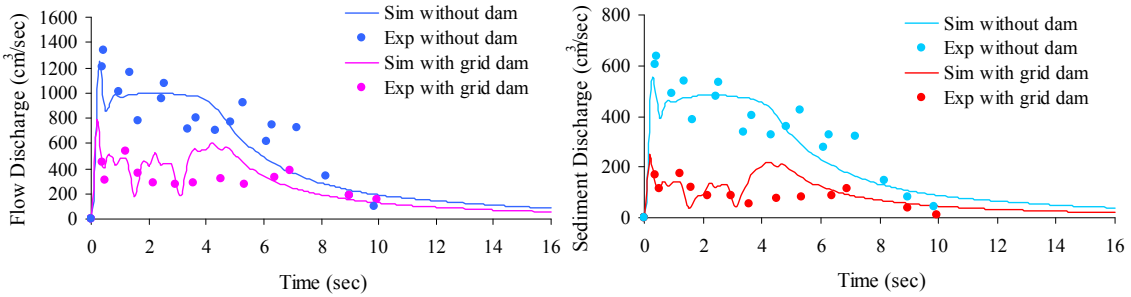

Grid dam type-2

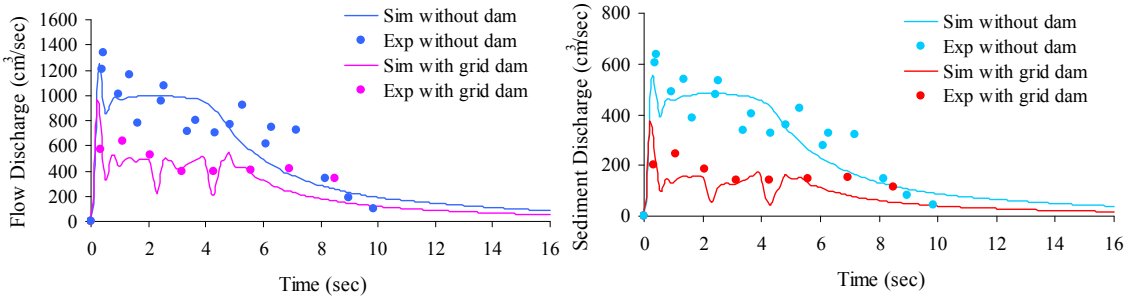

Grid dam type-3

Figure 2.18 Reduction of flow and sediment discharge at downstream end of the flume, (using proposed deposition velocity model of upstream of check dam and the constitutive equations of Takahashi et al.), flume slope $\theta = 18^{o}$

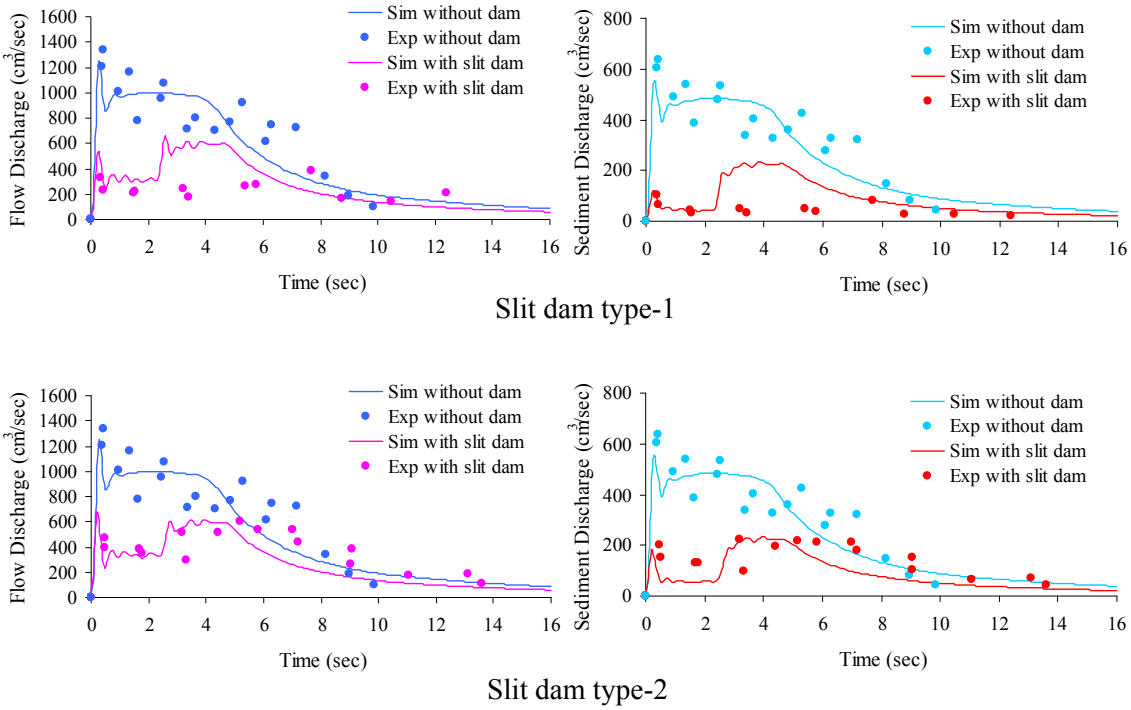

Figure 2.19 Reduction of flow and sediment discharge at downstream end of the flume, (using proposed deposition velocity model of upstream of check dam and the constitutive equations of Takahashi et al.), flume slope $\theta = 18^o$, slit dam case

The experiments were carried out in the fixed bed condition, in which the debris flow jumps due to the collision with a check dam or the deposited surface and flows on it. The deposited sediment in the most upstream area of the deposition is eroded by the coming debris flow from the upstream and the many sediments discharge downstream, which affects in the experimental results on depth of sediment deposition in the most upstream area.

The debris flow deposition phenomenon upstream of a closed or an open type check dam could be calculated by the proposed deposition velocity model and both the constitutive equations. Some variations are found in the simulated results with the comparison between Figure 2.16 and Figure 2.17, which may be due to the effect of the static pressures. The static pressures in Equation (2.16) (Takahashi et al., 1997) are influential when sediment concentration is higher than the limitative sediment concentration C_3, while in Equation (2.33) (Egashira et al., 1997) they are predominant even for lower sediment concentrations. However in both the constitutive equations, the static pressures are increased as sediment concentration increases.

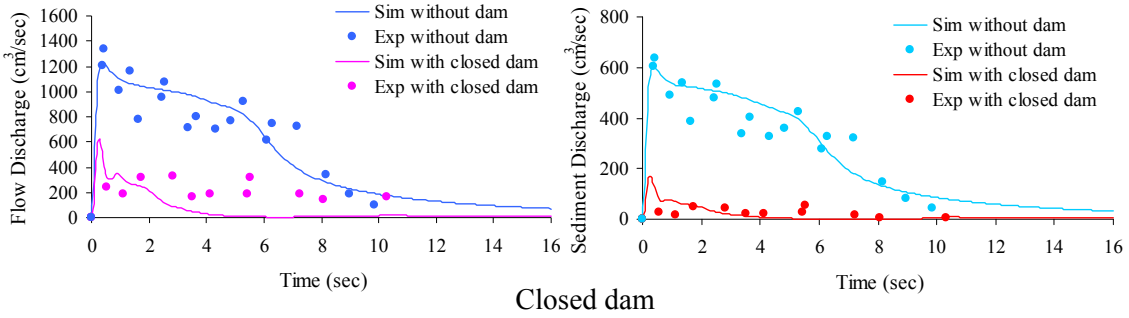

Closed dam

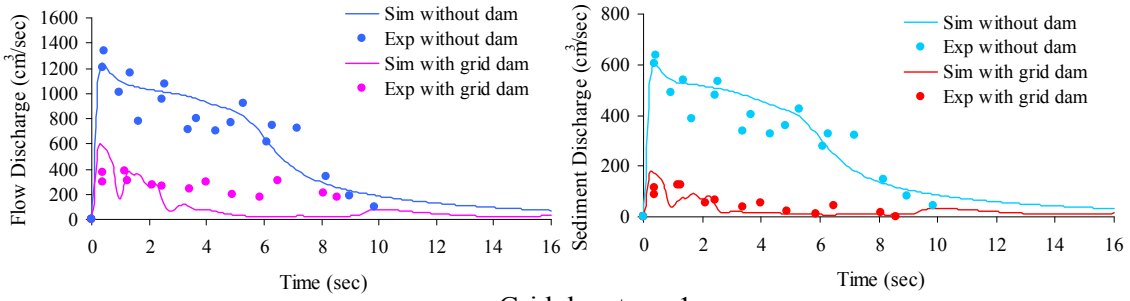

Grid dam type-1

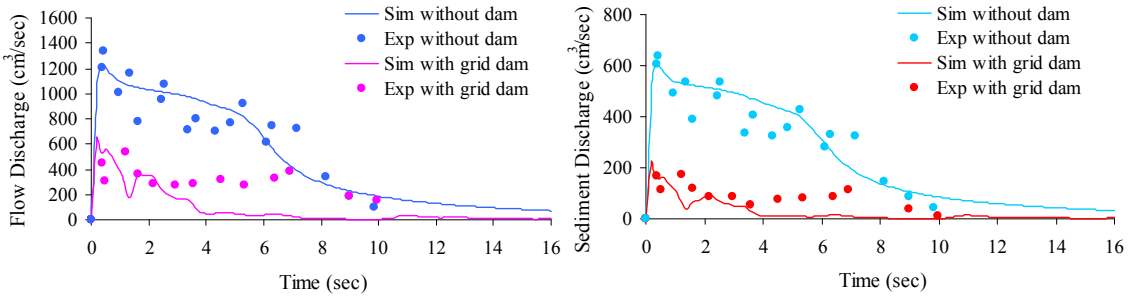

Grid dam type-2

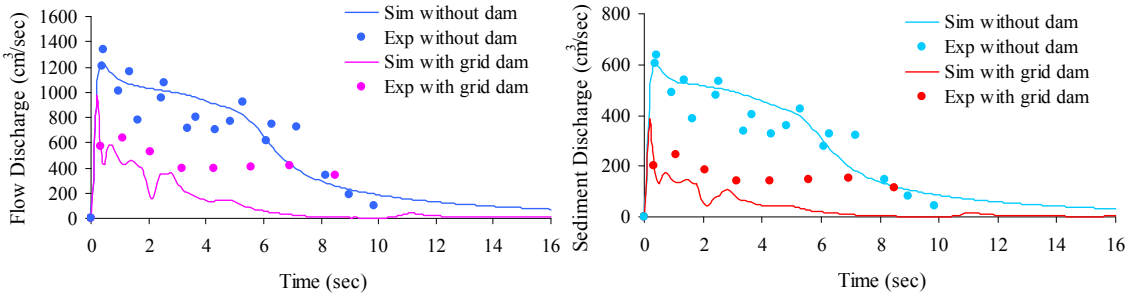

Grid dam type-3

Figure 2.20 Reduction of flow and sediment discharge at downstream end of the flume, (using proposed deposition velocity model of upstream of check dam and the constitutive equations of Egashira et al.), flume slope $\theta = 18^{o}$

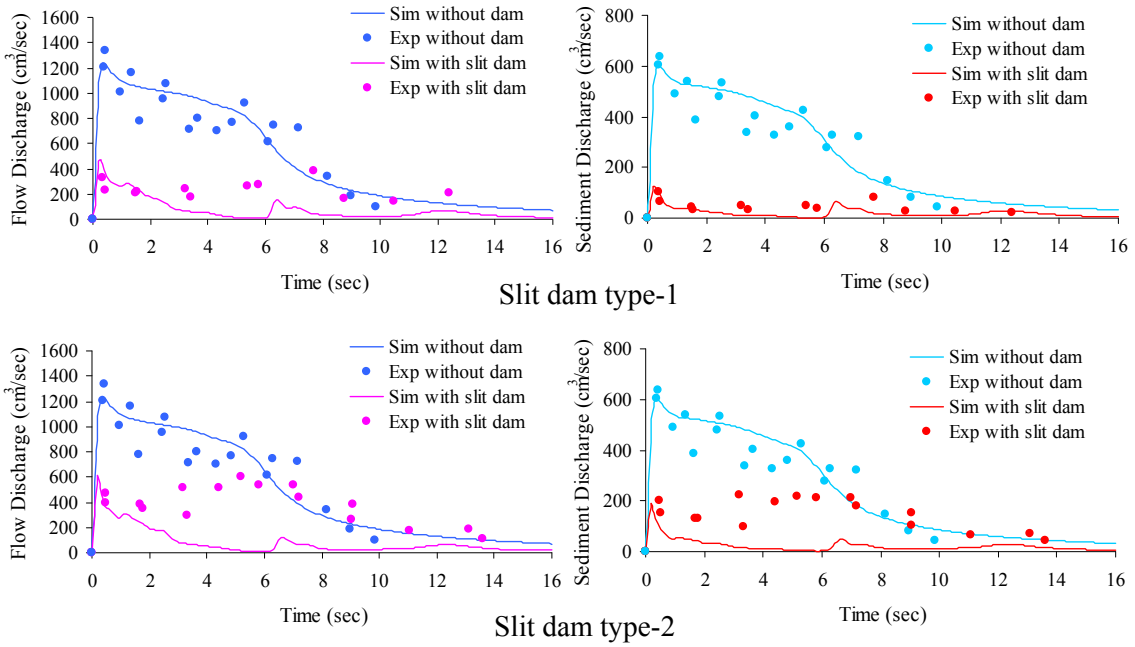

Figure 2.21 Reduction of flow and sediment discharge at downstream end of the flume, (using proposed deposition velocity model of upstream of check dam and the constitutive equations of Egashira et al.), flume slope $\theta = 18^{o}$, slit dam case

The simulated results of outflow discharge and sediment discharge at the downstream end of the flume with check dams using the constitutive equations of Takahashi et al. (1997) are shown in Figures 2.18 and 2.19 for flume slope 18 degrees. The results of flow discharge and sediment discharge using the constitutive equations of Egashira et al. (1997) are shown in Figures 2.20 and 2.21. The simulated results of outflow discharge are also agreeable with the experimental results. The results of outflow discharge and sediment concentration at the downstream end of the flume without check dam for the flume slope 20 degrees using the constitutive equations of Takahashi et al. (1997) and Egashira et al. (1997) are shown in Figure 2.22 and Figure 2.23, respectively. The results of debris flow deposition upstream of check dams using the constitutive equations of Takahashi et al. (1997) and Egashira et al. (1997) are shown in Figure 2.24 and Figure 2.25, respectively for flume slope 20 degrees. Figures 2.26 and 2.27 show the calculated results of reduction of flow and sediment discharge using the constitutive equations of Takahashi et al. (1997) and Egashira et al. (1997), respectively for flume slope 20 degrees. The simulated results of debris flow deposition upstream of check dams, outflow discharge and sediment discharge using both the constitutive equations agree with the experimental results. Figure 2.28 shows the photographs of final depth of debris flow deposition upstream of check dams and clogging of open spaces of open type check dams by boulders in the experiments.

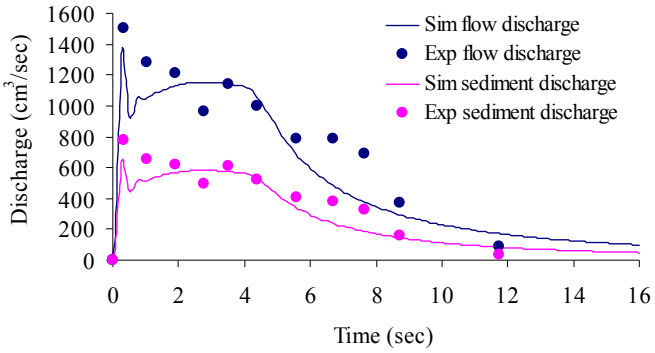

(a)

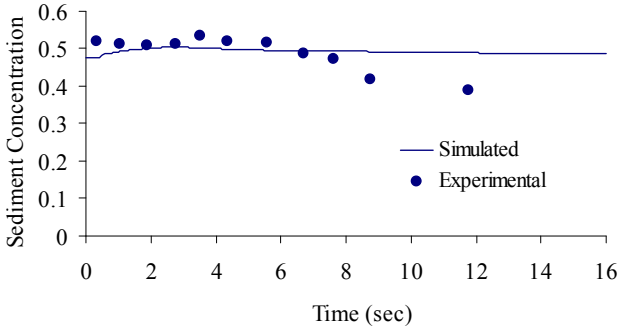

(b)

Figure 2.22 (a) Flow and sediment discharge, (b) sediment concentration at downstream end, without check dam, $\theta = 20^o$, using constitutive equations of Takahashi et al.

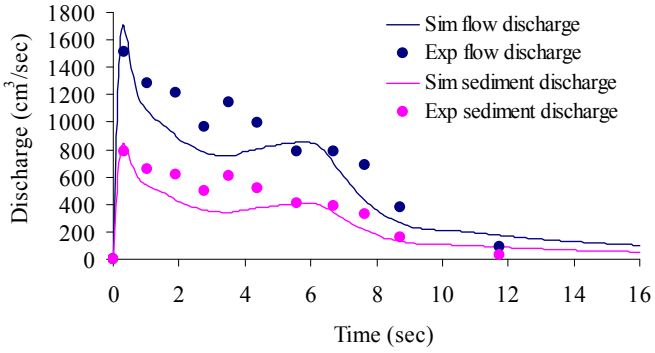

(a)

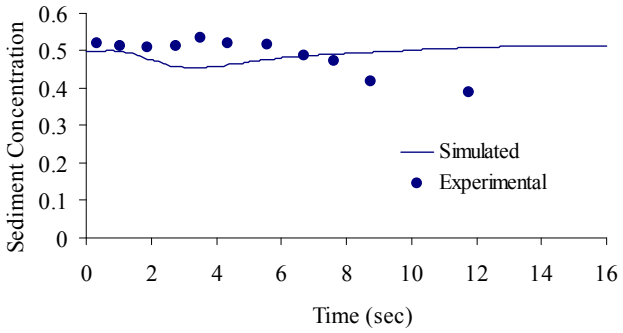

(b)

Figure 2.23 (a) Flow and sediment discharge, (b) sediment concentration at downstream end, without check dam, $\theta = 20^o$, using constitutive equations of Egashira et al.

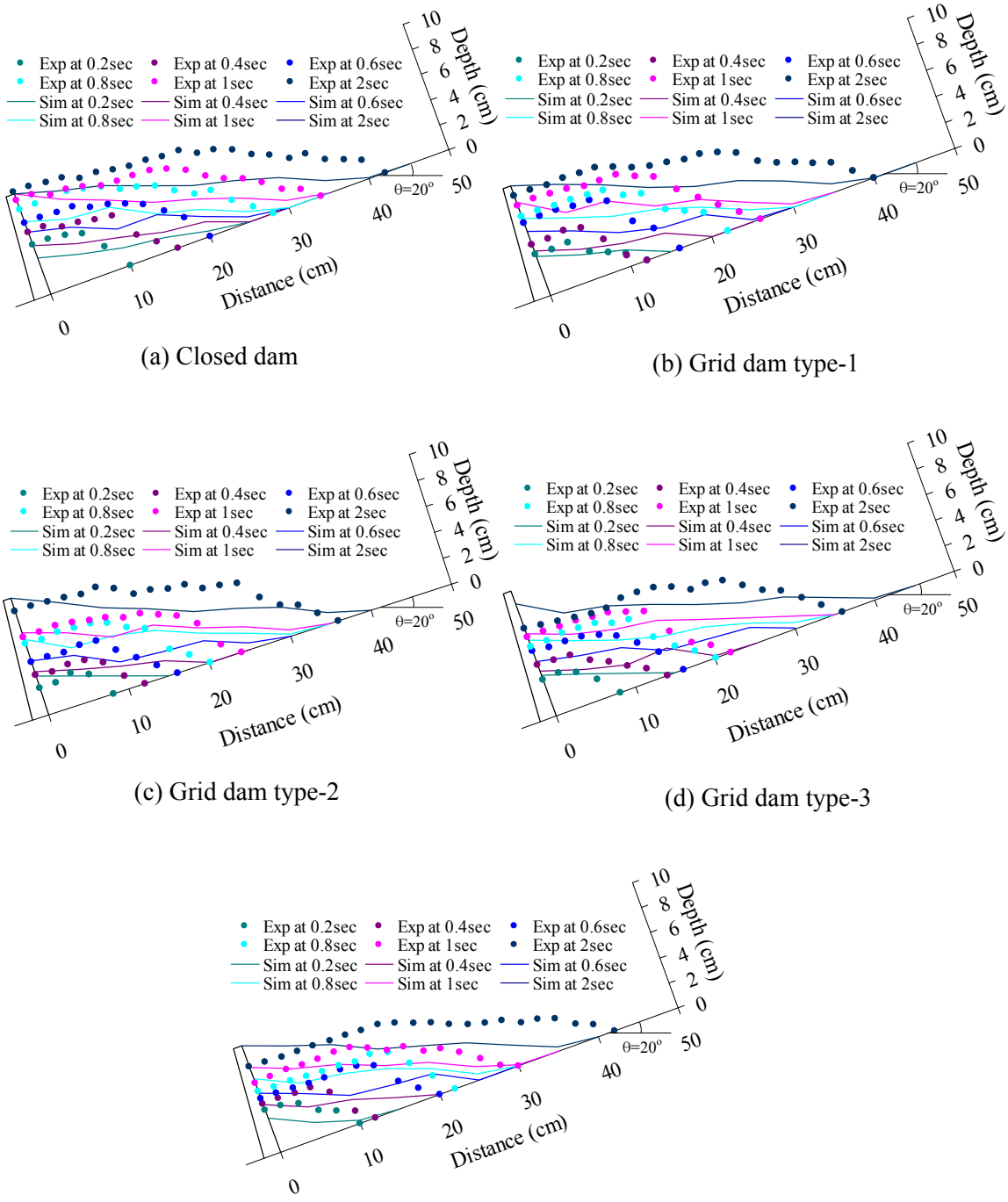

(a) Closed dam

(b) Grid dam type-1

(c) Grid dam type-2

(d) Grid dam type-3

(e) Slit dam type-1

Figure 2.24 Debris flow deposition upstream of check dams (using proposed deposition velocity model of upstream of check dam and the constitutive equations of Takahashi et al.), flume slope $\theta = 20^o$

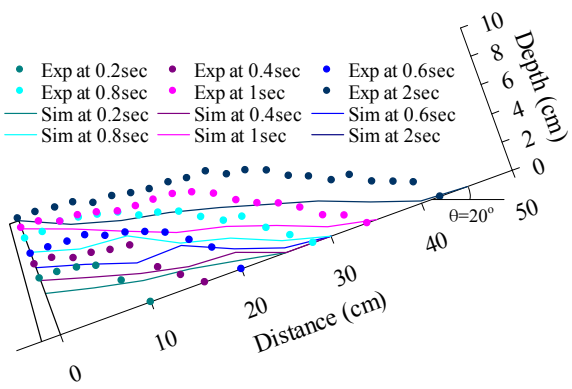

(a) Closed dam

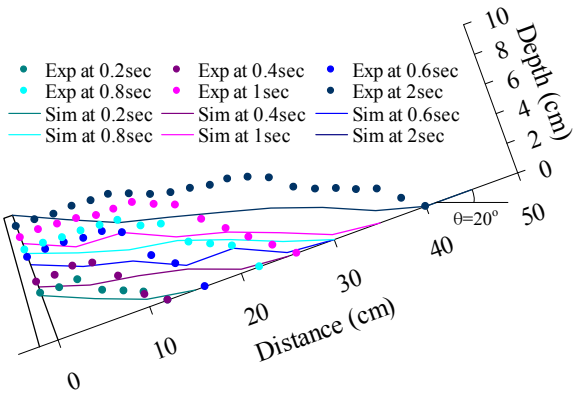

(b) Grid dam type-1

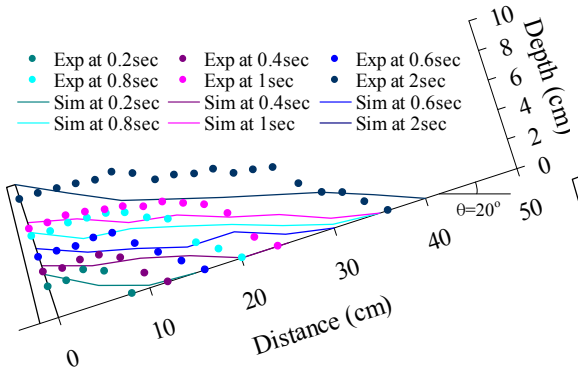

(c) Grid dam type-2

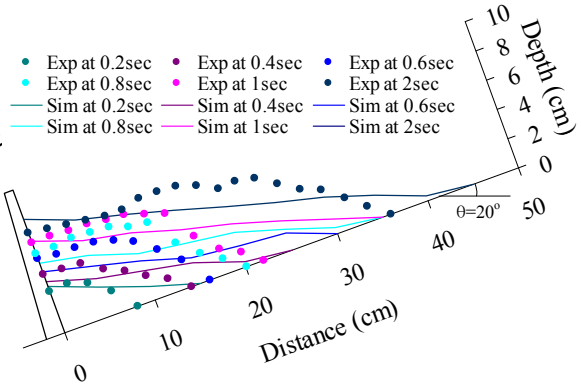

(d) Grid dam type-3

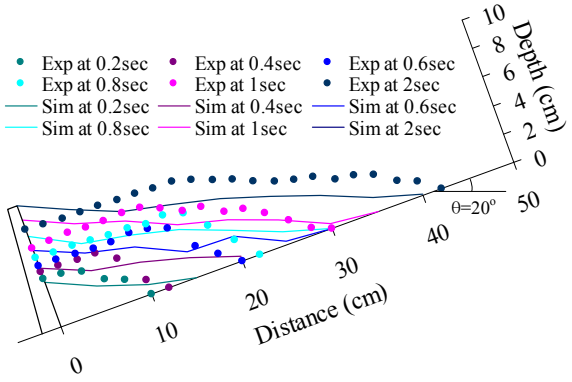

(e) Slit dam type-1

Figure 2.25 Debris flow deposition upstream of check dams (using proposed deposition velocity model of upstream of check dam and the constitutive equations of Egashira et al.), flume slope $\theta = 20^o$

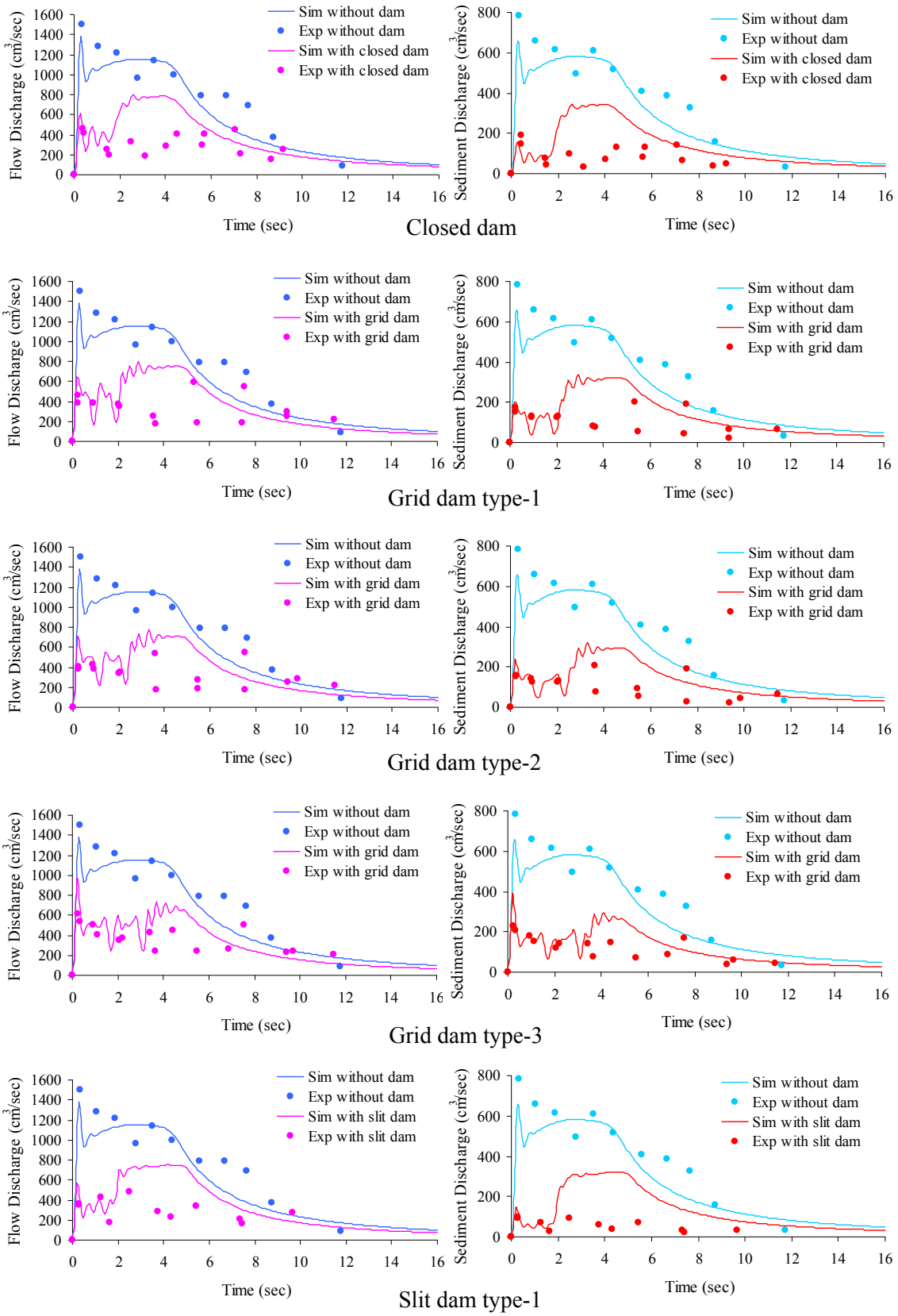

Figure 2.26 Discharge at downstream end of the flume (using deposition velocity model of upstream of check dam and the constitutive equations of Takahashi et al.), $\theta = 20^o$

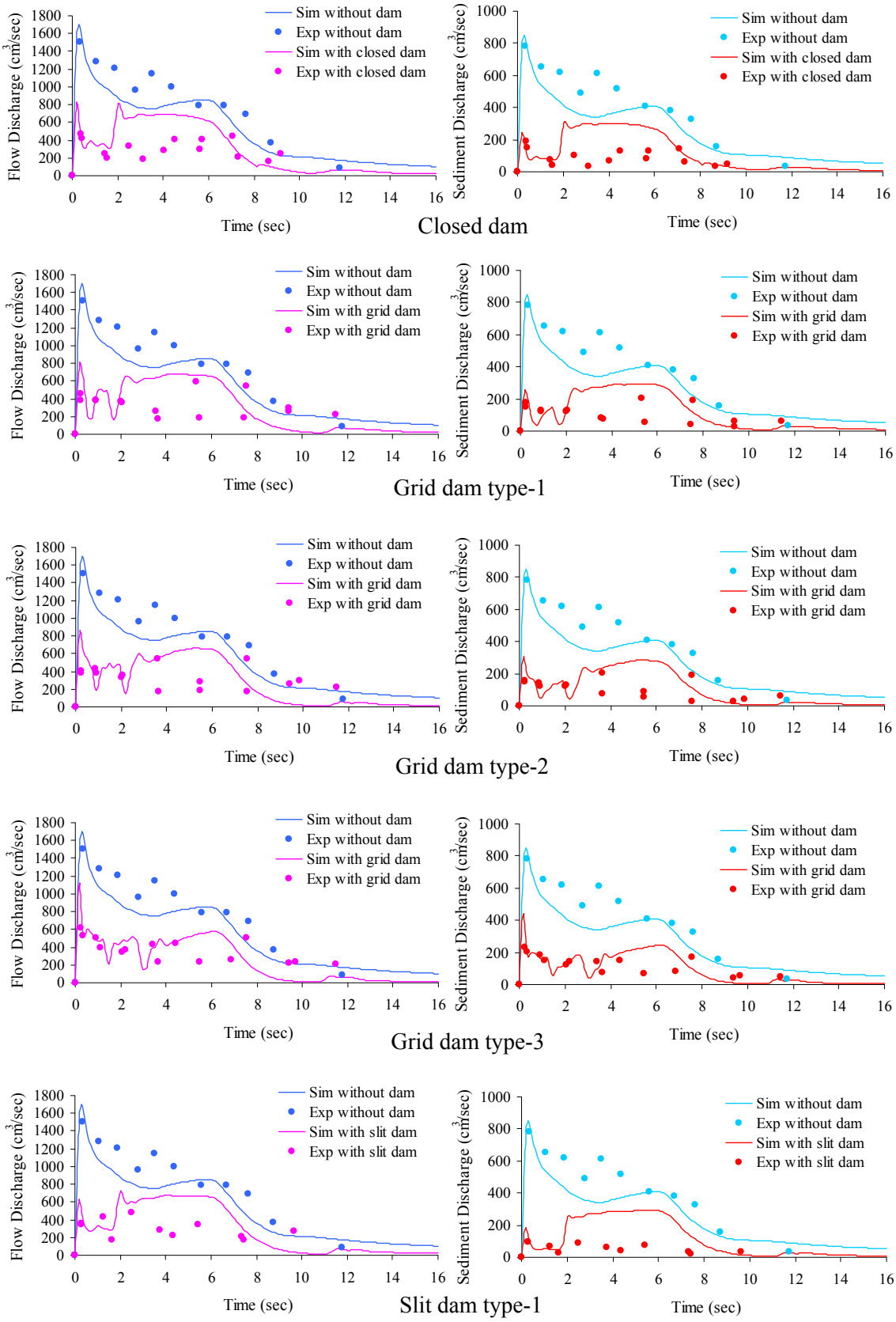

Figure 2.27 Discharge at downstream end of the flume (using deposition velocity model of upstream of check dam and the constitutive equations of Egashira et al.), $\theta = 20^o$

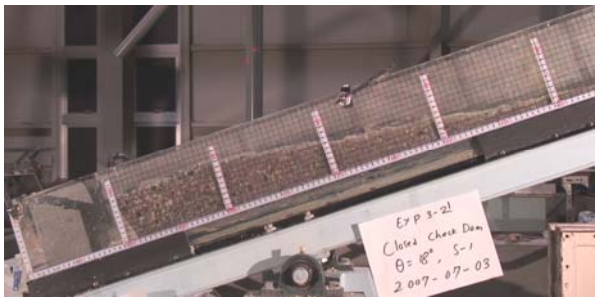

(a) Final debris flow deposition upstream of closed dam

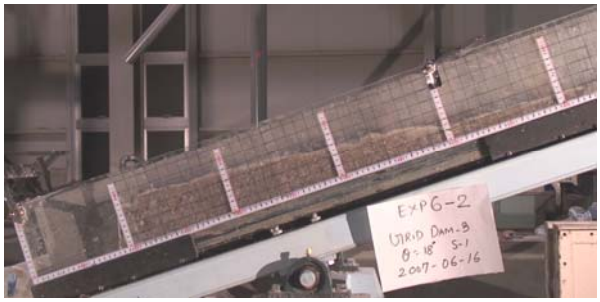

(b) Final debris flow deposition upstream of grid dam

(c) Final debris flow deposition upstream of slit dam

(d) Clogging of open spaces of grid or slit type check dam by boulders

Figure 2.28 Photographs of debris flow deposition upstream of check dams and clogging of open spaces of open type check dams by boulders in the experiments

2.6.2 Erosion of deposited sediment

CASE-I

The water discharge was supplied after removing the blockaded and deposited large boulders from the upstream of the check dams to investigate the erosion of deposited sediment upstream of the check dams. Figure 2.29 shows the experimental results of the time variation in shape of deposited sediment upstream of the check dams due to erosion process after supplying the normal flow discharge. In which, dashed line indicates initially deposited depth of sediment and continuous line indicates depth of deposition after the erosion. The sediment deposited upstream of a grid dam is flushed out more effectively than the closed dam. The used basic governing equations are described in section 2.2.1. The erosion process of deposited sediment upstream of grid dams was investigated using a one-dimensional riverbed erosion model and comparison between experimental and simulated results are shown in Figure 2.30 for Grid Dam Type (GDT)-1, GDT-2 and GDT-3. Deposited sediment upstream of grid dams is effectively transported to the downstream due to the erosion process by a normal flow discharge. Thus, the grid type check dams will have debris flow storage capacity to control the next debris flow event. In the numerical simulation, measured mean diameter 3.21mm of deposited sediment was used.

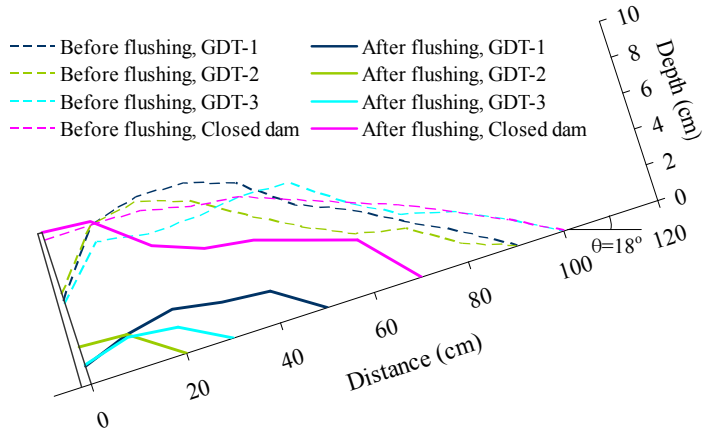

Figure 2.29 Experimental results of flushing out of deposited sediment due to erosion and variations in depth, CASE-I

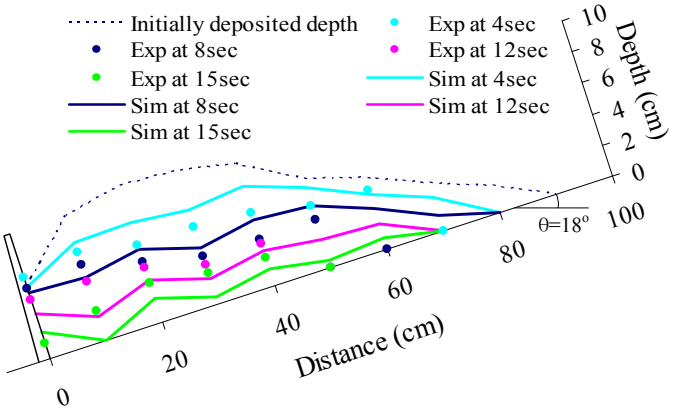

Grid dam type-1 (GDT-1)

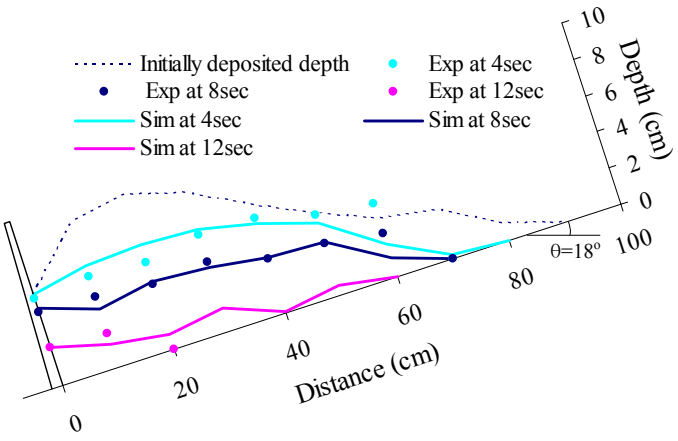

Grid dam type-2 (GDT-2)

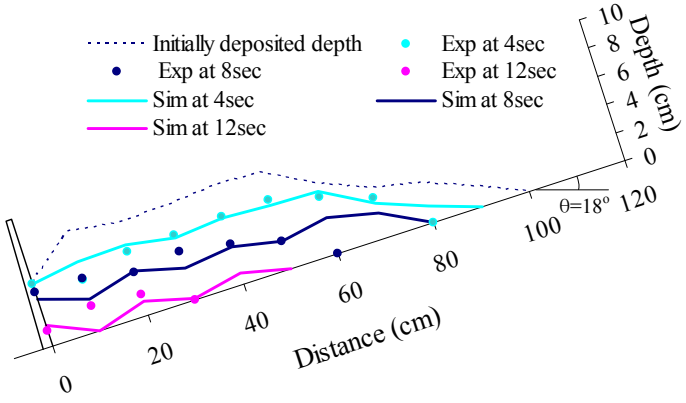

Grid dam type-3 (GDT-3)

Figure 2.30 Simulated and experimental bed variations of deposited sediment upstream of grid dams due to erosion, CASE-I

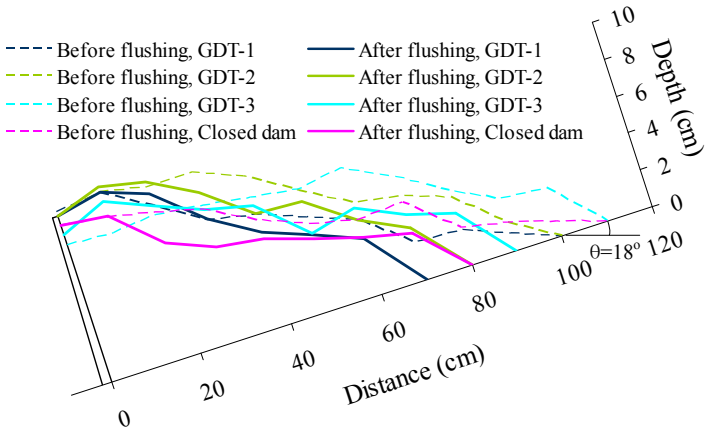

Figure 2.31 Experimental results of flushing out of deposited sediment before removing large boulders, CASE-II

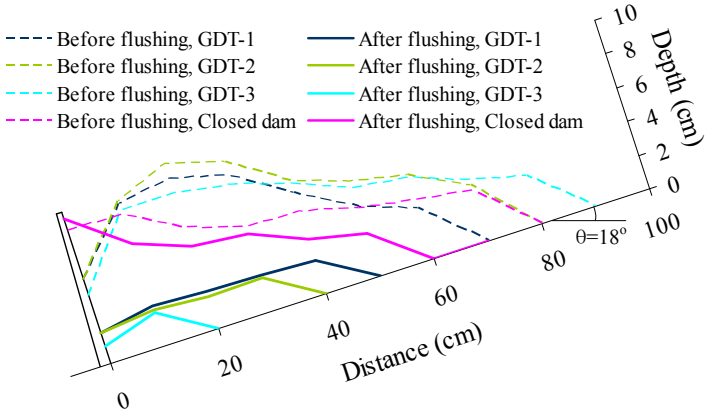

Figure 2.32 Experimental results of flushing out of deposited sediment after removing large boulders, CASE-II

CASE-II

In this case, firstly clear water discharge was supplied without removing any blockaded and deposited large boulders from the upstream of check dams, and Figure 2.31 shows the experimental results of erosion of deposited sediment, in which deposited sediment may not be effectively transported to the downstream. After that some blockaded and deposited large boulders from upstream of check dams were removed, then again clear water discharge was supplied, and Figure 2.32 shows the experimental results of erosion of deposited sediment by

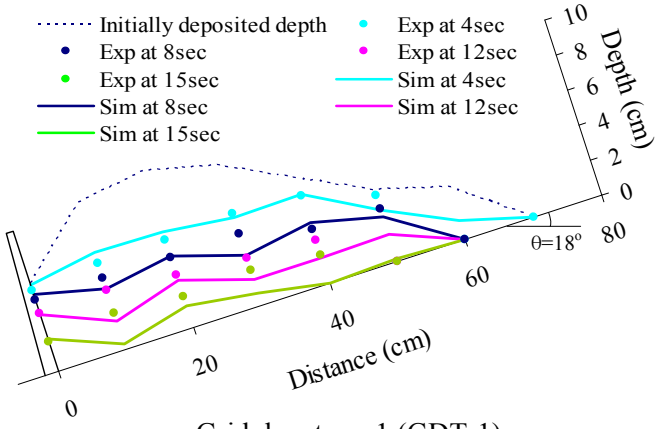

Grid dam type-1 (GDT-1)

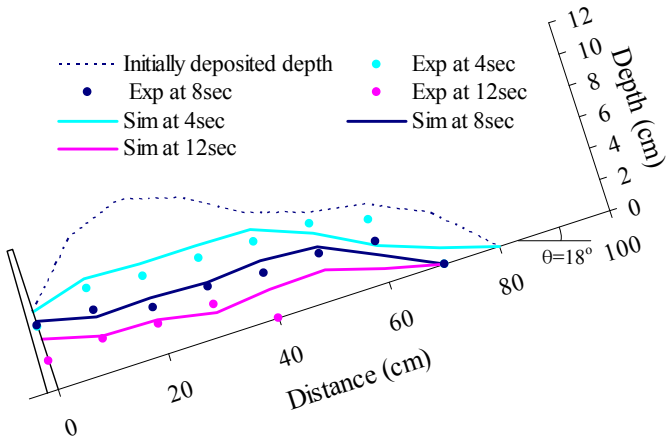

Grid dam type-2 (GDT-2)

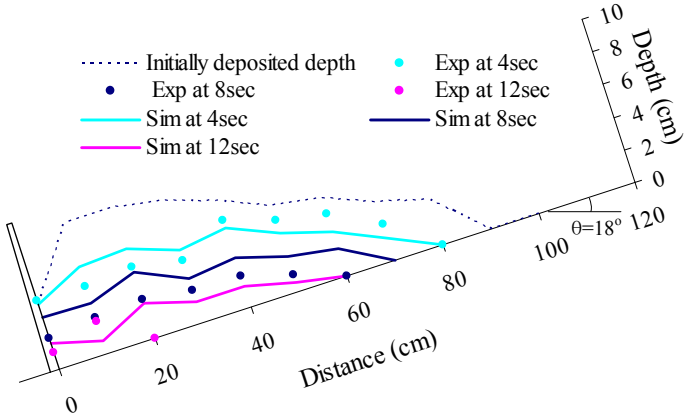

Grid dam type-3 (GDT-3)

Figure 2.33 Simulated and experimental bed variations of deposited sediment upstream of grid dams due to erosion, CASE-II

supplying flushing discharge after removing some large boulders, where dashed line indicates the deposition shape after removing boulders at the end of the first water supply. The deposited sediment could not be flushed out effectively due to erosion by water supplying before removing large boulders. Figure 2.33 shows the comparison of the simulated and experimental results of bed variations of deposited sediment upstream of GDT-1, GDT-2 and GDT-3 at different time steps due to erosion process after removing some large boulders from upstream of the grid dam.

In all three types of grid dam, deposited sediment upstream of grid dam could be effectively transported to the downstream due to the erosion process by normal flow discharge, when some large boulders blockaded in open spaces of grid and deposited upstream of the grid dam are removed. The simulated results of erosion process of deposited sediment upstream of the grid dam are in good agreement with the experimental results.

Summary

A numerical model was developed to investigate the phenomenon of debris flow deposition upstream of check dams. The proposed model was tested for different experimental conditions using various types of check dams. A new deposition velocity equation to calculate the debris flow deposition upstream of a check dam was also presented. The simulated results of debris flow deposition upstream of check dam and the reduction of outflow discharge at the downstream end of the flume are in good agreement with the experimental results.

The erosion process of deposited sediment upstream of check dams were investigated numerically and experimentally. A riverbed erosion model under unsaturated bed condition was used to simulate the erosion process of deposited sediment upstream of check dams. The simulated results of erosion of deposited sediment upstream of check dams are agreeable with the experimental results.

Chapter 3

Debris Flow with Driftwood Model

3.1 Introduction

In mountainous areas of many countries, debris flow flows with driftwood, due to heavy downpours over mountainous rivers. The driftwood means standing trees, fallen trees, felled trees, etc. that may flow out when a hillside collapse, a riverbank collapse, or a debris flow occurs and the resulting sediment flows out. When debris flow flows with driftwood, it is clear that the greatest damage has occurred, which results in destruction of bridge or culvert and sometimes resulting in considerable loss of lives and properties. Therefore, the countermeasures against debris flow disasters with driftwood are to be implemented in the basin areas where debris flow flows with driftwood for protecting human life and property.

Many researchers such as Takahashi et al. (1992), Honda and Egashira (1997), Brufau et al. (2000), Nakagawa et al. (2000), Satofuka and Mizuyama (2005), and others have proposed numerical models of debris flow as a mixture of sediment and water, but they have not considered the behavior of debris flow with driftwood. On the other hand, some numerical studies to compute the behavior of driftwood in the Lagrangian form only with clear water flow have been carried out by Nakagawa et al. (1994, 1995), Gotoh et al. (2002), Shimizu and Osada (2008), and others but they have not focused on computing the behavior of driftwood with debris flow or sediment water mixture flow.

To clarify the nature of debris flow disasters with driftwood, it is necessary to understand the characteristics of debris flow with driftwood. Takahashi et al. (1992), Nakagawa and Takahashi (1997), Hirano et al. (1997), Jan (1997), Wada et al. (2008) and others have developed two-dimensional (2D) debris flow models. However, they have not considered driftwood behavior and each model has its limit in application. Two-dimensional (2D) debris flow models are essential to compute the driftwood position in longitudinal and lateral directions and rotational angle of the driftwood. To also consider the flow discharge and change in riverbed in lateral direction, 2D debris model is very important.

A two-dimensional numerical model is presented for computing the behavior of debris flow with driftwood. Equations of the rotational motion and the translational motion of driftwood are evaluated dynamically in the Lagrangian form. A numerical model has been developed with an interacting combination of Eulerian expression of the debris flow and Lagrangian expression of the driftwood, in which the fluctuation components of the position and the rotational angular velocity of the driftwood are dealt with stochastically as random variables based on the results of a statistical analysis of experimental values. The motion of driftwood is restricted near the flow surface.

3.2 Numerical model of debris flow with driftwood

3.2.1 Basic equations of debris flow motion

The basic equations used to compute the behavior of flow motion of debris flow are the two-dimensional momentum equations, continuity equation of flow, continuity equation of sediment and river bed surface equation. The motion of driftwood is restricted near the flow surface and the shear stresses at the flow surface are generated as the reaction of the drag force acting on the driftwood. By introducing these shear stresses at the flow surface, the depth-wise averaged two-dimensional momentum equations of debris flow for the *x*–wise (down valley) and *y*-wise (lateral) directions are described as follows.

$$\frac{\partial M}{\partial t}+\beta\frac{\partial(uM)}{\partial x}+\beta\frac{\partial(vM)}{\partial y}=gh\sin\theta_{bx0}-gh\cos\theta_{bx0}\frac{\partial(z_b+h)}{\partial x}-\frac{\tau_{bx}}{\rho_T}+\frac{\tau_{sx}}{\rho_T} \tag{3.1}$$

$$\frac{\partial N}{\partial t}+\beta\frac{\partial(uN)}{\partial x}+\beta\frac{\partial(vN)}{\partial y}=gh\sin\theta_{by0}-gh\cos\theta_{by0}\frac{\partial(z_b+h)}{\partial y}-\frac{\tau_{by}}{\rho_T}+\frac{\tau_{sy}}{\rho_T} \tag{3.2}$$

The continuity equation of the total volume is

$$\frac{\partial h}{\partial t}+\frac{\partial M}{\partial x}+\frac{\partial N}{\partial y}=i_b \tag{3.3}$$

The continuity equation of the coarse particle fraction that is sustained in the flow by the action of particle encounters is

$$\frac{\partial(C_L h)}{\partial t}+\frac{\partial(C_L M)}{\partial x}+\frac{\partial(C_L N)}{\partial y}=\begin{cases} i_b C_{*L} & (i_b\geq 0)\\ i_b C_{*DL} & (i_b<0)\end{cases} \tag{3.4}$$

The continuity equation for fine particle fraction that is suspended in the interstitial fluid by the action of turbulence is

$$\frac{\partial\{(1-C_L)C_F h\}}{\partial t}+\frac{\partial\{(1-C_L)C_F M\}}{\partial x}+\frac{\partial\{(1-C_L)C_F N\}}{\partial y}=\begin{cases} i_b(1-C_{*L})C_{*F}\,; & (i_b \geq 0) \\ i_b(1-C_{*DL})C_F\,; & (i_b < 0) \end{cases} \tag{3.5}$$

where M (= uh) and N (= vh) are the flow discharge per unit width in x and y directions, u and v are the velocity components in x and y directions, θ_{bx0} and θ_{by0} are the x and y components of the slope of the original bed surface, τ_{bx} and τ_{by} are the bottom shear stresses in x and y directions, τ_{sx} and τ_{sy} are the shear stresses at the flow surface in x and y directions, C_L is the volumetric sediment concentration of the coarse fraction in the flow, C_F is the volumetric sediment concentration of the fine fraction in the interstitial fluid, C_{*L} and C_{*F} are the volumetric concentrations of the coarse and fine fractions in the original bed, and C_{*DL} is the volumetric concentration of the coarse fraction in the static bed produced by deposition of the debris flow. The erosion or deposition thickness to calculate the bed surface elevation is given by Equation (2.4).

Bottom shear stress equations

The bottom resistance for a two-dimensional flow is described as follows.

For a fully developed stony debris flow ($C_L > 0.4C_*$);

$$\tau_{bx}=\frac{u}{\sqrt{u^2+v^2}}\tau_{yx}+\rho f_b u\sqrt{u^2+v^2} \tag{3.6}$$

$$\tau_{by}=\frac{v}{\sqrt{u^2+v^2}}\tau_{yy}+\rho f_b v\sqrt{u^2+v^2} \tag{3.7}$$

in which τ_{yx} and τ_{yy} are the yield stresses in x and y directions, which can be expressed by using constitutive equations of Takahashi et al. (1997) as follows:

$$\tau_{yx}=f(C_L)(\sigma-\rho)C_L gh\cos\theta_x\tan\phi \tag{3.8}$$

$$\tau_{yy}=f(C_L)(\sigma-\rho)C_L gh\cos\theta_y\tan\phi \tag{3.9}$$

$$f(C_L)=\begin{cases}\dfrac{C_L-C_3}{C_*-C_3} & ;\quad C_L > C_3 \\ 0 & ;\quad C_L \leq C_3\end{cases} \tag{3.10}$$

where θ_x and θ_y are the x and y components of slope of the bed surface.

The coefficient of resistance, f_b, is described similar to Equation (2.27) as

$$f_b = \frac{1}{8}\frac{(\sigma/\rho)}{\left\{(C_*/C_L)^{1/3}-1\right\}^2}\left(\frac{d_m}{h}\right)^2 \tag{3.11}$$

For an immature debris flow ($0.02 \le C_L \le 0.4C_*$);

$$\tau_{bx} = \frac{\rho_T}{0.49}\left(\frac{d_m}{h}\right)^2 u\sqrt{u^2+v^2} \tag{3.12}$$

$$\tau_{by} = \frac{\rho_T}{0.49}\left(\frac{d_m}{h}\right)^2 v\sqrt{u^2+v^2} \tag{3.13}$$

For a turbulent flow ($C_L < 0.02$);

$$\tau_{bx} = \frac{\rho g n^2 u\sqrt{u^2+v^2}}{h^{1/3}} \tag{3.14}$$

$$\tau_{by} = \frac{\rho g n^2 v\sqrt{u^2+v^2}}{h^{1/3}} \tag{3.15}$$

Surface shear stress equations

The shear stresses at the flow surface in x and y directions generated as the reaction of the drag force acting on the driftwood are described as follows.

$$\tau_{sx} = \frac{1}{A}\sum_{k=1}^{N_t}\left\{\frac{1}{2}\rho_T C_{Dx} W_k (u_k - U_k) A_{kx}\right\} \tag{3.16}$$

$$\tau_{sy} = \frac{1}{A}\sum_{k=1}^{N_t}\left\{\frac{1}{2}\rho_T C_{Dy} W_k (v_k - V_k) A_{ky}\right\} \tag{3.17}$$

where u_k and v_k are the respective driftwood velocity components in x and y directions, U_k and V_k are the respective local velocity components of the fluid in x and y directions at the position of the centroid of the driftwood, $W_k = \sqrt{(u_k - U_k)^2 + (v_k - V_k)^2}$, A_{kx} and A_{ky} are the respective projected areas of the submerged part of the driftwood in x and y directions, C_{Dx} and C_{Dy} are the drag coefficients in x and y directions, A is the flow surface area which is

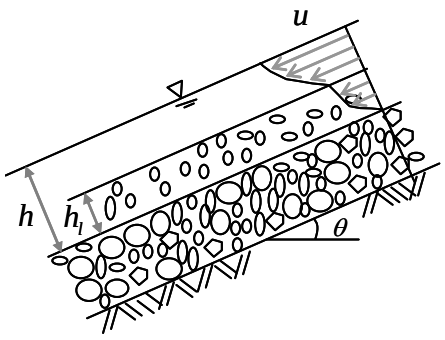

Figure 3.1 Schematic illustration of the immature debris flow

written as $A = \Delta x \Delta y$ (Δx and Δy are the grid sizes of the finite difference equations), and N_t is the number of total pieces of driftwood in area A.

Surface flow velocity equations

As the motion of the piece of driftwood is restricted near the flow surface, the surface flow velocity components u_s and v_s in x and y directions to compute the driftwood motion are described by integrating the velocity distribution functions given by Takahashi (1991) as follows.

For a fully developed stony debris flow;

$$u_s = \frac{2}{3d_m}\left[\frac{g\sin\theta_x}{a\sin\alpha}\left\{C_L + (1-C_L)\frac{\rho}{\sigma}\right\}\right]^{1/2}\left\{\left(\frac{C_*}{C_L}\right)^{1/3} - 1\right\}h^{3/2} \tag{3.18}$$

$$v_s = \frac{2}{3d_m}\left[\frac{g\sin\theta_y}{a\sin\alpha}\left\{C_L + (1-C_L)\frac{\rho}{\sigma}\right\}\right]^{1/2}\left\{\left(\frac{C_*}{C_L}\right)^{1/3} - 1\right\}h^{3/2} \tag{3.19}$$

For an immature debris flow;

$$\frac{u_s}{u_*} = \frac{u_l}{u_*} + \frac{2}{\kappa}\left\{-\left(1-\frac{h_l}{h}\right)^{1/2}\right\} - \frac{1}{\kappa}\psi\ln\left|\frac{\psi\left\{\left(1-\frac{h_l}{h}\right)^{1/2} - \psi\right\}}{(-\psi)\left\{\left(1-\frac{h_l}{h}\right)^{1/2} + \psi\right\}}\right| \tag{3.20}$$

$$\frac{v_s}{v_*}=\frac{v_l}{v_*}+\frac{2}{\kappa}\left\{-\left(1-\frac{h_l}{h}\right)^{1/2}\right\}-\frac{1}{\kappa}\psi\ln\left|\frac{\psi\left\{\left(1-\frac{h_l}{h}\right)^{1/2}-\psi\right\}}{(-\psi)\left\{\left(1-\frac{h_l}{h}\right)^{1/2}+\psi\right\}}\right| \tag{3.21}$$

$$\psi=\left(\frac{d_m}{\kappa h}\frac{\varsigma}{\lambda}+1-\frac{h_l}{h}\right)^{1/2} \tag{3.22}$$

where u_l and v_l are the velocity components in x and y directions at the thickness of the particle mixture layer in an immature debris flow h_l (Figure 3.1) , $u_*=\sqrt{gh\sin\theta_x}$ and $v_*=\sqrt{gh\sin\theta_y}$ are the friction velocity components in x and y directions, $\varsigma=3$ is constant to describe the mixing length, $\kappa=0.4$ is Karman constant, and λ is the linear concentrations. The thickness of particle mixture layer and the linear concentration are described as

$$\frac{h_l}{h}=\frac{C_\infty}{C_{dl}} \tag{3.23}$$

$$C_{dl}\approx 0.4C_{*L} \tag{3.24}$$

$$\lambda=\left\{\left(\frac{C_*}{C_L}\right)^{1/3}-1\right\}^{-1} \tag{3.25}$$

and the velocity components u_l and v_l are described as

$$\frac{u_l}{u_*}=\frac{2}{3}\frac{h}{d_m}\frac{1}{\left\{(\sigma/\rho)\lambda^2 a_i\sin\alpha_i+\varsigma^2/\lambda^2\right\}^{1/2}\left\{C_{dl}(\sigma-\rho)/\rho+1\right\}}\eta' \tag{3.26}$$

$$\frac{v_l}{v_*}=\frac{2}{3}\frac{h}{d_m}\frac{1}{\left\{(\sigma/\rho)\lambda^2 a_i\sin\alpha_i+\varsigma^2/\lambda^2\right\}^{1/2}\left\{C_{dl}(\sigma-\rho)/\rho+1\right\}}\eta' \tag{3.27}$$

$$\eta'=\left[\eta^{3/2}-\left\{\eta-\left(\frac{\sigma-\rho}{\rho}C_{dl}+1\right)\frac{h_l}{h}\right\}^{3/2}\right] \tag{3.28}$$

$$\eta=\left(\frac{\sigma-\rho}{\rho}C_{dl}\frac{h_l}{h}+1\right) \tag{3.29}$$

For a turbulent flow;

$$\frac{u_s}{u_*} = \frac{1}{\kappa} \ln \frac{1 + \sqrt{1 + \psi_1}}{a_0 / R_{*x} + \sqrt{(a_0 / R_{*x})^2 + \psi_1}} \tag{3.30}$$

$$\frac{v_s}{v_*} = \frac{1}{\kappa} \ln \frac{1 + \sqrt{1 + \psi_1}}{a_0 / R_{*y} + \sqrt{(a_0 / R_{*y})^2 + \psi_1}} \tag{3.31}$$

$$\psi_1 = \lambda^2 (a_i \sin \alpha_i / \kappa^2)(\sigma / \rho)(d_m / h)^2 \tag{3.32}$$

in which $R_{*x} = u_* h / \upsilon_0$, $R_{*y} = v_* h / \upsilon_0$, $a_0 = 1/9.025$ and $\upsilon_0 = 0.01 cm^2 / \sec$ is the kinematic viscosity of plain water.

Erosion and deposition velocity equations

The erosion and deposition velocity equations for 2D debris flow model given by Takahashi et al. (1992) are described as follows.

Erosion velocity equation;

$$i_b = \delta_e \frac{C_\infty - C_L}{C_* - C_\infty} \frac{\sqrt{u^2 + v^2}\, h}{d_m} \tag{3.33}$$

Deposition velocity equation for a fully developed stony debris flow;

$$i_b = \delta_d \left(1 - \frac{\sqrt{u^2 + v^2}}{p U_e} \right) \frac{C_\infty - C_L}{C_{*DL}} \sqrt{u^2 + v^2} \tag{3.34}$$

where $p(= 2/3)$ is numerical constant and U_e is the equilibrium velocity at which neither erosion nor deposition takes place as follows:

$$U_e = \frac{2}{5 d_m} \left[\frac{g \sin \theta_e}{a_i \sin \alpha_i} \left\{ C_L + (1 - C_L) \frac{\rho_m}{\sigma} \right\} \right]^{1/2} \left\{ \left(\frac{C_{*DL}}{C_L} \right)^{1/3} - 1 \right\} h^{3/2} \tag{3.35}$$

where θ_e channel slope in which coarse sediment concentration is in equilibrium, which can be obtained as follows.

$$\tan \theta_e = \frac{C_L (\sigma - \rho_m) \tan \phi}{C_L (\sigma - \rho_m) + \rho_m} \tag{3.36}$$

In this study, the inertial motion is not considered in the deposition velocity Equation (3.34) to calculate the deposition, i.e. $\sqrt{u^2 + v^2} / p U_e = 0$ is used. For the cases of an immature debris

flow and a turbulent flow, the respective deposition equation is expressed as

$$i_b = \delta_d \frac{C_\infty - C_L}{C_{*DL}} \sqrt{u^2 + v^2} \tag{3.37}$$

The inclination of the surface of the flow to the direction of the velocity vector, which is necessary for the calculation of C_∞ using Equation (2.7) or (2.8) or (2.9), is described as

$$\tan\theta_w = \frac{u \sin\theta_{bx}^{'} + v \sin\theta_{by}^{'}}{\sqrt{u^2 \cos^2\theta_{bx}^{'} + v^2 \cos^2\theta_{by}^{'}}} \tag{3.38}$$

where,

$$\tan\theta_{bx}^{'} = \tan\left(\theta_{bx0} + \theta_{bzhx}\right) \; ; \quad \tan\theta_{by}^{'} = \tan\left(\theta_{by0} + \theta_{bzhy}\right)$$

$$\tan\theta_{bzhx} = \frac{-\partial\left(z_b + h\right)}{\partial x} \; ; \quad \tan\theta_{bzhy} = \frac{-\partial\left(z_b + h\right)}{\partial y}$$

3.2.2 Basic equations of driftwood motion

It is assumed that no driftwood coalescence or breakup occurs. This implies that the pieces of driftwood are sufficiently dispersed so that collisions between them are infrequent. Based on the numerical model of driftwood proposed by Nakagawa et al. (1994), the equations of motion of each piece of driftwood in x and y directions, individually labeled by subscript k are expressed as follows.

$$(m_k + mC_M)\frac{du_k}{dt} = -m_k g \frac{\partial H_k}{\partial x} - \frac{1}{2}\rho_T C_{Dx} W_k (u_k - U_k) A_{kx} \tag{3.39}$$

$$(m_k + mC_M)\frac{dv_k}{dt} = -m_k g \frac{\partial H_k}{\partial y} - \frac{1}{2}\rho_T C_{Dy} W_k (v_k - V_k) A_{ky} \tag{3.40}$$

The equations for the position of the driftwood are as

$$\frac{dX_k}{dt} = u_k \; ; \quad \frac{dY_k}{dt} = v_k \tag{3.41}$$

where X_k and Y_k are the position of the centroid of the driftwood, m_k is the mass of the driftwood, i.e., $m_k = \rho_d \pi r^2 L_d$, ρ_d is the density of the driftwood, π is the ratio of the circumference of a circle to its diameter, r is the radius of the driftwood, L_d is the length of the driftwood piece, m is the mass of the fluid occupied by volume of a piece of driftwood, C_M is

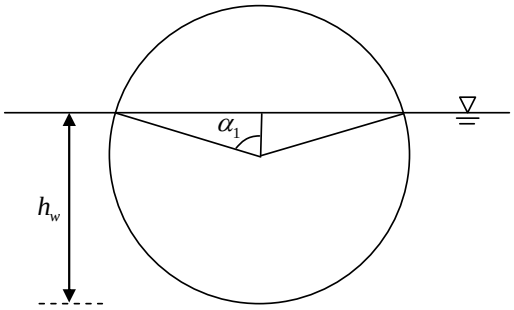

Figure 3.2 Definition sketch of angle α_1

the virtual mass coefficient, H_k is the flow surface level at the position of the centroid of the driftwood, and $\partial H_k / \partial x$ and $\partial H_k / \partial y$ are described as follows:

$$-\frac{\partial H_k}{\partial x} = \sin(\theta_{bx0})_k - \cos(\theta_{bx0})_k \frac{\partial (z_b + h)_k}{\partial x} \tag{3.42}$$

$$-\frac{\partial H_k}{\partial y} = \sin(\theta_{by0})_k - \cos(\theta_{by0})_k \frac{\partial (z_b + h)_k}{\partial y} \tag{3.43}$$

in which, $(\theta_{bx0})_k$ and $(\theta_{by0})_k$ are the x and y components of the slope of the original bed surface at the position of the centroid of the driftwood, and $(z_b + h)_k$ is the flow surface stage $(z_b + h)$ at the position of the centroid of the driftwood. The projected areas A_{kx} and A_{ky} of the submerged part of the driftwood are described as follows.

$$A_{kx} = h_w L_d \left|\sin\theta_k\right| \tag{3.44}$$

$$A_{ky} = h_w L_d \left|\cos\theta_k\right| \tag{3.45}$$

and,

$$A_{kx} = r^2(\pi - \alpha_1 + \sin\alpha_1 \cos\alpha_1); \quad \text{when } \theta_k = 0 \tag{3.46}$$

$$A_{ky} = r^2(\pi - \alpha_1 + \sin\alpha_1 \cos\alpha_1); \quad \text{when } \theta_k = \pi/2 \tag{3.47}$$

$$h_w = r(1 + \cos\alpha_1) \tag{3.48}$$

where θ_k is the rotational angle of the piece of driftwood, and α_1 is angle as shown in Figure 3.2, which can be determined by equating the weight of driftwood pieces and weight of fluid occupied by the volume of a piece of driftwood as follows.

$$\rho_d \pi r^2 L_d g = \rho_T r^2 (\pi - \alpha_1 + \sin\alpha_1 \cos\alpha_1) g L_d \tag{3.49}$$

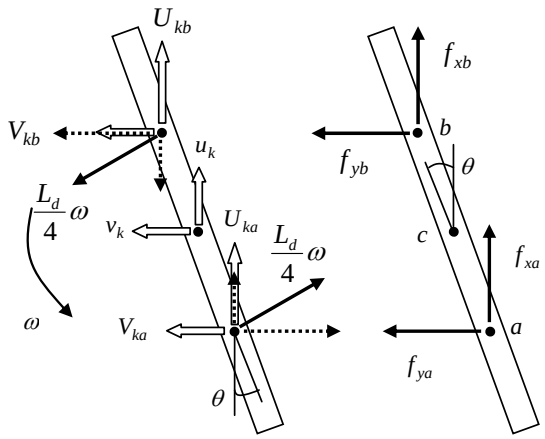

Figure 3.3 Definition sketch of the rotational angle of pieces of driftwood

The rotational motion of driftwood

The rotational motion around the axis of the centroid of the driftwood is described by evaluating the moment N_0 produced by the hydrodynamic force acting on the driftwood. On the supposition that the driftwood can be divided into two pieces at the centroid 'c' and that the drag force acts on both centroids, 'a' and 'b', of these pieces as shown in Figure 3.3, the rotational motion of the driftwood is written as follows (Nakagawa et al., 1995).

$$Id^2\theta_k / dt^2 = \sum N_0 = (L_d / 4)\{(f_{xa} - f_{xb})\sin\theta_k - (f_{ya} - f_{yb})\cos\theta_k\} \quad (3.50)$$

where,

$$f_{xa} = (1/2)\rho C_{Dx}\sqrt{(U_{ka} - u_k - u_{rka})^2 + (V_{ka} - v_k - v_{rka})^2}\,(U_{ka} - u_k - u_{rka})(A_{kx} / 2) \quad (3.51)$$

$$f_{ya} = (1/2)\rho C_{Dy}\sqrt{(U_{ka} - u_k - u_{rka})^2 + (V_{ka} - v_k - v_{rka})^2}\,(V_{ka} - v_k - v_{rka})(A_{ky} / 2) \quad (3.52)$$

$$f_{xb} = (1/2)\rho C_{Dx}\sqrt{(U_{kb} - u_k - u_{rkb})^2 + (V_{kb} - v_k - v_{rkb})^2}\,(U_{kb} - u_k - u_{rkb})(A_{kx} / 2) \quad (3.53)$$

$$f_{yb} = (1/2)\rho C_{Dy}\sqrt{(U_{kb} - u_k - u_{rkb})^2 + (V_{kb} - v_k - v_{rkb})^2}\,(V_{kb} - v_k - v_{rkb})(A_{ky} / 2) \quad (3.54)$$

$$u_{rka} = (L_d / 4)(d\theta_k / dt)\sin\theta_k \quad ; \quad v_{rka} = -(L_d / 4)(d\theta_k / dt)\cos\theta_k \quad (3.55)$$

$$u_{rkb} = -(L_d / 4)(d\theta_k / dt)\sin\theta_k \quad ; \quad v_{rkb} = (L_d / 4)(d\theta_k / dt)\cos\theta_k \quad (3.56)$$

in which I is the moment of inertia around the centroid, 'c', which is written as $I = m_k(r^2 / 4 + L_d{}^2 / 12)$. The rotational motion of the driftwood is also supposed to be restricted on the flow surface and the rotation on the vertical plane is not considered.

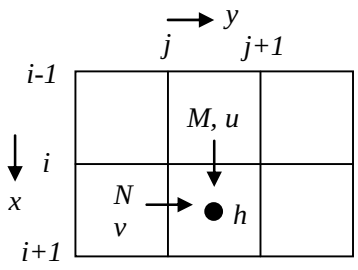

Figure 3.4 Arrangement of variables on meshes

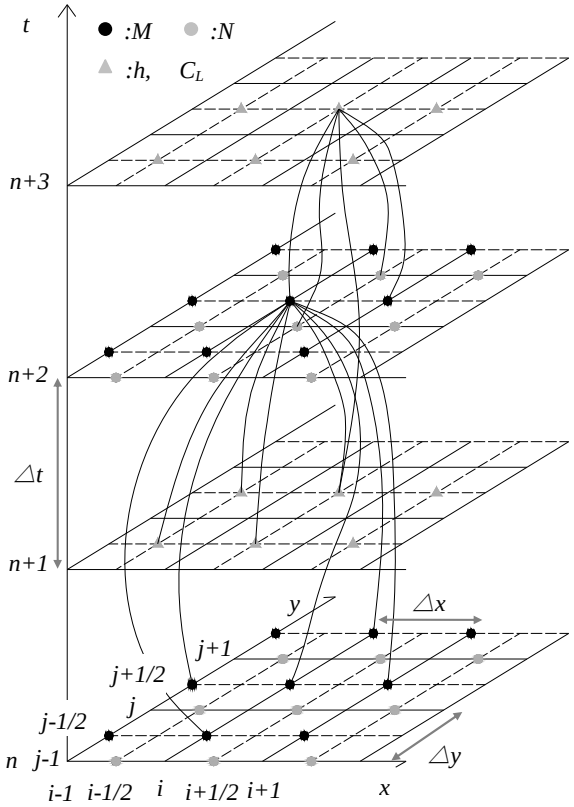

Figure 3.5 Arrangement of variables and the way of advancing the calculation

3.3 Solution methods

3.3.1 Flow motion of debris flow

The partial differential equations of basic equations of debris flow are obtained from the methods of Nakagawa (1989) by using Leap-Frog scheme. In which vector quantities such as

M , N and u , v are defined in the middle of the cell face and scalar quantities such as h , C_L , C_F are defined in the center of the cell (Figure 3.4). The arrangement of variables and the way of advancing the calculation are shown in Figure 3.5. The finite difference form of Equation (3.1) for momentum equation in the x direction is as follows.

$$\frac{M_{i,j+1/2}^{n+2} - M_{i,j+1/2}^{n}}{2\Delta t} + \beta.XDX + \beta.XDY = g\bar{h}\sin\theta_{bx0}$$
$$- g\bar{h}\cos\theta_{bx0}\frac{(h+z_b)_{i+1/2,j+1/2}^{n+1} - (h+z_b)_{i-1/2,j+1/2}^{n+1}}{\Delta x} - \frac{u_{i,j+1/2}}{\sqrt{(u_{i+1/2,j}^{n})^2 + (v_{i+1/2,j}^{n})^2}}$$
$$.\frac{f(\overline{C}_L)(\sigma-\rho)g\bar{h}}{\overline{\rho_T}}\frac{\cos\theta_{x\,i+1/2,j+1/2}^{n+1} + \cos\theta_{x\,i-1/2,j+1/2}^{n+1}}{2}\tan\phi -$$
$$- \rho.\frac{1}{\overline{\rho}_T}\frac{f_{bi+1/2,j+1/2}^{n+1} + f_{bi-1/2,j+1/2}^{n+1}}{2}u_{i,j+1/2}\sqrt{(u_{i+1/2,j}^{n})^2 + (v_{i+1/2,j}^{n})^2} + \frac{\tau_{sx}}{\overline{\rho}_T} \qquad (3.57)$$

where,

$$XDX = \begin{cases} \dfrac{u_{i,j+1/2}^{n}M_{i,j+1/2}^{n} - u_{i-1,j+1/2}^{n}M_{i-1,j+1/2}^{n}}{\Delta x} & : \ u_{i,j+1/2}^{n} \geq 0, \quad u_{i-1,j+1/2}^{n} \geq 0 \\ \dfrac{u_{i,j+1/2}^{n}M_{i,j+1/2}^{n} - 0}{\Delta x} & : \ u_{i,j+1/2}^{n} \geq 0, \quad u_{i-1,j+1/2}^{n} < 0 \\ \dfrac{u_{i+1,j+1/2}^{n}M_{i+1,j+1/2}^{n} - u_{i,j+1/2}^{n}M_{i,j+1/2}^{n}}{\Delta x} & : \ u_{i,j+1/2}^{n} < 0, \quad u_{i-1,j+1/2}^{n} < 0 \\ \dfrac{0 - u_{i,j+1/2}^{n}M_{i,j+1/2}^{n}}{\Delta x} & : \ u_{i,j+1/2}^{n} < 0, \quad u_{i+1,j+1/2}^{n} \geq 0 \end{cases} \qquad (3.58)$$

$$XDY = \begin{cases} \dfrac{\tilde{v}_{i,j+1/2}^{n}M_{i,j+1/2}^{n} - \tilde{v}_{i,j-1/2}^{n}M_{i,j-1/2}^{n}}{\Delta y} & : \ \tilde{v}_{i,j+1/2}^{n} \geq 0, \quad \tilde{v}_{i,j-1/2}^{n} \geq 0 \\ \dfrac{\tilde{v}_{i,j+1/2}^{n}M_{i,j+1/2}^{n} - 0}{\Delta y} & : \ \tilde{v}_{i,j+1/2}^{n} \geq 0, \quad \tilde{v}_{i,j-1/2}^{n} < 0 \\ \dfrac{\tilde{v}_{i,j+3/2}^{n}M_{i,j+3/2}^{n} - \tilde{v}_{i,j+1/2}^{n}M_{i,j+1/2}^{n}}{\Delta y} & : \ \tilde{v}_{i,j+1/2}^{n} < 0, \quad \tilde{v}_{i,j+3/2}^{n} < 0 \\ \dfrac{0 - \tilde{v}_{i,j+1/2}^{n}M_{i,j+1/2}^{n}}{\Delta y} & : \ \tilde{v}_{i,j+1/2}^{n} < 0, \quad \tilde{v}_{i,j+3/2}^{n} \geq 0 \end{cases} \qquad (3.59)$$

$$u_{i,j+1/2}^{n} = \frac{2M_{i,J+1/2}^{n}}{h_{i-1/2,j+1/2}^{n+1} + h_{i+1/2,j+1/2}^{n+1}} \quad ; \quad v_{i+1/2,j}^{n} = \frac{2N_{i+1/2,J}^{n}}{h_{i+1/2,j-1/2}^{n+1} + h_{i+1/2,j+1/2}^{n+1}} \qquad (3.60)$$

$$\tilde{v}_{i,j+1/2}^{n} = \frac{1}{4}\left(v_{i-1/2,j}^{n} + v_{i-1/2,j+1}^{n} + v_{i+1/2,j}^{n} + v_{i+1/2,j+1}^{n}\right) \qquad (3.61)$$

$$\bar{h} = \frac{h_{i-1/2,j+1/2}^{n+1} + h_{i+1/2,j+1/2}^{n+1}}{2} \qquad (3.62)$$

$$\overline{\rho}_T = (\sigma-\rho)\overline{C_L} + \rho \qquad (3.63)$$

$$\overline{C_L} = \frac{C^{n+1}_{Li-1/2,j+1/2} + C^{n+1}_{Li+1/2,j+1/2}}{2} \tag{3.64}$$

$$f(\overline{C_L}) = \begin{cases} \dfrac{\overline{C_L} - C_3}{C_* - C_3} & ; \quad \overline{C_L} > C_3 \\ 0 & ; \quad \overline{C_L} \le C_3 \end{cases} \tag{3.65}$$

Similarly, we can get the finite difference form of Equation (3.2) for momentum equation in the y direction. The finite difference form of Equations (3.3) and (3.4) for continuity equation of flow and coarse sediment are expressed as follows:

$$\frac{h^{n+3}_{i+1/2,j+1/2} - h^{n+1}_{i+1/2,j+1/2}}{2\Delta t} + \frac{M^{n+2}_{i+1,j+1/2} - M^{n+2}_{i,j+1/2}}{2\Delta x} + \frac{N^{n+2}_{i+1/2,j+1} - N^{n+2}_{i+1/2,j}}{2\Delta y} = i^{n+1}_{bi+1/2,j+1/2} \tag{3.66}$$

$$\frac{(C_L h)^{n+3}_{i+1/2,j+1/2} - (C_L h)^{n+1}_{i+1/2,j+1/2} h^{n+1}_{i+1/2,j+1/2}}{2\Delta t} + \frac{Q^{n+2}_{Lxi+1,j+1/2} - Q^{n+2}_{Lxi,j+1/2}}{2\Delta x}$$

$$+ \frac{Q^{n+2}_{Lyi+1/2,j+1} - Q^{n+2}_{Lyi+1/2,j}}{2\Delta y} = i^{n+1}_{bi+1/2,j+1/2} C_{*L} \tag{3.67}$$

where,

$$Q^{n+2}_{Lxi,j+1/2} = \begin{cases} M^{n+2}_{i,j+1/2} C^{n+1}_{Li-1/2,j+1/2}; & M^{n+2}_{i,j+1/2} \ge 0 \\ M^{n+2}_{i,j+1/2} C^{n+1}_{Li+1/2,j+1/2}; & M^{n+2}_{i,j+1/2} < 0 \end{cases} \tag{3.68}$$

$$Q^{n+2}_{Lxi+1,j+1/2} = \begin{cases} M^{n+2}_{i+1,j+1/2} C^{n+1}_{Li-1/2,j+1/2}; & M^{n+2}_{i+1,j+1/2} \ge 0 \\ M^{n+2}_{i+1,j+1/2} C^{n+1}_{Li+1/2,j+1/2}; & M^{n+2}_{i+1,j+1/2} < 0 \end{cases} \tag{3.69}$$

$$Q^{n+2}_{Lyi+1/2,j} = \begin{cases} N^{n+2}_{i+1/2,j} C^{n+1}_{Li+1/2,j-1/2}; & N^{n+2}_{i+1/2,j} \ge 0 \\ N^{n+2}_{i+1/2,j} C^{n+1}_{Li+1/2,j+1/2}; & N^{n+2}_{i+1/2,j} < 0 \end{cases} \tag{3.70}$$

$$Q^{n+2}_{Lyi+1/2,j+1} = \begin{cases} N^{n+2}_{i+1/2,j+1} C^{n+1}_{Li+1/2,j-1/2}; & N^{n+2}_{i+1/2,j+1} \ge 0 \\ N^{n+2}_{i+1/2,j+1} C^{n+1}_{Li+1/2,j+1/2}; & N^{n+2}_{i+1/2,j+1} < 0 \end{cases} \tag{3.71}$$

Similarly, we can get the finite difference form of Equation (3.5) for continuity equation of fine fraction.

3.3.2 Flow motion of driftwood

For driftwood motion, the space-centered and time-forward differencing approximation proposed by Nakagawa et al. (1992, 1993) is adopted. The finite difference form of equations of motion and position of driftwood are expressed as follows.

$$(m_k + mC_M)\frac{u_k^{n+2} - u_k^n}{2\Delta t} = m_k g(HFSX) - \frac{1}{2}\rho_T C_{Dx} W_k^n (\frac{u_k^{n+2} + u_k^n}{2} - U_k^n) A_{kx} \tag{3.72}$$

$$(m_k + mC_M)\frac{v_k^{n+2} - v_k^n}{2\Delta t} = m_k g(HFSY) - \frac{1}{2}\rho_T C_{Dy} W_k^n (\frac{v_k^{n+2} + v_k^n}{2} - V_k^n) A_{ky} \tag{3.73}$$

$$\frac{X_k^{n+3} - X_k^{n+1}}{2\Delta t} = u_k^{n+2} \; ; \quad \frac{Y_k^{n+3} - Y_k^{n+1}}{2\Delta t} = v_k^{n+2} \tag{3.74}$$

where,

$$W_k^n = \sqrt{(u_k^n - U_k^n)^2 + (v_k^n - V_k^n)^2} \tag{3.75}$$

$$HFSX = \sin(\theta_{bx0})_k - \cos(\theta_{bx0})_k \frac{(z_b + h)_{kfx}^{n+1} - (z_b + h)_{kbx}^{n+1}}{\Delta x} \tag{3.76}$$

$$HFSY = \sin(\theta_{by0})_k - \cos(\theta_{by0})_k \frac{(z_b + h)_{kfy}^{n+1} - (z_b + h)_{kby}^{n+1}}{\Delta y} \tag{3.77}$$

in which $(z_b + h)_{kfx}^{n+1}$ and $(z_b + h)_{kbx}^{n+1}$ are the flow surface stages $(z_b + h)$ measured from the original bed surface elevation at downstream and upstream of the position of the centroid of the driftwood k in x direction, and $(z_b + h)_{kfy}^{n+1}$ and $(z_b + h)_{kby}^{n+1}$ are in y direction. U_k^n and V_k^n are expressed as follows.

$$U_k^n = \left(1 - \frac{\mathrm{E}_k^{n+1}}{\Delta x}\right) u_{sI_k^{n+1}, J_k^{n+1}+1/2}^n + \frac{\mathrm{E}_k^{n+1}}{\Delta x} u_{sI_k^{n+1}+1, J_k^{n+1}+1/2}^n \tag{3.78}$$

$$V_k^n = \left(1 - \frac{\Gamma_k^{n+1}}{\Delta y}\right) v_{sI_k^{n+1}+1/2, J_k^{n+1}}^n + \frac{\Gamma_k^{n+1}}{\Delta y} v_{sI_k^{n+1}+1/2, J_k^{n+1}+1}^n \tag{3.79}$$

and $(z_b + h)_k^{n+1}$ at the position of the driftwood k is expressed as

$$(z_b + h)_k^{n+1} = (z_b + h)_{I_k^{n+1}+1/2, J_k^{n+1}+1/2}^{n+1} \tag{3.80}$$

where,

$$I_k^{n+1} = \left| X_k^{n+1} / \Delta x \right| + 1 \quad ; \quad J_k^{n+1} = \left| Y_k^{n+1} / \Delta y \right| + 1 \tag{3.81}$$

$$\mathrm{E}_k^{n+1} = X_k^{n+1} - \Delta x (I_k^{n+1} - 1) \quad ; \quad \Gamma_k^{n+1} = Y_k^{n+1} - \Delta y (J_k^{n+1} - 1) \tag{3.82}$$

in which I_k^{n+1} and J_k^{n+1} are the spatial position of the computational cell of the driftwood position in x and y directions, and $\left|x\right|$ means the integer value, rounds number x down to the nearest integer.

3.4 Fluctuation of position and angular velocity of driftwood

3.4.1 Fluctuation of position of driftwood

Driftwood positions can be evaluated by integrating Equation (3.41) deterministically under suitable initial conditions, but they fluctuate due to the collision of driftwood with boulders and disturbances on the flow surface during the collision of the sediment particles, which are considered in the diffusions coefficients. The fluctuation components of driftwood position ΔX_k and ΔY_k are evaluated as Nakagawa et al. (1994, 1995).

$$\Delta X_k = \sqrt{4K_x(2\Delta t)}erf^{-1}(\alpha') \tag{3.83}$$

$$\Delta Y_k = \sqrt{4K_y(2\Delta t)}erf^{-1}(\beta') \tag{3.84}$$

where K_x and K_y are the longitudinal and transverse diffusion coefficients, α' and β' are random variables uniformly distributed in the range (0,1), and erf^{-1} is the inverse of error function, erf , given by

$$\left.\begin{aligned} erf(s) &= \left\{1-\Phi(\sqrt{2}s)\right\} = \left(1/\sqrt{\pi}\right)\int_s^{\infty}\exp(-\varepsilon^2)d\varepsilon \\ \Phi(s) &= \left(1/\sqrt{2\pi}\right)\int_{-\infty}^{s}\exp(-\varepsilon^2/2)d\varepsilon \end{aligned}\right\} \tag{3.85}$$

The driftwood position is estimated by adding the fluctuation value to the value obtained from the equations of motion deterministically as

$$X_k^{n+3} = X_k^{n+1} + u_k^{n+2}(2\Delta t) + \sqrt{4K_x(2\Delta t)}erf^{-1}(\alpha') \tag{3.86}$$

$$Y_k^{n+3} = Y_k^{n+1} + v_k^{n+2}(2\Delta t) + \sqrt{4K_y(2\Delta t)}erf^{-1}(\beta') \tag{3.87}$$

3.4.2 Fluctuation of angular velocity of driftwood

The rotational angle of a piece of driftwood can be evaluated deterministically by solving Equation (3.50), but it also fluctuates due to the collision of driftwood with boulders and disturbances on the flow surface during the collision of the sediment particles. Therefore, the rotational angle of driftwood is evaluated by considering the fluctuation component as follows.

$$d\theta_k / dt = \omega_d + \omega_p \tag{3.88}$$

$$\theta_k^{n+3} = \theta_k^{n+1} + 2\Delta t(\omega_d + \omega_p) \tag{3.89}$$

where ω_d is the angular velocity of the piece of driftwood obtained deterministically and ω_p is the fluctuation of the angular velocity of the driftwood evaluated stochastically. Assuming the rotational angular velocity of the fluctuating component of a piece of driftwood follows a normal distribution, its distribution function, Φ, is given by

$$\Phi(\gamma) = \frac{1}{\sqrt{2\pi}} \int_{-\infty}^{\gamma} \exp(-\varepsilon^2 / 2) d\varepsilon \tag{3.90}$$

where $\gamma = (\omega_p - \overline{\omega}) / \sigma_w$ is obtained from the inverse function, Φ^{-1}, for uniformly distributed random numbers within (0,1), $\overline{\omega}$ and σ_w are the mean and standard deviation of angular velocity of driftwood. After γ is obtained, ω_p is estimated from $\omega_p = \gamma\sigma_w + \overline{\omega}$.

It is difficult to evaluate the integral of inverse of error function and normal distribution in closed form in terms of elementary functions, but by expanding the integrand in a Taylor series, we can evaluate the inverse of error function and normal distribution as follows (Abramowitz and Stegun, 1972).

$$erf^{-1}(A) = \sqrt{\pi}\left\{(1-A) + \pi\frac{(1-A)^3}{12} + 7\pi^2\frac{(1-A)^5}{480} + 127\pi^3\frac{(1-A)^7}{40320} + 4369\pi^4\frac{(1-A)^9}{5806080} + 34807\pi^5\frac{(1-A)^{11}}{182476800} + \ldots\right\} \tag{3.91}$$

$$\Phi^{-1}(A) = \sqrt{2\pi}\left\{A + \pi\frac{A^3}{12} + 7\pi^2\frac{A^5}{480} + 127\pi^3\frac{A^7}{40320} + 4369\pi^4\frac{A^9}{5806080} + 34807\pi^5\frac{A^{11}}{182476800} + \ldots\right\} \tag{3.92}$$

3.5 Determination of diffusion coefficients and rotational angle of driftwood

The fluctuation components of driftwood position and rotational angular velocity of the driftwood are evaluated as method proposed by Nakagawa et al. (1994). The diffusion coefficients of driftwood only with clear water flow have been determined from the experiments with driftwood by previous researchers such as Gotoh (1983), Nakagawa et al. (1992, 1994, 1995) and others. However, they have not determined diffusion coefficients of driftwood by interacting with debris flow or sediment water mixture flow. Therefore, it is necessary to

determine the diffusion coefficients to evaluate the fluctuation components of position and angular velocity of the driftwood in debris flow case.

3.5.1 Laboratory experiments and method

A rectangular flume of 5m long, 30cm wide and 45cm deep was used for the experiments. The slope of flume was set at 18 degrees. To measure the position and rotational angle of the driftwood, 19 pieces measuring rods having the same length as the flume width, were stretched across the flume at intervals of 10cm in the downstream direction from x = 0cm (2.6m downstream from the upstream end) along the 1.8m measuring reach (Figure 3.6). Sediment (mean size = 1.86mm, maximum size = 4.75mm) was supplied with a sediment feeder at 0.8m downstream from the upstream end and water discharge was supplied from the upstream end of the flume. Figures 3.7 and 3.8 show the photo of the flume and the particle size distribution curve of sediment material, respectively. A piece of driftwood was supplied at x = -10cm after supplying designated water and sediment mixture flow discharge. The position and rotational angle of the moving driftwood were measured with a video camera in each of the 19 sections for x = 0, 10, 20,…..180cm. Such measurement was repeated 30 times for each experiment under the same hydraulic conditions. A 3.5cm long, cylindrical piece of driftwood with a diameter of 3mm and a mass density $\rho_d = 0.785\text{g/cm}^3$ was used. The data obtained in the experiments were analyzed statistically, after which the diffusion coefficients and other hydraulic parameters were determined.

The experimental conditions and results are shown in Table 3.1, where Q_{in} is the inflow water discharge supplied at the upstream end, Q_{flow} is the sediment-water mixture flow discharge in the flume, C is the sediment concentration in the flow, h is the flow depth, u is the cross-sectional averaged velocity of the flow, $u_* = \sqrt{gh\sin\theta}$ is the friction velocity (θ = flume slope) and $Fr = u/\sqrt{gh}$ is the Froude number. Eight experiments were carried out with different hydraulic conditions.

3.5.2 Diffusion coefficients of driftwood

Figure 3.9 shows the path lines of the driftwood centroids of 30 pieces of driftwood and it demonstrate statistical variety of them. Based on the data as shown in Figure 3.9, the scattering

process is described as a diffusion process and the diffusion coefficients might be defined. In general, the spatial distribution of a substance diffusing in a uniform flow is a normal distribution (Nakagawa et al., 1994), and the longitudinal and transverse diffusion coefficients, K_x and K_y, and the longitudinal and transverse variances, $\overline{X^2}$ and $\overline{Y^2}$, are related to each other and which can be evaluated as follows.

$$K_x = \frac{1}{2}\left(\frac{\overline{dX^2}}{dt}\right) \tag{3.93}$$

$$K_y = \frac{1}{2}\left(\frac{\overline{dY^2}}{dt}\right) \tag{3.94}$$

To obtain the frequency distribution of the positions of the driftwood in longitudinal direction from the hydraulic experiments, the distance moved in longitudinal direction by each piece of driftwood during each $dt = 0.1\text{sec}$ time interval for $T_L (= ndt)$ time period was determined. The possible distance moved during dt time interval from 0 to 20cm (20cm maximum) was divided into m (=20) number of section at the interval of 1cm. The number of pieces of driftwood, which distance moved in dt time interval in each section, was counted, after which the ratio of this number to the multiplication of the total number of time interval (n) and the total pieces of driftwood (30) was calculated (i.e., P= N_i /(n x 30), i =1, …., m). The frequency distributions of the longitudinal positions of the driftwood are shown in Figure 3.10, in which solid line is calculated by assuming a normal distribution with the mean value, X_{mean} and variance, $\overline{X^2}$.

To obtain the frequency distribution of the transverse positions of the driftwood, the flume width (30cm) was divided into 30 sections transversely. The number of pieces of the driftwood in each section was counted, after which the ratio of this number to the total pieces of the driftwood (30) was calculated. The frequency distributions of the transverse positions of the driftwood are shown in Figures 3.11 and 3.12, in which solid line is calculated by assuming a normal distribution with the mean value, Y_{mean} and variance, $\overline{Y^2}$. The variance becomes large as x increases, and the calculated normal distributions are in fairly good agreement with the experimental frequency distribution. This means that the diffusion coefficients of the driftwood have relations as Equation (3.93) and Equation (3.94) for longitudinal and transverse directions, respectively. Table 3.2 shows the experimental results of transverse diffusivity of driftwood in

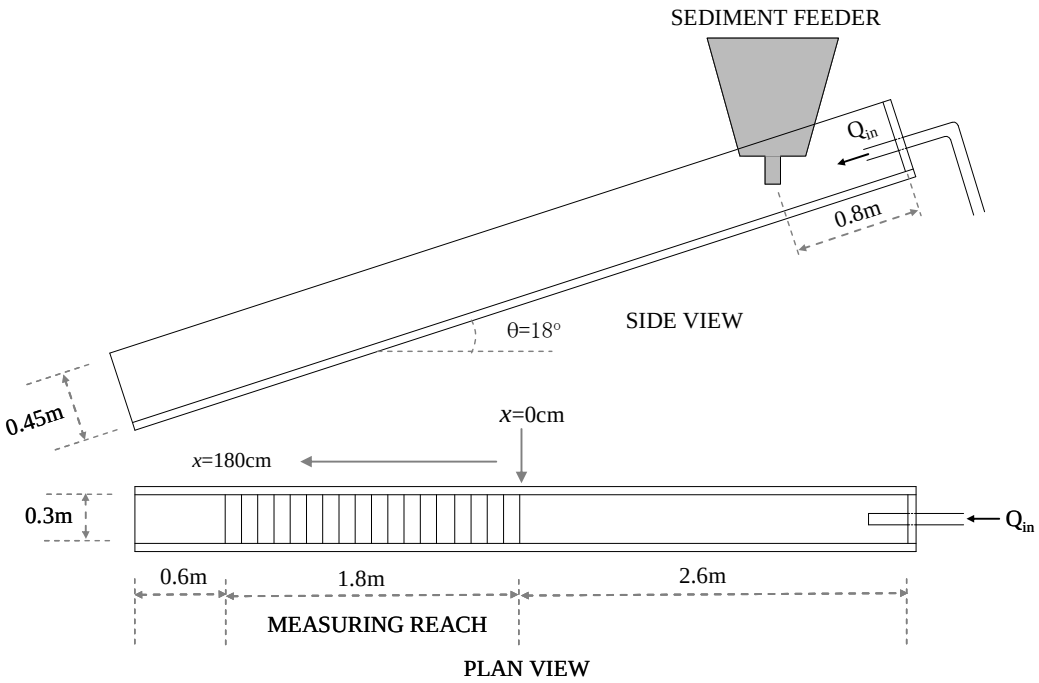

Figure 3.6 Experimental setup for the determination of diffusion coefficients and rotational angular velocity of driftwood

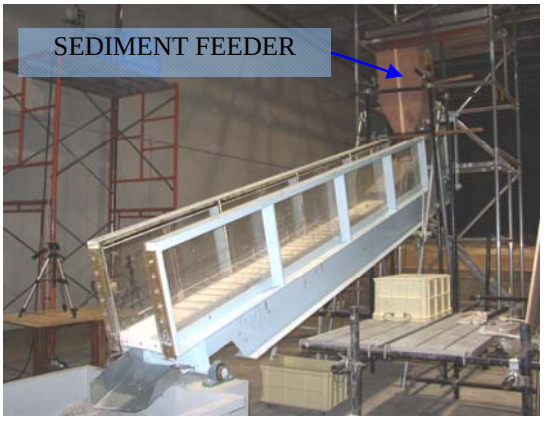

Figure 3.7 Photo of the experimental flume

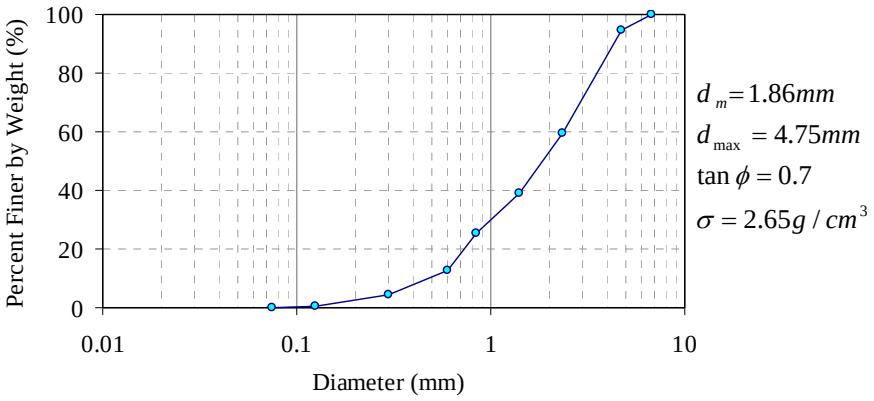

Figure 3.8 Particle size distribution curve of the sediment

Table 3.1 Experimental conditions and results of diffusion coefficient and rotational angle of driftwood

EXP NO.	Q_{in} (cm^3/sec)	Q_{flow} (cm^3/sec)	C	h (cm)	u (cm/sec)	u_* (cm/sec)	Fr	K_x (cm^2/sec)	K_y (cm^2/sec)	$\frac{K_x}{u_* h}$	$\frac{K_y}{u_* h}$	ϖ (deg/sec)	σ_w (deg/sec)
1	646.020	843.489	0.283	0.830	33.875	15.854	1.188	11.270	6.408	0.856	0.487	-0.881	28.896
2	742.105	976.006	0.320	0.900	36.148	16.509	1.217	13.817	4.804	0.930	0.323	0.550	29.645
3	888.563	1028.305	0.323	0.910	37.667	16.601	1.261	4.192	5.873	0.278	0.389	0.727	38.970
4	993.644	1538.425	0.340	1.100	46.619	18.252	1.420	14.234	5.875	0.709	0.293	-2.385	41.134
5	873.729	1130.734	0.265	0.960	39.262	17.051	1.280	8.890	6.676	0.543	0.408	-2.099	27.268
6	924.146	1215.897	0.270	0.990	40.939	17.315	1.314	14.203	4.644	0.829	0.271	0.470	34.483
7	844.030	1318.343	0.339	1.030	42.665	17.661	1.343	14.073	4.439	0.774	0.244	1.518	33.945
8	873.627	1284.487	0.269	1.020	41.977	17.575	1.328	4.869	5.922	0.272	0.330	-2.611	30.291
Mean										**0.649**	**0.343**	**-0.589**	**33.079**

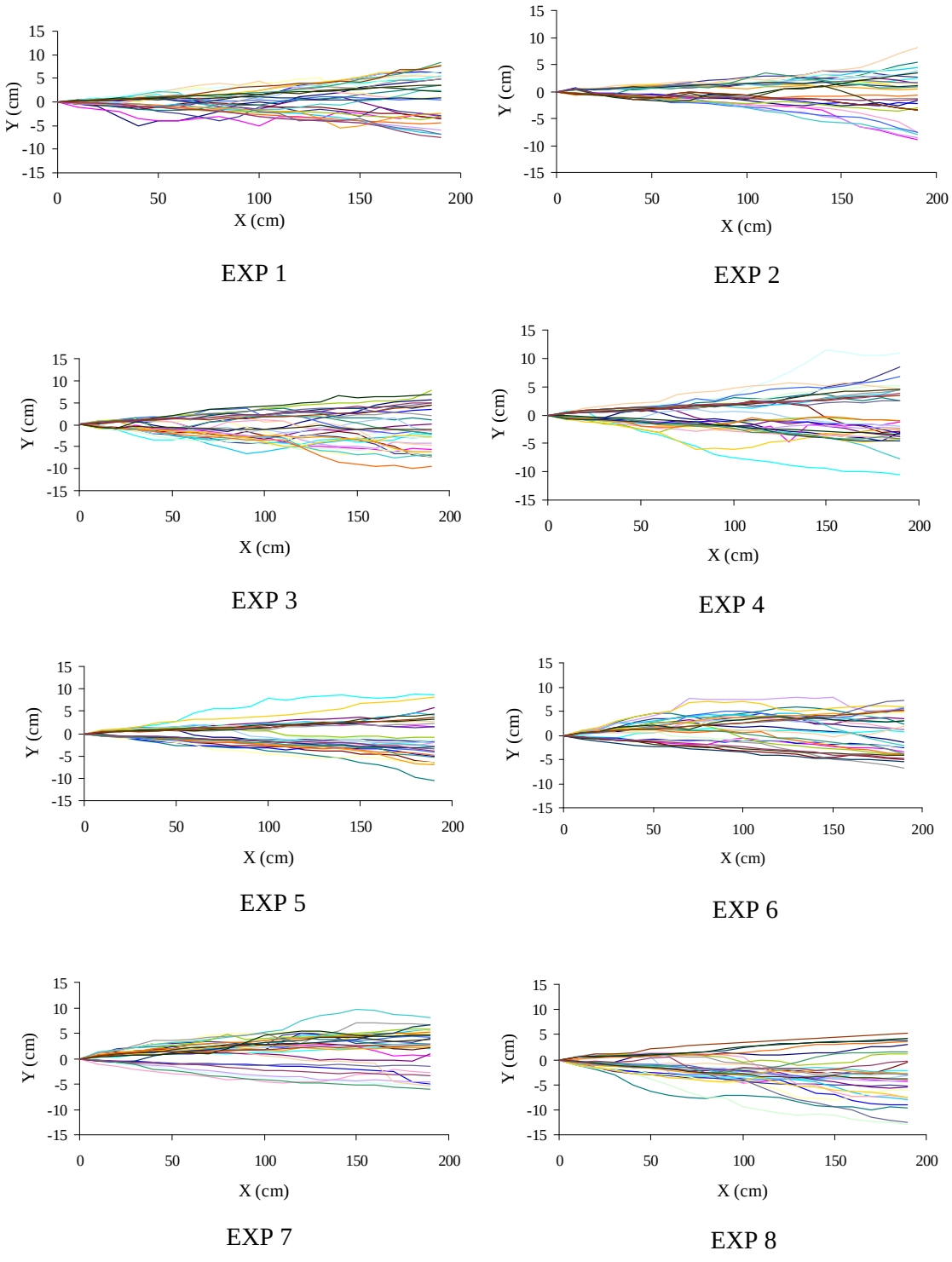

Figure 3.9 Path lines of the centroid of the driftwood

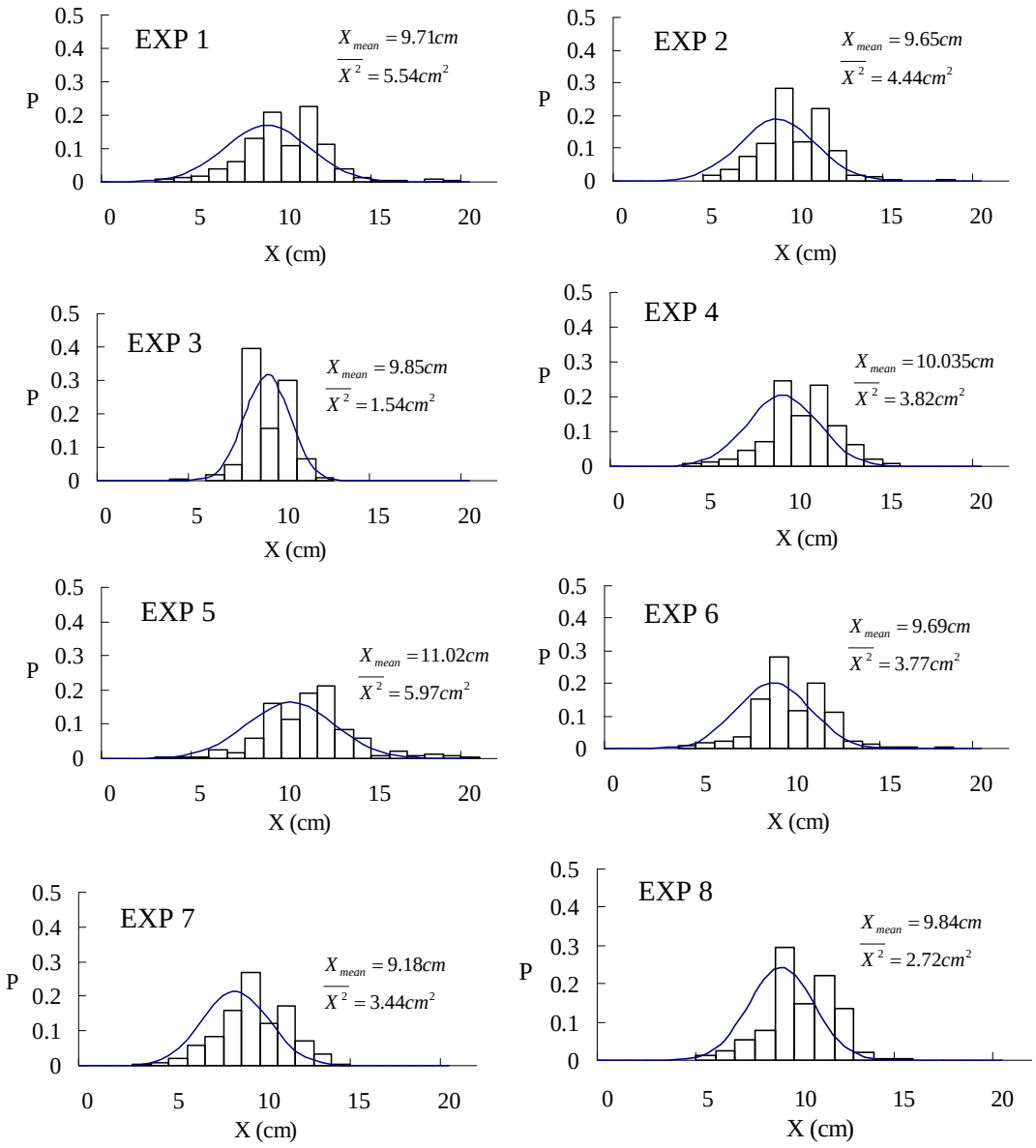

Figure 3.10 Frequency distribution of longitudinal position of driftwood

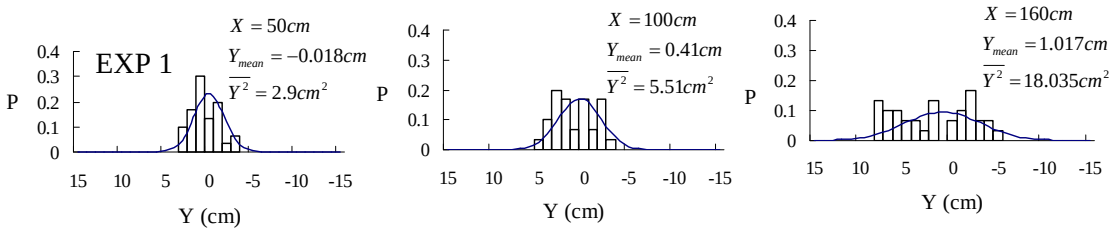

Figure 3.11 Frequency distribution of transverse position of driftwood, Experiment 1

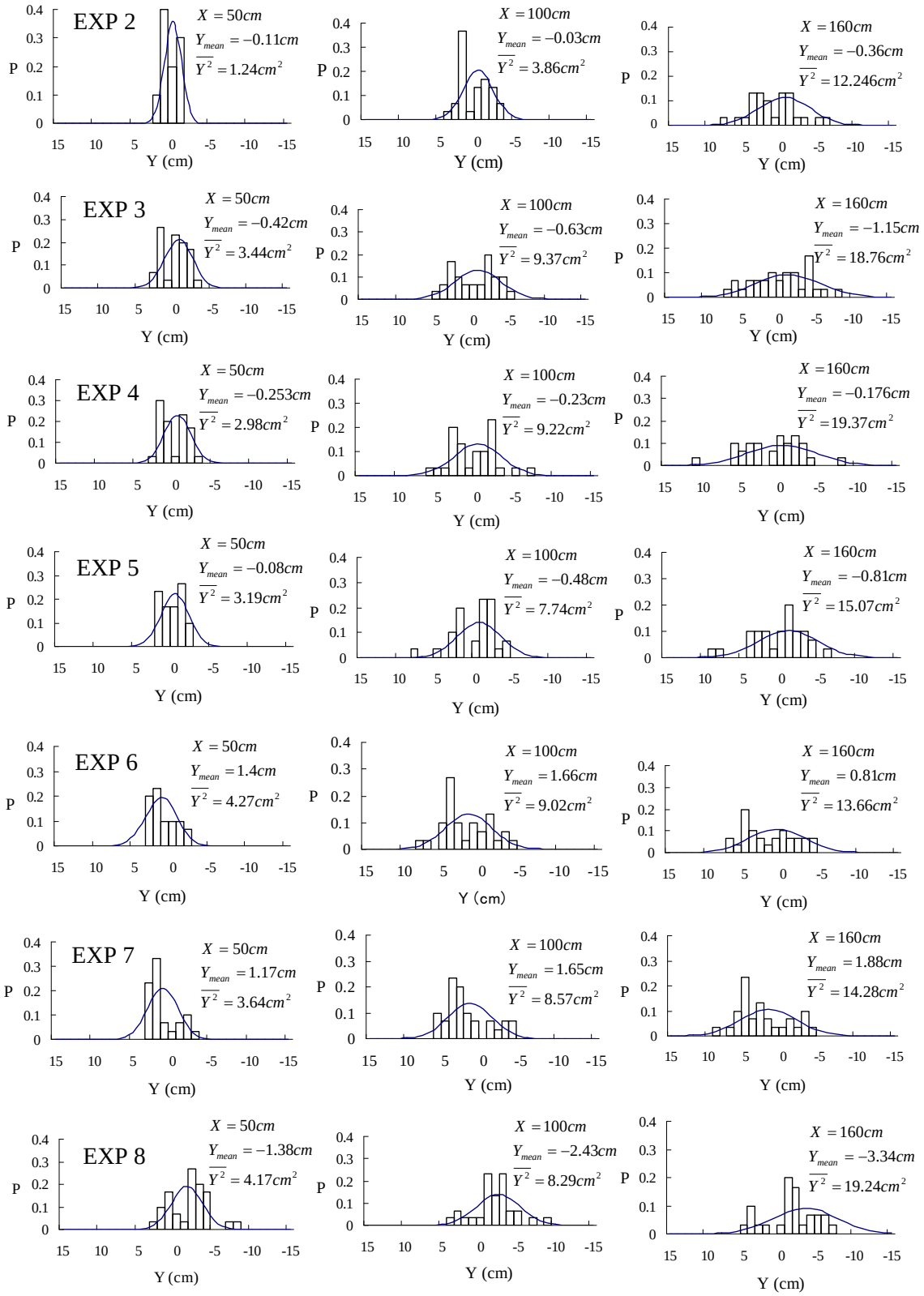

Figure 3.12 Frequency distribution of transverse position of driftwood, Experiments 2 to 8

Table 3.2 Experimental results of transverse diffusivity of driftwood in each section

	EXP1	EXP2	EXP3	EXP4	EXP5	EXP6	EXP7	EXP8
x (cm)	K_y (cm^2/sec)							
10	0.814	0.0429	2.040	1.5606	1.820	1.768	2.598	2.344
20	2.366	0.9588	2.916	1.5889	2.066	3.970	2.570	2.490
30	5.508	1.7538	4.236	2.2525	3.518	4.141	4.150	4.523
40	1.811	0.6847	3.698	3.4633	3.501	4.881	3.099	5.569
50	2.151	1.3950	2.978	3.4969	6.466	5.189	3.837	4.001
60	-0.041	0.7475	10.074	4.6245	5.956	11.102	4.891	4.663
70	1.540	1.5290	4.878	6.7206	1.988	1.303	5.225	4.130
80	3.875	2.2708	6.331	3.4964	4.291	2.877	2.882	2.090
90	6.779	3.8488	3.400	7.0950	8.767	4.039	6.342	5.155
100	0.066	3.1546	3.499	5.6395	4.847	4.440	3.982	4.343
110	9.188	2.5884	7.473	4.8674	5.368	4.121	8.908	6.858
120	5.514	4.6388	5.196	12.0064	6.336	2.488	4.045	9.107
130	6.316	6.4989	5.224	6.3022	3.715	5.001	1.701	8.156
140	8.007	3.7892	6.914	11.6202	8.716	4.444	4.214	8.280
150	12.727	10.5960	7.434	7.0158	6.272	0.376	2.050	9.837
160	17.744	9.3026	10.132	3.1982	12.535	6.074	5.714	10.963
170	14.913	14.7958	8.406	10.5038	19.933	7.638	8.626	5.269
180	16.069	17.8791	10.888	10.3038	14.071	9.733	5.069	8.819
MEAN	6.408	4.804	5.873	5.875	6.676	4.644	4.439	5.922

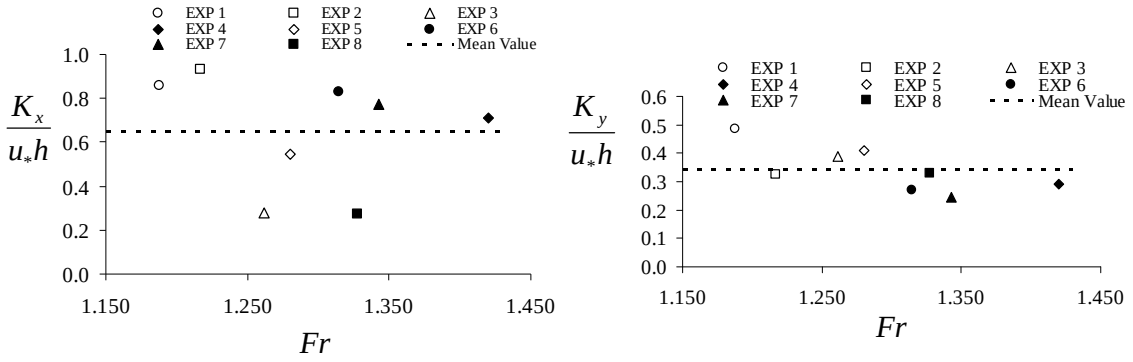

Figure 3.13 Relation of non-dimensional diffusion coefficients and Froude number

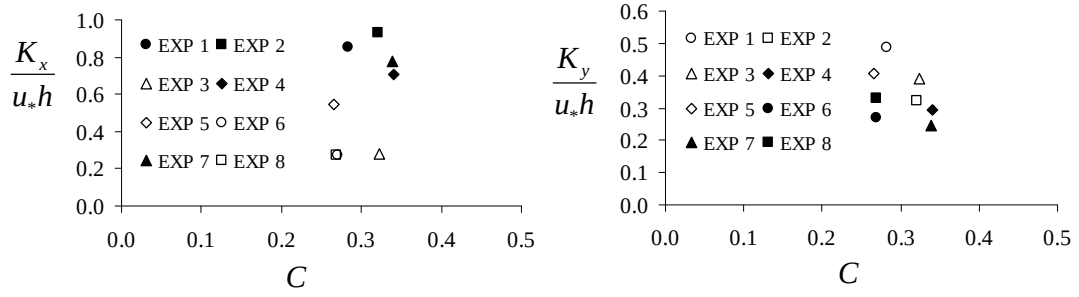

Figure 3.14 Relation of non-dimensional diffusion coefficients and sediment concentration

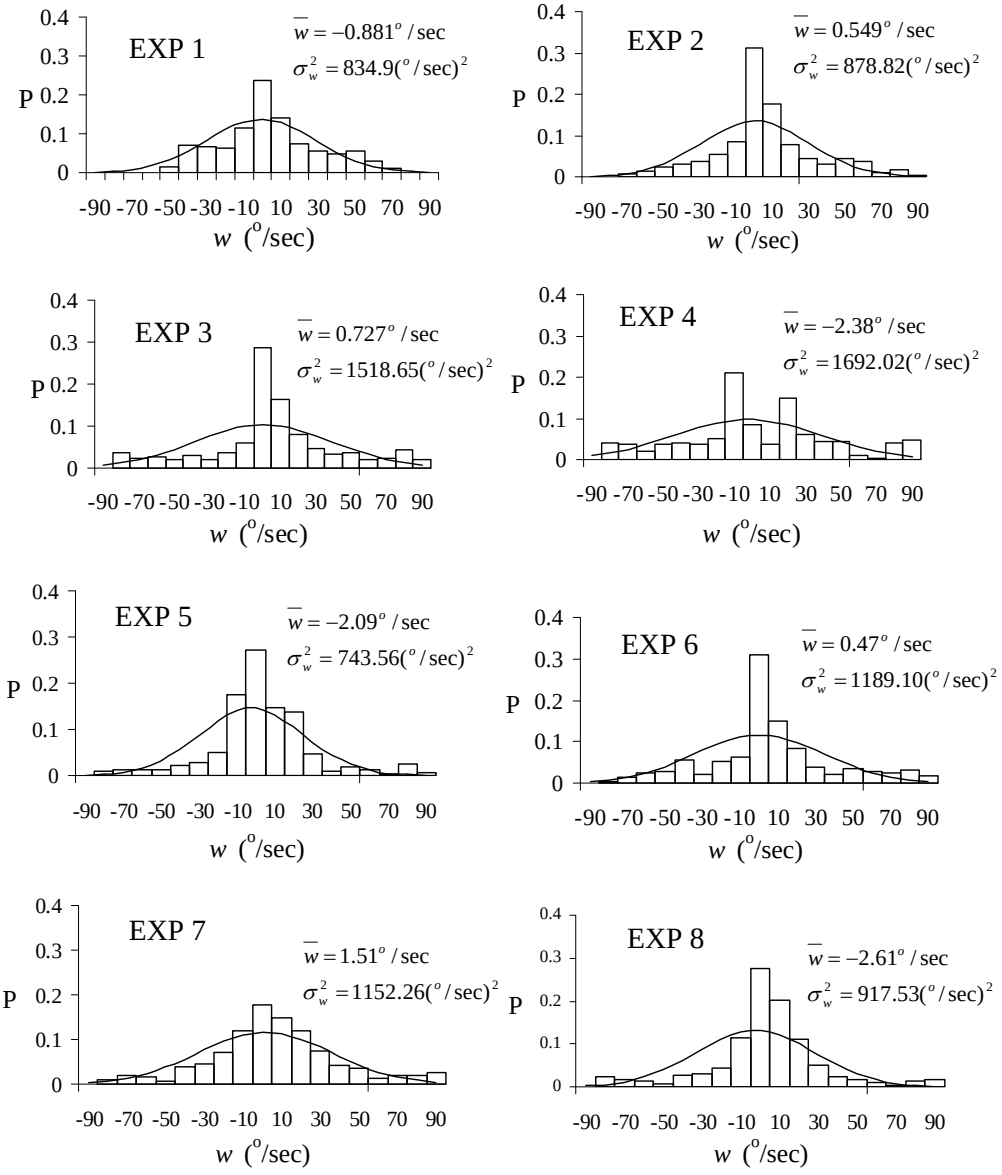

Figure 3.15 Frequency distribution of the rotational angular velocities of the driftwood

each section. The frequency distributions of the longitudinal and transverse positions of the pieces of driftwood are well explained by the normal distribution.

The average values of the longitudinal and transverse diffusion coefficients, K_x and K_y, of each experiments are shown in Table 3.1. The average values of the non-dimensional diffusion coefficients of eight experiments, $K_x / u_* h = 0.649$ and $K_y / u_* h = 0.343$ are obtained. The relations of non-dimensional diffusion coefficients with Froude number and sediment concentration of the flow are shown in Figure 3.13 and Figure 3.14, respectively.

3.5.3 Rotational angle of driftwood

To obtain the frequency distributions of the rotational angular velocities of the driftwood, the range of angular velocity from -90 deg/sec to 90 deg/sec was divided with Δw=10 deg/sec interval in to m number of divisions. The frequency distribution of the rotational angular velocity, P, is evaluated as

$$P = \sum_{i=1}^{18} N_{i,j} \Big/ \sum_{i=1}^{18} \sum_{j=1}^{m} N_{i,j} \tag{3.95}$$

in which i is measurement sections (x =10, 20, …..,180, 18 sections), j is the division of angular velocity, $N_{i,j}$ is the number of driftwood pieces which change in angular velocity for i section in each of j division of angular velocity.

The frequency distributions of the rotational angular velocities of the driftwood obtained experimentally is shown in Figure 3.15, in which solid line is calculated by assuming the normal distribution with the experimentally determined values of the parameters, the mean, $\overline{\omega}$ and variance, σ_w^2. The frequency distributions of the rotational angular velocities of pieces of driftwood are well explained by the normal distribution. The values of mean, $\overline{\omega}$, and standard deviation, σ_w, of rotational angular velocity of the driftwood for each experiments are given in Table 3.1. The mean angular velocity of the driftwood pieces is approximately zero, $\overline{\omega} \approx 0$. The standard deviation appears to be prescribed by the hydraulic parameters, and it is related to the Froude number. The reason why the Froude number is related to the standard deviation of the

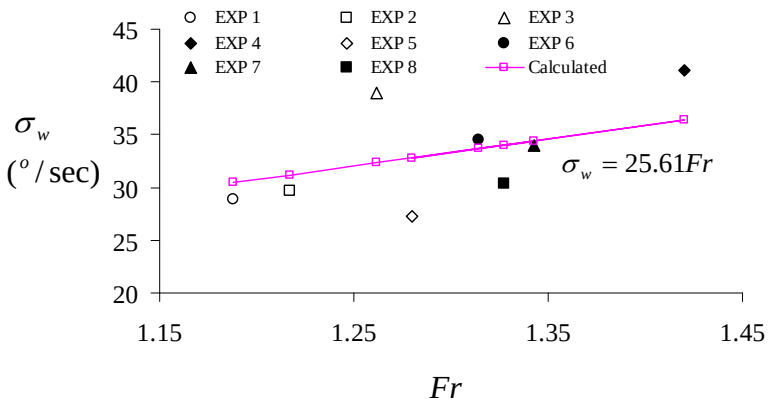

Figure 3.16 Relation of Froude number, Fr , to standard deviation, σ_w, of the rotational angular velocities of the driftwood

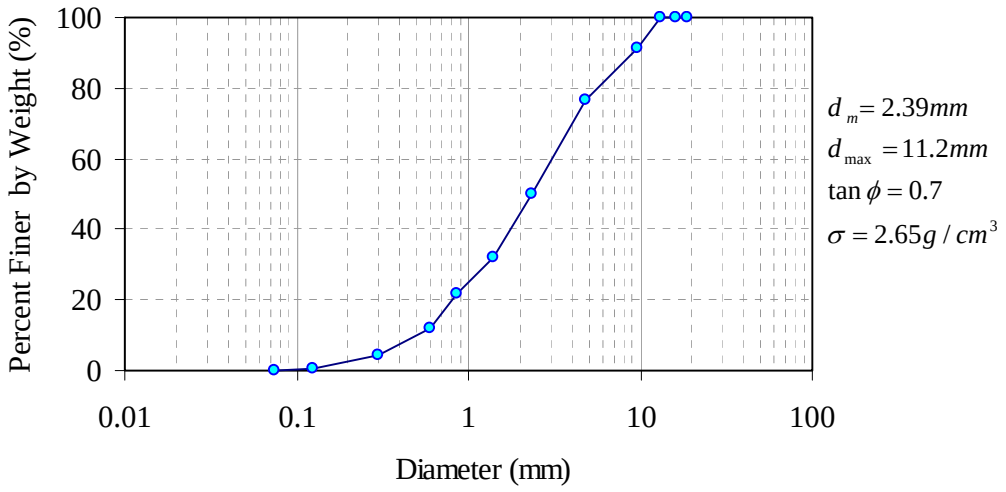

Figure 3.17 Particle size distribution curve for experiment of debris flow with driftwood

rotational angular velocity is not clear; but, as the flow field of driftwood is restricted on the flow surface, its fluctuation, which is related to the Froude number, affects the rotational motion of the driftwood (Nakagawa et al., 1994). The relation between the Froude number, Fr , and the standard deviation of the rotational angular velocity of the driftwood, σ_w , is shown in Figure 3.16, and the relation is obtained as $\sigma_w = 25.61Fr$ from the regression analysis of the values obtained in the hydraulic experiments.

3.6 Experiments of debris flow with driftwood

To investigate the flow characteristic of debris flow with driftwood and the verification of the model, a series of experiments were carried out. For the experiments, a rectangular flume of 5m long, 10cm wide and 13cm deep was used. The experiments were carried out for flume slope of 18 degrees and 20 degrees. A sediment bed of 1.9m long and 7cm deep was positioned from 2.8m to 4.7m upstream measured from the outlet of the flume. Sediment materials with mean diameter $d_m = 2.39$mm, maximum diameter d_{max}=11.2mm, $\tan\phi = 0.7$ and sediment density σ = 2.65g/cm^3 were used. The sediment materials were prepared by mixing the uniformly distributed different sizes of silica sands and gravels. The particle size distribution of the sediment bed is shown in Figure 3.17. Cylindrical pieces of 38 driftwood pieces (Ramin wood, $\rho_d = 0.785$g/cm^3) were positioned on the sediment bed at intervals of 10cm c/c along the downstream direction from 7.5cm downstream from the upstream end of the sediment bed in

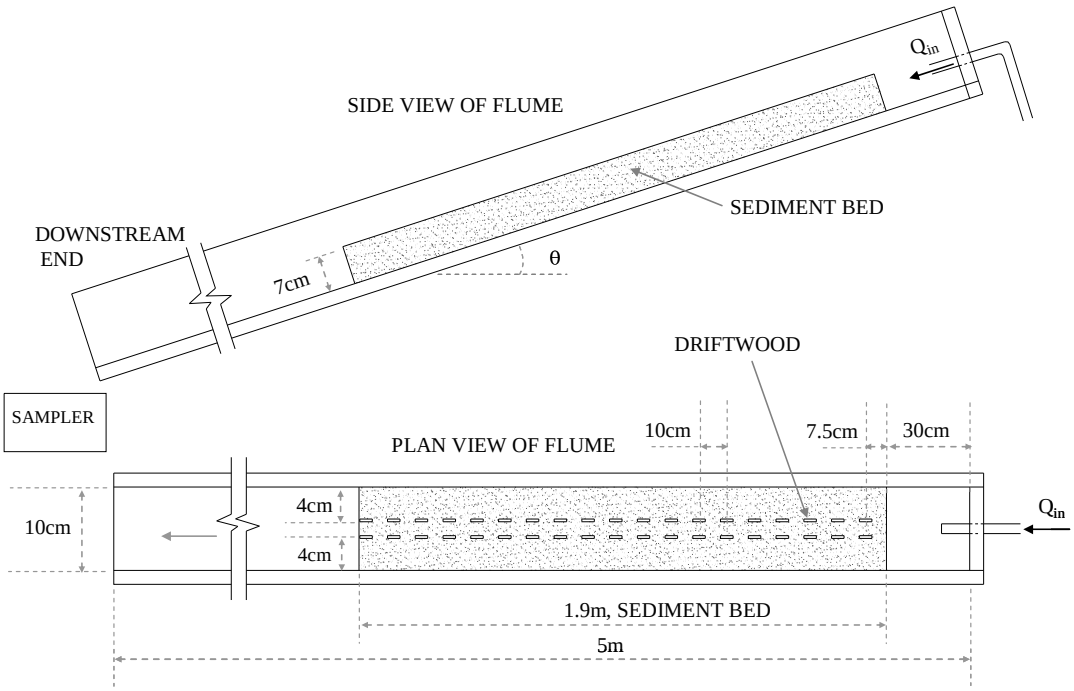

Figure 3.18 Experimental setup and positions of the driftwood for the experiments of debris flow with driftwood

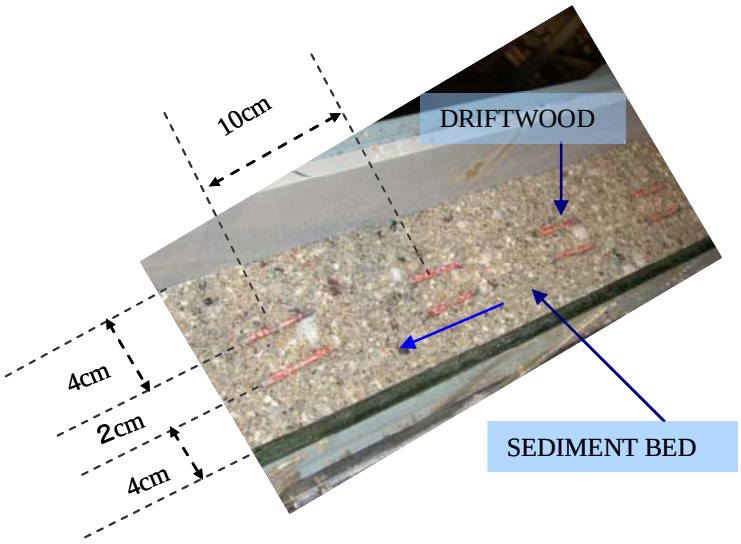

Figure 3.19 Photo of the driftwood position on the sediment bed

two columns 2cm apart as shown in Figure 3.18 and Figure 3.19. The sediment bed was saturated by water. Debris flow was produced by supplying a constant water discharge 270cm^3/sec for 10sec from the upstream end of the flume. The experiments were carried out for driftwood pieces of diameter 3mm and 4mm with 3.5cm, 4.0cm and 4.5cm in length.

The experiments were repeated three times under the same identical conditions, because the sediment composition and degree of saturation might not be uniform throughout the sediment layer. The flow discharge and outflow of the driftwood at the downstream end of the flume were determined by collecting outflow discharge using series of manually movable sampler boxes. The flow motion of driftwood at forefront of debris flow is shown in Figure 3.20.

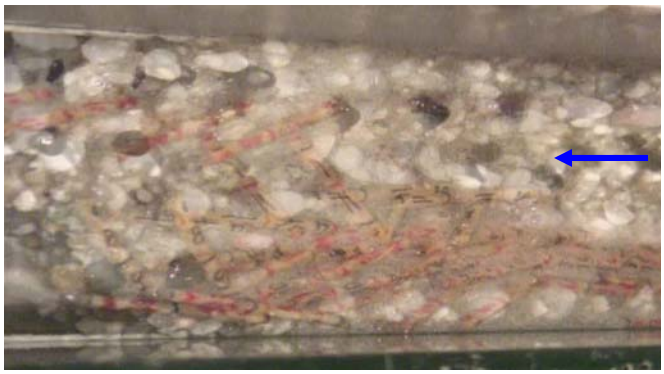

Figure 3.20 Flow motion of driftwood at forefront of debris flow

3.7 Results and discussions

The numerical simulations and experiments were performed to determine the characteristics of debris flow with driftwood. The parameters of the numerical simulation are as follows; $\Delta x =$ 5cm, $\Delta y =$ 1cm, $\Delta t =$ 0.001sec, $\rho =$ 1.0g/cm^3, $\rho_m =$ 1.15g/cm^3, $g =$ 980cm/sec^2, $C_3 =$ 0.48, $n =$0.04, $C_* = C_{*L} = C_{*DL} =$0.65, $C_{*F} =$0, $C_{Dx} =$1.0, $C_{Dy} =$1.0, $\delta_e =$0.0018, $\delta_d =$0.045 and $C_M =$1.0. The outflow condition of the downstream end of the channel was used the drop flow equation M or $N = h\sqrt{2gh}$. It is noted that in the calculations concentration of a fine sediment $C_F = 0$.

The numerical simulations were carried out for the series of experimental cases. A numerical simulation model was developed with an interacting combination of Eulerian expression of the debris flow and Lagrangian expression of the driftwood, in which the fluctuation components of the driftwood position and the rotational angular velocity of the driftwood were dealt with as random variables based on the results of a statistical analysis of experimental values. The scattering process of driftwood in the flow field was supposed to be treated as diffusion process.

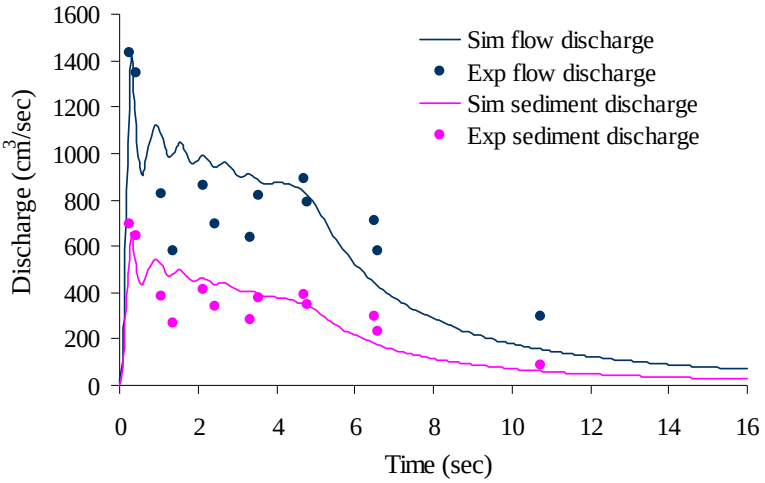

(a) Flow and sediment discharge

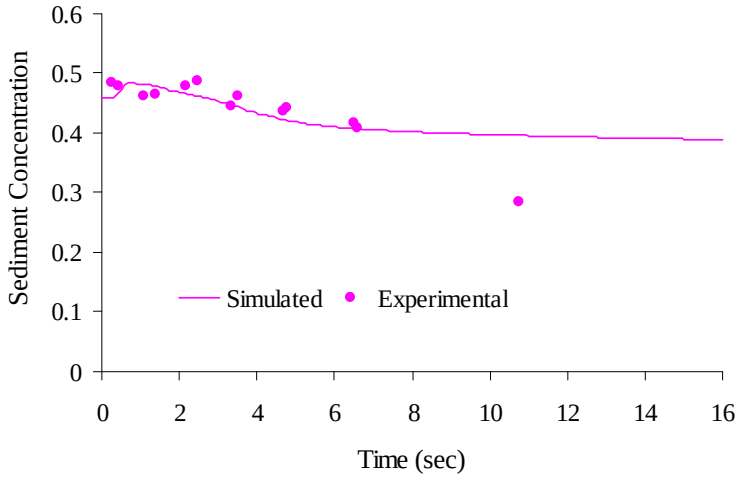

(b) Sediment concentration

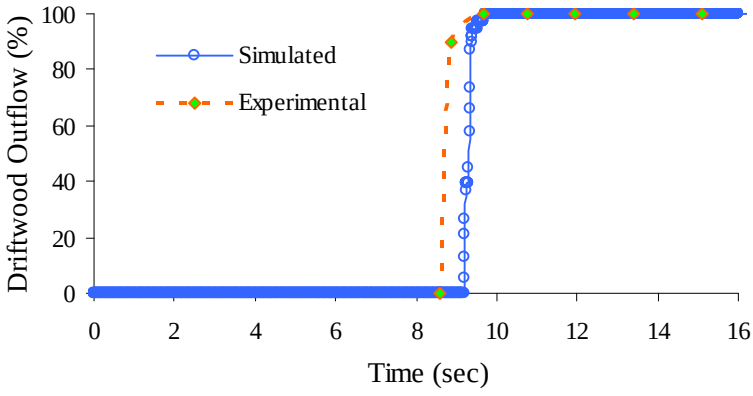

(c) Accumulated percentage of driftwood outflow

Figure 3.21 (a) Flow and sediment discharge, (b) sediment concentration, and (c) driftwood outflow at downstream end, case with driftwood D_d=3mm and L_d =3.5cm, $\theta = 18^o$

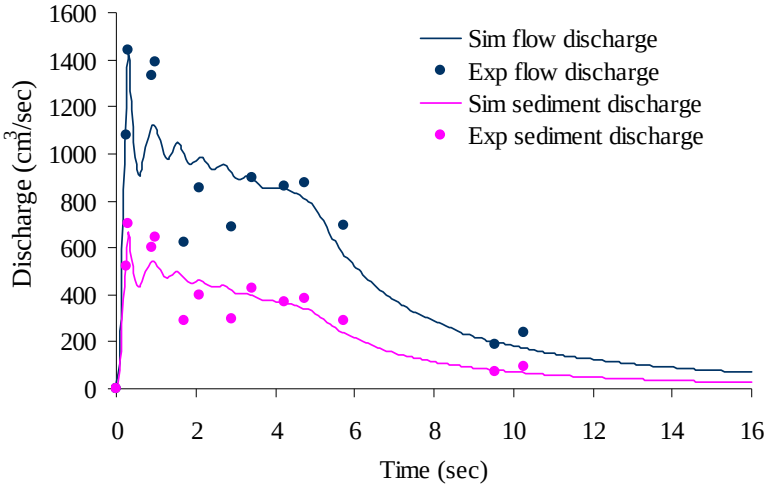

(a) Flow and sediment discharge

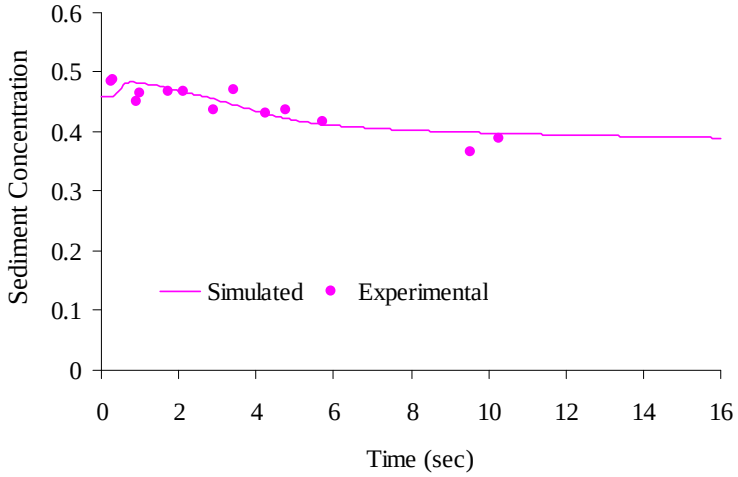

(b) Sediment concentration

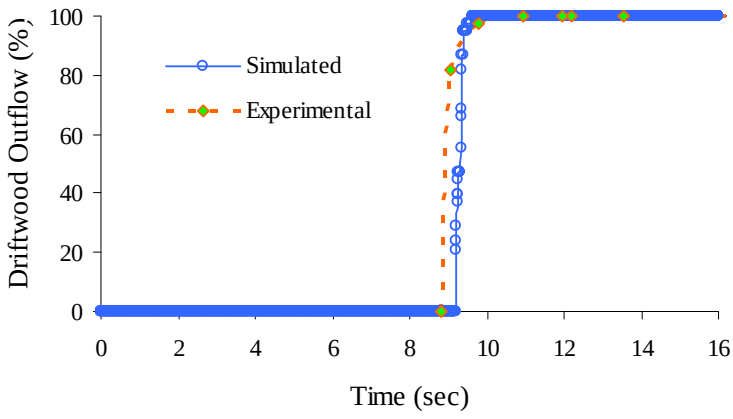

(c) Accumulated percentage of driftwood outflow

Figure 3.22 (a) Flow and sediment discharge, (b) sediment concentration, and (c) driftwood outflow at downstream end, case with driftwood D_d=3mm and L_d =4.0cm, $\theta = 18^o$

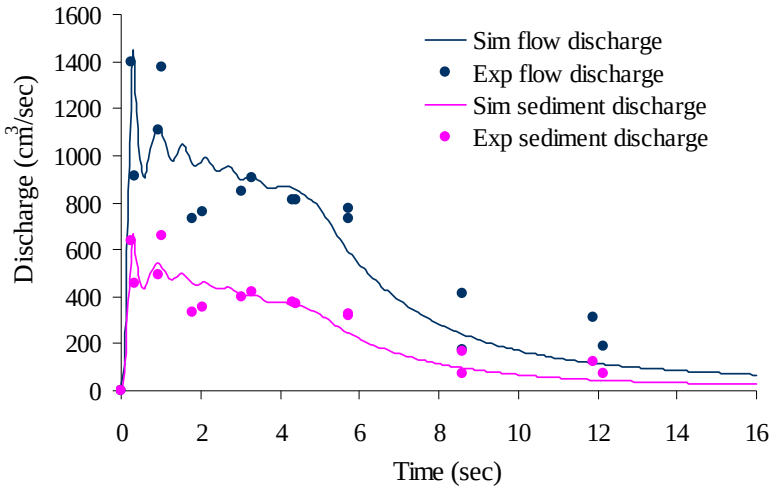

(a) Flow and sediment discharge

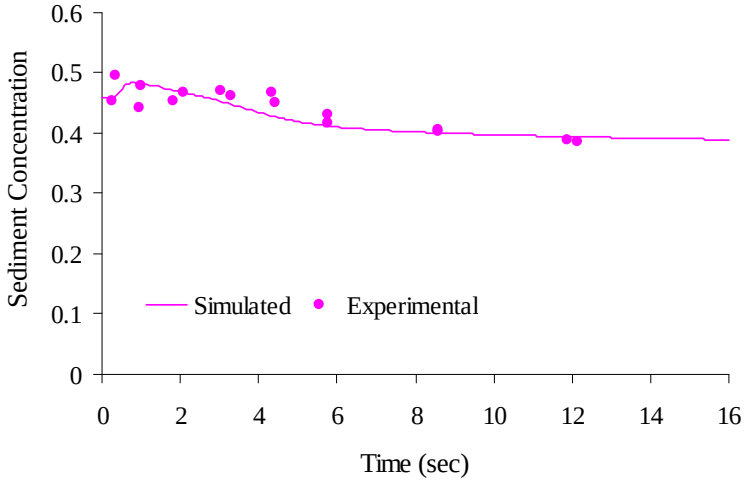

(b) Sediment concentration

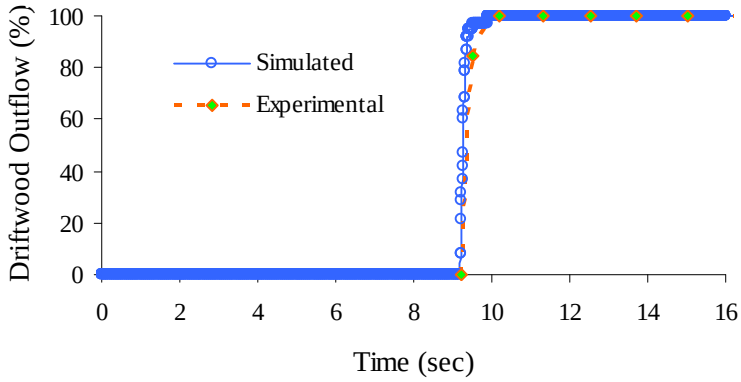

(c) Accumulated percentage of driftwood outflow

Figure 3.23 (a) Flow and sediment discharge, (b) sediment concentration, and (c) driftwood outflow at downstream end, case with driftwood D_d=3mm and L_d =4.5cm, $\theta = 18^o$

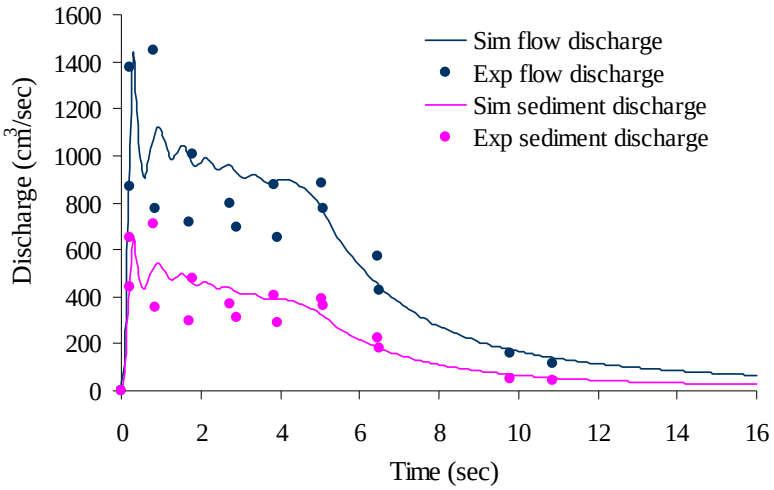

(a) Flow and sediment discharge

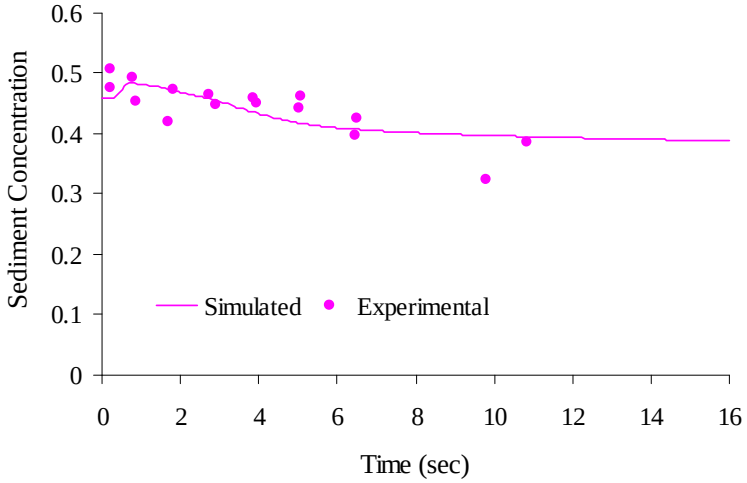

(b) Sediment concentration

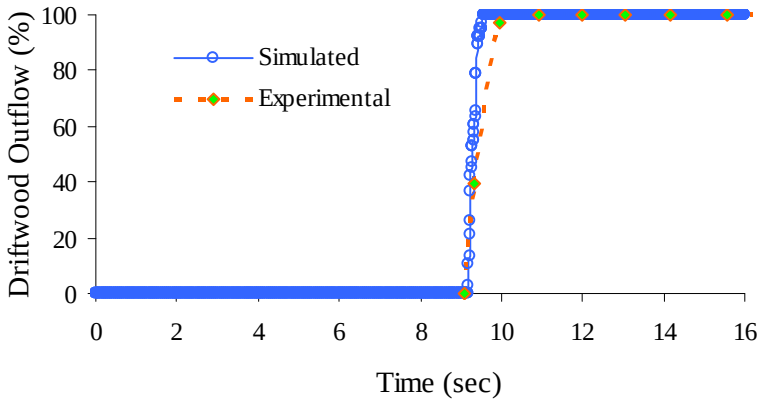

(c) Accumulated percentage of driftwood outflow

Figure 3.24 (a) Flow and sediment discharge, (b) sediment concentration, and (c) driftwood outflow at downstream end, case with driftwood D_d=4mm and L_d=4.5cm, $\theta = 18^o$

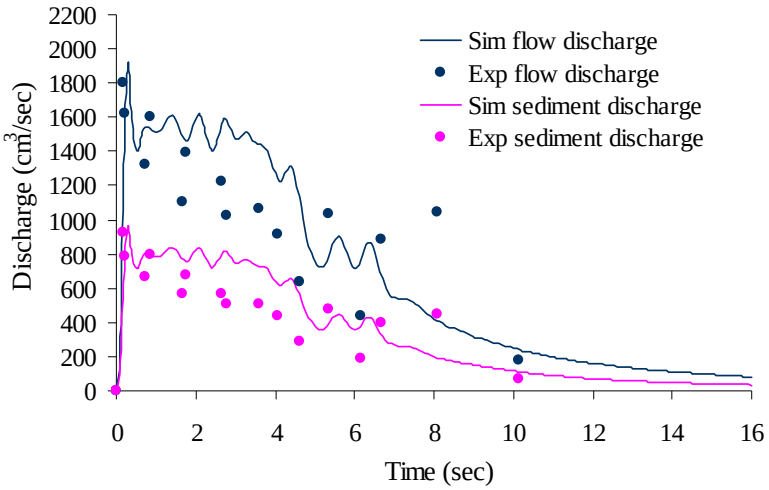

(a) Flow and sediment discharge

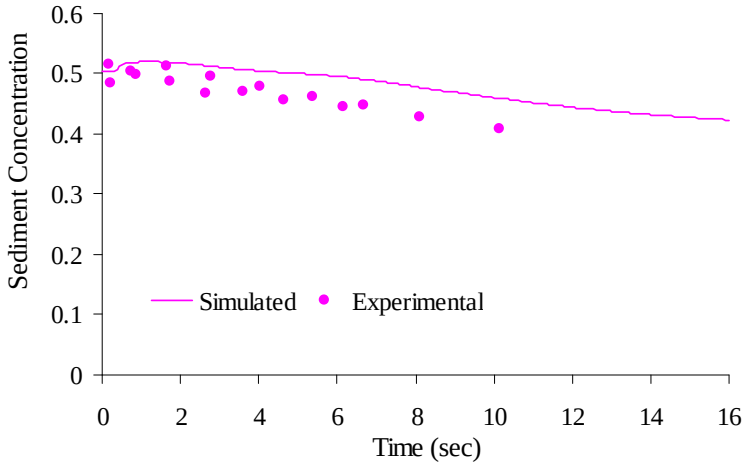

(b) Sediment concentration

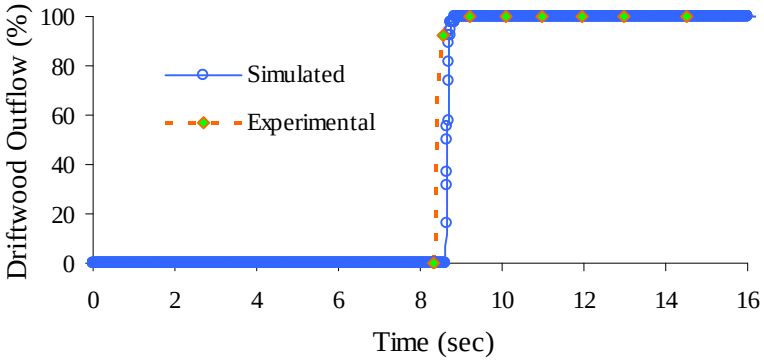

(c) Accumulated percentage of driftwood outflow

Figure 3.25 (a) Flow and sediment discharge, (b) sediment concentration, and (c) driftwood outflow at downstream end, case with driftwood D_d=4mm and L_d =4.5cm, $\theta = 20^o$

The diffusion coefficients and the relation of Froude number to the rotational angular velocity of driftwood were obtained from a statistical analysis of the experimental values. The motion of driftwood was restricted near the flow surface. Thus, the flow motion of driftwood was calculated by using surface velocity components of the debris flow. The driftwood positions and rotational angle of the driftwood were evaluated by deterministically and stochastically.

Figure 3.21 (a) shows the simulated and experimental results of temporal variations of flow and sediment discharge at downstream end of the flume for flume slope 18 degrees, in case of driftwood D_d=3mm and L_d=3.5cm. The temporal change in the sediment concentration of the debris flow discharge is shown in Figure 3.21 (b) and the sediment concentration is found higher in frontal part of the flow. The simulated results of flow discharge, sediment discharge and the sediment concentration of the debris flow are in good agreement with the experimental results. The simulated and experimental results of the percentage of temporal driftwood outflow at the downstream end of the flume are shown in Figure 3.21 (c). The percentage of driftwood outflow is the ratio of the number of pieces of driftwood outflow at the downstream end to the total amount of driftwood (38 pieces) supplied at the inflow boundary. The simulated result of percentage of temporal driftwood outflow is agreeable with the results obtained from the experiment.

Similar results of outflow discharge, sediment concentration and the percentage of driftwood outflows at the downstream end with flume slope 18 degrees for the cases with driftwood D_d=3mm and L_d=4.0cm, D_d=3mm and L_d=4.5cm, and D_d=4mm and L_d=4.5cm are shown in Figure 3.22, Figure 3.23 and Figure 3.24, respectively. Figure 3.25 shows the simulated results of flow discharge, sediment concentration and the percentage of driftwood outflow for flume slope 20 degrees with driftwood D_d=4mm and L_d=4.5cm case. The simulated results of flow discharge, sediment concentration and the percentage of driftwood outflow at the downstream end of the flume are agreeable with the experimental results.

The driftwood positions and the rotational angle of the driftwood were determined by proposed numerical simulation model. In all the cases, the simulated results of driftwood outflow time at the downstream end of the flume are close to the results obtained from the experiments. Thus, the positions and rotational angle of the driftwood dealt with deterministically and stochastically are well explained in the simulations.

Summary

Numerical simulations and experimental works were carried out to determine the characteristics of debris flow with driftwood. A two-dimensional numerical model was developed for computing the characteristics of debris flow with driftwood. Equations of the rotational motion and the translational motion of driftwood were evaluated dynamically in the Lagrangian form. A numerical model was developed with an interacting combination of Eulerian expression of the debris flow and Lagrangian expression of the driftwood, in which the fluctuation components of the position and the rotational angular velocity of the driftwood were dealt with stochastically. The position and rotational angular velocity of the driftwood fluctuated due to the collision of driftwood with boulders and disturbances on the flow surface during the collision of the sediment particles, which were considered in the diffusions coefficients. The scattering process of driftwood was described as a diffusion process and the diffusion coefficients were defined by the hydraulic experiments. The calculated results of frequency distribution of the longitudinal positions, the transverse positions and the rotational angular velocities of the driftwood are fairly good agreement with the experimental results. The simulated results of outflow discharge, sediment concentration and the percentage of driftwood outflow at the downstream end of the flume are in good agreement with the experimental results.

Chapter 4

Capturing Process of Debris Flow with Driftwood

4.1 Introduction

Based on the observations of past experiences it is clear that the greatest damage has occurred when the debris flow flows with driftwood. Thus the countermeasures should be aimed at the linking the measures for debris flow and driftwood outflows. There is a close relationship between countermeasure of driftwood and debris flow control. Open type check dams such as grid type or slit type check dams are commonly used for debris flow control and capturing driftwood because they are preferable over closed type check dams for conserving the natural environment and landscape of mountain torrents as much as possible (Mizuyama and Mizuno, 1997). In the debris flow section where driftwood is assumed to flow down with a debris flow, both of them are captured together by open type check dam. Debris flow may be captured due to jamming of driftwood on grid or slit type check dams. Therefore, it is very important to study on capturing process of debris flow with driftwood by open type check dams. Figure 4.1 shows the debris flow and driftwood captured by check dams.

Agi River, Nakatsugawa, Gifu Prefecture, Japan, September 2000

Tenryu River, Okaya city, Nagano Prefecture, Japan, July 2006

Figure 4.1 Photographs of debris flow and driftwood captured by check dams

(*Source: Sabo department, MLIT, Japan)*

Debris flow control by check dams considering sediments of the flow only is reported in many numerical and experimental studies (Honda and Egashira, 1997; Takahashi et al., 2001b; Wang, 2001; Shrestha, 2004; Satofuka and Mizuyama, 2006; Osti and Egashira, 2008). Only very few research works on debris flow and driftwood capturing by check dams have been carried out (Ozaki et al., 1998; Doi et al., 2000). Furthermore, these studies are limited to the experimental study only.

The capturing process of debris flow with driftwood by open type check dams such as grid or slit type check dams is presented. The jamming of driftwood on open type check dams is evaluated based on the geometric conditions and probabilistic approaches. A deposition velocity model is also presented to calculate the debris flow deposition due to driftwood jamming on open type check dams. To simulate the debris flow with driftwood capturing by open type check dams, a driftwood jamming model and a model of sediment deposition behind check dam, are incorporated in a two-dimensional flow model of the debris flow with driftwood. The results of outflow discharge and the percentage of driftwood outflows at the downstream end of the flume are compared with those obtained from the hydraulic model experiments.

4.2 Experiments of debris flow with driftwood capturing

To investigate the capturing process of debris flow with driftwood and the verification of the model, a series of experiments were carried out. A rectangular flume of 5m long, 10cm wide and 13cm deep was used for the experiments. The experiments were carried out for flume slope of 18 degrees and 20 degrees. A sediment bed of 1.9m long and 7cm deep was positioned from 2.8m to 4.7m upstream measured from the outlet of the flume. The particle size distribution of the sediment bed is shown in Figure 3.17. Cylindrical pieces of 38 driftwood pieces were positioned on the sediment bed at intervals of 10cm c/c along the downstream direction from 7.5cm downstream from the upstream end of the sediment bed in two columns 2cm apart as shown in Figure 3.18 and Figure 3.19. Check dams were set at 20cm upstream from the downstream end of the flume as shown in Figure 4.2. The sediment bed was saturated by water. Debris flow was produced by supplying a constant water discharge 270cm^3/sec for 10sec from the upstream end of the flume. The experiments were carried out for driftwood pieces of diameter 3mm and 4mm with 3.5cm, 4.0cm and 4.5cm in length. The length and diameter of driftwood were determined based on the clear opening of check dam and availability of the experimental flume size. The experiments were carried out for grid dam and slit dam cases.

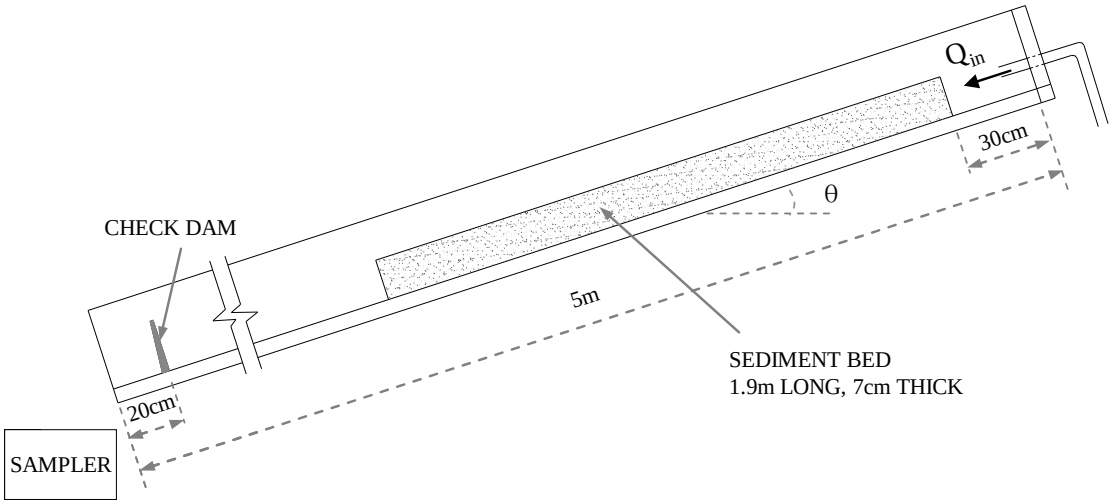

Figure 4.2 Check dam setup in the experimental flume

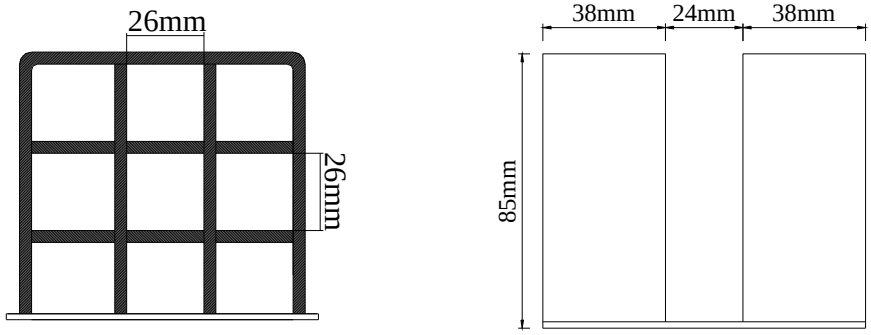

(4mm column/beam diameter)

(a) Grid dam

(b) Slit dam

Figure 4.3 Details of the check dams (a) Grid dam, (b) Slit dam

For effective capturing of debris flow by clogging of large boulders on open type check dam, the ratio of the open spacing of grid or slit dam, L_g or b (L_g =open spacing of grid dam, b = open spacing of slit dam), to the maximum size of sediment should be within the range of 1.5 ~ 2 (i.e., L_g/d_{max}=1.5 ~ 2) (Ashida and Takahashi, 1980). To investigate the jamming of driftwood on open type check dams, clear open spacing of the grid or slit dam was determined by making $L_g/d_{\max} > 2$ or $b/d_{\max} > 2$ to prevent clogging of the open spaces of grid or slit dam by large boulders (i.e., $L_g/d_{\max} = 2.32$ and $b/d_{\max} = 2.14$). Figure 4.3 shows the details of grid or slit

dam used for the experiments. The details of the experimental conditions are shown in Table 4.1. The experiments were repeated three times under the same identical conditions. The flow discharge and driftwood outflows at the downstream end of the flume were determined by collecting outflow discharge using series of manually movable sampler boxes. The jamming of driftwood and deposition upstream of check dams were evaluated by capturing the images shot by video cameras located at side, front and above the downstream end of the flume.

Table 4.1 The experimental conditions of debris flow with driftwood

S. No.	Exp. Ref.	Supply discharge (cm^3/sec)	Flume slope θ (deg)	Check dam type	Diameter of driftwood (mm)	Length of driftwood (mm)	Remarks
1	D5	270	18	Grid dam	-	-	
2	D6	270	18	-	-	-	
3	D7	270	18	Grid dam	3	35	
4	D8	270	18	Grid dam	3	40	
5	D9	270	18	Grid dam	3	45	
6	D10	270	18	Grid dam	4	35	
7	D11	270	18	Grid dam	4	40	
8	D12	270	18	Grid dam	4	45	
9	D13	270	18	Slit dam	3	35	
10	D14	270	18	Slit dam	3	40	
11	D15	270	18	Slit dam	3	45	
12	D16	270	18	Slit dam	4	35	
13	D17	270	18	Slit dam	4	40	
14	D18	270	18	Slit dam	4	45	
15	D19	270	18	Slit dam	-	-	
16	D20a	270	18	-	3	35	
17	D20b	270	18	-	3	40	
18	D20c	270	18	-	3	45	
19	D20d	270	18	-	4	35	
20	D20e	270	18	-	4	40	
21	D20f	270	18	-	4	45	
22	D21	270	20	Grid dam	3	35	
23	D22	270	20	Grid dam	3	45	
24	D23	270	20	Grid dam	4	45	
25	D24	270	20	Grid dam	-	-	
26	D25	270	20	Slit dam	3	35	
27	D26	270	20	Slit dam	3	45	
28	D27	270	20	Slit dam	4	45	
29	D28	270	20	Slit dam	-	-	
30	D29a	270	20	-	3	35	
31	D29b	270	20	-	3	45	
32	D29c	270	20	-	4	45	
33	D30	270	20	-	-	-	

EXP D8

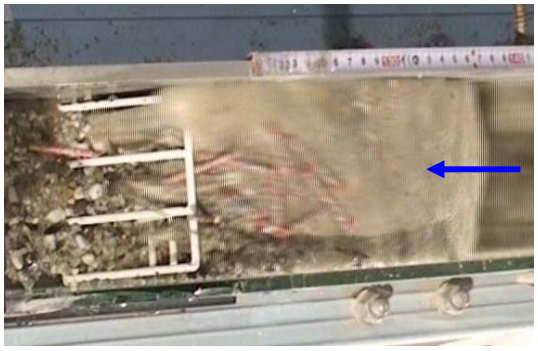

EXP D9

EXP D10

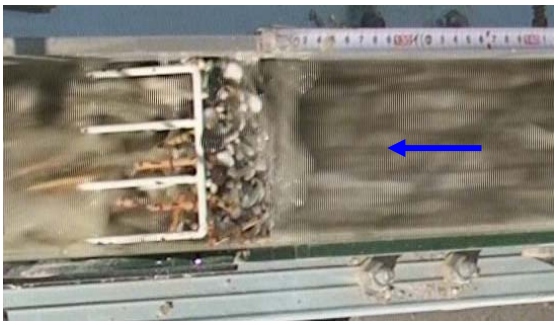

EXP D12

Figure 4.4 Flow motion of driftwood at upstream of grid dam

EXP D10

EXP D12

Figure 4.5 Driftwood and debris flow captured by grid dam

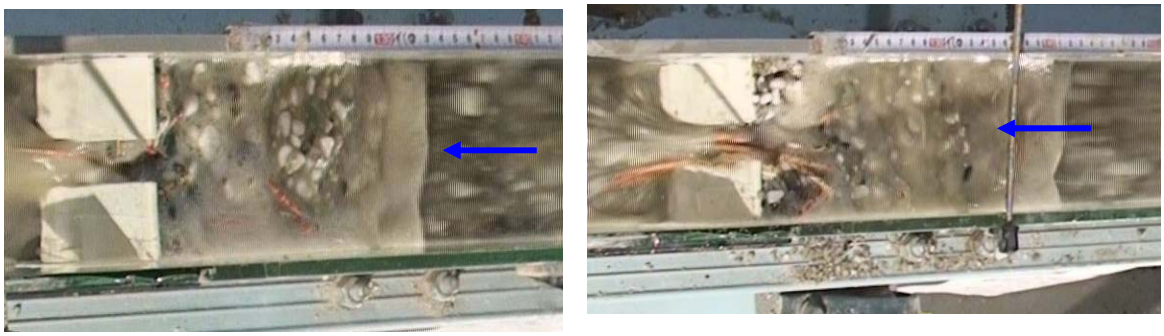

EXP D15　　EXP D17

Figure 4.6 Flow motion of driftwood at upstream of slit dam

EXP D15　　EXP D17

Figure 4.7 Driftwood and debris flow captured by slit dam

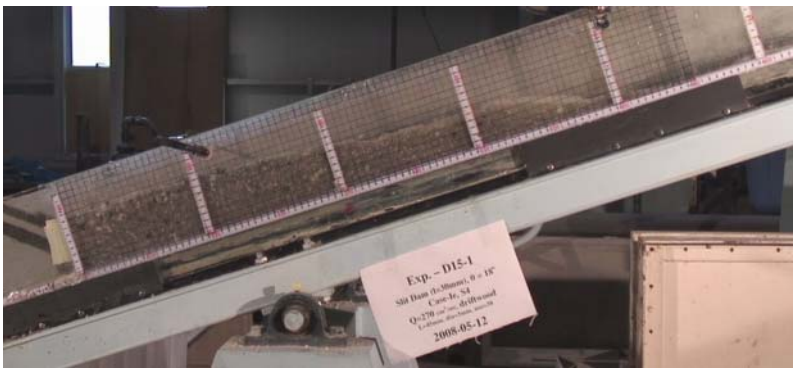

Figure 4.8 Debris flow deposition upstream of grid dam due to dirftwood jamming

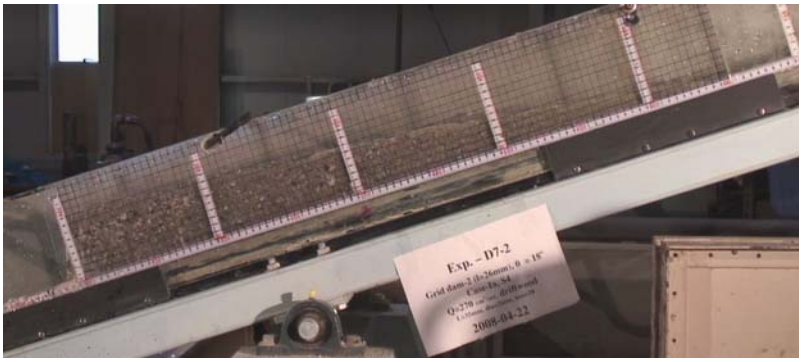

Figure 4.9 Debris flow deposition upstream of slit dam due to dirftwood jamming

Figures 4.4 and 4.5 show the flow motion of driftwood at upstream of grid dam and driftwood jamming, respectively. In the case of slit dam flow motion of driftwood and driftwood jamming are shown in Figure 4.6 and Figure 4.7, respectively. Debris flow deposition due to driftwood jamming on grid type check dam and slit type check dam are shown in Figure 4.8 and Figure 4.9, respectively.

4.3 Jamming of driftwood on open type check dams

When the driftwood is jammed on open space of open type check dam such as grid or slit dam, the sediment is deposited upstream side of the dam. The jamming of driftwood on open type check dams is evaluated based on the geometric conditions and probabilistic approaches.

4.3.1 Jamming of driftwood on grid dam

Four cases are considered as conditions under which driftwood is jammed on open spaces of a grid dam as follows:

(1) A piece of driftwood will be jammed on a grid dam with a large rotational angle (Figure 4.10 (a)). On the basis of the experimental results, it is considered that the rotational angle of the driftwood to be in the range of $80^o \le \theta_k \le 90^o$.

(2) A piece of driftwood will be jammed on a grid dam due to the geometric conditions as $y_{d1} < y_{g1}$ and $y_{d2} > y_{g2}$ (Figure 4.10 (b)).

(3) A piece of driftwood coming from the rear will be also jammed by the pieces of driftwood already jammed on a grid dam (Figure 4.10 (c)). It is considered that when more than five

pieces of driftwood already jammed at previous time level of calculation, all pieces of driftwood coming from the rear are also considered to be jammed on a grid dam.

(4) The pieces of driftwood will be jammed when the number of pieces of driftwood arrival at open spaces of grid dam at same time (Figure 4.10 (d)). In this case, the probability of a piece of driftwood jamming depends on the number of driftwood arrival at grid opening at same time. This probability, $p(n)$, can be assessed in hydraulic experiments with assuming the functions of length (L_d) and diameter (D_d) of driftwood, clear opening between two columns of grid dam (L_g) and number of driftwood (n) arrival at same time. To determine this probability, series of experiments were carried out with different hydraulic conditions. A rectangular flume of 5m long, 10cm wide and 13cm deep was used. A grid dam was set at 20cm upstream from the downstream end of the flume. Debris flow was produced with similar sediment conditions and properties as described in section 4.2. In this case, n (n=1, 2, 3, 4) pieces of driftwood was

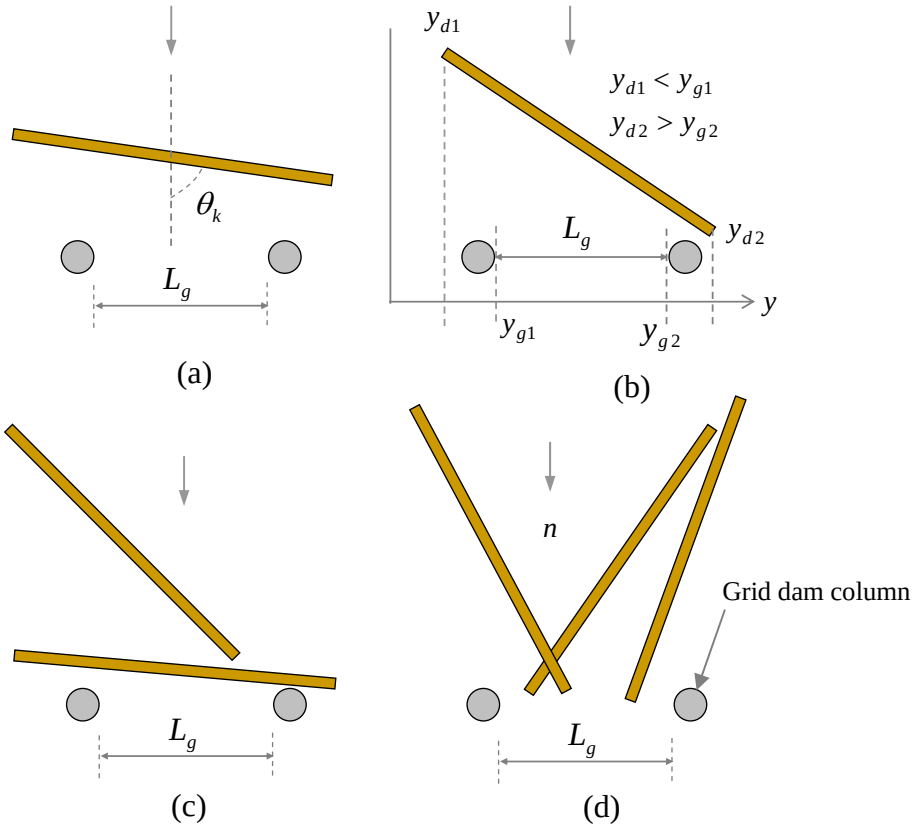

Figure 4.10 Jamming of driftwood on a grid dam

Table 4.2 The summary of experiments and results of jamming probability for grid dam

S. No.	Q (cm^3/sec)	θ (deg)	L_g (mm)	L_d (mm)	D_d (mm)	n	RUN 1		RUN 2		RUN 3		*Avg. P(n)*	Remarks
							N_T	N_b	N_T	N_b	N_T	N_b		
1	270	18	26	35	3	1	10	4	10	4	20	9	0.425	
2	270	18	26	35	3	2	20	8	20	7	40	17	0.400	
3	270	18	26	35	3	3	18	8	18	7	39	16	0.413	
4	270	18	26	35	3	4	24	17	24	15	56	33	0.628	
5	270	18	26	40	3	1	10	3	10	4	21	7	0.341	
6	270	18	26	40	3	2	20	6	20	7	40	17	0.375	
7	270	18	26	40	3	3	21	17	24	14	24	15	0.673	
8	270	18	26	40	3	4	32	20	28	21	32	26	0.729	
9	270	18	26	45	3	1	8	3	13	8	10	7	0.563	
10	270	18	26	45	3	2	20	11	20	11	20	12	0.567	
11	270	18	26	45	3	3	27	18	21	14	27	19	0.679	
12	270	18	26	45	3	4	28	21	32	22	32	20	0.688	
13	270	18	24	35	3	1	12	6	12	7	10	5	0.528	
14	270	18	24	35	3	2	20	9	20	14	20	15	0.633	
15	270	18	24	35	3	3	21	17	24	17	24	18	0.756	
16	270	18	24	35	3	4	28	24	28	18	28	21	0.750	
17	270	18	24	40	3	1	11	6	10	7	10	5	0.582	
18	270	18	24	40	3	2	16	8	16	11	16	10	0.604	
19	270	18	24	40	3	3	18	14	21	14	21	17	0.751	
20	270	18	24	40	3	4	32	25	24	18	28	21	0.760	
21	270	18	24	45	3	1	11	6	10	5	9	4	0.497	
22	270	18	24	45	3	2	14	9	18	10	16	9	0.587	
23	270	18	24	45	3	3	21	14	24	19	24	19	0.750	
24	270	18	24	45	3	4	28	17	28	19	32	25	0.689	
25	310	18	26	35	3	1	10	4	11	5	-	-	0.427	
26	310	18	26	35	3	2	14	10	14	4	-	-	0.500	
27	310	18	26	35	3	3	21	14	21	12	-	-	0.619	
28	310	18	26	35	3	4	32	27	32	20	-	-	0.734	
29	310	18	26	40	3	1	10	4	10	3	-	-	0.350	
30	310	18	26	40	3	2	16	6	16	7	-	-	0.406	
31	310	18	26	40	3	3	21	9	21	13	-	-	0.524	
32	310	18	26	40	3	4	28	21	28	22	-	-	0.768	
33	310	18	26	45	3	1	11	12	11	8	-	-	0.818	
34	310	18	26	45	3	2	18	5	14	7	-	-	0.389	
35	310	18	26	45	3	3	21	10	21	14	-	-	0.571	
36	310	18	26	45	3	4	28	22	28	19	-	-	0.732	
37	270	20	26	35	3	1	8	4	-	-	-	-	0.500	
38	270	20	26	35	3	2	16	8	-	-	-	-	0.500	
39	270	20	26	35	3	3	24	15	-	-	-	-	0.625	
40	270	20	26	35	3	4	20	11	-	-	-	-	0.550	
41	270	20	26	40	3	1	9	4	-	-	-	-	0.444	
42	270	20	26	40	3	2	14	8	-	-	-	-	0.571	
43	270	20	26	40	3	3	18	12	-	-	-	-	0.667	
44	270	20	26	40	3	4	24	17	-	-	-	-	0.708	
45	270	20	26	45	3	1	10	4	-	-	-	-	0.400	
46	270	20	26	45	3	2	10	6	-	-	-	-	0.600	
47	270	20	26	45	3	3	21	14	-	-	-	-	0.667	
48	270	20	26	45	3	4	24	22	-	-	-	-	0.917	
49	270	18	26	45	4	1	20	9	-	-	-	-	0.450	
50	270	18	26	45	4	2	34	23	-	-	-	-	0.681	
51	270	18	26	45	4	3	45	30	-	-	-	-	0.664	
52	270	18	26	45	4	4	56	43	-	-	-	-	0.768	

supplied at 80cm upstream from the grid dam location (n = number of driftwood pieces supplied at a time). Such n pieces of driftwood were supplied for many times (m trials). The summary of experimental conditions and calculated average values of jamming probability, $p(n)$, are shown in Table 4.2, where, N_T (= n x m) is the total number of driftwood pieces supply in m trials, N_b is the total number of driftwood pieces jamming on a grid dam in m trials, and the probability of jamming $p(n)$ is calculated as

$$p(n) = \frac{N_b}{N_T} \tag{4.1}$$

From the regression analysis of values obtained in the experiments, the relation of jamming probability on a grid dam with n number of driftwood arrival at same time is obtained as

$$p(n) = 0.32\left(\frac{L_d}{L_g - D_d}\right)^{0.63} n^{0.3} \tag{4.2}$$

This equation is represented in Figure 4.11 and Figure 4.12 with experimental values. To determine which pieces of driftwood will be jammed, the random variable, q, uniformly distributed in the range (0,1), is generated for each piece of driftwood flowing down the flume. The driftwood is considered to be jammed when the condition $p(n) > q$ is satisfied.

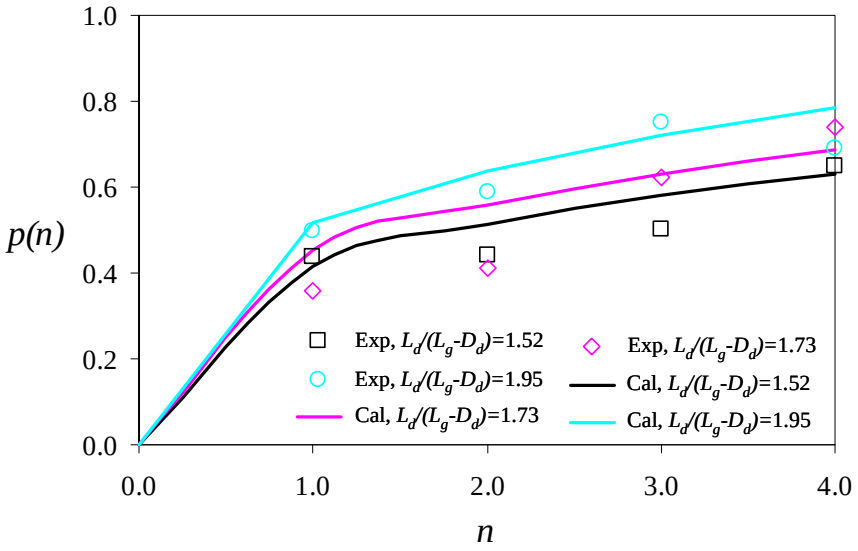

Figure 4.11 Plot of jamming probability, $p(n)$, and number of driftwood arrival, n, using Equation (4.2) with experimental data for grid dam

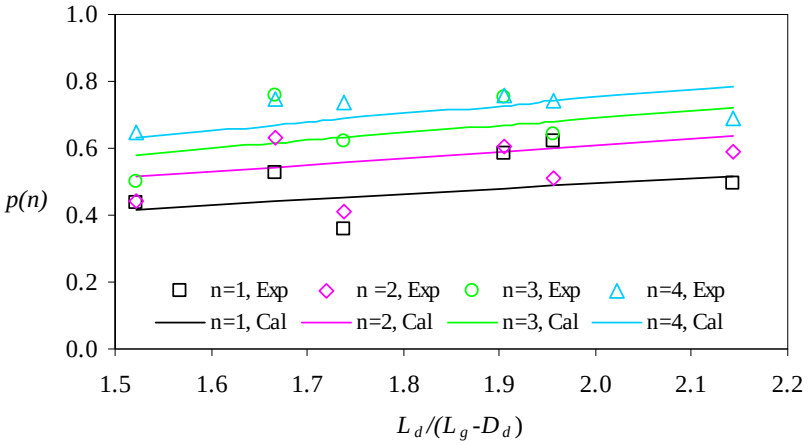

Figure 4.12 Plot of $p(n)$, and $L_d/(L_g - D_d)$, using Equation (4.2) with experimental data for a grid dam

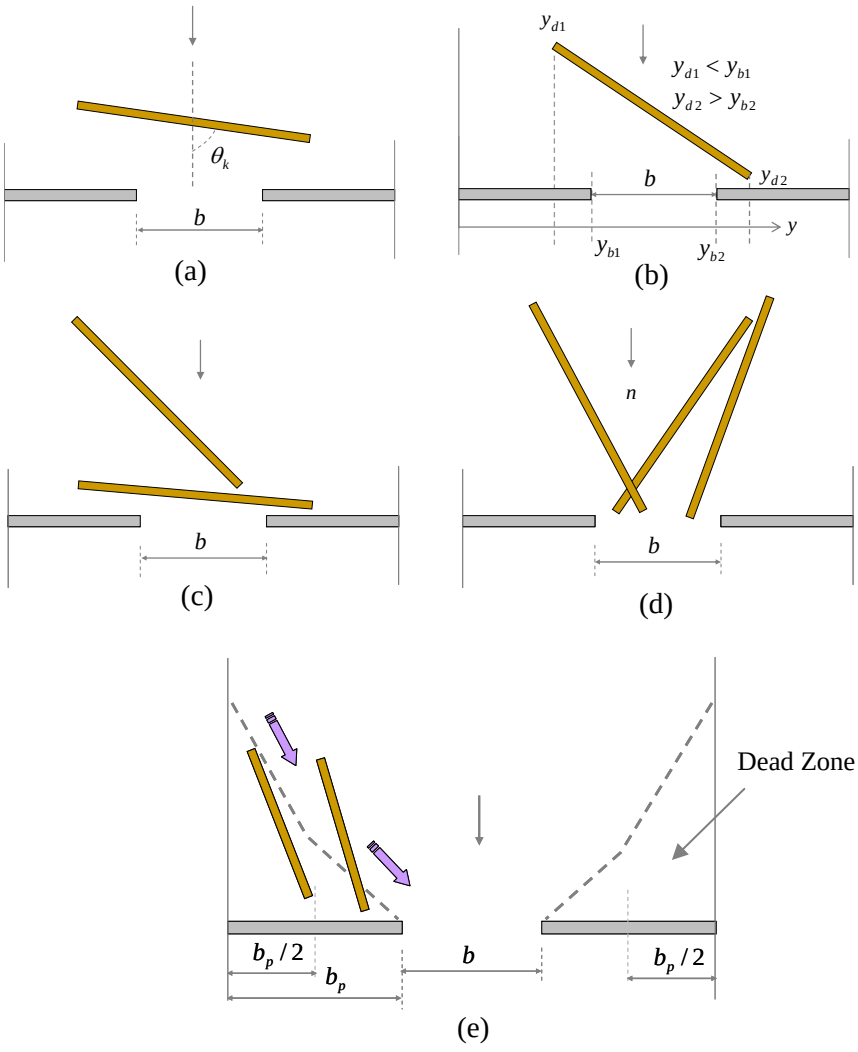

Figure 4.13 Jamming of driftwood on slit dam

Table 4.3 The summary of experiments and results of jamming probability for slit dam

S. No.	Q (cm^3/sec)	θ (deg)	b (mm)	L_d (mm)	D_d (mm)	n	RUN 1		RUN 2		RUN 3		*Avg.* p	Remarks
							N_T	N_b	N_T	N_b	N_T	N_b		
1	270	18	24	35	3	1	11	4	9	4	10	3	0.369	
2	270	18	24	35	3	2	16	8	18	7	16	8	0.463	
3	270	18	24	35	3	3	21	11	21	13	18	12	0.603	
4	270	18	24	35	3	4	28	15	28	18	24	17	0.629	
5	270	18	24	40	3	1	9	5	10	5	9	5	0.537	
6	270	18	24	40	3	2	16	10	16	8	14	8	0.565	
7	270	18	24	40	3	3	21	14	21	13	18	14	0.688	
8	270	18	24	40	3	4	24	18	28	19	28	20	0.714	
9	270	18	24	45	3	1	9	5	10	5	9	3	0.463	
10	270	18	24	45	3	2	14	8	14	7	14	9	0.571	
11	270	18	24	45	3	3	21	15	15	13	21	14	0.749	
12	270	18	24	45	3	4	20	13	20	14	24	18	0.700	
13	270	18	26	35	3	1	10	3	10	4	9	3	0.344	
14	270	18	26	35	3	2	14	6	14	5	14	4	0.357	
15	270	18	26	35	3	3	21	12	21	13	21	10	0.556	
16	270	18	26	35	3	4	24	14	24	15	24	13	0.583	
17	270	18	26	40	3	1	11	4	12	5	8	4	0.427	
18	270	18	26	40	3	2	14	7	14	6	14	5	0.429	
19	270	18	26	40	3	3	18	8	18	9	18	9	0.481	
20	270	18	26	40	3	4	20	11	20	14	20	12	0.617	
21	270	18	26	45	3	1	8	4	9	4	9	5	0.500	
22	270	18	26	45	3	2	14	7	14	8	14	8	0.548	
23	270	18	26	45	3	3	21	13	21	14	21	10	0.587	
24	270	18	26	45	3	4	24	17	24	16	24	17	0.694	
25	310	18	24	35	3	1	10	3	9	3	-	-	0.317	
26	310	18	24	35	3	2	14	9	14	6	-	-	0.536	
27	310	18	24	35	3	3	21	10	21	11	-	-	0.500	
28	310	18	24	35	3	4	20	13	20	10	-	-	0.575	
29	310	18	24	40	3	1	8	4	8	3	-	-	0.438	
30	310	18	24	40	3	2	12	6	12	5	-	-	0.458	
31	310	18	24	40	3	3	18	10	18	12	-	-	0.611	
32	310	18	24	40	3	4	24	15	24	16	-	-	0.646	
33	310	18	24	45	3	1	6	3	8	4	-	-	0.500	
34	310	18	24	45	3	2	14	6	12	7	-	-	0.506	
35	310	18	24	45	3	3	18	9	15	9	-	-	0.550	
36	310	18	24	45	3	4	20	15	20	16	-	-	0.775	
37	270	20	24	35	3	1	7	2	-	-	-	-	0.286	
38	270	20	24	35	3	2	10	4	-	-	-	-	0.400	
39	270	20	24	35	3	3	18	8	-	-	-	-	0.444	
40	270	20	24	35	3	4	16	8	-	-	-	-	0.563	
41	270	20	24	40	3	1	8	3	-	-	-	-	0.375	
42	270	20	24	40	3	2	12	8	-	-	-	-	0.667	
43	270	20	24	40	3	3	18	8	-	-	-	-	0.444	
44	270	20	24	40	3	4	16	10	-	-	-	-	0.625	
45	270	20	24	45	3	1	7	4	-	-	-	-	0.571	
46	270	20	24	45	3	2	10	5	-	-	-	-	0.500	
47	270	20	24	45	3	3	15	11	-	-	-	-	0.733	
48	270	20	24	45	3	4	16	11	-	-	-	-	0.688	
49	270	18	24	35	4	1	7	4	7	3	-	-	0.500	
50	270	18	24	35	4	2	12	8	12	4	-	-	0.500	
51	270	18	24	35	4	3	18	10	18	11	-	-	0.583	
52	270	18	24	35	4	4	20	15	20	10	-	-	0.625	
53	270	18	24	45	4	1	7	5	11	7	-	-	0.675	
54	270	18	24	45	4	2	12	8	12	7	-	-	0.625	
55	270	18	24	45	4	3	15	10	15	9	-	-	0.633	
56	270	18	24	45	4	4	16	10	20	18	-	-	0.763	

4.3.2 Jamming of driftwood on slit dam

In the case of slit dam, some conditions of driftwood jamming are similar to the conditions of grid dam case. Five cases are considered as conditions under which driftwood is jammed on a slit dam as follows:

(1) A piece of driftwood will be jammed on a slit dam with a large rotational angle in the range of $80^o \le \theta_k \le 90^o$ (Figure 4.13 (a)).

(2) A piece of driftwood will be jammed on a slit dam due to the geometric conditions as $y_{d1} < y_{b1}$ and $y_{d2} > y_{b2}$ (Figure 4.13 (b)).

(3) It is also considered that when more than five pieces of driftwood already jammed on open space of slit dam at previous time level of calculation, all pieces of driftwood coming from the rear are also considered to be jammed on a slit dam (Figure 4.13 (c)).

(4) The pieces of driftwood will be jammed when the number of pieces of driftwood arrival at open spaces of slit dam at same time (Figure 4.13 (d)). The probability, $p(n)$, of a piece of driftwood jamming depends on the number of driftwood arrival on open spacing of slit dam (b) at same time. To determine this probability in the case of slit dam, the series of experiments were carried out using slit dam as similar procedure described in grid dam case. Table 4.3 shows the experimental conditions and the calculated results of probability of jamming. From the

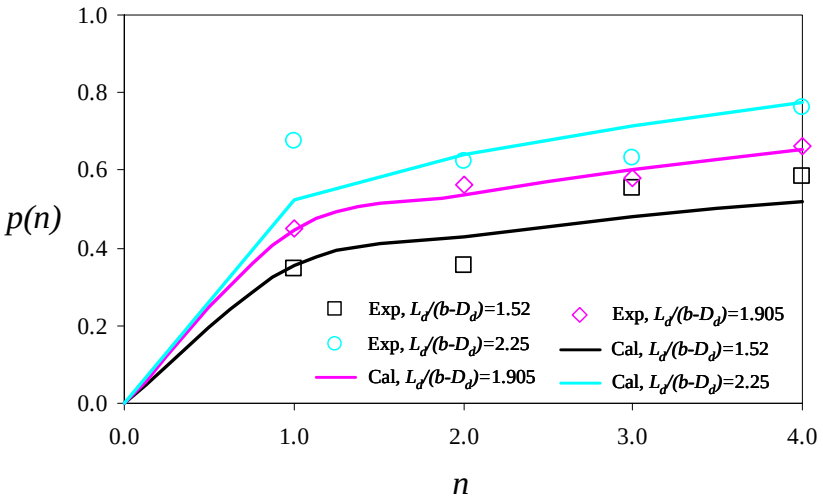

Figure 4.14 Plot of jamming probability, $p(n)$, and number of driftwood arrival, n, using Equation (4.3) with experimental data for slit dam

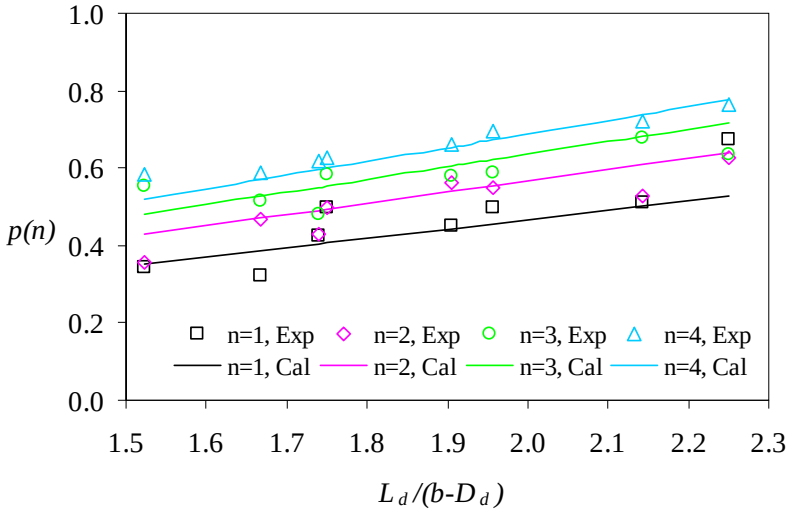

Figure 4.15 Plot of $p(n)$, and $L_d/(b-D_d)$, using Equation (4.3) with experimental data for slit dam

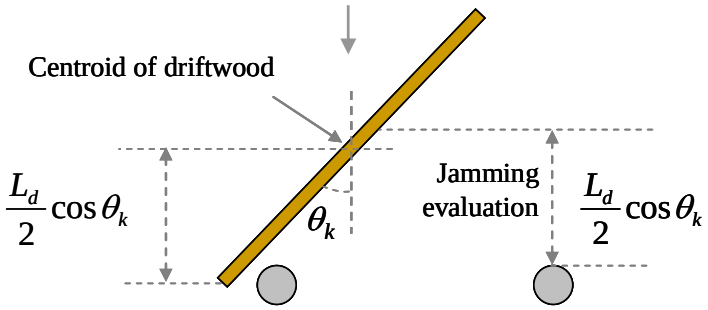

Figure 4.16 Schematic diagram of evaluation of driftwood jamming for grid or slit dam

regression analysis of experimental values, following relation is obtained for slit dam as

$$p(n) = 0.23\left(\frac{L_d}{b-D_d}\right)^{1.02} n^{0.28} \tag{4.3}$$

This equation is represented in Figure 4.14 and Figure 4.15 with experimental values. From the figures, it is clear that the probability of driftwood jamming becomes higher as the number of driftwood arrival at same time increases.

(5) A piece of driftwood will be jammed in impermeable width (b_p) of slit dam when the centroid of the driftwood is located only inside dead zone of flow as shown in Figure 4.13 (e). When the driftwood centroid is located outside of dead zone, it can be carried by coming flow from upstream. In this case, it is considered that when the centroid of a piece of driftwood is located inside half distance of impermeable width ($b_p/2$) from the channel wall, the piece of driftwood is considered to be jammed on slit dam.

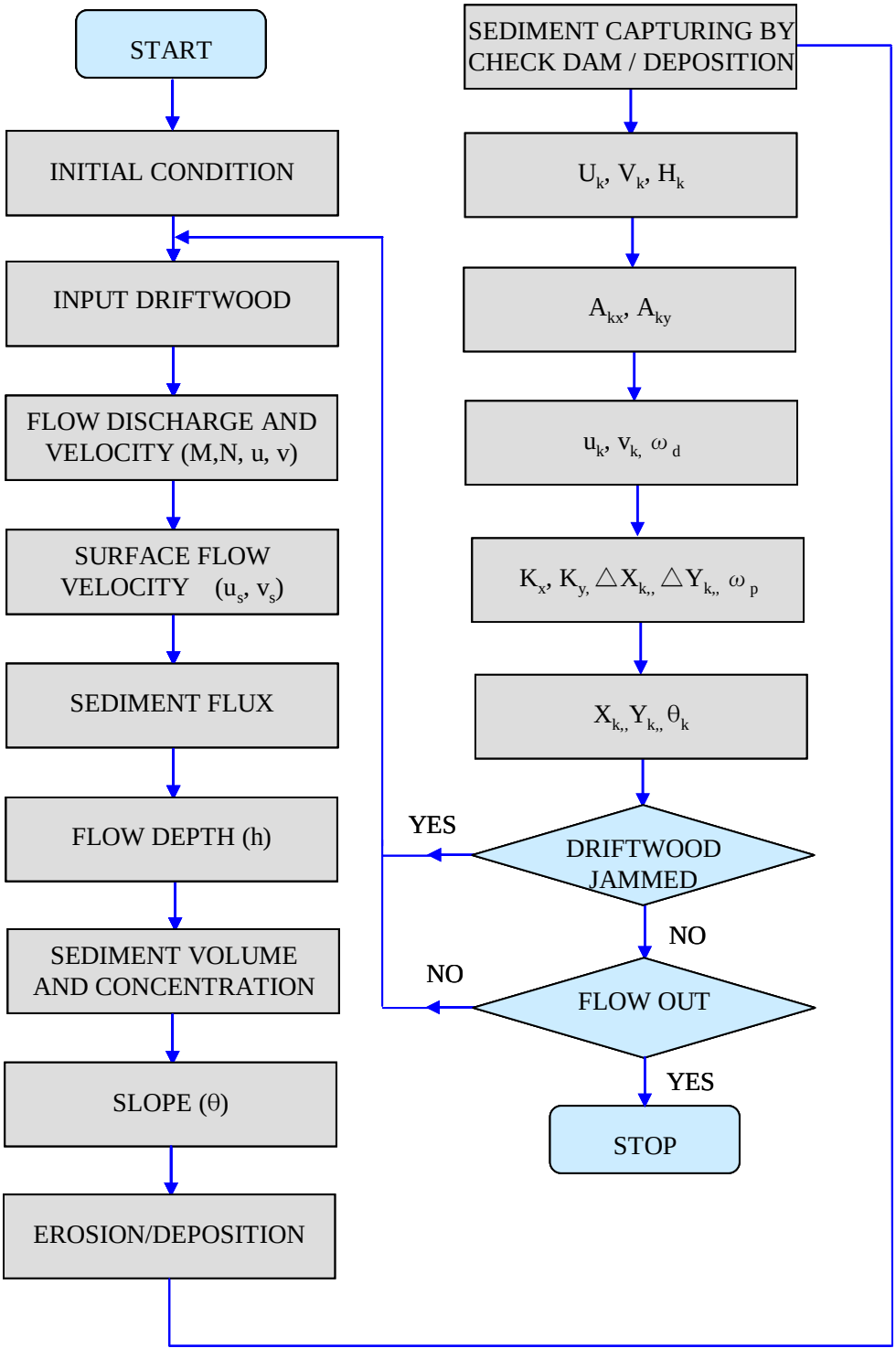

Figure 4.17 Flow chart for the method of simulating driftwood jamming process on open type check dam and sediment deposition behind a dam

The jamming of driftwood on a grid or slit dam is evaluated when the centroid of the driftwood piece is located within the half distance of projected horizontal length of driftwood in flow direction behind a grid or slit dam position as shown in Figure 4.16. Figure 4.17 shows the flow chart for the method of simulating driftwood jamming process and sediment deposition.

4.4 Debris flow deposition model

4.4.1 Debris flow deposition due to jamming of driftwood on grid dam

Due to the jamming of driftwood on a grid dam, sediment is deposited behind the grid dam. Figure 4.18 shows the schematic flow near a grid dam. The effects of the driftwood jamming on debris flow deposition on grid dam is evaluated based on the projected horizontal length of driftwood piece in y direction with its rotational angle and clear spacing of column of grid dam, and the sediment passing rate, P_s, through a grid dam is determined as $P_s = L_o / L_g$ (Figure 4.19 (a)). The deposition velocity, i_{dep}, is derived under the mass conservation law of sediment

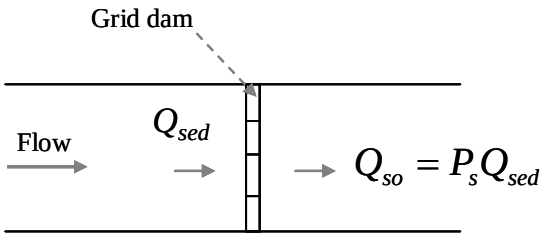

Figure 4.18 Schematic flow model near grid dam

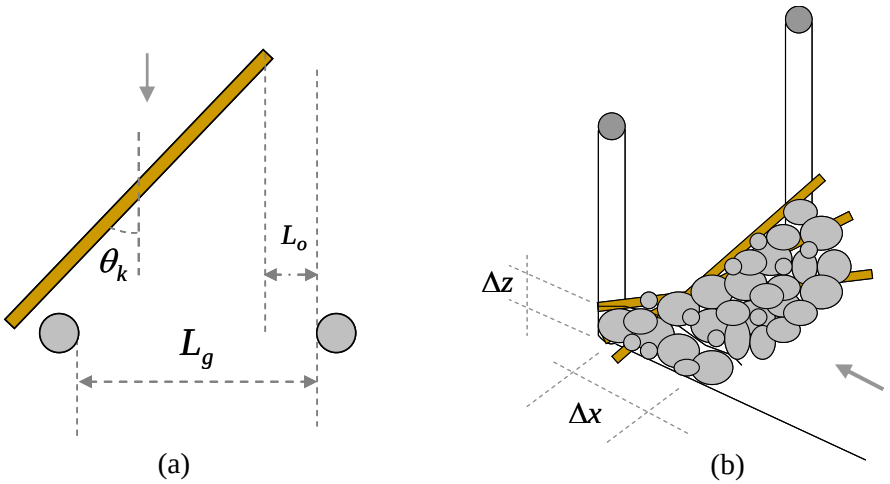

Figure 4.19 (a) Schematic diagram for sediment passing rate through grid dam, (b) schematic diagram for sediment deposition due to driftwood jamming on a grid dam

discharge per unit width (Q_{sed}) and sediment deposition as

$$\left.\begin{aligned} C_*\Delta x\Delta z &= (1-P_s)Q_{sed}\Delta t \\ i_{dep} &= -\Delta z/\Delta t = -(1-P_s)Q_{sed}/(C_*\Delta x) \end{aligned}\right\} \tag{4.4}$$

where Δx is the distance increment of calculating point and Δz is the thickness of the deposition. Figure 4.19 (b) shows the schematic of sediment deposition behind grid dam due to driftwood jamming.

4.4.2 Debris flow deposition due to jamming of driftwood on slit dam

Figure 4.20 (a) shows the schematic diagram of flow passing through a slit dam. In the case of slit dam, the deposition equation due to jamming of driftwood on open space of slit dam similar to as grid dam is described as

$$i_{dep} = -(1-P_s)Q_{sed}/(C_*\Delta x) \tag{4.5}$$

in which $P_s = L_o/b$ is the sediment passing rate through open spacing of slit dam (Figure 4.20 (b)) and in the case of impermeable space of slit dam P_s =0.

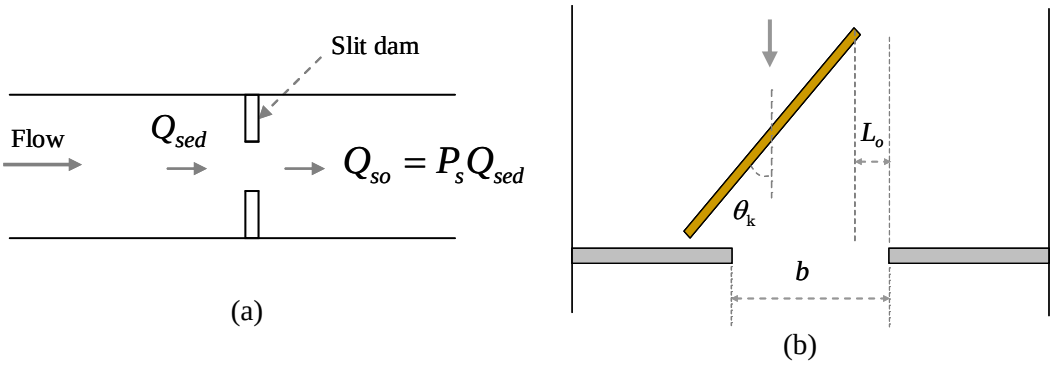

Figure 4.20 (a) Schematic flow model near slit dam, (b) schematic diagram for sediment passing rate through slit dam

4.4.3 Debris flow deposition due to clogging of large boulders

The open spaces of grid or slit dam may be also blockaded by large boulders. In the case of grid dam, the growing rate formula of grid dam blockage given by Equation (2.50) for two dimensional flow fields is written as

$$i_b^{'} = i_b - a_2 \frac{C_L h\sqrt{u^2+v^2}}{C_* \Delta x} \tag{4.6}$$

For the case of slit dam, sediment deposition by clogging of open space of slit dam due to simultaneous arrival of two or more particles given by Equation (2.59) is written as

$$i_{dep} = -K_{sd}(1-P_{sd})\frac{C_L h\sqrt{u^2+v^2}}{C_* \Delta x} \tag{4.7}$$

4.4.4 Deposition equation upstream area of check dam

The sediment deposition given by Equations (4.4) to (4.7) is used to calculate the deposition at check dam location. But in the upstream area of check dam (if $z_i < z_{dam}$ or $z_i < z_{i+1}$ and $\tau_{*y} > \tau_{*e}$), sediment deposition is calculated using deposition model described by Equation (2.44) as

$$i_{dep} = K_{dep}(\tau_{*e} - \tau_{*y})\frac{C_{L\,i-1} h_{i-1}\sqrt{u_{i-1}^2+v_{i-1}^2}}{C_* \Delta x} \tag{4.8}$$

The bed surface slope, which is necessary to calculate τ_{*e} and τ_{*y} using Equation (2.45) and Equation (2.46) is described as

$$\tan\theta = \frac{u\sin\theta_{bx} + v\sin\theta_{by}}{\sqrt{u^2\cos^2\theta_{bx} + v^2\cos^2\theta_{by}}} \tag{4.9}$$

where,

$$\tan\theta_{bx} = \tan(\theta_{bx0} + \theta_{bzx}); \quad \tan\theta_{by} = \tan(\theta_{by0} + \theta_{bhy})$$

$$\tan\theta_{bzx} = \frac{-\partial(z_b)}{\partial x}; \quad \tan\theta_{bzy} = \frac{-\partial(z_b)}{\partial y}$$

4.5 Results and discussions

The numerical simulations and experiments were performed to investigate the capturing process of debris flow with driftwood by open type check dams such as grid or slit type check dams. The jamming of driftwood on grid or slit dam was evaluated based on the geometric conditions and the probabilistic approaches. The geometric conditions under which jamming of driftwood on grid or slit dam were determined based on the evaluation of the experimental results and the

probabilistic approach was developed from the regression analysis of values obtained in the experiments. Debris flow deposition behind a grid or slit dam due to driftwood jamming was described. To simulate the debris flow with driftwood capturing by grid or slit dam, a jamming model of driftwood and a deposition model behind a grid or slit dam were incorporated in a flow model of debris flow with driftwood described in Chapter 3. The parameters of the numerical simulation are as follows; Δx =5cm, Δy =1cm, Δt = 0.001sec, ρ = 1.0g/cm^3, ρ_m = 1.15g/cm^3, g = 980cm/sec^2, C_3= 0.48, n =0.04, $C_* = C_{*L} = C_{*DL}$ =0.65, C_{*F} =0, C_{Dx} =1.0, C_{Dy} =1.0, δ_e =0.0018, δ_d =0.045, C_M =1.0, K_{sd} =0.1, K_{dep} =1.0 and C_F = 0.

Figures 4.21 (a), (b), (c), (d), (e) and (f) show the results of flow discharge at downstream end of the flume and reduction of outflow discharge by grid dam with debris flow capturing due to jamming of driftwood on open spaces of grid dam with driftwood cases D_d=3mm and L_d=3.5cm, D_d=3mm and L_d=4.0cm, D_d=3mm and L_d=4.5cm, D_d=4mm and L_d=3.5cm, D_d=4mm and L_d=4.0cm, and D_d=4mm and L_d=4.5cm, respectively for flume slope 18 degrees. Debris flow is captured effectively by a grid dam due to the driftwood jamming. The simulated results of flow discharge passed through grid dam and flow discharge without dam are quite close to the experimental results. Figure 4.21 (g) shows the flow discharge without driftwood case, in which flow discharge is not reduced effectively by a grid dam with compared to the flow discharge with driftwood cases. From the results, outflow discharge is reduced by a grid dam more effectively in the cases with driftwood due to jamming of driftwood on a grid dam. The results of sediment discharge at downstream end of the flume with different sizes of driftwood cases are shown in Figures 4.22 (a), (b), (c), (d), (e) and (f) for flume slope 18 degrees. The sediment discharge is reduced by sediment deposition behind a grid dam due to driftwood jamming on a grid dam. Figure 4.22 (g) shows the sediment discharge at downstream end of the flume without driftwood case. The simulated results of outflow sediment discharge from a grid dam are also agreeable with the experimental results. The effect of driftwood jamming on sediment deposition behind a grid dam using developed deposition equation is well explained in the numerical simulations. In the calculation, deposition due to blockage of grid dam by large boulders was also considered.

Figure 4.23 shows the comparison results of the reduction of flow discharge at downstream end of the flume by grid dam with different sizes of driftwood cases to the without driftwood case for flume slope 20 degrees. The comparison results of reduction of sediment discharge by grid dam with and without driftwood cases for flume slope 20 degrees are shown in Figure 4.24. The

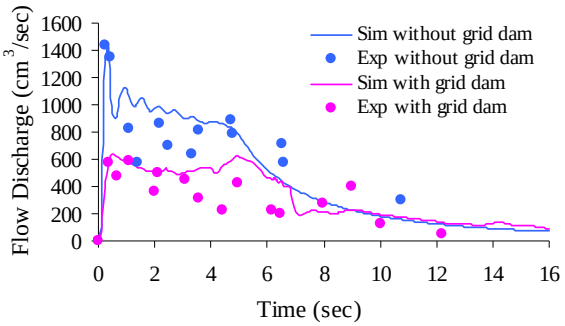

(a) Case with driftwood D_d=3mm and L_d =3.5cm

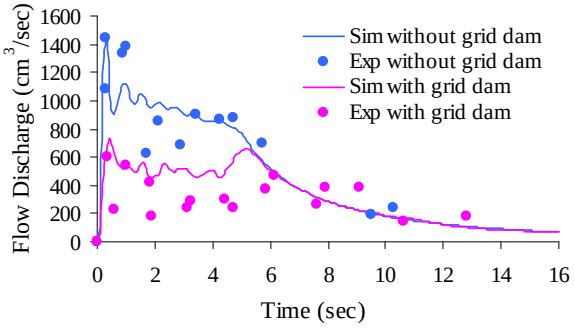

(b) Case with driftwood D_d=3mm and L_d =4.0cm

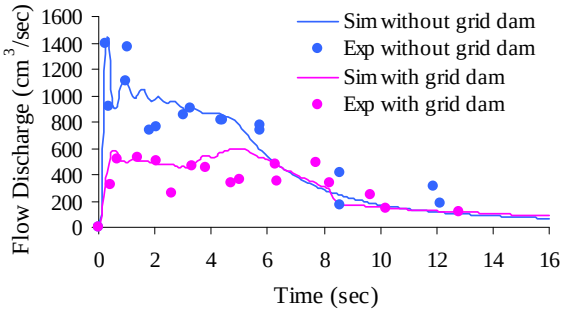

(c) Case with driftwood D_d=3mm and L_d =4.5cm

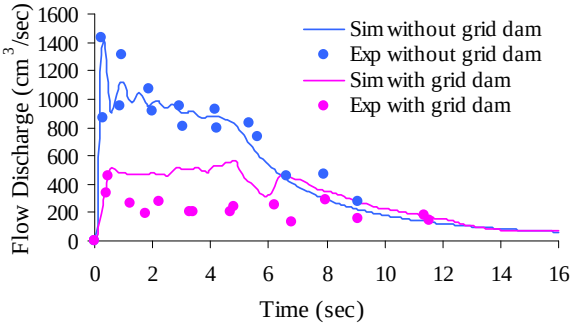

(d) Case with driftwood D_d=4mm and L_d =3.5cm

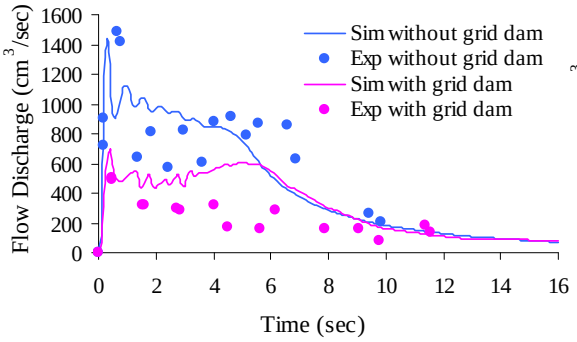

(e) Case with driftwood D_d=4mm and L_d =4.0cm

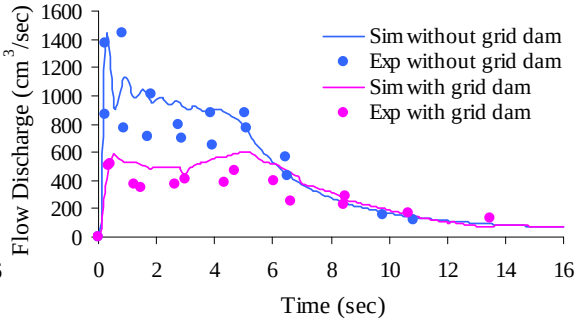

(f) Case with driftwood D_d=4mm and L_d =4.5cm

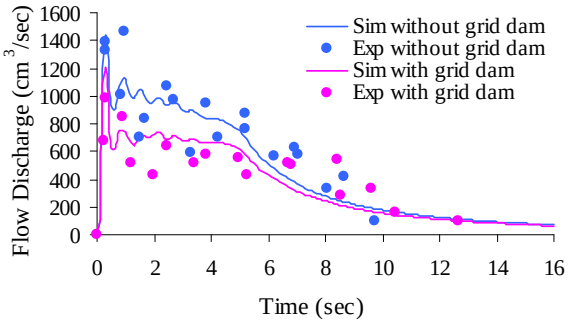

(g) Flow without driftwood case

Figure 4.21 Flow discharge at downstream end of flume and discharge reduction by grid dam due to driftwood jamming, flume slope θ=18^o

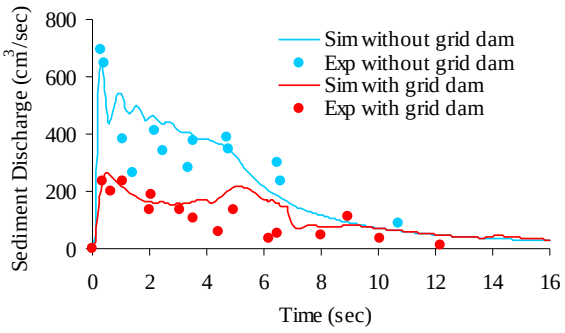

(a) Case with driftwood D_d=3mm and L_d =3.5cm

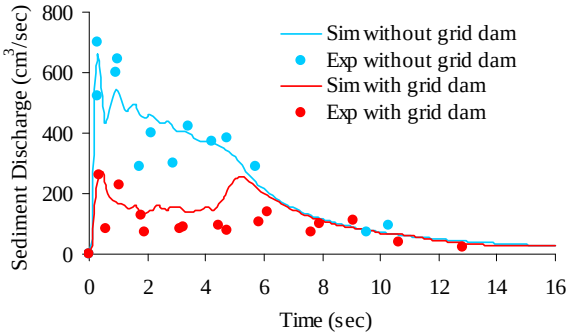

(b) Case with driftwood D_d=3mm and L_d =4.0cm

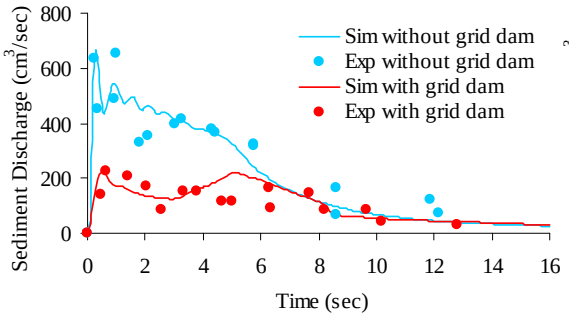

(c) Case with driftwood D_d=3mm and L_d =4.5cm

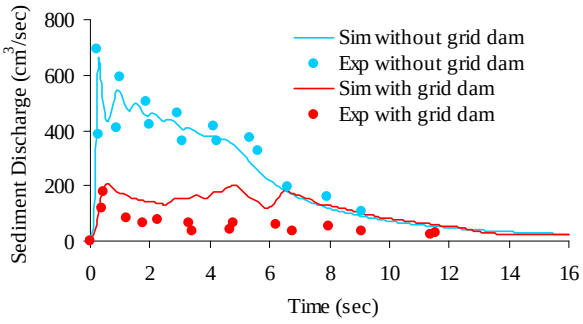

(d) Case with driftwood D_d=4mm and L_d =3.5cm

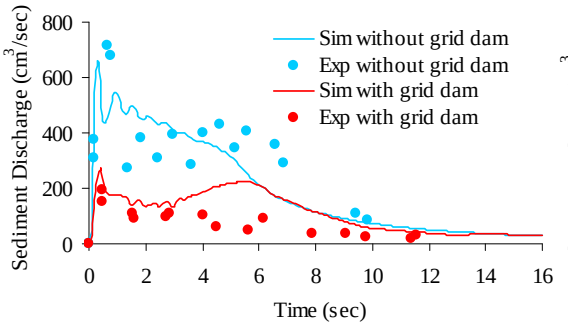

(e) Case with driftwood D_d=4mm and L_d =4.0cm

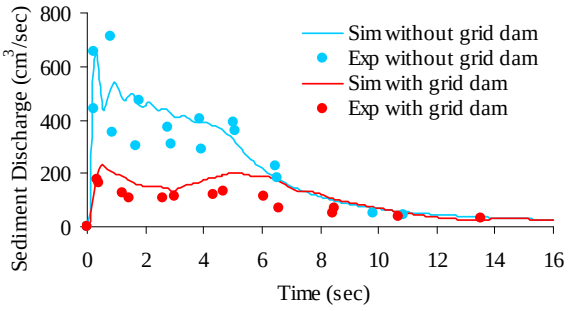

(f) Case with driftwood D_d=4mm and L_d =4.5cm

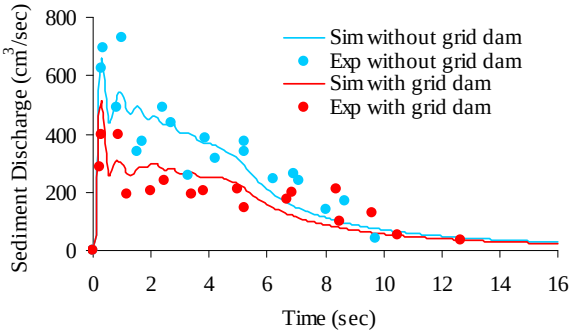

(g) Flow without driftwood case

Figure 4.22 Sediment discharge at downstream end and discharge reduction by grid dam due to driftwood jamming, flume slope θ=18^o

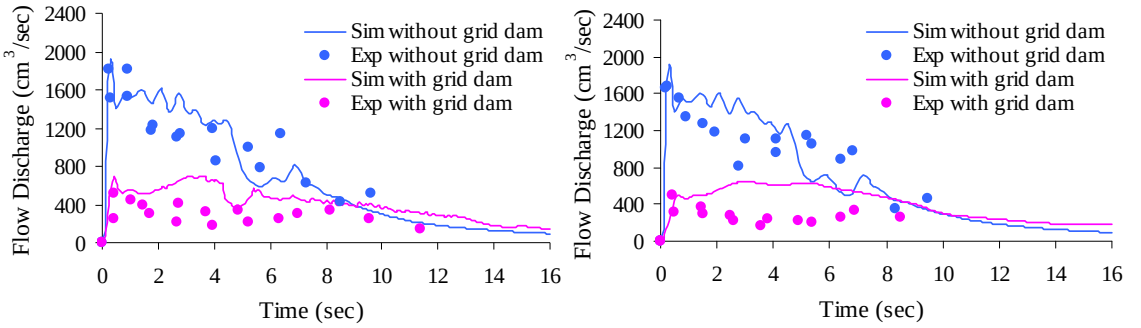

(a) Case with driftwood D_d=3mm and L_d =3.5cm

(b) Case with driftwood D_d=3mm and L_d =4.5cm

(c) Case with driftwood D_d=4mm and L_d =4.5cm

(d) Flow without driftwood case

Figure 4.23 Reduction of outflow discharge by grid dam at downstream end, flume slope θ=20°

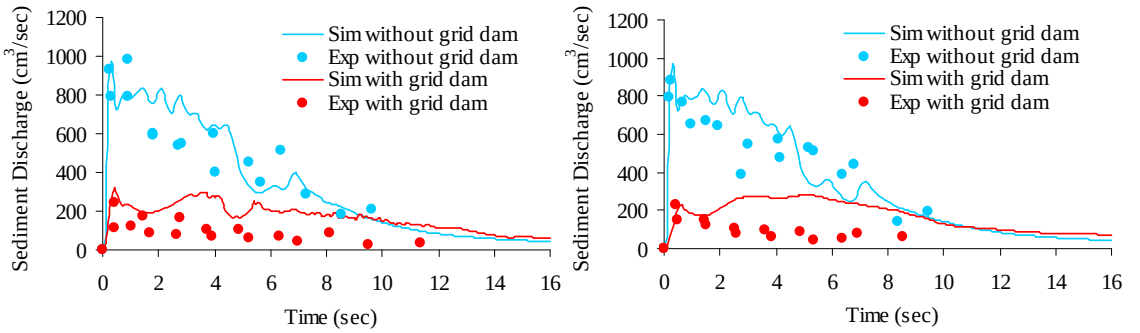

(a) Case with driftwood D_d=3mm and L_d =3.5cm

(b) Case with driftwood D_d=3mm and L_d =4.5cm

(c) Case with driftwood D_d=4mm and L_d =4.5cm

(d) Flow without driftwood case

Figure 4.24 Reduction of sediment discharge by grid dam at downstream end, flume slope θ=20°

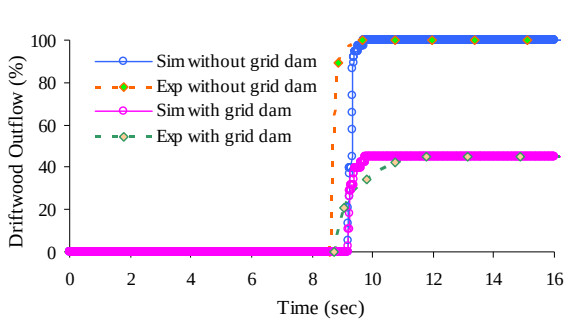

(a) Driftwood D_d=3mm and L_d =3.5cm case

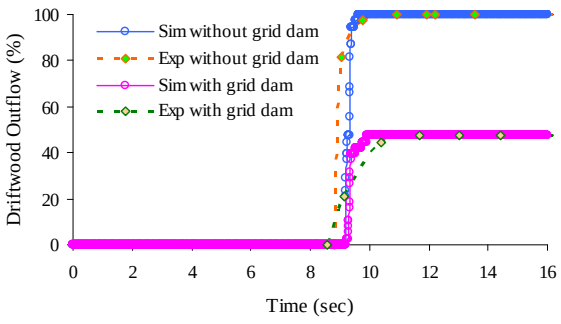

(b) Driftwood D_d=3mm and L_d =4.0cm case

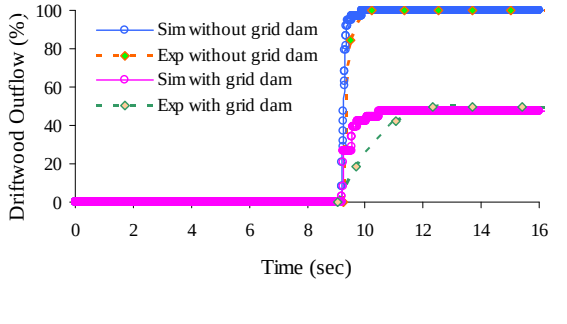

(c) Driftwood D_d=3mm and L_d =4.5cm case

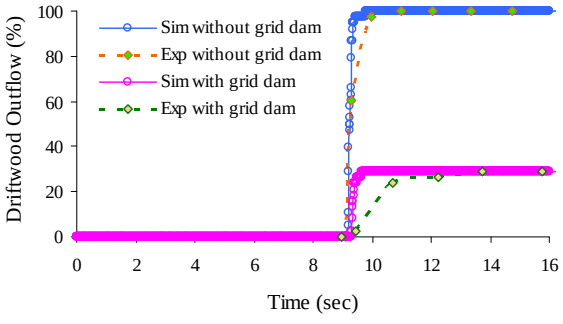

(d) Driftwood D_d=4mm and L_d =3.5cm case

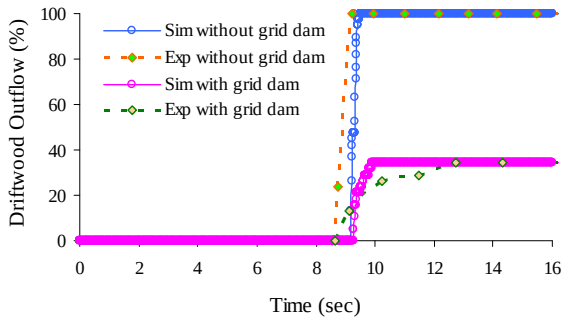

(e) Driftwood D_d=4mm and L_d =4.0cm case

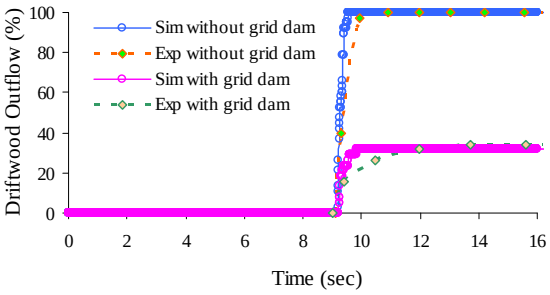

(f) Driftwood D_d=4mm and L_d =4.5cm case

Figure 4.25 Accumulated driftwood outflow at downstream end of the flume and reduction of driftwood outflow by grid dam, flume slope θ=18^o

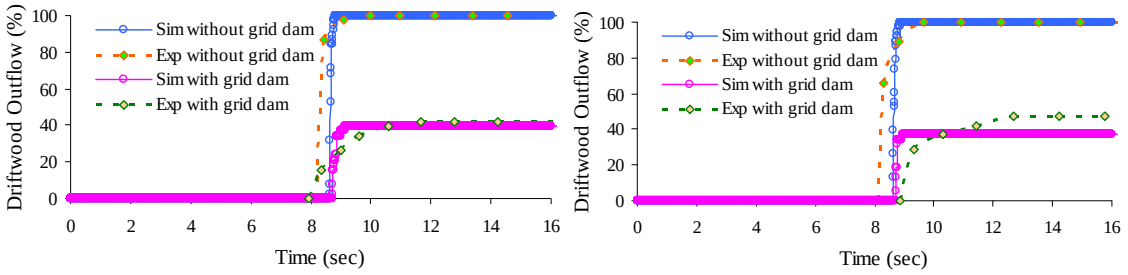

(a) Driftwood D_d=3mm and L_d =3.5cm case

(b) Driftwood D_d=3mm and L_d =4.5cm case

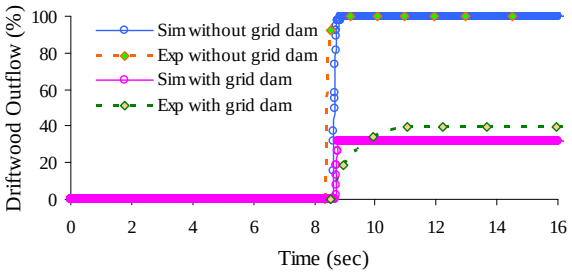

(c) Driftwood D_d=4mm and L_d =4.5cm case

Figure 4.26 Accumulated driftwood outflow at downstream end of the flume and reduction of driftwood outflow by grid dam, flume slope θ=20°

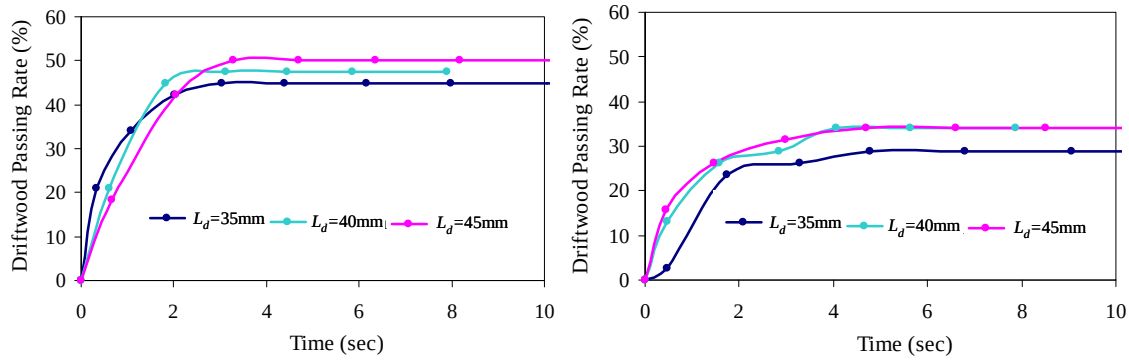

(a) Driftwood, D_d=3mm case

(b) Driftwood, D_d=4mm case

Figure 4.27 Comparison of experimental results of driftwood passing rate through a grid dam, flume slope θ=18°

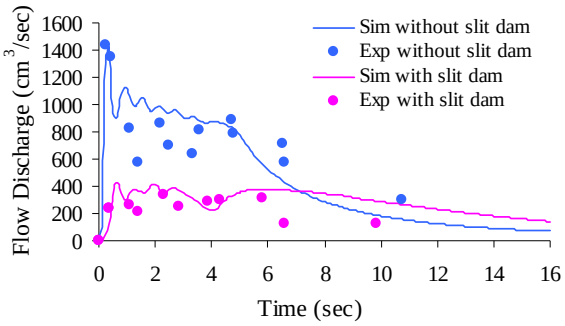

(a) Case with driftwood D_d=3mm and L_d =3.5cm

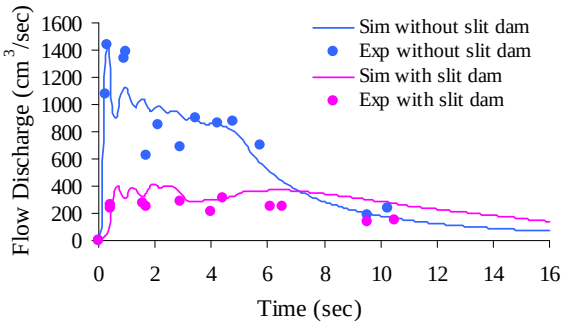

(b) Case with driftwood D_d=3mm and L_d =4.0cm

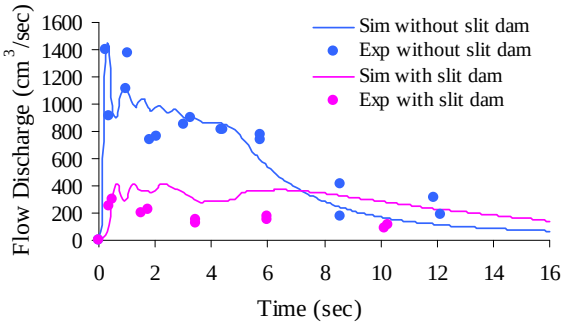

(c) Case with driftwood D_d=3mm and L_d =4.5cm

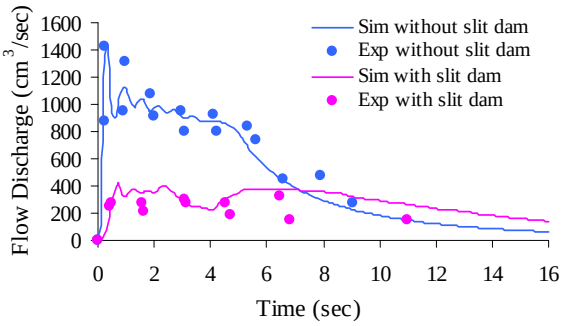

(d) Case with driftwood D_d=4mm and L_d =3.5cm

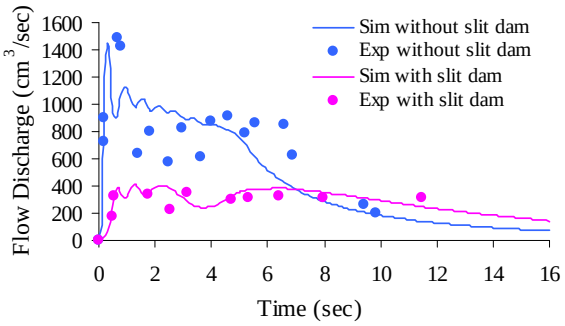

(e) Case with driftwood D_d=4mm and L_d =4.0cm

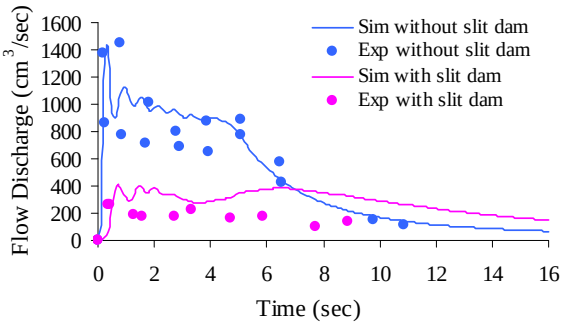

(f) Case with driftwood D_d=4mm and L_d =4.5cm

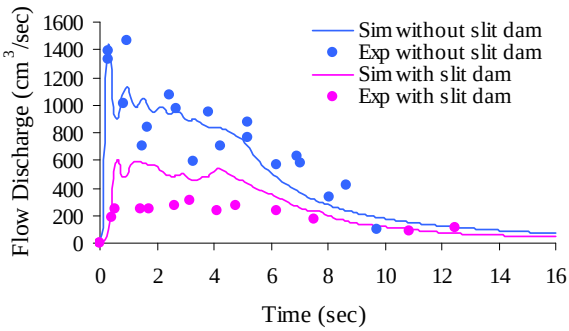

(g) Flow without driftwood case

Figure 4.28 Flow discharge at downstream end of flume and discharge reduction by slit dam due to driftwood jamming, flume slope θ=18°

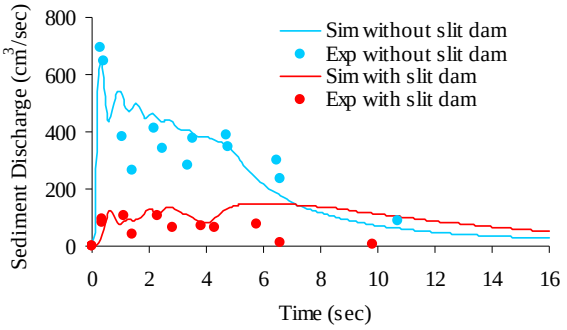

(a) Case with driftwood D_d=3mm and L_d =3.5cm

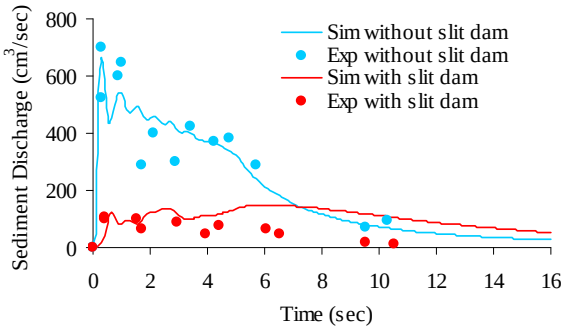

(b) Case with driftwood D_d=3mm and L_d =4.0cm

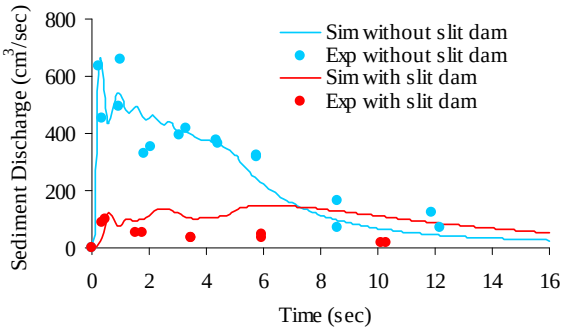

(c) Case with driftwood D_d=3mm and L_d =4.5cm

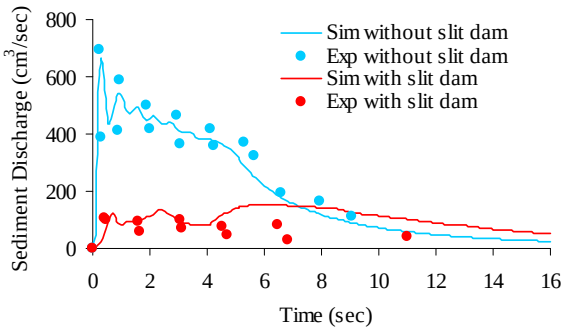

(d) Case with driftwood D_d=4mm and L_d =3.5cm

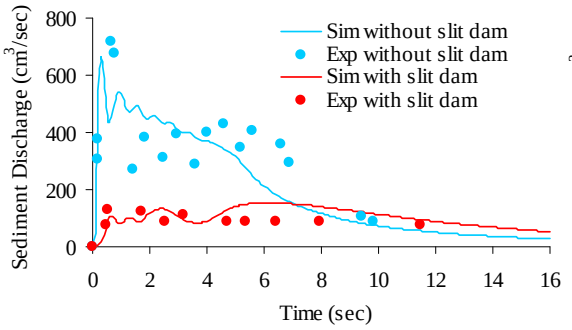

(e) Case with driftwood D_d=4mm and L_d =4.0cm

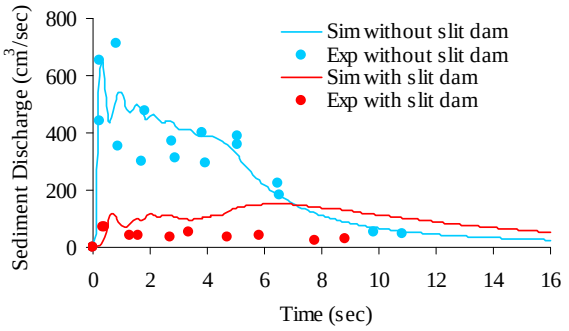

(f) Case with driftwood D_d=4mm and L_d =4.5cm

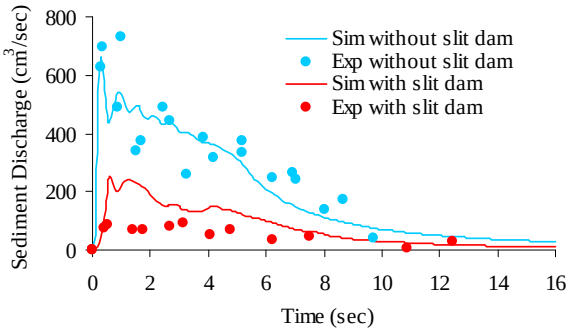

(g) Flow without driftwood case

Figure 4.29 Sediment discharge at downstream end and discharge reduction by slit dam due to driftwood jamming, flume slope θ=18^o

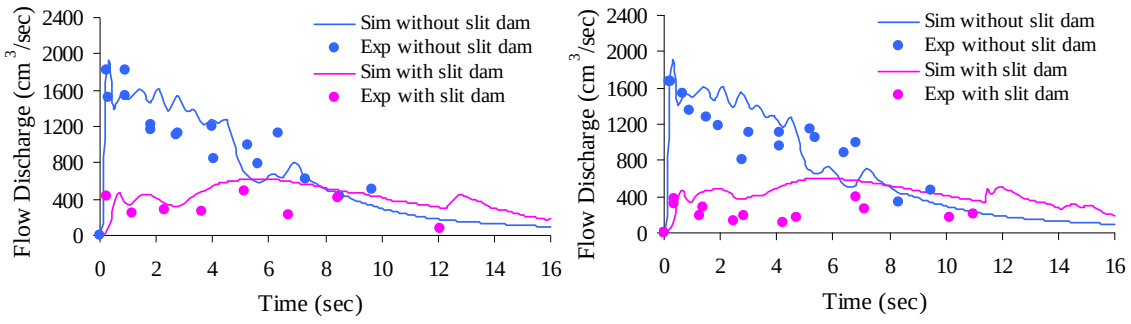

(a) Case with driftwood D_d=3mm and L_d =3.5cm (b) Case with driftwood D_d=3mm and L_d =4.5cm

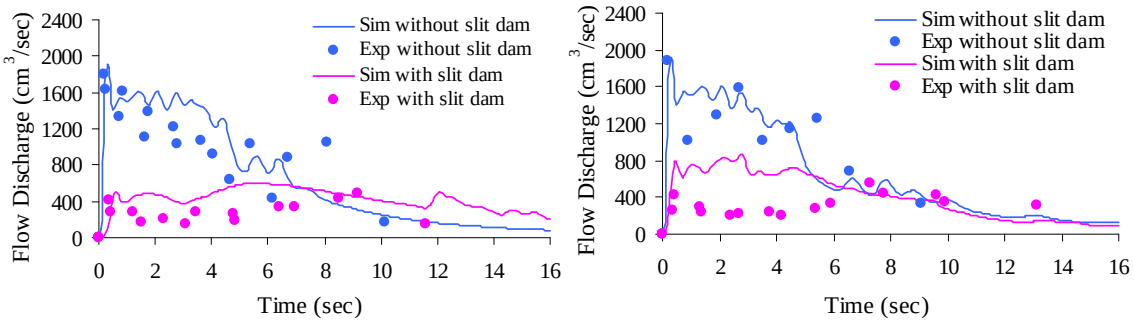

(c) Case with driftwood D_d=4mm and L_d =4.5cm (d) Flow without driftwood case

Figure 4.30 Reduction of outflow discharge by slit dam at downstream end, flume slope θ=20°

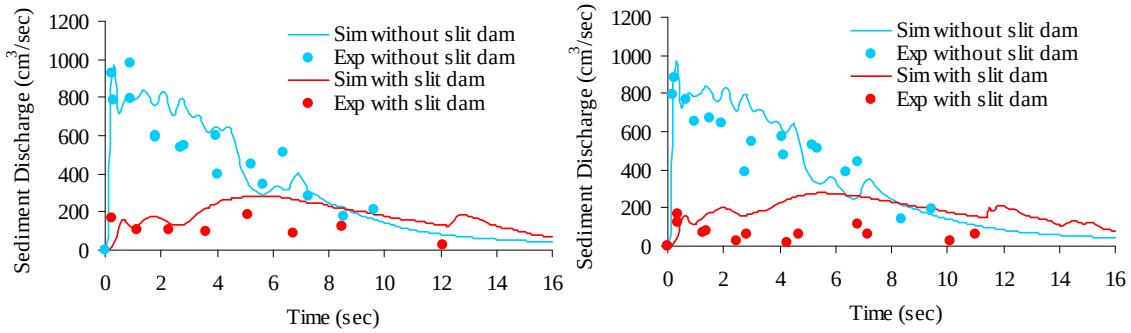

(a) Case with driftwood D_d=3mm and L_d =3.5cm (b) Case with driftwood D_d=3mm and L_d =4.5cm

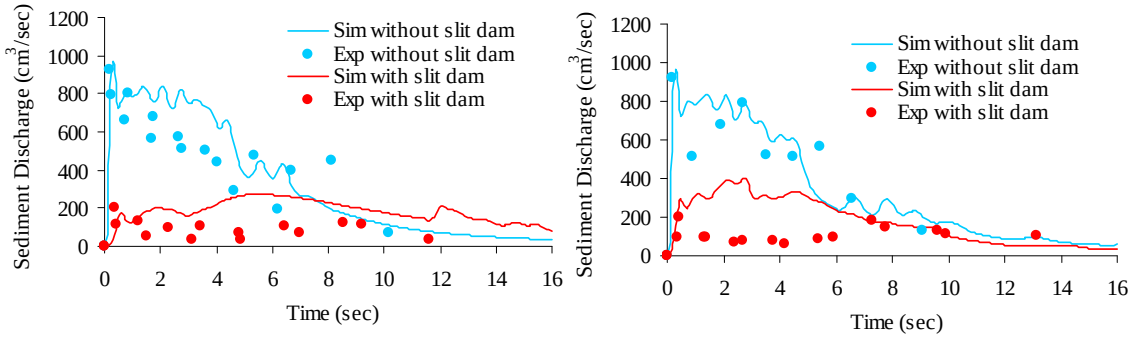

(c) Case with driftwood D_d=4mm and L_d =4.5cm (d) Flow without driftwood case

Figure 4.31 Reduction of sediment discharge by slit dam at downstream end, flume slope θ=20°

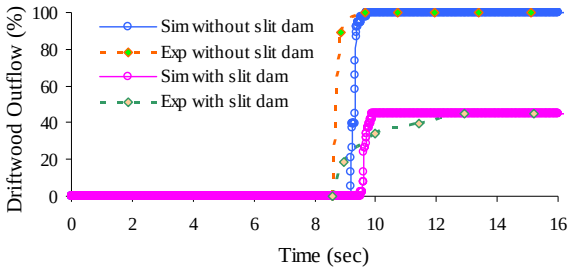

(a) Driftwood D_d=3mm and L_d =3.5cm case

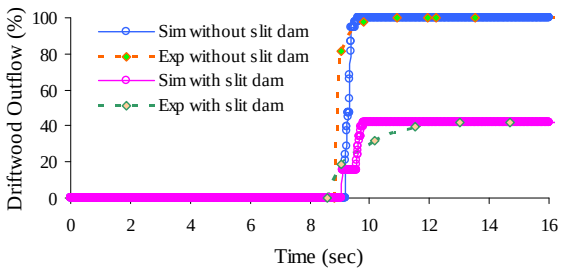

(b) Driftwood D_d=3mm and L_d =4.0cm case

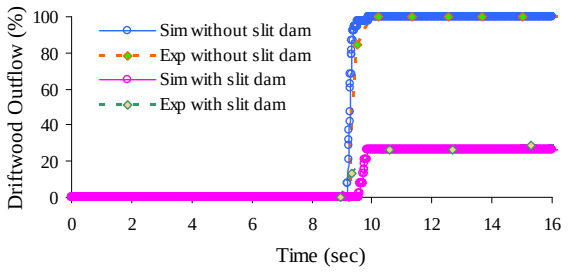

(c) Driftwood D_d=3mm and L_d =4.5cm case

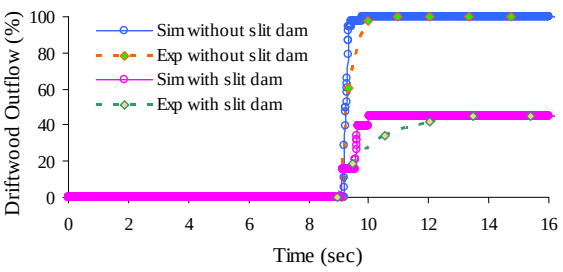

(d) Driftwood D_d=4mm and L_d =3.5cm case

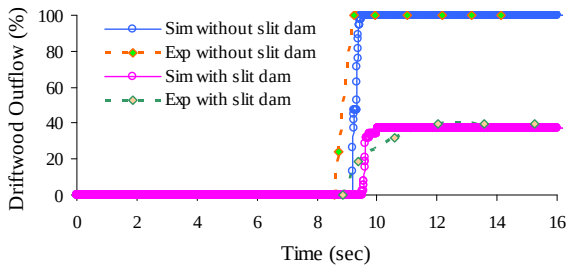

(e) Driftwood D_d=4mm and L_d =4.0cm case

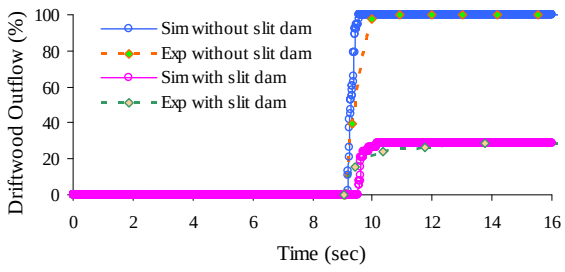

(f) Driftwood D_d=4mm and L_d =4.5cm case

Figure 4.32 Accumulated driftwood outflow at downstream end of the flume and reduction of driftwood outflow by slit dam, flume slope $\theta=18^o$

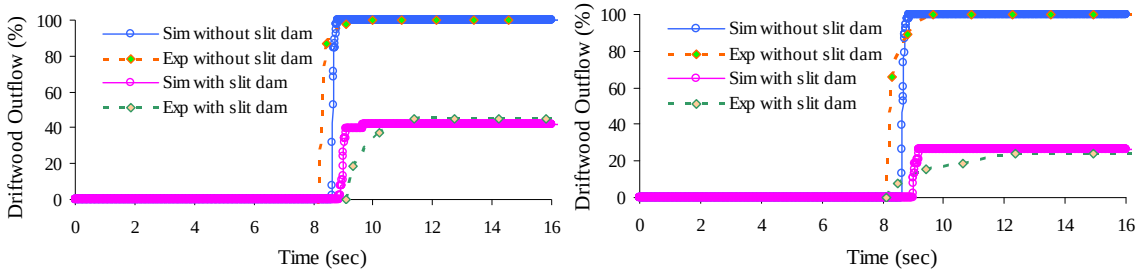

(a) Driftwood D_d=3mm and L_d =3.5cm case

(b) Driftwood D_d=3mm and L_d =4.5cm case

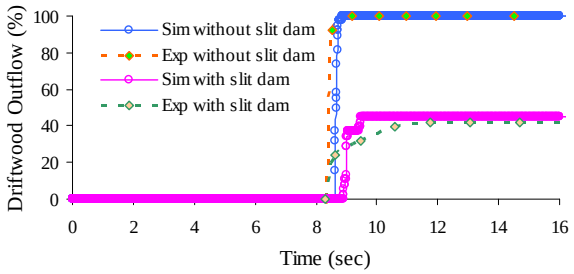

(c) Driftwood D_d=4mm and L_d =4.5cm case

Figure 4.33 Accumulated driftwood outflow at downstream end of the flume and reduction of driftwood outflow by slit dam, flume slope θ=20^o

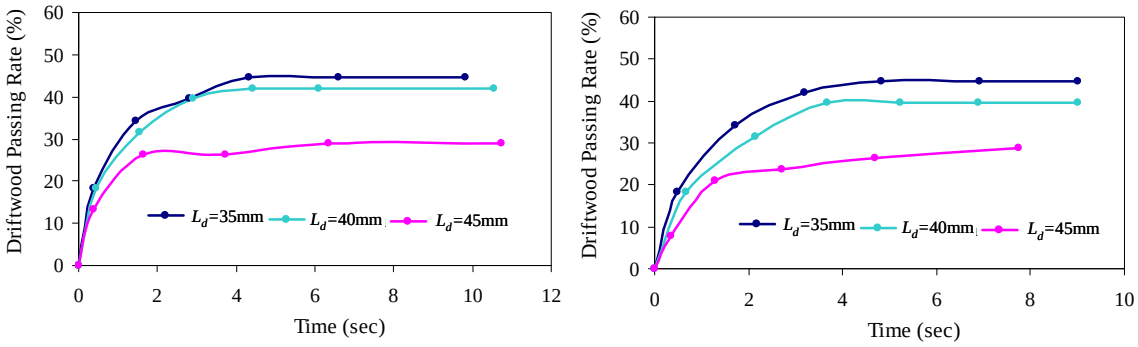

(a) Driftwood, D_d=3mm case

(b) Driftwood, D_d=4mm case

Figure 4.34 Comparison of experimental results of driftwood passing rate through a slit dam, flume slope θ=18^o

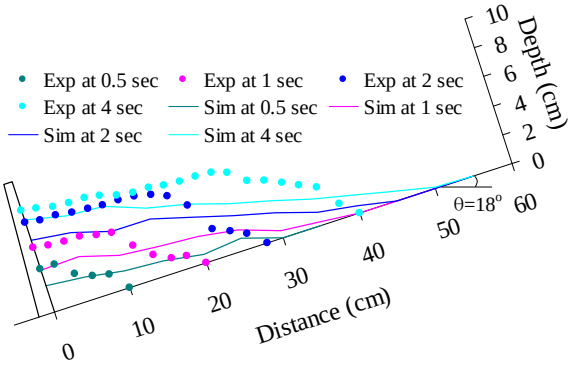

(a) Driftwood D_d=3mm and L_d =3.5cm case

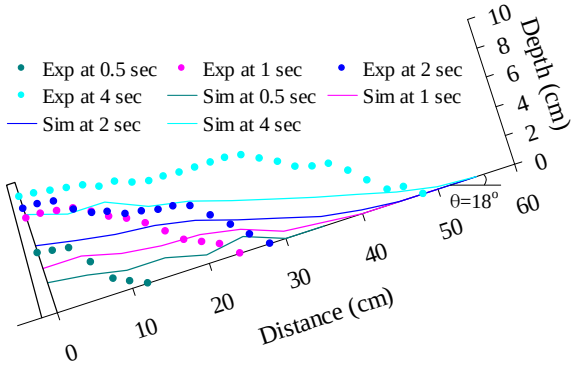

(b) Driftwood D_d=3mm and L_d =4.0cm case

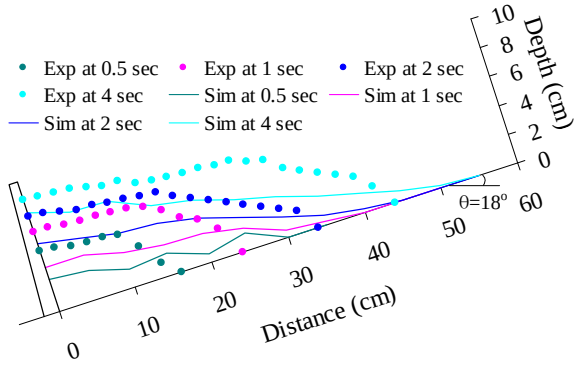

(c) Driftwood D_d=3mm and L_d =4.5cm case

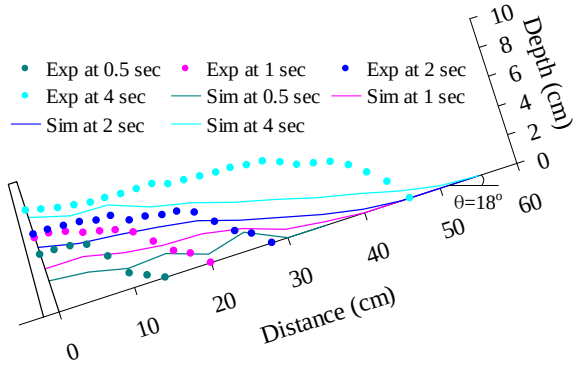

(d) Driftwood D_d=4mm and L_d =3.5cm case

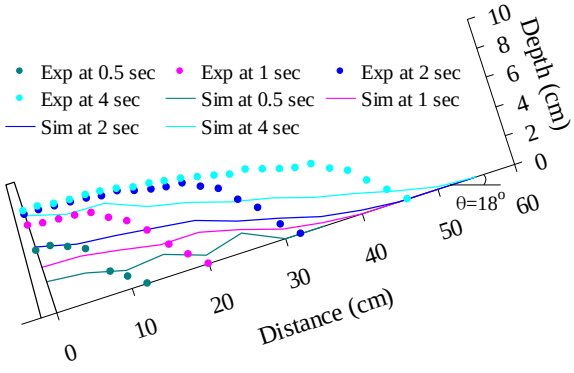

(e) Driftwood D_d=4mm and L_d =4.0cm case

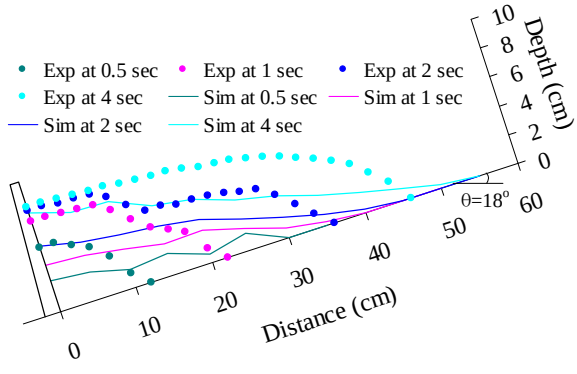

(f) Driftwood D_d=4mm and L_d =4.5cm case

Figure 4.35 Numerical and experimental results of temporal variation of deposition upstream of grid dam, flume slope θ=18°

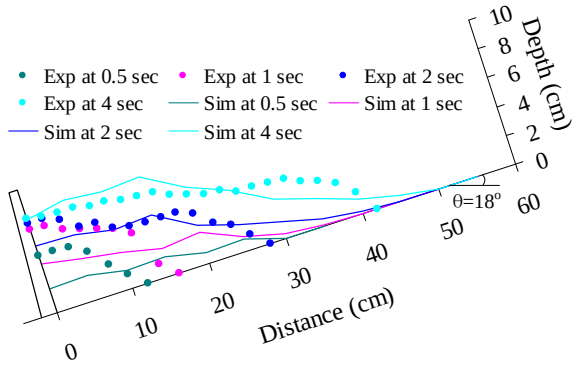

(a) Driftwood D_d=3mm and L_d =3.5cm case

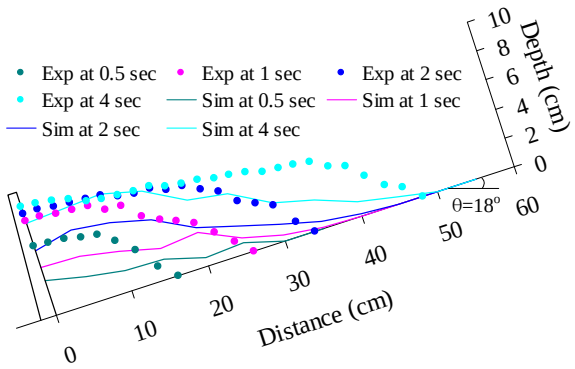

(b) Driftwood D_d=3mm and L_d =4.0cm case

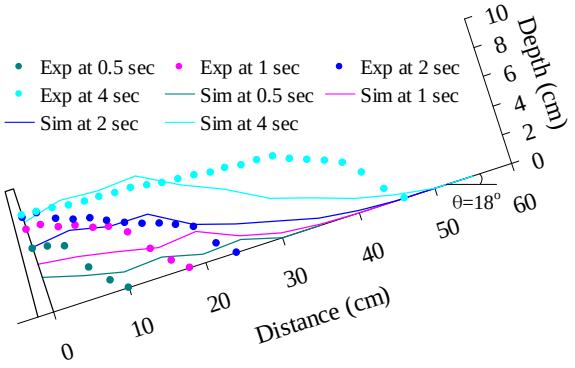

(c) Driftwood D_d=3mm and L_d =4.5cm case

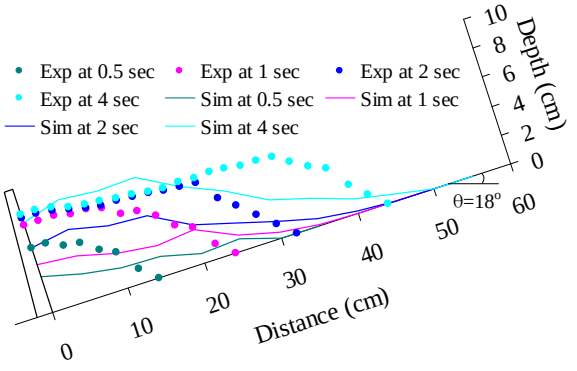

(d) Driftwood D_d=4mm and L_d =3.5cm case

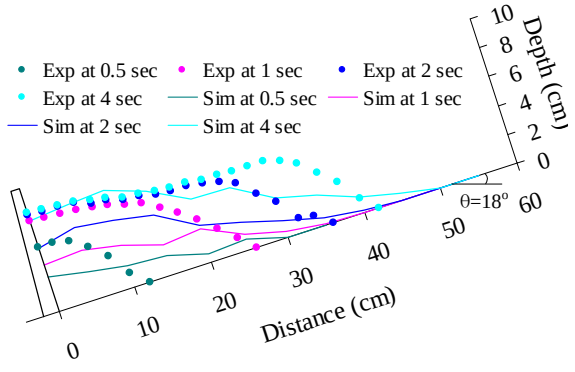

(e) Driftwood D_d=4mm and L_d =4.0cm case

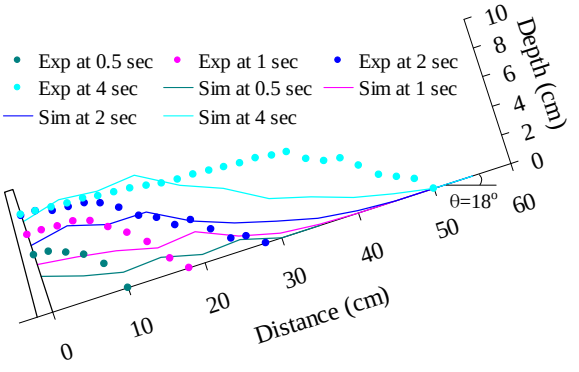

(f) Driftwood D_d=4mm and L_d =4.5cm case

Figure 4.36 Numerical and experimental results of temporal variation of deposition upstream of slit dam, flume slope θ=18^o

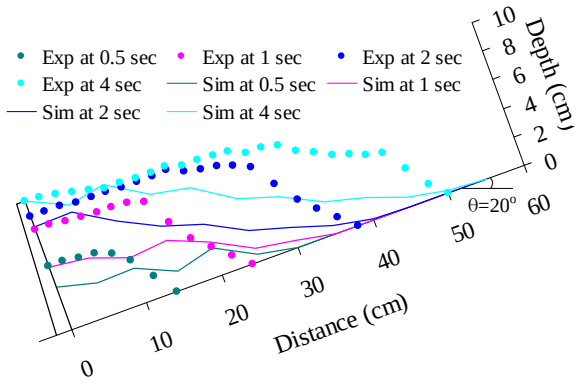

(a) Grid dam, Driftwood D_d=3mm and L_d =3.5cm

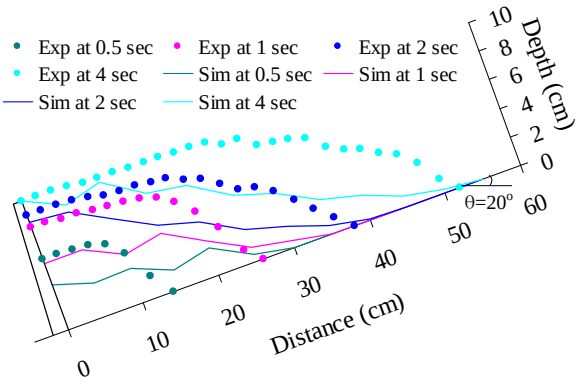

(b) Grid dam, Driftwood D_d=3mm and L_d =4.5cm

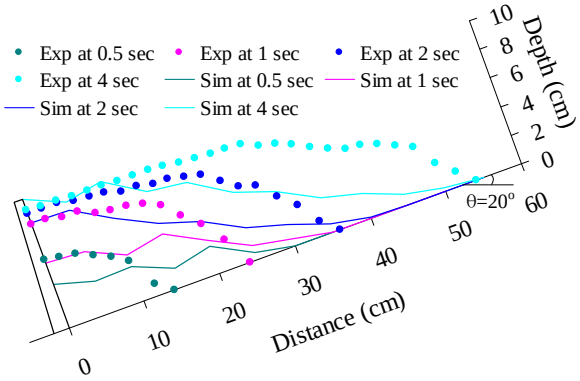

(c) Grid dam, Driftwood D_d=4mm and L_d =4.5cm

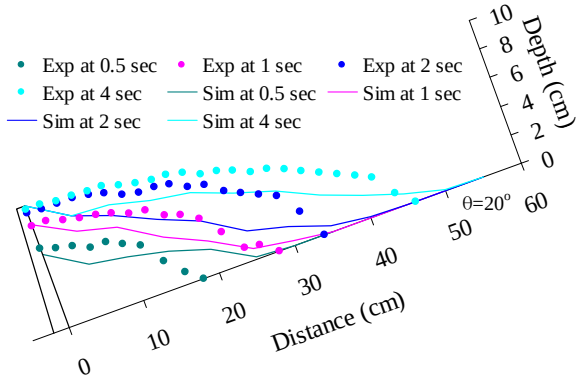

(d) Slit dam, Driftwood D_d=3mm and L_d =3.5cm

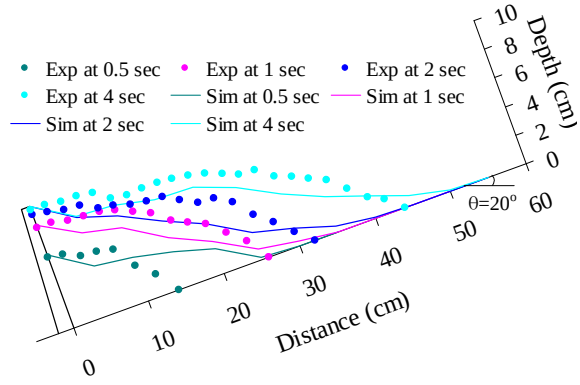

(e) Slit dam, Driftwood D_d=3mm and L_d =4.5cm

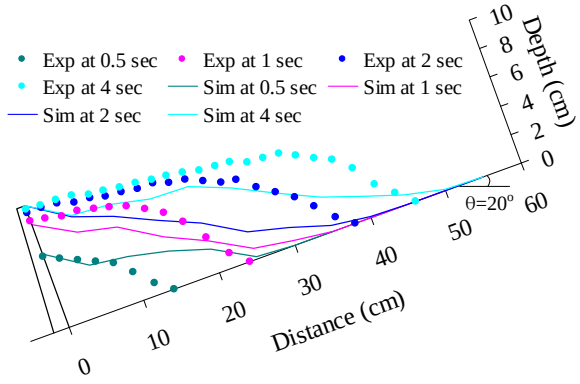

(f) Slit dam, Driftwood D_d=4mm and L_d =4.5cm

Figure 4.37 Temporal variation of deposition upstream of grid dam (a), (b) and (c), and slit dam (d), (e) and (f), flume slope θ=20°

simulated results of reduction of flow and sediment discharge by grid dam for flume slope 20 degrees cases are also agreeable with the experimental results.

The results of percentage of temporal driftwood passed through grid dam at the downstream end of the flume with different sizes of driftwood cases are shown in Figure 4.25 and Figure 4.26 for flume slope 18 and 20 degrees, respectively. The percentage of driftwood outflow is the ratio of the number of pieces of driftwood outflow at downstream end to the total amount of driftwood (38 pieces) supplied at the inflow boundary. The driftwood passed through a grid dam is reduced due to the driftwood jamming on grid dam. The number of pieces of the driftwood outflows from a grid dam based on the developed driftwood jamming model under the geometric conditions and probabilistic approaches are well explained in the numerical simulations. The simulated results of driftwood outflow time at the downstream end of the flume are also close to the results obtained from the experiments.

Figure 4.27 shows the comparison of experimental results of the percentage of driftwood passing through a grid dam with various sizes of driftwood diameter and length. Driftwood passing rate is decreased as diameter of driftwood pieces increases. The driftwood passing rate through a grid dam is determined as the ratio of the number of pieces of driftwood outflow at downstream end to the total amount of driftwood supplied at the inflow boundary.

The results of flow discharge and reduction of flow discharge by slit dam at the downstream end of the flume with or without driftwood cases are shown in Figure 4.28 for flume slope 18 degrees. Figure 4.29 shows the results of sediment discharge at the downstream end of the flume in the case of slit dam. The simulated results of flow discharge and sediment discharge passing through a slit dam are agreeable with the experimental results. The debris flow deposition behind a slit dam due to driftwood jamming is well explained in the numerical simulations. The simulated results of flow discharge and sediment discharge for flume slope 20 degrees with slit dam case are shown in Figure 4.30 and Figure 4.31, respectively.

The results of the percentage of driftwood outflow at the downstream end of the flume in slit dam case with different sizes of driftwood pieces are shown in Figure 4.32 and Figure 4.33 for flume slope 18 and 20 degrees, respectively. The driftwood passed through a slit dam is reduced due to the driftwood jamming on slit dam. The jamming of driftwood on slit dam is well explained in the numerical simulations with compared to the experimental results. Figure 4.34

shows the comparison of experimental results of driftwood passing rate through a slit dam with various sizes of driftwood diameter and length.

The simulated and experimental results of temporal variation of debris flow deposition upstream of a grid dam for different sizes of driftwood cases are shown in Figure 4.35 for flume slope 18 degrees. Similar results of debris flow deposition upstream of a slit dam are shown in Figure 4.36. The simulated results of debris flow deposition upstream of grid or slit dam for flume slope 20 degrees are shown in Figure 4.37. The simulated results of deposition upstream of grid and slit type check dams are also agreeable with the experimental results.

Summary

The capturing process of debris flow with driftwood by grid or slit dam was investigated. A numerical model was developed for computing the debris flow with driftwood capturing by open type check dams such as grid or slit dam. The jamming of driftwood on open type check dams was evaluated based on the geometric conditions and probabilistic approaches. A deposition velocity model was also developed to calculate the debris flow deposition due to driftwood jamming on a grid or slit dam. To simulate the debris flow with driftwood capturing by grid or slit dam, a jamming model of driftwood and a deposition model behind a grid or slit dam were incorporated in a two-dimensional flow model of debris flow with driftwood. The flow discharge and sediment discharge passing through a grid or slit dam are reduced due to driftwood jamming. The simulated results of flow discharge, sediment discharge and the percentage of driftwood passed through a grid or slit dam are in good agreement with the experimental results. The simulated results of debris flow deposition upstream of check dams also agree with the experimental results.

Chapter 5

Debris Flow with Driftwood Fan Deposition

5.1 Introduction

Debris flow is generally described as gravity flow of a mixture of soil, rocks and water (Sharp and Nobles, 1953; Fisher, 1971; Carter, 1975; Varnes, 1978; Naylor, 1980; Pierson, 1981; Costa, 1984; Takahashi et al., 1992; Nakagawa et al., 2002a; Takahashi, 2007). Debris flow is often generated by the erosion of steep debris beds in gullies. When the debris flow reaches a gentle basin from the steep channel, it spreads out, reduces its momentum and then stops after reaching a flatter area. Sediment deposits and leaves mud fluid or clear water flowing downstream. This process gradually creates a debris flow fan (Takahashi et al., 1992; Tsai, 2006). Many settlement areas are located at the foot of mountain, when debris flow spreads and deposits in these areas, which results in disastrous damage and sometimes considerable loss of life and property. Thus, it is necessary to study on the deposition of debris flow with driftwood on the fan to establish soft countermeasures for debris flow hazards.

Debris flow consists of several stages such as initiation, transportation and erosion, and deposition (Figure 5.1). Initiation generally requires a channel gradient greater than 25^{o} (47%); transportation and erosion generally require a gradient of greater than 15^{o} (27%); partial deposition, in the form of levees, generally occurs at a gradient of less than 15^{o} (27%); and deposition on the debris fan usually begins once the gradient flattens to less than a 10^{o} (18%) gradient (Takahashi, 1991; VanDine, 1996).

Numerical analysis and experimental studies are carried out to investigate the deposition of debris flows with driftwood on the fan. A two-dimensional integrated numerical model is developed for computing the characteristics of debris flow with driftwood, which can simulate all stages of debris flow from initiation to deposition stages. A numerical simulation model is developed with an interacting combination of Eulerian expression of the debris flow and Lagrangian expression of the driftwood. A capturing model of debris flow with driftwood by

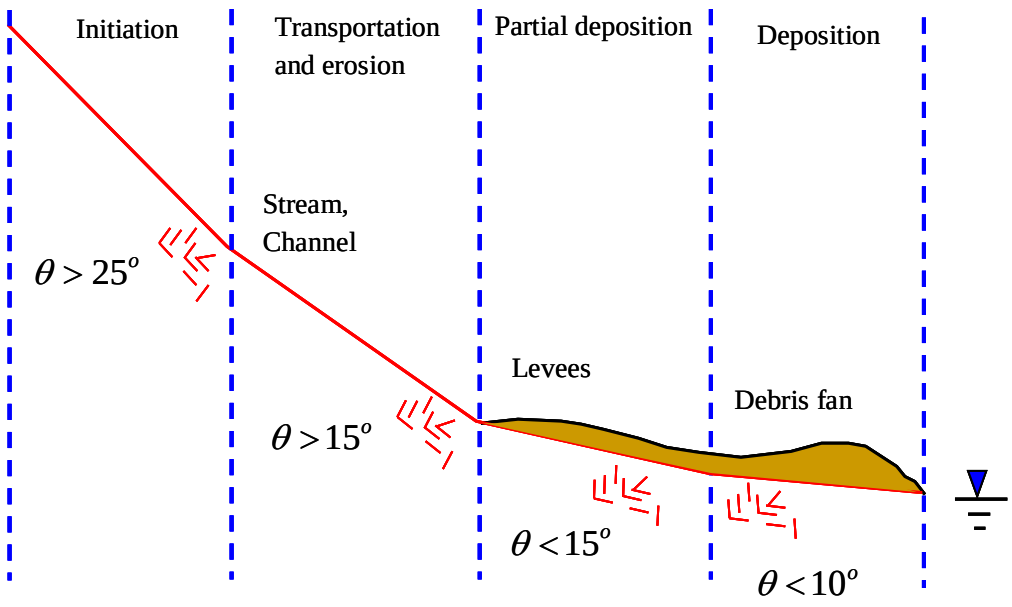

Figure 5.1 Stages of debris flow

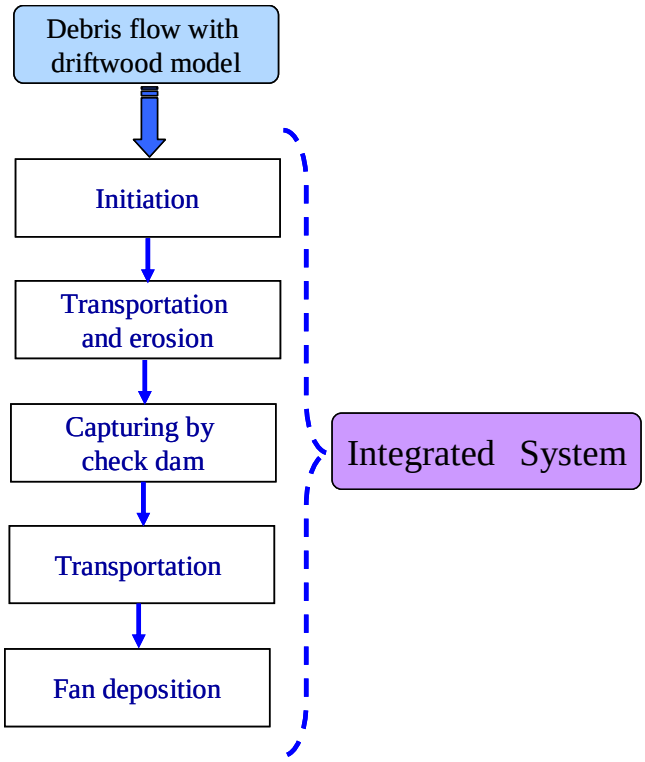

Figure 5.2 Schematic diagram of integrated numerical model

open type check dams is also incorporated into an integrated numerical model. The driftwood deposition process to investigate the positions and rotational angle of deposited driftwood in a debris flow fan is also considered into an integrated numerical model. The effects of driftwood and check dams on debris flow fan formation are also investigated numerically and experimentally. Figure 5.2 shows the schematic diagram of an integrated numerical model of debris flow with driftwood. The simulated results of the deposition of debris flow with driftwood on the fan are compared with those obtained from hydraulic model experiments.

5.2 Numerical simulation model

The depth-wise averaged two-dimensional used basic equations of debris flow are described in section 3.2.1. The inertial motion is not considered to calculate the deposition of debris flow on the fan in Equation (3.34). The basic equations of driftwood motion are described in section 3.2.2. The flow motion of driftwood is restricted near the flow surface. However, when a debris flow debouches from a canyon mouth at which the slope abruptly becomes flat, its competence to transport sediment markedly decreases and its materials are deposited on a debris fan. The flow motion of driftwood becomes contact with bed surface after reducing certain flow depth due to debris flow deposition in a fan area. The driftwood stops due to the friction forces generated between driftwood and bed surface. To compute the driftwood deposition in a fan area, equations of driftwood motion, Equation (3.39) and Equation (3.40) described in section 3.2.2 are modified respectively as follows:

$$(m_k + mC_M)\frac{du_k}{dt} = -m_k g \frac{\partial H_k}{\partial x} - \frac{1}{2}\rho_T C_{Dx} W_k (u_k - U_k) A_{kx} \pm F_{fx} \tag{5.1}$$

$$(m_k + mC_M)\frac{dv_k}{dt} = -m_k g \frac{\partial H_k}{\partial y} - \frac{1}{2}\rho_T C_{Dy} W_k (v_k - V_k) A_{ky} \pm F_{fy} \tag{5.2}$$

where F_{fx} and F_{fy} are the friction forces in x and y directions, which are opposite in direction to the flow motion of driftwood. These forces can be described as follows:

$$F_{fx} = \mu_{kx} m_k g \cos(\theta_x)_k \tag{5.3}$$

$$F_{fy} = \mu_{ky} m_k g \cos(\theta_y)_k \tag{5.4}$$

where μ_{kx} and μ_{ky} are the kinetic friction coefficients in x and y directions and $(\theta_x)_k$ and $(\theta_y)_k$ are the bed slope at the position of the centroid of the driftwood in x and y directions.

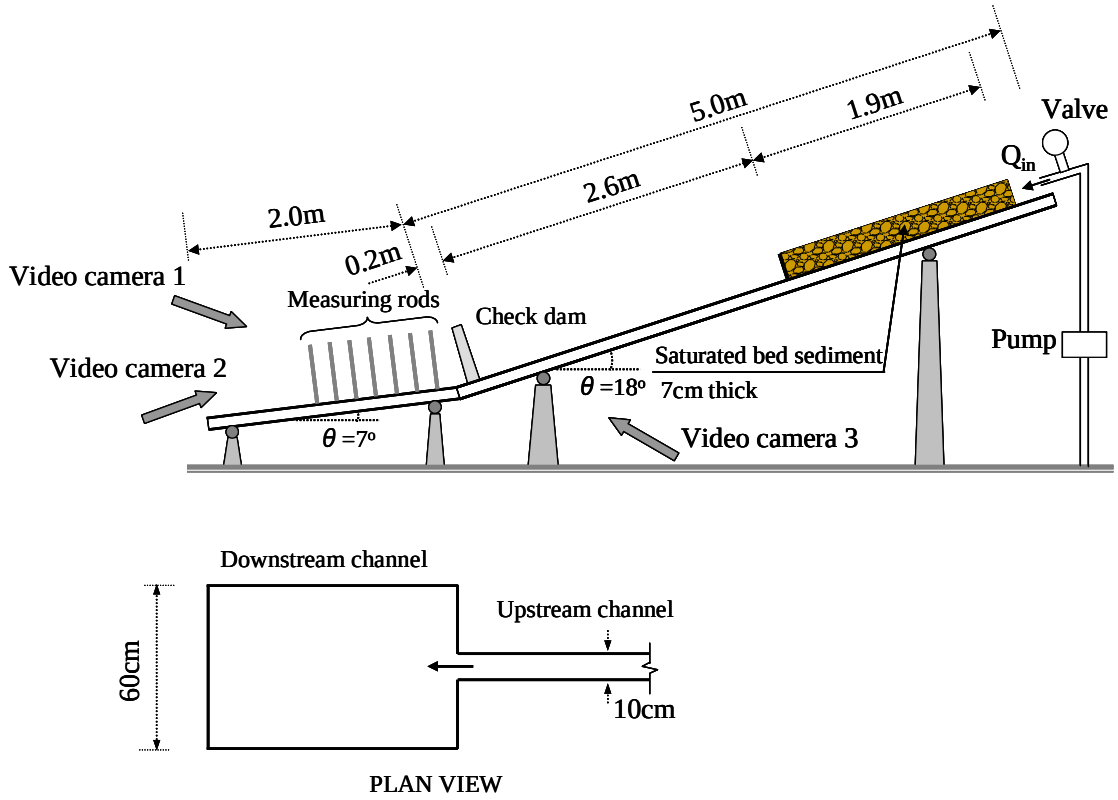

Figure 5.3 Experimental flume setup for debris flow fan deposition

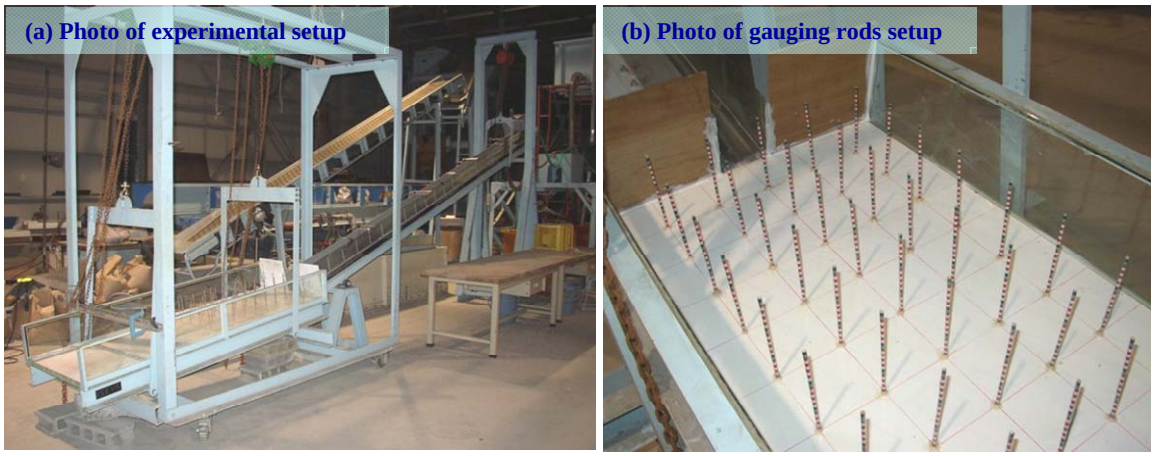

Figure 5.4 Photos of experimental setup and gauging rods

5.3 Laboratory experiments of debris flow fan deposition

For the verification of numerical model and investigation of the deposition process of debris flow with driftwood on the fan, flume experiments were conducted. A flume channel of 2m long, 60cm wide and 20cm deep was connected to the downstream end of 5m long, 10cm wide and

13cm deep flume as shown in Figure 5.3 and Figure 5.4 (a). The slopes of the upstream channel and downstream channel were 18 degrees and 7 degrees, respectively. A sediment bed of 1.9m long and 7cm deep was positioned from 2.8m to 4.7m upstream measured from the debouching point and soaked by the seepage flow. The particle size distribution of the sediment bed is shown in Figure 3.17. In the experiments with driftwood case, cylindrical pieces of 38 driftwood pieces were positioned on the sediment bed at intervals of 10cm c/c along the downstream direction from 7.5cm downstream from the upstream end of the sediment bed in two columns 2cm apart as shown in Figure 3.18 and Figure 3.19. To investigate the effectiveness of check dams on debris flow fan deposition, check dams were set at 20 cm upstream from the debouching point. The grid or slit type check dams as shown in Figure 4.3 were used.

Debris flow was produced by supplying a constant water discharge 270cm^3/sec for 10sec from the upstream end of the flume. The variations of the shape and thickness of the deposit were measured by two video cameras, in which the thickness of deposit was measured on the video image by reading out the elevations of the deposit surface using the gauging rods set on the downstream deposition channel. The gauging rods were set at the rate of 10cm c/c interval in both longitudinally and laterally as shown in Figure 5.4 (b). The depth of flow and deposition just upstream of the downstream end of the upstream channel were measured by other video camera. The positions and rotational angle of deposited driftwood were also determined by video cameras. Table 5.1 shows the details of the experimental conditions. The experiments were repeated three times under the same identical conditions. Figure 5.5 shows the debris flow and driftwood deposited in the experiments with driftwood case. Driftwood is deposited at the foot of the deposition area. Figure 5.6 shows the final stage of the deposition of debris flow on the fan and effectiveness of check dam on the fan deposition without driftwood case.

Table 5.1 The details of the experimental conditions for debris flow fan deposition

S. No.	Exp. Ref.	Supply discharge (cm^3/sec)	Check dam type	Diameter of driftwood (mm)	Length of driftwood (mm)	Remarks
1	G1	270	-	3	35	
2	G2	270	-	3	45	
3	G3	270	-	4	45	
4	G4	270	Grid dam	3	35	
5	G5	270	Grid dam	3	45	
6	G6	270	Slit dam	3	35	
7	G7	270	Slit dam	-	-	
8	G8	270	Grid dam	-	-	
9	G9	270	-	-	-	

(a) Without check dam, EXP G1

(b) With grid dam, EXP G4

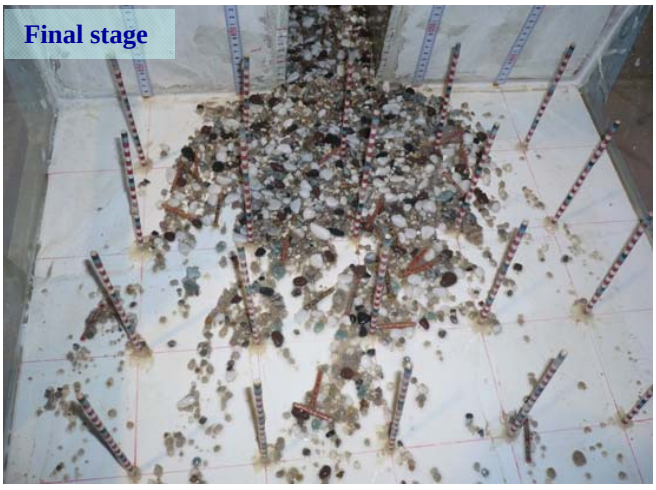

(c) With slit dam, EXP G6

Figure 5.5 Debris flow and driftwood deposition, with driftwood D_d=3mm and L_d =3.5cm

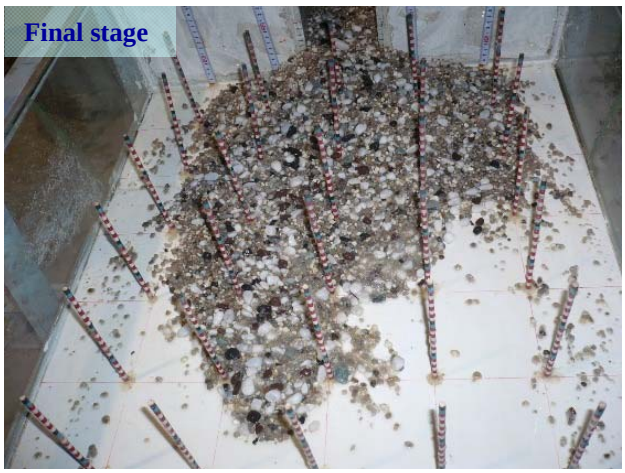

(a) Without check dam, EXP G9

(b) With grid dam, EXP G8

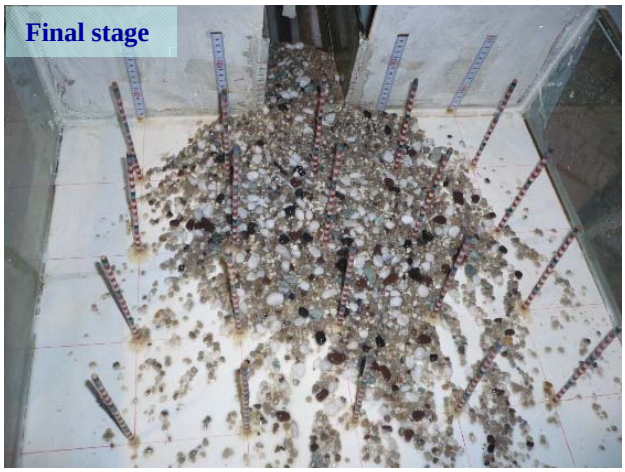

(c) With slit dam, EXP G7

Figure 5.6 Debris flow fan deposition, without driftwood case

5.4 Results and discussions

The numerical simulations and experiments were performed to investigate the deposition of debris flows with driftwood on the fan. The parameters of the numerical simulation are as follows; Δx =5cm, Δy =1cm, $\Delta t = 0.001$sec, $\rho = 1.0$g/cm^3, $\rho_m = 1.15$g/cm^3, $g = 980$cm/sec^2, C_3= 0.48, n =0.04, $C_* = C_{*L} = C_{*DL}$ =0.65, C_{*F} =0, C_{Dx} =1.0, C_{Dy} =1.0, δ_e =0.0018, δ_d =0.045 (for upstream channel) and δ_d =1.0 (for downstream channel), C_M =1.0, K_{sd} =0.1, K_{dep} =1.0, $\mu_{kx} = 0.3$, $\mu_{ky} = 0.11$ and $C_F = 0$.

Figure 5.7 shows the simulated flow and sediment discharge at 150cm and at 10cm upstream from a debouching point in the case of without driftwood and check dam. Figure 5.8 compares the temporal variations of the shapes and thicknesses (i.e., the flow depth plus the deposit thickness before the final stop, but only the deposit thickness after the final stop) in the process of a debris flow fan formation in a hydraulic model experiment with those obtained from the simulation by the integrated numerical model in the case of without driftwood and check dam. The numbers on the contour lines indicate the thickness in centimeters measured from the surface of the downstream deposition channel. The simulated and experimental results of final longitudinal bed profile along the center axis of a debris flow fan are shown in Figure 5.9. The simulated flow and sediment discharge at 10cm upstream from a debouching point in case of driftwood are shown in Figure 5.10 (a), Figure 5.10 (b) and Figure 5.17 for the cases with driftwood D_d=3mm and L_d=3.5cm, D_d=3mm and L_d=4.5cm, and D_d=4mm and L_d=4.5cm, respectively. The simulated and experimental results of shapes and thicknesses (flow depth plus

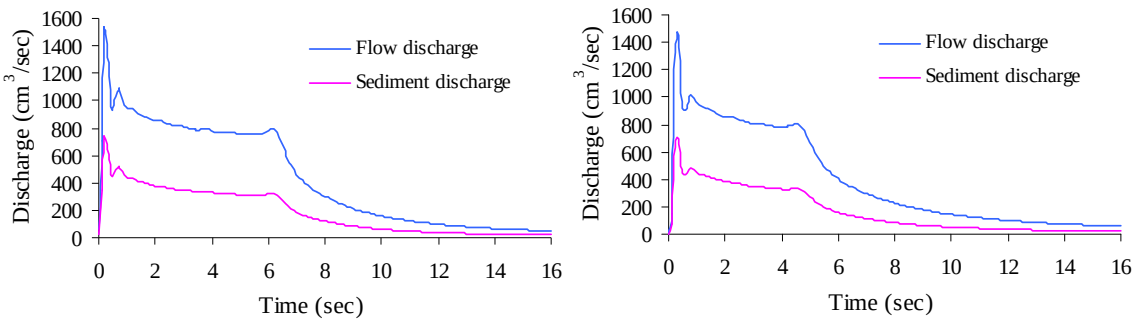

Figure 5.7 Flow and sediment discharge at (a) 150cm, (b) 10cm upstream from a debouching point (downstream end of upstream channel) without driftwood and check dam case

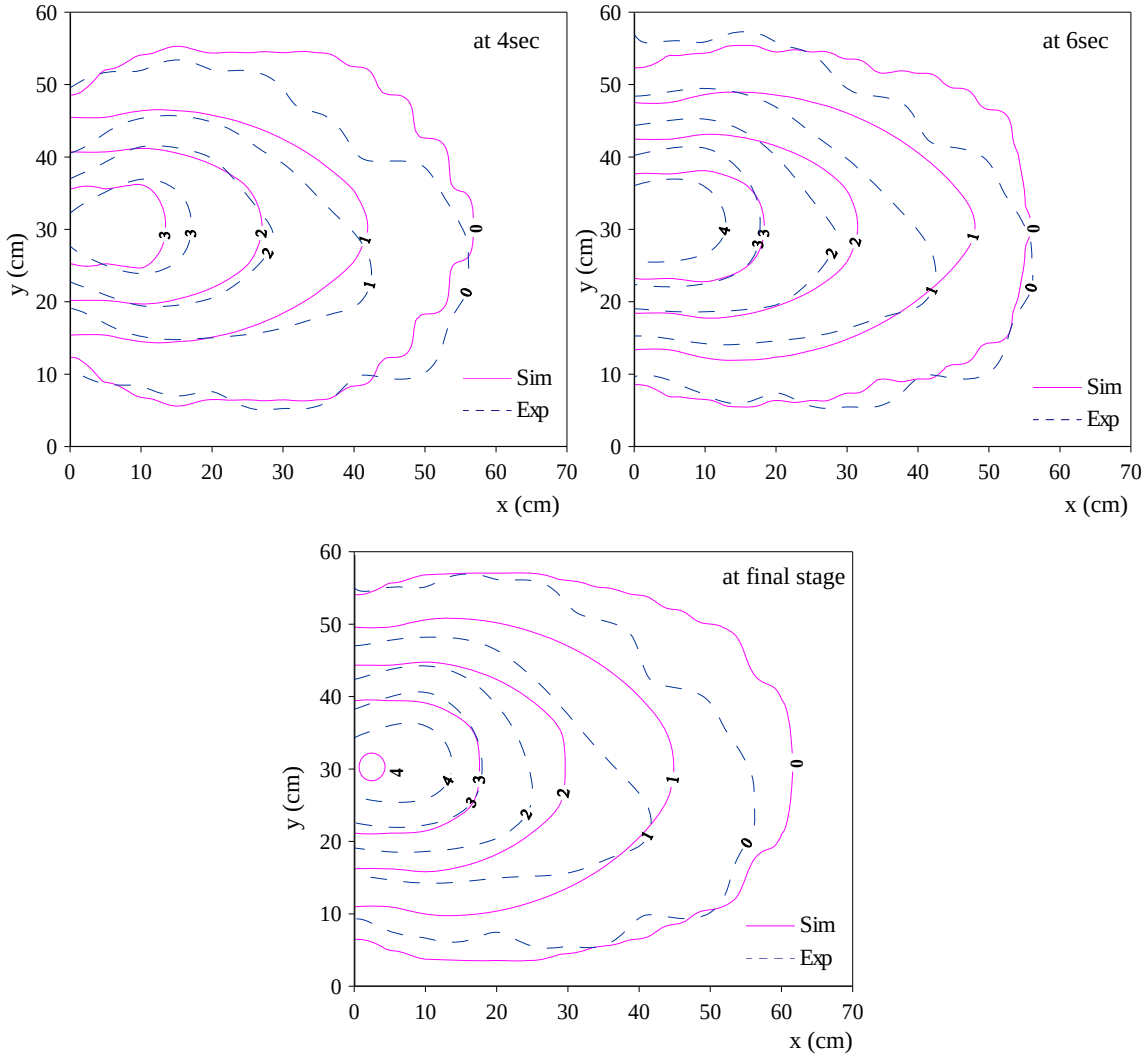

Figure 5.8 Temporal changes of shapes and thicknesses of a debris flow fan , without driftwood and check dam case

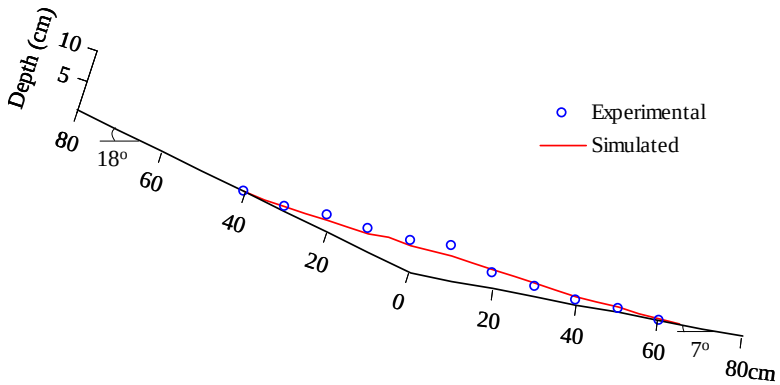

Figure 5.9 The final stage longitudinal bed profile along the center axis of a debris flow fan, without driftwood and check dam case

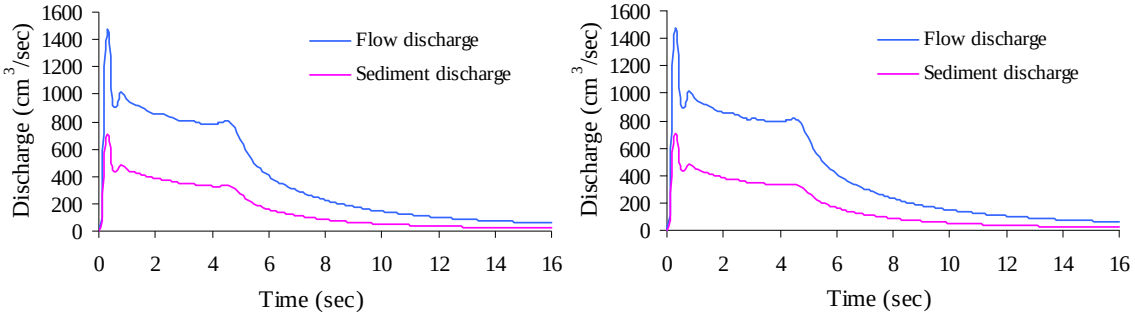

(a) With driftwood D_d=3mm and L_d =3.5cm case (b) With driftwood D_d=3mm and L_d =4.5cm case

Figure 5.10 Simulated flow and sediment discharge at 10cm upstream from a debouching point, driftwood D_d=3mm and L_d=3.5cm, D_d=3mm and L_d=4.5cm, without check dam

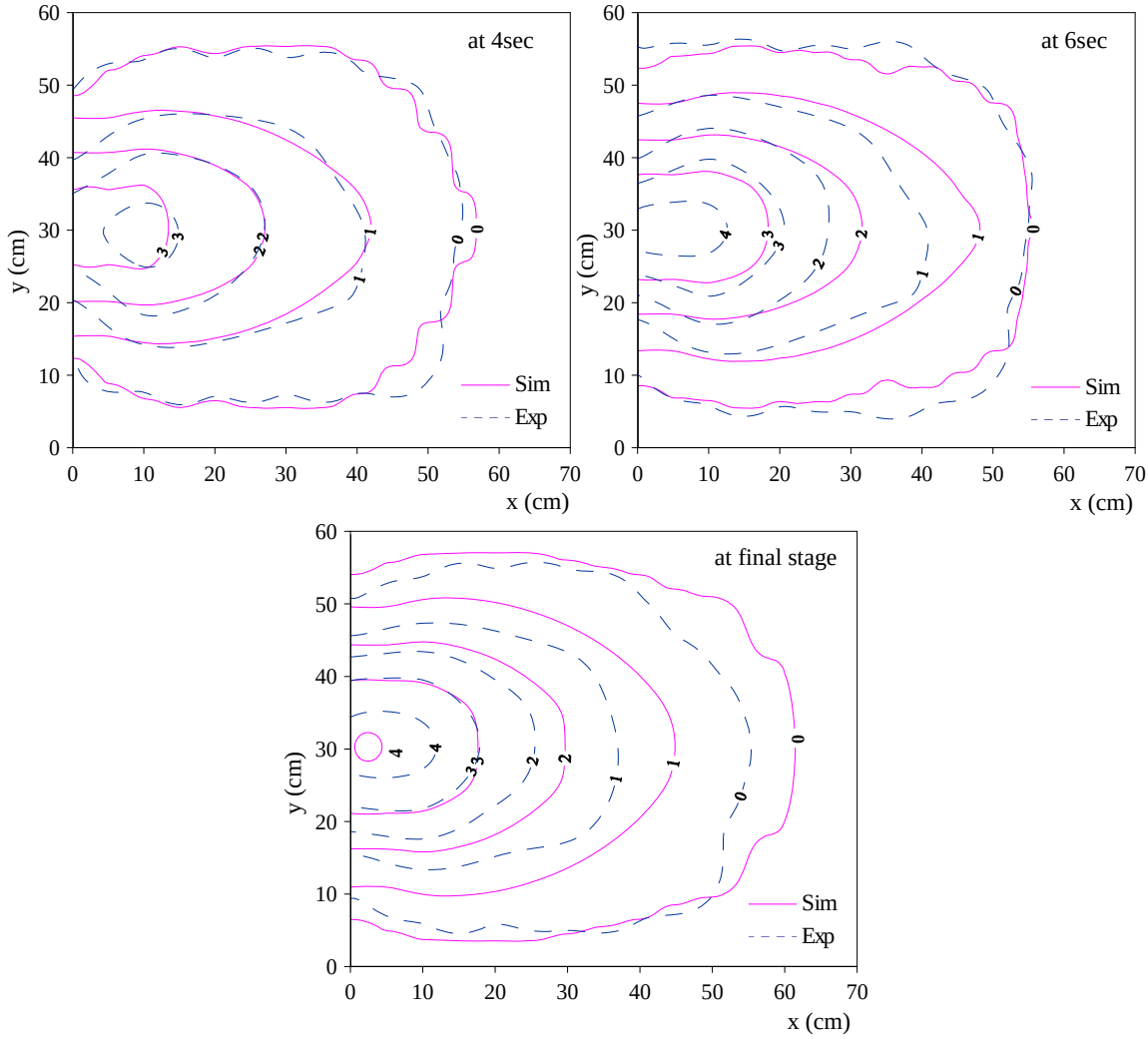

Figure 5.11 Temporal changes of shapes and thicknesses of a debris flow fan, with driftwood D_d=3mm and L_d =3.5cm, without check dam case

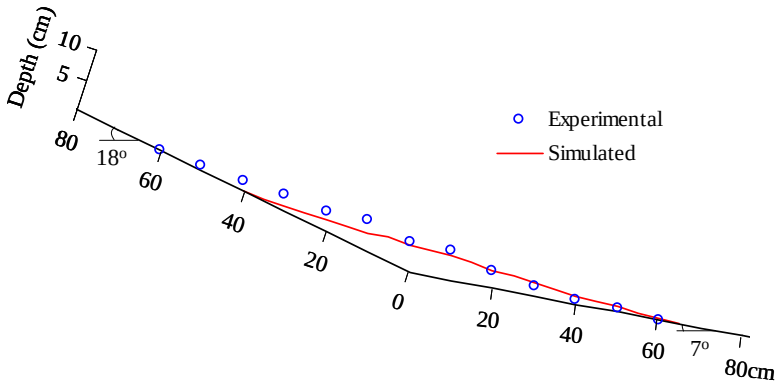

Figure 5.12 The final stage longitudinal bed profile along the center axis of a debris flow fan, with driftwood D_d=3mm and L_d =3.5cm, without check dam case

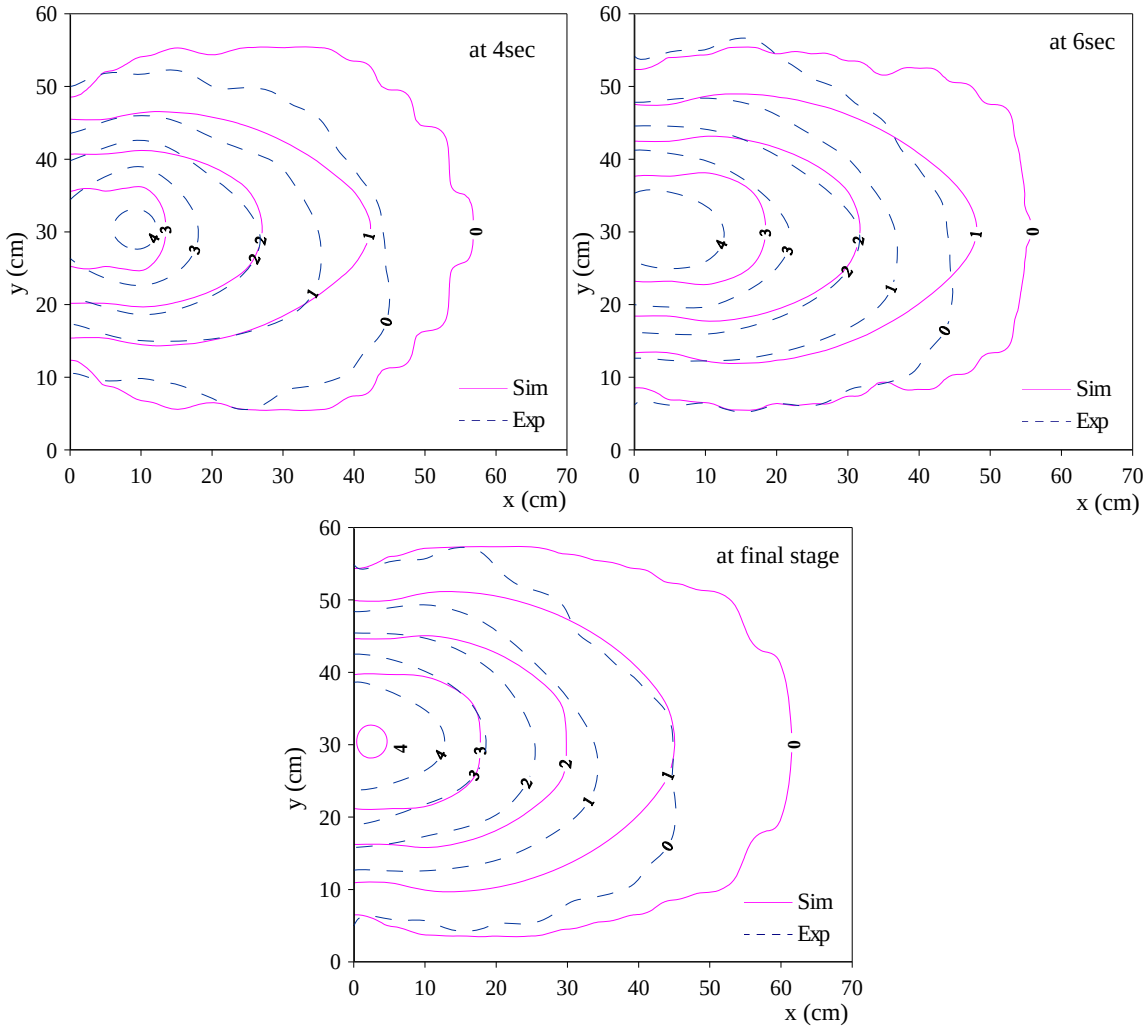

Figure 5.13 Temporal changes of shapes and thicknesses of a debris flow fan, with driftwood D_d=3mm and L_d =4.5cm, without check dam case

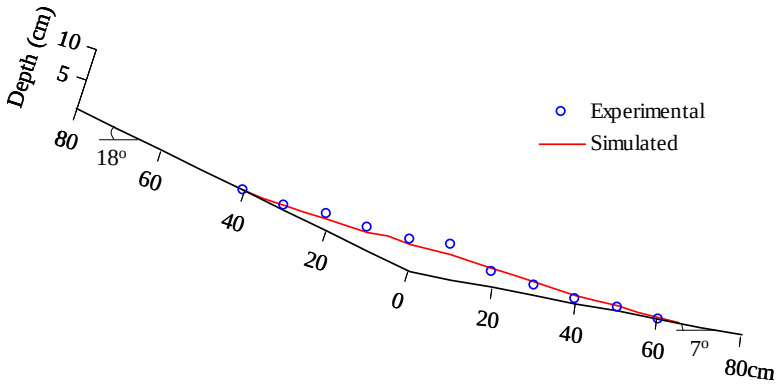

Figure 5.14 The final stage longitudinal bed profile along the center axis of a debris flow fan, with driftwood D_d=3mm and L_d =4.5cm, without check dam case

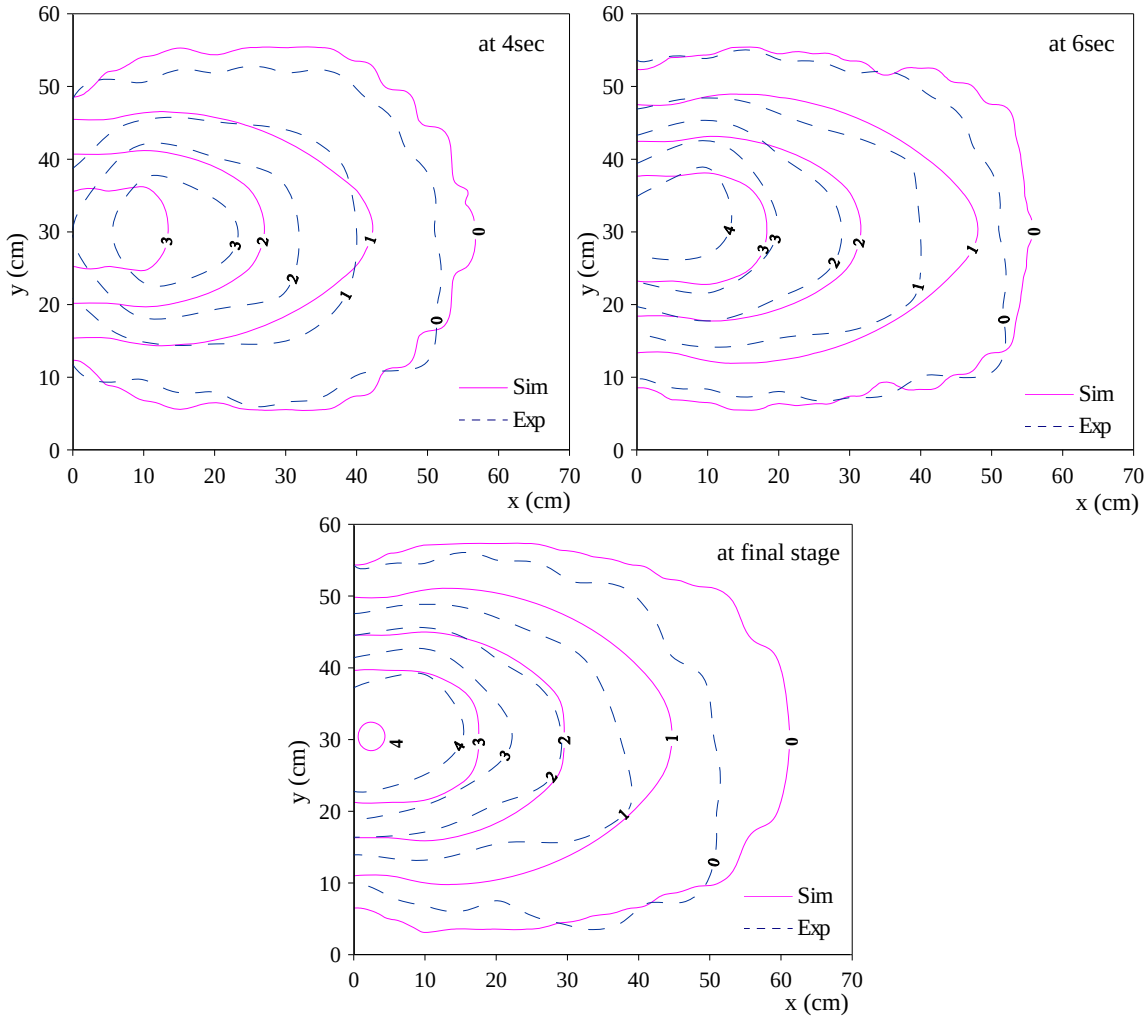

Figure 5.15 Temporal changes of shapes and thicknesses of a debris flow fan, with driftwood D_d=4mm and L_d =4.5cm, without check dam case

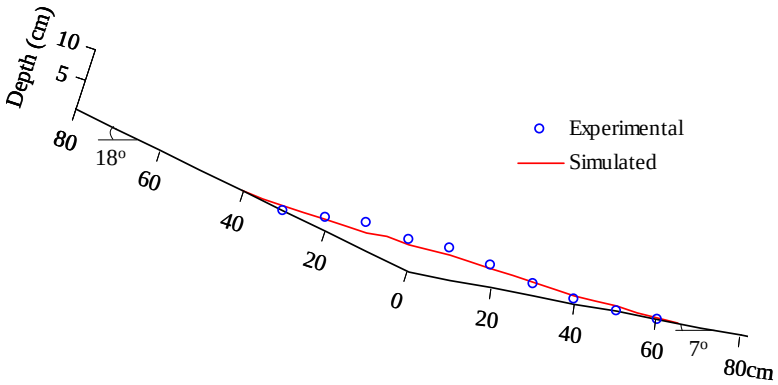

Figure 5.16 The final stage longitudinal bed profile along the center axis of a debris flow fan, with driftwood D_d=4mm and L_d =4.5cm, without check dam case

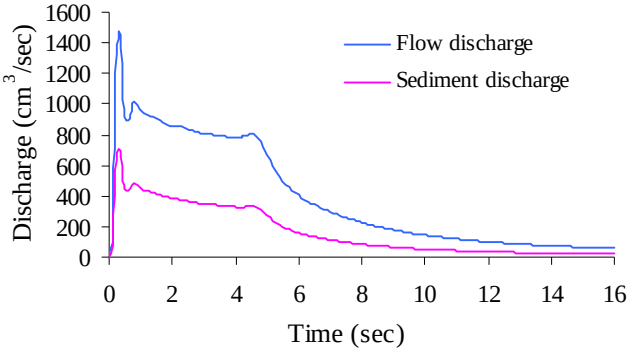

Figure 5.17 Simulated flow and sediment discharge at 10cm upstream from a debouching point, with driftwood D_d=4mm and L_d=4.5cm case, without check dam

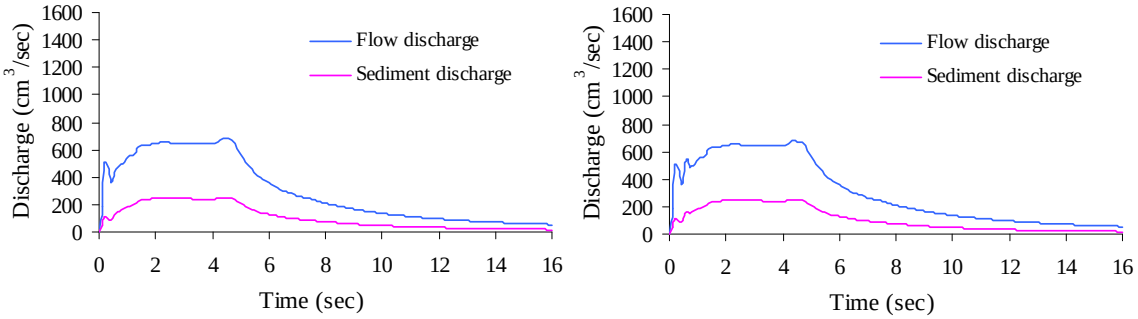

(a) With driftwood D_d=3mm and L_d =3.5cm

(b) With driftwood D_d=3mm and L_d =4.5cm

Figure 5.18 Simulated flow and sediment discharge at 10cm upstream from a debouching point, with driftwood and grid dam cases

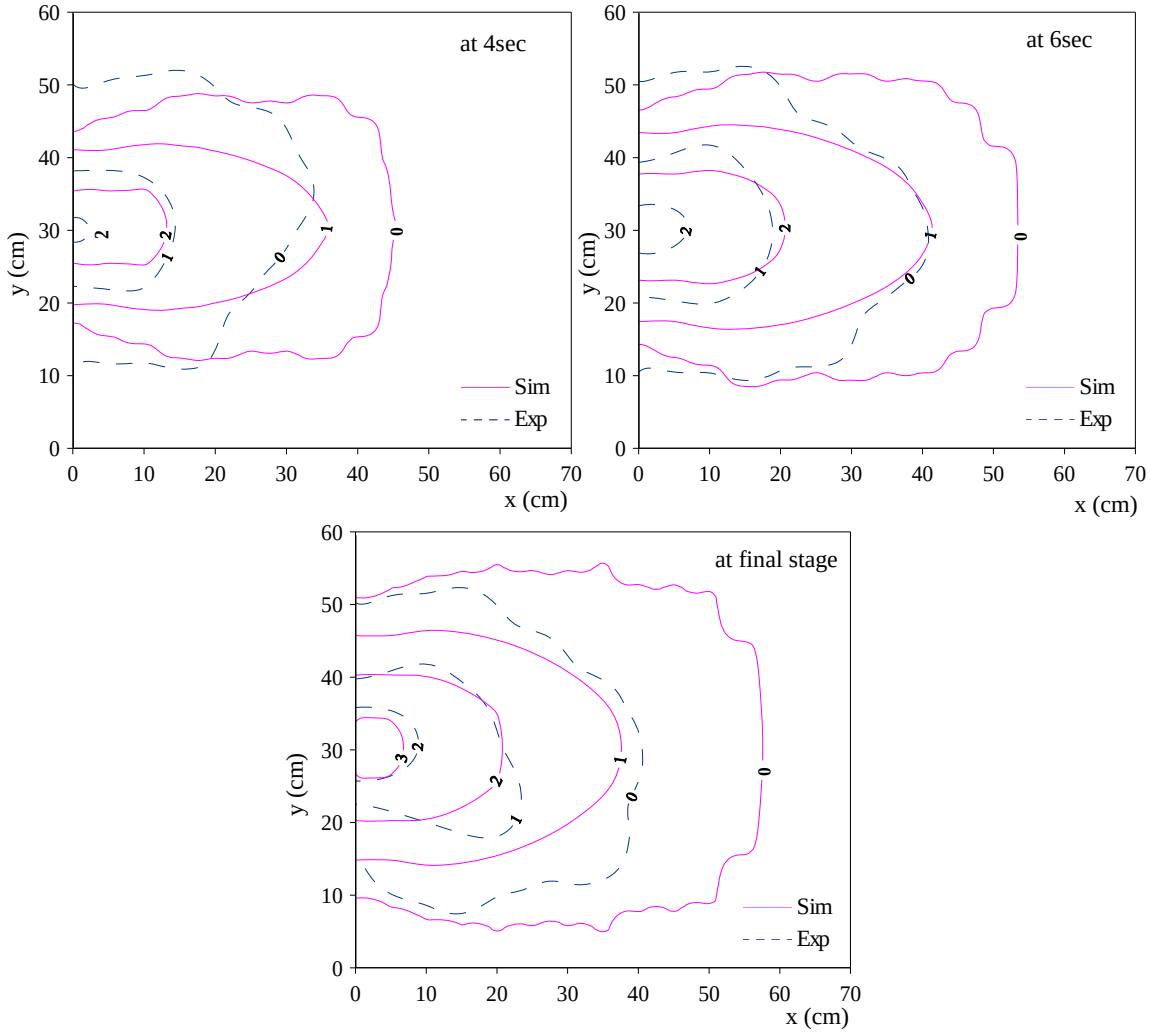

Figure 5.19 Temporal changes of shapes and thicknesses of a debris flow fan, with driftwood D_d=3mm and L_d =3.5cm, and grid dam case

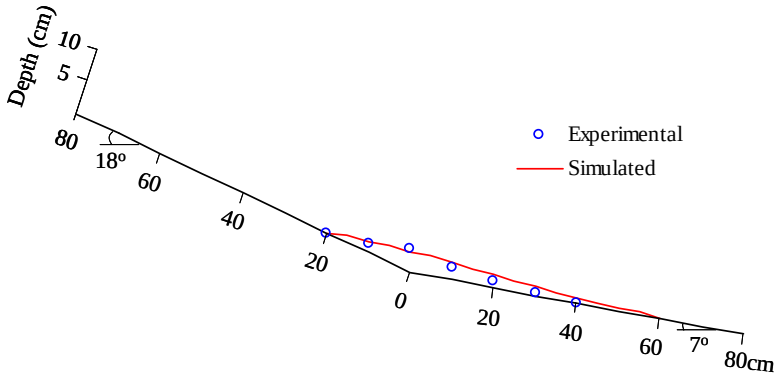

Figure 5.20 The final stage longitudinal bed profile along the center axis of a debris flow fan, with driftwood D_d=3mm and L_d =3.5cm, and grid dam case

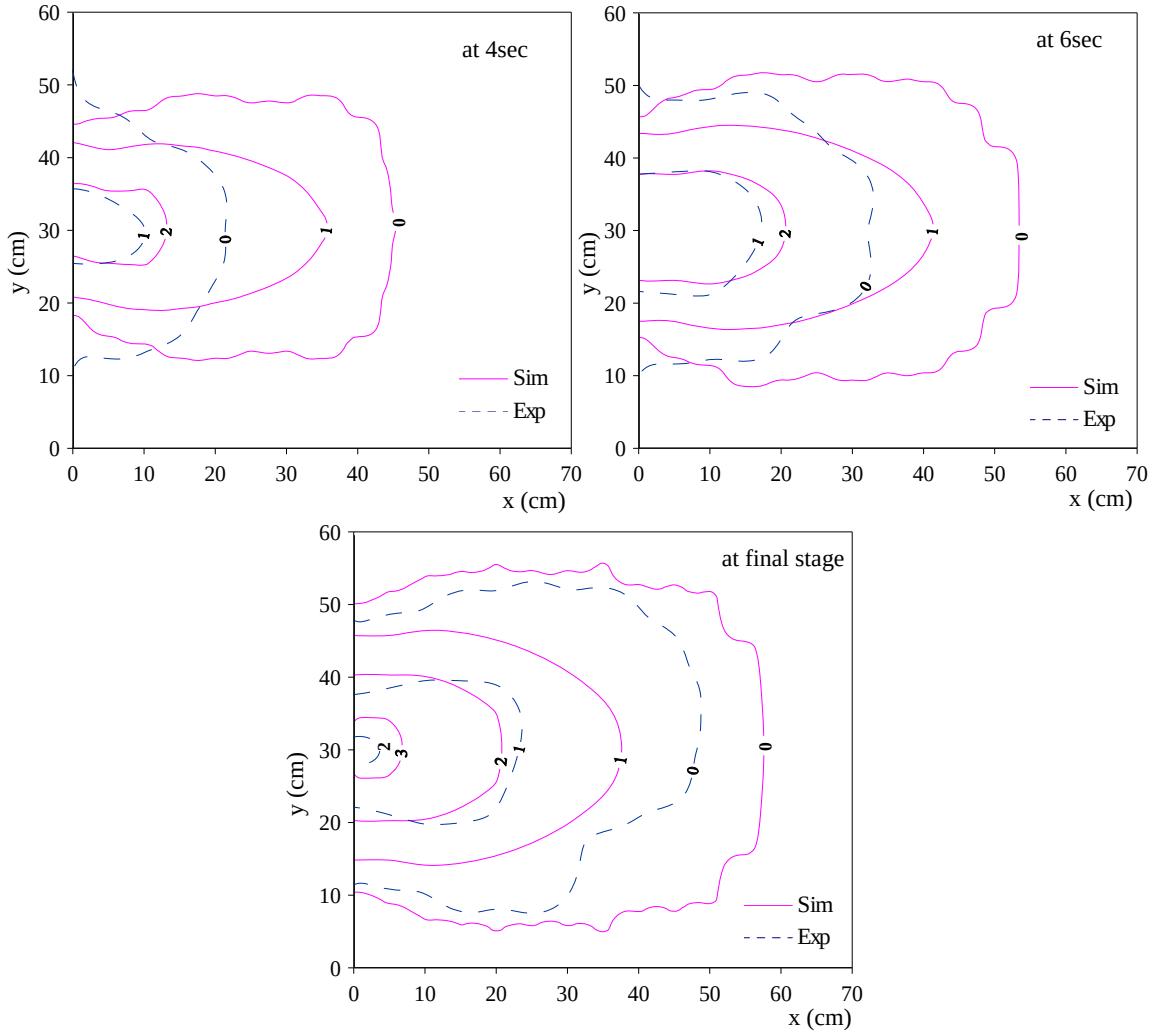

Figure 5.21 Temporal changes of shapes and thicknesses of a debris flow fan, with driftwood D_d=3mm and L_d =4.5cm, and grid dam case

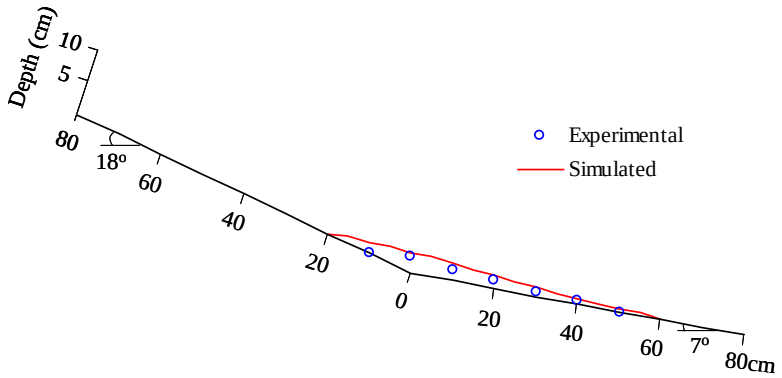

Figure 5.22 The final stage longitudinal bed profile along the center axis of a debris flow fan, with driftwood D_d=3mm and L_d =4.5cm, and grid dam case

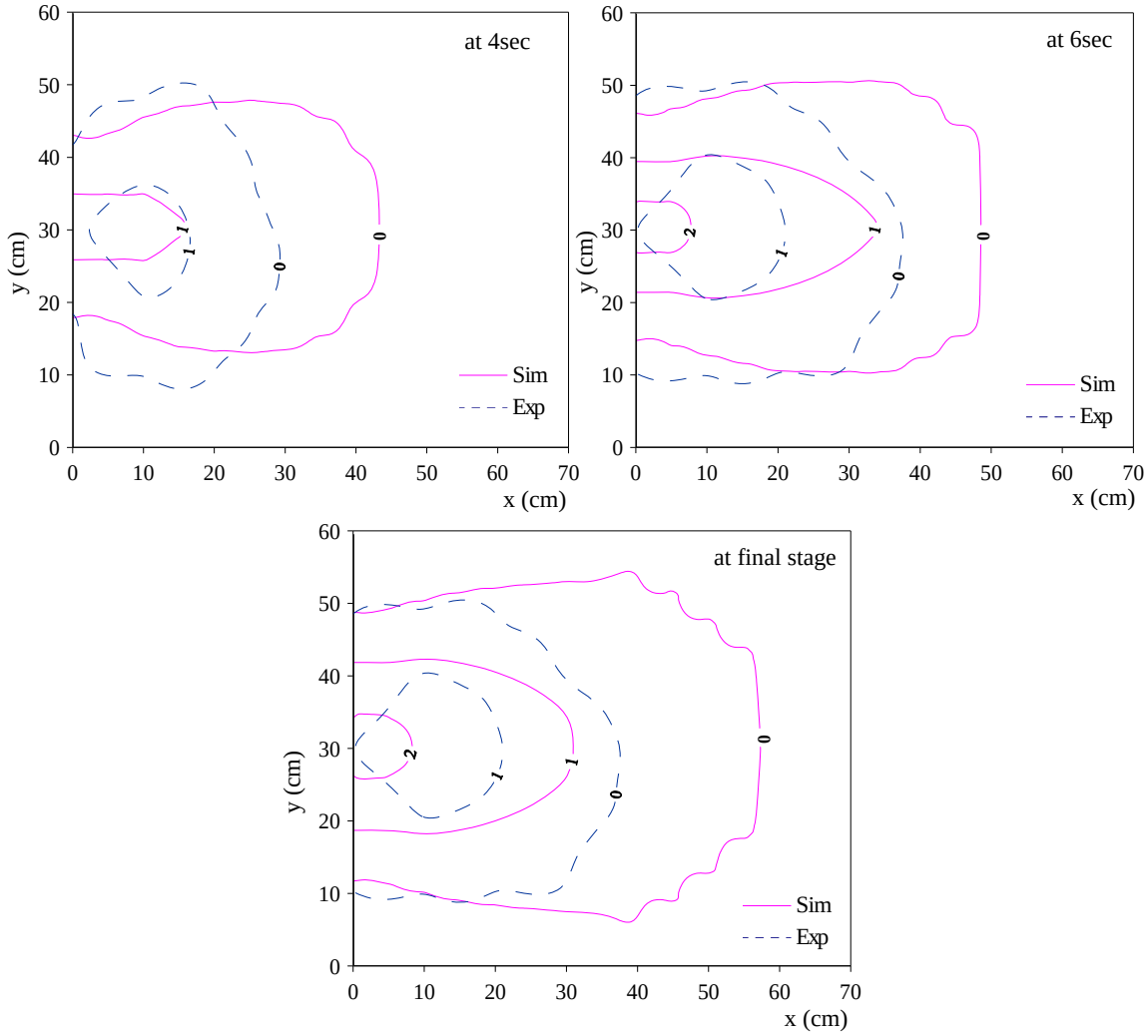

Figure 5.23 Temporal changes of shapes and thicknesses of a debris flow fan, with driftwood D_d=3mm and L_d =3.5cm, and slit dam case

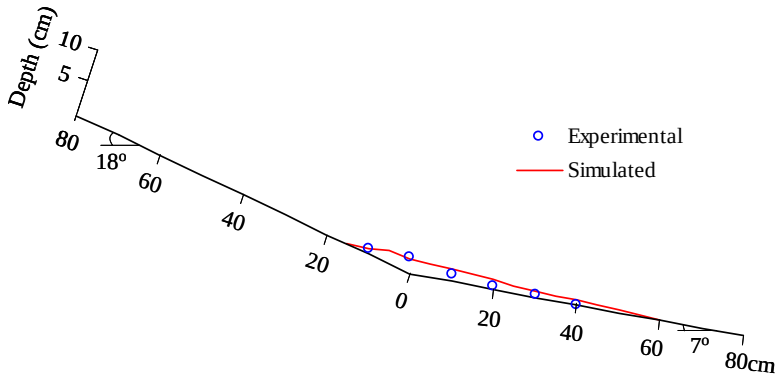

Figure 5.24 The final stage longitudinal bed profile along the center axis of a debris flow fan, with driftwood D_d=3mm and L_d =3.5cm, and slit dam case

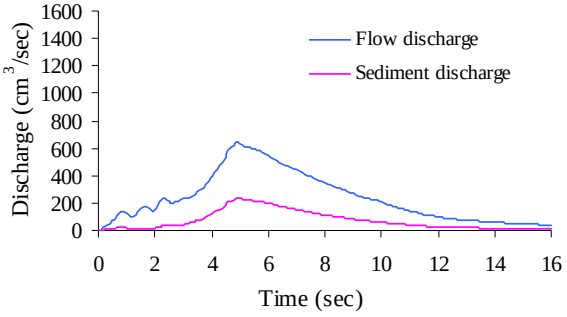

Figure 5.25 Simulated flow and sediment discharge at 10cm upstream from a debouching point, with driftwood D_d=3mm and L_d =3.5cm, and slit dam case

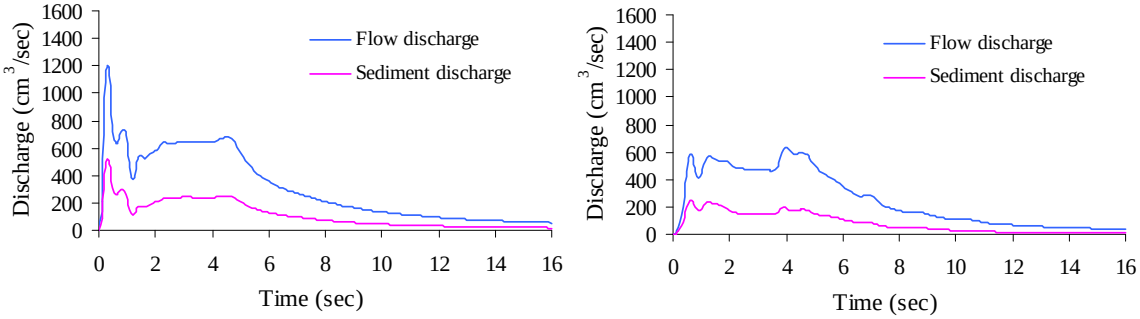

(a) Grid dam case

(b) Slit dam case

Figure 5.26 Simulated flow and sediment discharge at 10cm upstream from a debouching point, with check dams but without driftwood case

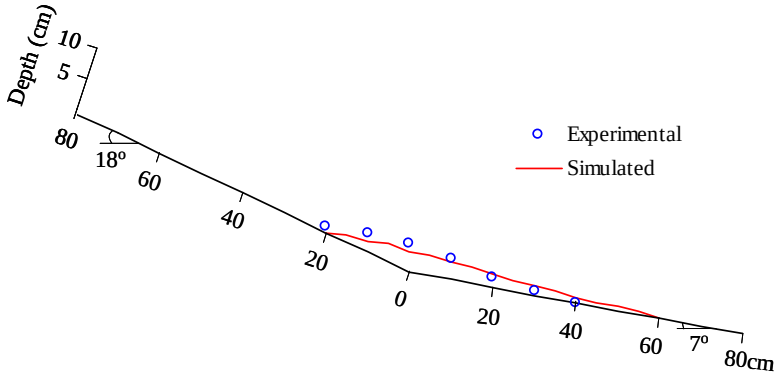

Figure 5.27 The final stage longitudinal bed profile along the center axis of a debris flow fan, with grid dam and without driftwood case

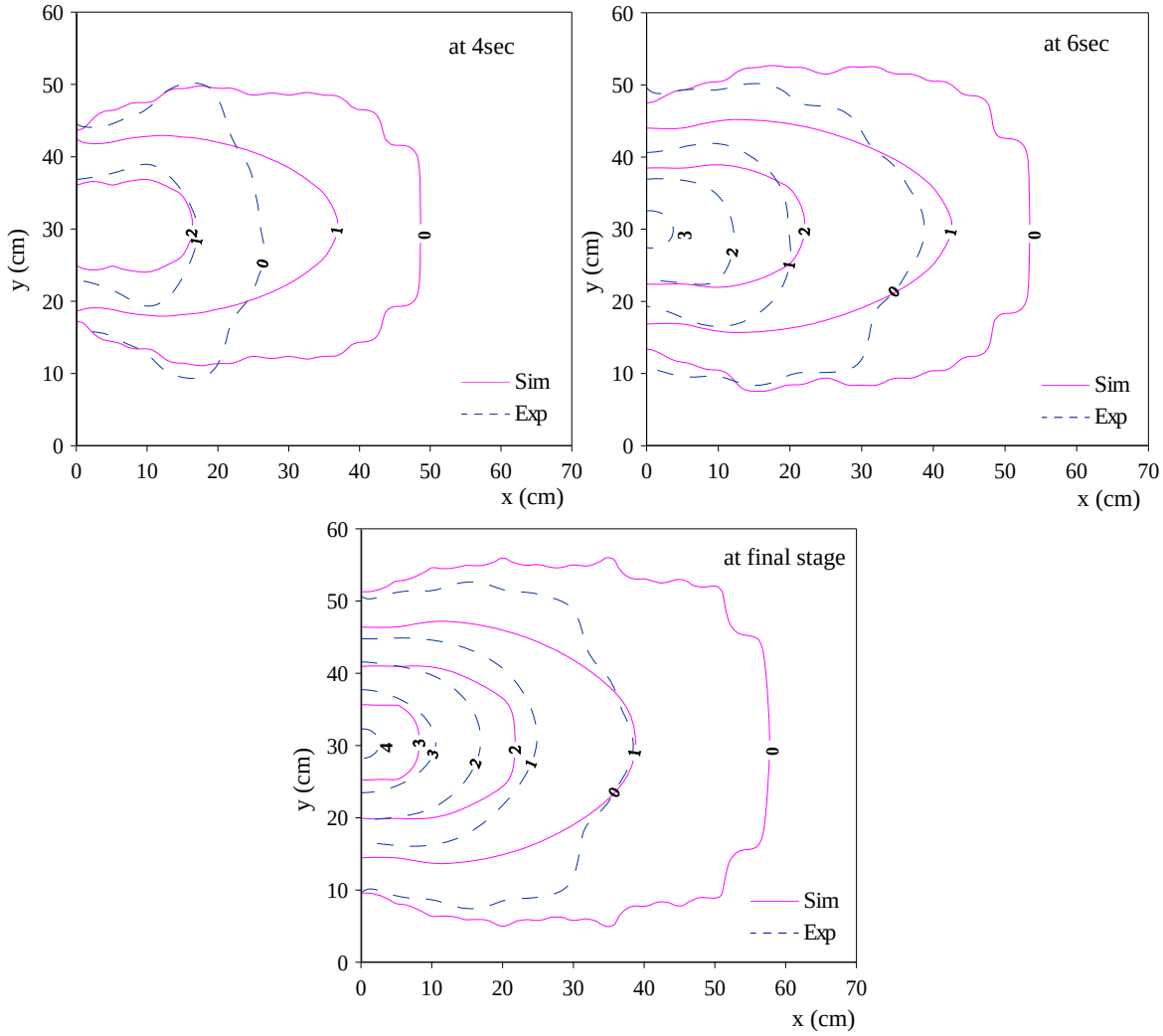

Figure 5.28 Temporal changes of shapes and thicknesses of a debris flow fan, with grid dam and without driftwood case

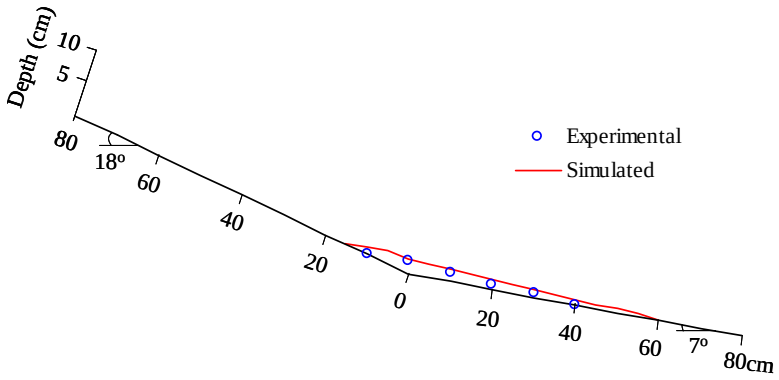

Figure 5.29 The final stage longitudinal bed profile along the center axis of a debris flow fan, with slit dam and without driftwood case

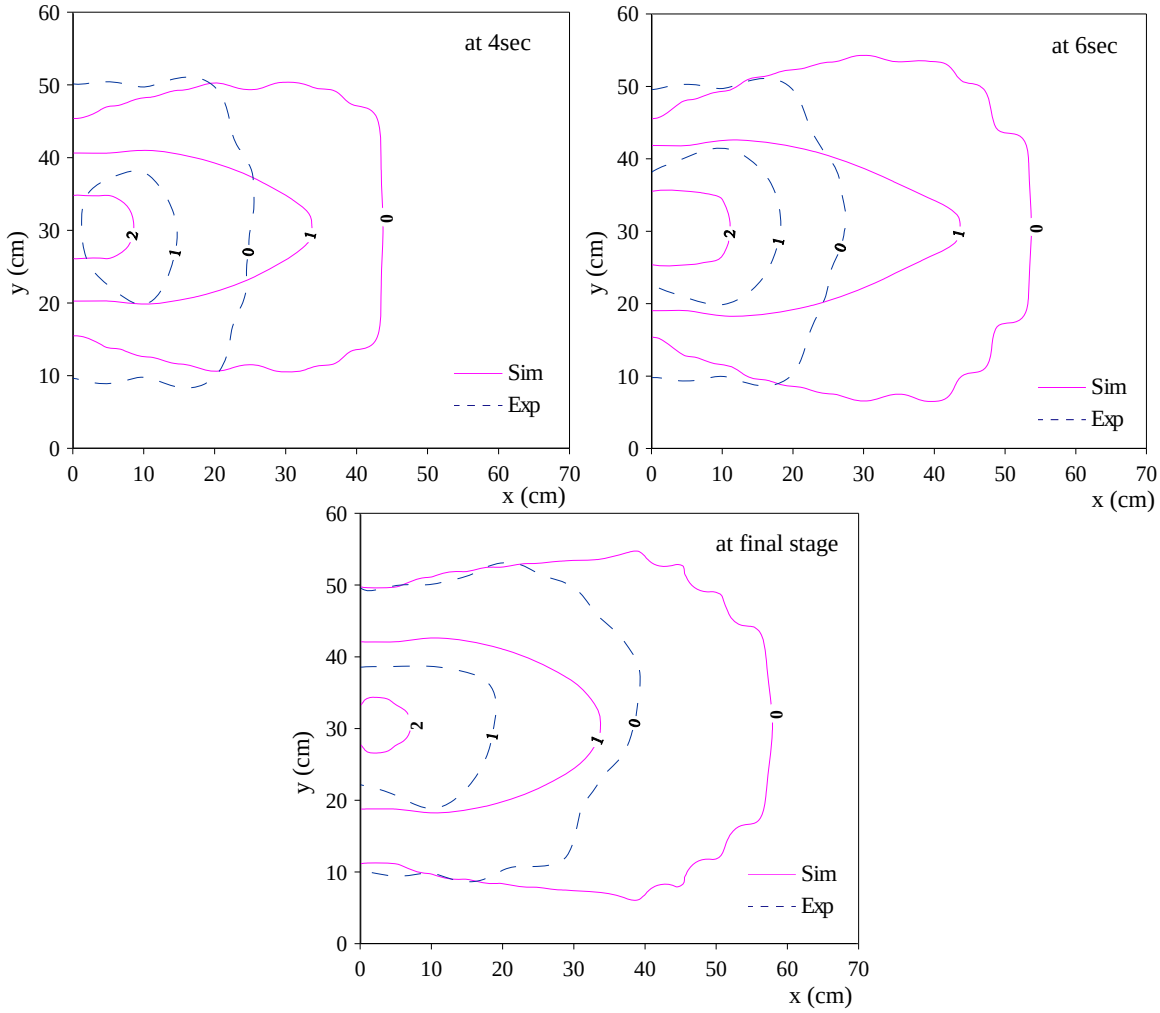

Figure 5.30 Temporal changes of shapes and thicknesses of a debris flow fan, with slit dam and without driftwood case

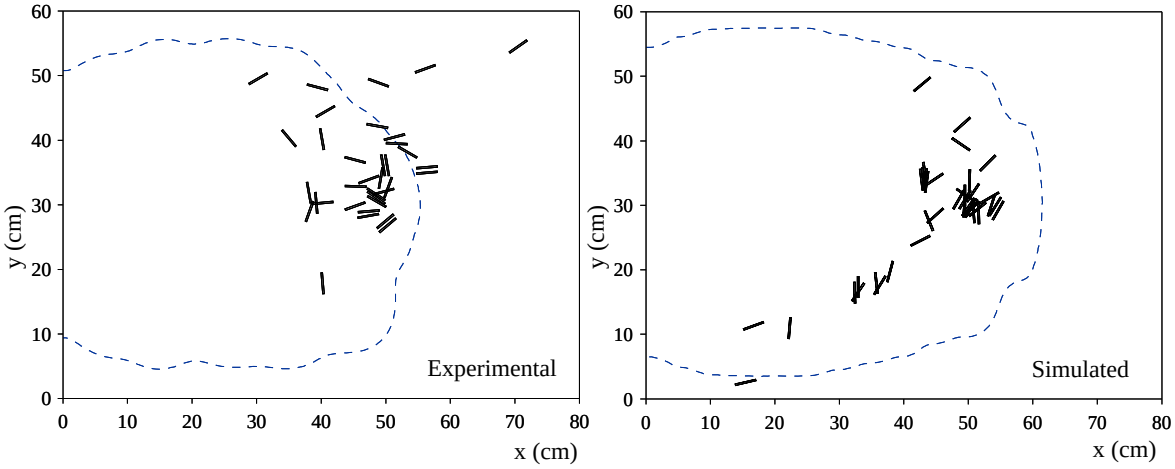

Figure 5.31 Positions and rotational angles of deposited driftwood in a debris flow fan, with driftwood D_d=3mm and L_d =3.5cm case, without check dam

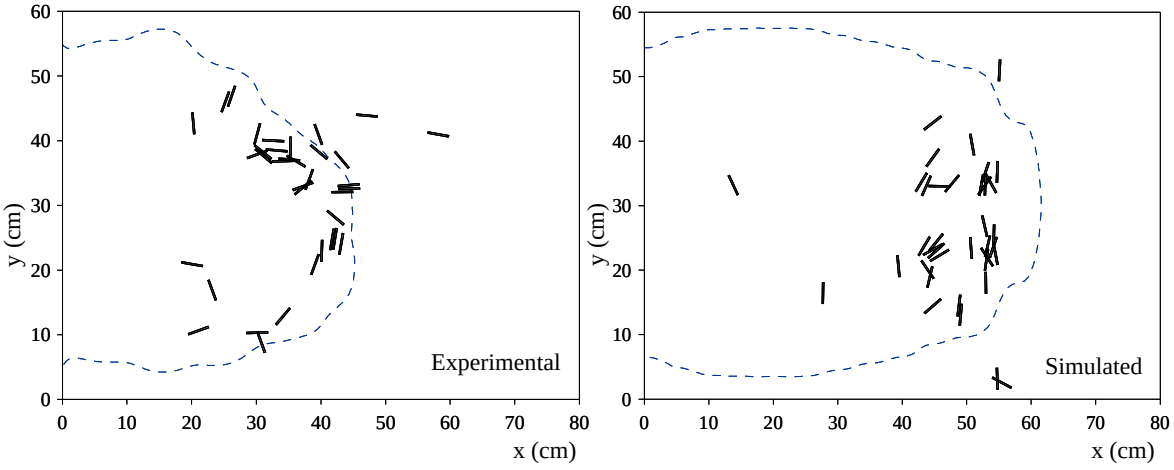

(a)

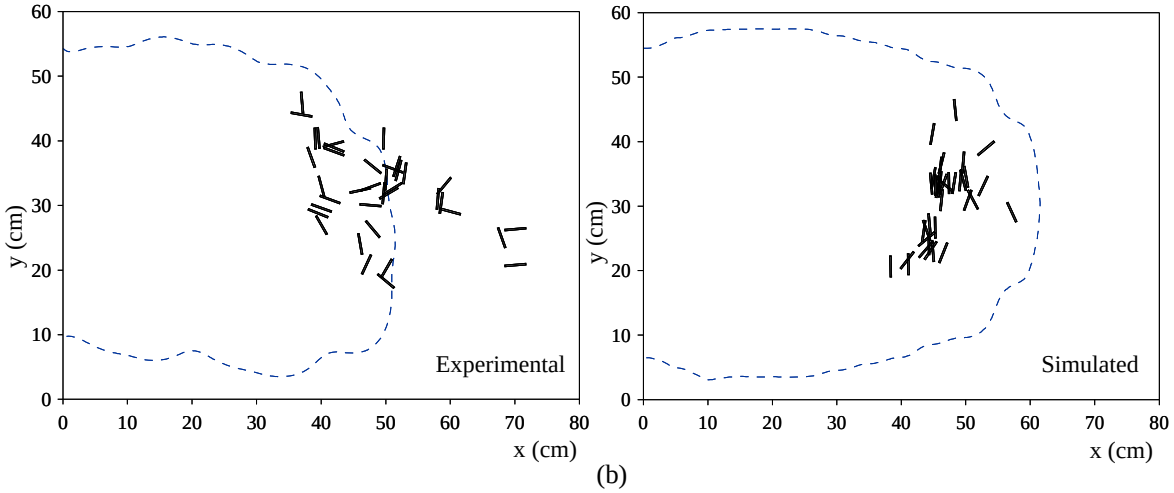

(b)

Figure 5.32 Positions and rotational angles of deposited driftwood in a debris flow fan, driftwood cases (a) D_d=3mm and L_d =4.5cm, (b) D_d=4mm and L_d =4.5cm, without check dam

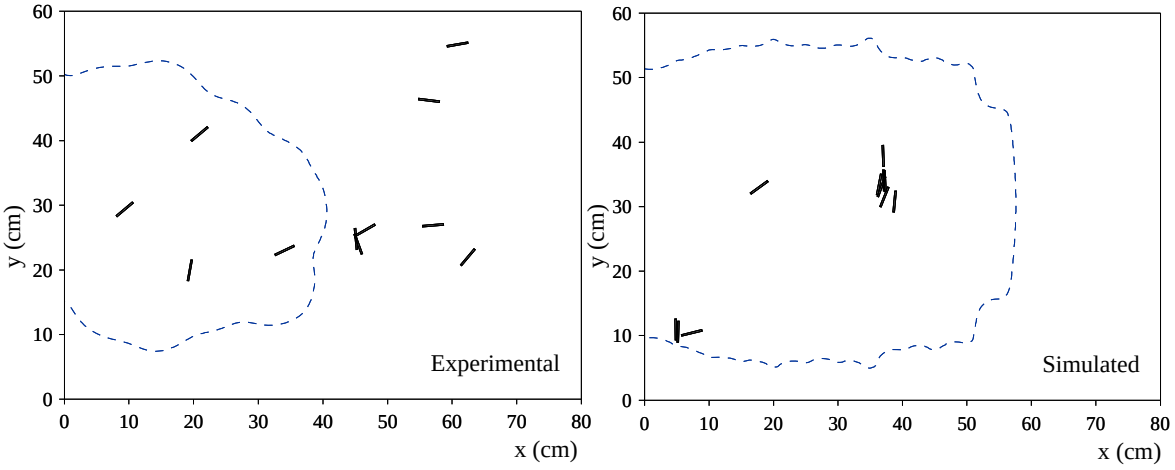

Figure 5.33 Positions and rotational angles of deposited driftwood in a debris flow fan, with driftwood D_d=3mm and L_d =3.5cm case, with grid dam

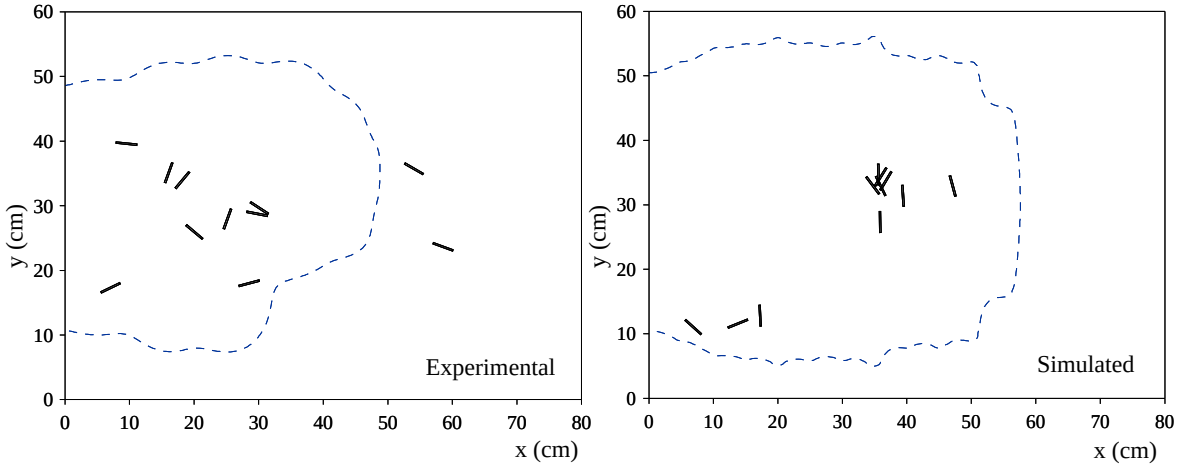

Figure 5.34 Positions and rotational angles of deposited driftwood in a debris flow fan, with driftwood D_d=3mm and L_d =4.5cm case, with grid dam

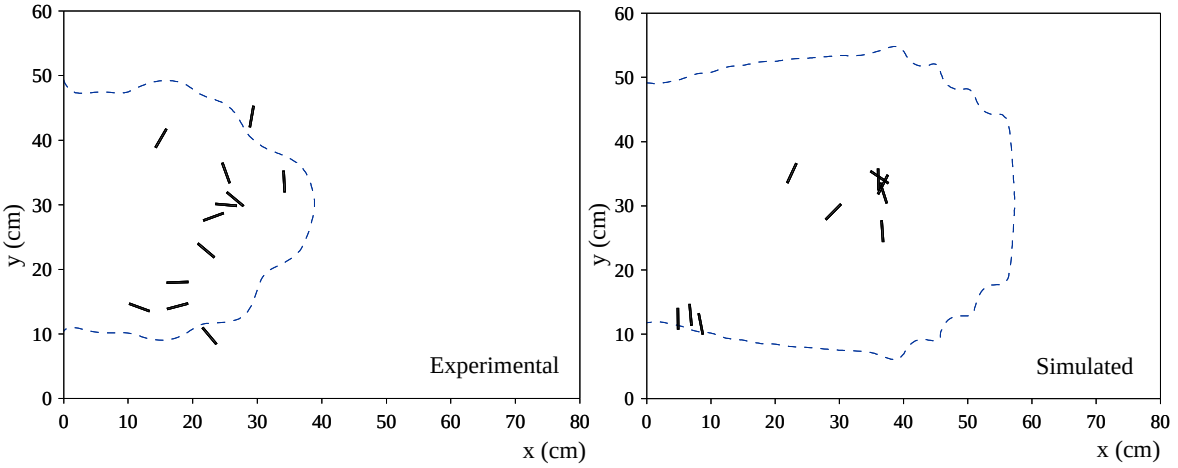

Figure 5.35 Positions and rotational angles of deposited driftwood in a debris flow fan, with driftwood D_d=3mm and L_d =3.5cm case, with slit dam

deposit thickness) of a debris flow fan with driftwood cases are shown in Figure 5.11, Figure 5.13 and Figure 5.15 for driftwood D_d=3mm and L_d=3.5cm, D_d=3mm and L_d=4.5cm, and D_d=4mm and L_d=4.5cm cases, respectively. The results of final longitudinal bed profile along the center axis of a debris flow fan for the cases with driftwood D_d=3mm and L_d=3.5cm, D_d=3mm and L_d=4.5cm, and D_d=4mm and L_d=4.5cm are shown in Figure 5.12, Figure 5.14 and Figure 5.16, respectively. The simulated results of shapes and thicknesses of a debris flow fan and final stage longitudinal bed profile are comparatively good agreement with the experimental results. By comparing the simulated results of the deposition of debris flow on the fan with and without

driftwood cases, it is found that the effect of driftwood in the deposition of debris flow on the fan is very small.

The effectiveness of check dams in a debris flow fan was also investigated through numerical model and hydraulic experiments. Figure 5.18 shows the simulated discharge at 10cm upstream from a debouching point in the case of grid dam with driftwood. The simulated results of temporal variations of shapes and thicknesses (flow depth plus deposit thickness) of a debris flow fan in the case of grid dam are shown in Figure 5.19 and Figure 5.21 for driftwood D_d=3mm and L_d=3.5cm, and D_d=3mm and L_d=4.5cm cases, respectively. The simulated results of the temporal variations of shapes and thicknesses of the deposition of debris flow on the fan are agreeable with the experimental results. The final longitudinal bed profiles along the center axis of a debris flow fan with grid dam are shown in Figure 5.20 and Figure 5.22 for driftwood D_d=3mm and L_d=3.5cm, and D_d=3mm and L_d=4.5cm cases, respectively. The temporal variations of the deposition of debris flow on the fan, longitudinal deposition profile and flow discharge in the case of slit dam with driftwood D_d=3mm and L_d=3.5cm are shown in Figure 5.23, Figure 5.24 and Figure 5.25, respectively. By comparing the results of deposition of debris flow on the fan with and without check dam, it is clear that the deposition areas and thicknesses in the cases of check dams are smaller than without check dam case. The thickness and deposition area of a debris flow fan are reduced due to the sediment capturing by grid or slit dam due to driftwood jamming.

Figure 5.26 shows the simulated flow discharge at 10cm upstream from a debouching point in the cases of grid dam and slit dam for the flow without driftwood. Figures 5.27 and 5.29 show the final longitudinal bed profiles along the center axis of a debris flow fan for grid dam and slit dam, respectively. In the case of flow without driftwood, the simulated and experimental results of temporal variations of the deposition of debris flow on the fan are shown in Figure 5.28 and Figure 5.30 for grid dam and slit dam, respectively. From the experiments, it is clear that check dams not only capture the debris flow but also reduce the energy of flow. The simulated results of thicknesses and shapes are somewhat higher and larger than experimental results which may be caused by the excessive energy loss of flow due to the existence of check dam in the experiments.

The friction forces generated between driftwood and bed surface in Equations (5.1) and (5.2) were considered in downstream channel only (i.e., downstream from a debouching point) to calculate the driftwood deposition in a debris flow fan. The comparisons between the

experimental and simulated positions and rotational angles of deposited driftwood in a debris flow fan without check dam case are shown in Figures 5.31, Figure 5.32 (a) and Figure 5.32 (b) for driftwood D_d=3mm and L_d=3.5cm, D_d=3mm and L_d=4.5cm, and D_d=4mm and L_d=4.5cm cases, respectively. The dashed line in the figures indicates the debris flow fan area. The positions and the rotational angles of the pieces of driftwood in a group found experimentally are fairly well explained by the numerical simulation. The results of positions and rotational angles of deposited driftwood in a debris flow fan with grid dam are shown in Figure 5.33 and Figure 5.34 for driftwood D_d=3mm and L_d=3.5cm, and driftwood D_d=3mm and L_d=4.5cm cases, respectively. The results of driftwood deposition in a debris flow fan with slit dam case are shown in Figure 5.35. The number of driftwood deposition on the debris flow fan is reduced by open type check dams due to driftwood jamming on the check dam.

Summary

Numerical analysis and experimental studies were carried out to investigate the deposition of debris flows with driftwood on the fan. A two-dimensional integrated numerical model was developed for computing the characteristics of debris flow with driftwood, which can simulate all stages of debris flow from initiation, transportation and deposition stages. A numerical simulation model was developed with an interacting combination of Eulerian expression of the debris flow and Lagrangian expression of the driftwood. A capturing model of debris flow with driftwood by open type check dams was also incorporated into an integrated numerical model. The calculated results of the shapes and thicknesses of a debris flow fan and the positions and rotational angles of deposited driftwood in a debris flow fan are in good agreement with the experimental results. The effects of check dams in a debris flow fan formation were also investigated.

Chapter 6

Conclusions and Recommendations

In this study, the most effective and reliable methods to reduce the debris flow disasters with driftwood were investigated by numerical simulation and laboratory experimental approaches. A numerical model was developed to simulate the debris flow deposition upstream of check dams. A new deposition equation to calculate the debris flow deposition upstream of check dams was also developed. The erosion of deposited sediment upstream of a check dam was investigated by using one-dimensional river bed erosion model. A two-dimensional numerical model was developed for computing the characteristics of debris flow with driftwood and its capturing process due to jamming of driftwood on open type check dams. A numerical model of debris flow with driftwood was developed with an interacting combination of Eulerian expression of the debris flow and Lagrangian expression of the driftwood, in which the fluctuation components of the position and the rotational angular velocity of the driftwood were dealt with stochastically. The jamming of driftwood on open type check dams such as grid or slit dam was evaluated based on the geometric conditions and probabilistic approaches. An integrated numerical model was developed for computing the characteristics of debris flow with driftwood, which can simulate all stages of debris flow from initiation to deposition stages. The driftwood deposition process to compute the positions and rotational angle of deposited driftwood in a debris flow fan was also considered into an integrated numerical model. The simulated results were compared with those obtained from the hydraulic experiments.

6.1 Conclusions

The conclusions of this study are summarized as follows.

Debris flow deposition and erosion of deposited sediment upstream of check dams

A numerical model was presented to investigate the process of debris flow deposition upstream of a check dam. A new deposition equation to calculate the debris flow deposition upstream of a check dam was also developed. The debris flow deposition upstream of a check dam was

investigated using the constitutive equations of Takahashi et al. (1997) and those of Egashira et al. (1997). The simulated results of debris flow deposition upstream of check dams and the reduction in flow discharge at downstream end of the flume are in good agreement with the experimental results. The debris flow deposition phenomenon upstream of check dams can be calculated by the proposed deposition velocity model and both the constitutive equations of Takahashi et al. (1997) and Egashira et al. (1997).

The experiments were carried out in the fixed bed condition, in which the debris flow jumps due to the collision with a check dam or the deposited surface and flows on it. The deposited sediment in the most upstream area of the deposition is eroded by the coming debris flow from the upstream and the many sediments discharge downstream.

The simulated results of erosion of deposited sediment upstream of grid dams by normal flow discharge using a one-dimensional riverbed erosion model agree well with the experimental results. The deposited sediment upstream of a grid dam can be flushed out more effectively than that of a closed dam due to erosion process by a normal scale of flood flow when some deposited large boulders from the upstream of the dam are removed. From the results, it is shown that the grid type check dam can keep their sediment trapping capacity more effectively than the closed type check dam. An open type check dam not only provides adequate debris flow disaster prevention effects, but also conserves the natural environment and landscape.

Debris flow with driftwood model

A two-dimensional numerical model of debris flow with driftwood was developed with an interacting combination of Eulerian expression of the debris flow and Lagrangian expression of the driftwood. The position and the rotational angular velocity of the driftwood fluctuated due to the collision of driftwood with boulders and disturbances on the flow surface during the collision of the sediment particles, which were considered in the diffusions coefficients. The fluctuation components of the position and the rotational angular velocity of the driftwood were dealt with stochastically as random variables based on the results of a statistical analysis of experimental values. The scattering process of driftwood was described as a diffusion process and the diffusion coefficients were defined by the hydraulic experiments. The calculated results of frequency distribution of the longitudinal positions, the transverse positions and the rotational angular velocities of the driftwood are fairly good agreement with the experimental results. The scattering process of the driftwood can be expressed by the normal distribution. The average

values of the non-dimensional diffusion coefficients $K_x / u_* h = 0.649$ and $K_y / u_* h = 0.343$ are obtained. The relation between the Froude number, Fr, and the standard deviation of the rotational angular velocity of the driftwood, σ_w, is obtained as $\sigma_w = 25.61 Fr$.

The simulated results of outflow discharge, sediment concentration and the percentage of driftwood outflow at the downstream end of the flume are in good agreement with the experimental results. The positions and rotational angle of the driftwood dealt with deterministically and stochastically are well explained in the simulations. The proposed model can predict the characteristics of debris flow with driftwood such as outflow hydrograph, sediment concentrations and driftwood outflows.

Capturing process of debris flow with driftwood by open type check dams

A numerical model was developed for computing the debris flow with driftwood capturing by open type check dams such as grid or slit dam. A deposition model was also developed to calculate the debris flow deposition due to driftwood jamming on a grid or slit dam. To simulate the debris flow with driftwood capturing by grid or slit dam, a jamming model of driftwood and a deposition model behind a grid or slit dam were incorporated in a two-dimensional flow model of debris flow with driftwood. The jamming of driftwood on open type check dams was evaluated based on the geometric conditions and probabilistic approaches. The flow and sediment discharge passing through a grid or slit dam are reduced due to driftwood jamming on open spaces of dam. The results of flow discharge, sediment discharge and the percentage of driftwood passed through a grid or slit dam are in good agreement with the experimental results. The simulated results of debris flow deposition upstream of check dams are also agreeable with the experimental results. The proposed model can evaluate the capturing process of debris flow with driftwood by open type check dams.

The driftwood passing through a grid or slit dam is reduced due to the driftwood jamming on the dam. The number of pieces of the driftwood outflows from a grid or slit dam based on the developed driftwood jamming model under the geometric conditions and probabilistic approaches are well explained in the numerical simulations. The experimental results show that driftwood passing rate through open type check dams is decreased as diameter of driftwood pieces increases.

Debris flow with driftwood fan deposition

Numerical analysis and experimental studies are carried out to investigate the deposition of debris flows with driftwood on the fan. A two-dimensional integrated numerical model was developed for computing the characteristics of debris flow with driftwood, which can simulate all stages of debris flow from initiation, transportation and deposition stages. A numerical simulation model was developed with an interacting combination of Eulerian expression of the debris flow and Lagrangian expression of the driftwood. The driftwood deposition in a debris flow fan was calculated by considering the friction forces generated between driftwood and bed surface. A capturing model of debris flow with driftwood by open type check dams was also incorporated into an integrated numerical model. The calculated results of the shapes and thicknesses of a debris flow fan and the positions and rotational angles of deposited driftwood in a debris flow fan are in good agreement with the experimental results.

It is found that the effect of driftwood in the deposition of debris flow on the fan is very small. Driftwood is deposited at the foot of a debris flow fan. The positions and rotational angle of the deposited driftwood are well explained in the numerical simulations. The proposed model helps to reduce the debris flow disasters with driftwood.

The effects of check dams in a debris flow fan formation were also investigated. It is clear that the deposition areas and thicknesses in the cases of check dams are smaller than without check dam case. The thicknesses and shapes of the debris flow fan are reduced due to the sediment captured by check dams. Thus, we can reduce the hazards area by constructing check dams in the river basin. The proposed model can be used to investigate the preventive measures of debris flow disasters with driftwood by combining structural and non-structural countermeasures.

6.2 Recommendations for future researches

Future work is required to improve the performance of the model. The recommendations for future researches are discussed here.

(a) The proposed model of debris flow deposition upstream of a check dam is verified with the experimental results. The application of the model to the real field cases is necessary to be conducted for examine the applicability of the model. It is also necessary to investigate the effectiveness of check dams for debris flow control in river basin scale.

(b) In this study, a two-dimensional numerical model of debris flow with driftwood is developed with an interacting combination of Eulerian expression of the debris flow and Lagrangian expression of the driftwood. In the present study, the similarity of the driftwood to the actual one is not considered, which will be necessary to investigate the similarity conditions. The proposed model is verified with the experimental results. It is also necessary to check the applicability of the model with actual field cases.

(c) In this study, the fluctuation components of the position and rotational angular velocity of the driftwood due to the collision of driftwood with boulders and disturbances on the flow surface during the collision of the sediment particles are considered in the diffusion coefficients. The flow motion of driftwood may be affected by the collisions of driftwood with boulders, which is not considered. It is very difficult to evaluate the collisions between driftwood and boulders. However, further study is necessary to consider the collisions between driftwood and boulders in the flow motion of driftwood with deterministically.

(d) In this study, the diffusion coefficients relate with the friction velocity and flow depth and the standard deviation of rotational angular velocity of the driftwood relates with Froude number. They may also depend on other hydraulic parameters, so further study is necessary to clarify their relations.

(e) In this study, cylindrical pieces of driftwood model are used, further it is also necessary to investigate the driftwood pieces with branches to improve the models of debris flow with driftwood and driftwood capturing by open type check dams.

(f) To evaluate the risk of debris flow disasters with driftwood, it is also necessary to investigate the driftwood caught by houses and other structures in low land areas.

(g) The bed surfaces of low land areas or fan areas may not be always saturated even in a heavy rainfall, because of the high permeability of the bed materials. In such conditions, the excessive infiltration may occur, which may strongly affect on the formation, shapes and thicknesses, and travel distance of the deposition of debris flow on the fan. Further experimental and numerical studies are necessary to consider the infiltration in fan areas.

(h) When debris flow flows down along the river with driftwood, such driftwood clogs narrows in the river course or bridge/piers or culvert sites giving rise to flooding, bridge/piers or embankments damage or destruction, which results in disastrous damage and considerable loss of life and property. Thus, it is necessary to investigate the effects of driftwood carried by debris flow on bridge/piers, culvert and embankment such as accumulation process, clogs and others, in order to prevent the destruction of river structures and reduce the hazards from debris flow disasters with driftwood. In addition, development of design

criteria such as clear spacing, height, shape and other specifications of bridge/piers and culvert are also very important.

(i) Other limitations of the present study are as follows; the motion of driftwood is restricted near the flow surface, the rotational motion of the driftwood is also supposed to be restricted on the flow surface and the rotation on the vertical plane is not considered, and it is assumed that the pieces of driftwood are sufficiently dispersed so that collisions between them are infrequent. Further study is necessary to consider these limitations.

References:

Abramowitz, M. and Stegun, I. A.: Handbook of Mathematical Functions with Formulas, Graphs, and Mathematical Tables, *New York: Dover*, 1972.

Ackermann, N. L. and Shen, H.: Stresses in rapidly sheared fluid-solid mixtures, *Journal of the Engineering Mechanics Division*, ASCE, Vol. 108, No. 1, pp.95-113, 1982.

Armanini, A. and Gregoretti, C.: Triggering of debris-flow by overland flow: A comparison between theoretical and experimental results, *Proceedings of the Second International Conference on Debris-Flow Hazards Mitigation: Mechanics, Prediction, and Assessment*, Taiwan, Balkema, Rotterdam, pp.117-124, 2000.

Armanini, A. and Larcher, M.: Rational criterion for designing opening of slit-check dam, *Journal of Hydraulic Engineering*, ASCE, Vol. 127, No. 2, pp.94–104, 2001.

Ashida, K., Egashira, S., Kurita, M. and Aramaki, H.: Debris flow control by grid dams, *Annuals of the Disaster Prevention Research Institute*, Kyoto University, No. 30 B-2, pp.441-456, 1987 (in Japanese).

Ashida, K. and Takahashi, T.: Study on debris flow control -hydraulic function of grid type open dam-, *Annuals of the Disaster Prevention Research Institute*, Kyoto University, No. 23 B-2, pp.433-441, 1980 (in Japanese).

Bouchut, F. and Westdickenberg, M.: Gravity driven shallow water models for arbitrary topography, *Communications in Mathematical Science*, Vol. 2, No. 3, pp.359-389, 2004.

Bovolin, V. and Mizuno, H.: Experimental study on the effect of a check dam against mudflow, *Proceedings of the Second Conference on Debris-Flow Hazards Mitigation: Mechanics, Prediction, and Assessment*, Taiwan, Balkema, Rotterdam, pp.573-578, 2000.

Brufau, P., Garcia-Navarro, P., Ghilardi, P., Natale, L. and Savi, F.: 1D mathematical modelling of debris flow, *Journal of Hydraulic Research*, Vol. 38, No. 6, pp.435-446, 2000.

Busnelli, M. M., Stelling, G. S. and Larcher, M.: Numerical morphological modeling of open-check dams, *Journal of Hydraulic Engineering*, ASCE, Vol. 127, No. 2, pp.105-114, 2001.

Carter, R. M.: A discussion and classification of subaqueous mass-transport with particular application to grain-flow, slurry-flow, and fluxoturbidites, *Earth Science Reviews*, Vol. 11, pp.145−177, 1975.

Chau, K. T., Chan, L. C. P., Luk, S. T. and Wai, W. H.: Shape of deposition fan and runout distance of debris-flow: Effects of granular and water contents, *Proceedings of the Second Conference on Debris-Flow Hazards Mitigation: Mechanics, Prediction, and Assessment*, Taiwan, Balkema, Rotterdam, pp.387-395, 2000.

Chau, K. T. and Lo, K. H.: Hazard assessment of debris flows for Leung King Estate of Hong Kong by incorporating GIS with numerical simulations, *Natural Hazards and Earth System Sciences*, Vol. 4, pp.103-116, 2004.

Chen, C. L.: Generalized viscoplastic modeling of debris flow, *Journal of Hydraulic Engineering*, ASCE, Vol. 114, No. 3, pp.237-257, 1988.

Chen, C. L. and Ling, C. H.: Fully developed snout profiles of noncohesive debris-flow with internal friction, *Proceedings of the Second International Conference on Debris-Flow Hazards Mitigation: Mechanics, Prediction, and Assessment*, Taiwan, Balkema, Rotterdam, pp.335-344, 2000.

Costa, J. E.: Physical geomorphology of debris flows, *In: Costa, J. E. and Fleischer, P. J. (eds.), Developments and Applications of Geomorphology*, Springer-Verlag, New York, pp.268−317, 1984.

Daido, A.: On the occurrence of mud-debris flows, *Bulletin of Disaster Prevention Research Institute*, Kyoto University, Japan, Vol. 21, No. 2, pp.109-135, 1971.

Doi, Y., Minami, N., Yamada, T. and Amada, T.: Experimental analysis of woody debris trapping by impermeable type sabo dam, filled with sediment -woody debris carried by debris flow-, *Journal of the Japan Society of Erosion Control Engineering*, Vol. 52, No. 6, pp.49-55, 2000 (in Japanese).

Egashira, S.: Mechanism of sediment deposition from debris flow (part 1), *Journal of the Japan Society of Erosion Control Engineering*, Vol. 46, No. 1, ser.186, pp.45-49, 1993a (in Japanese).

Egashira, S.: Mechanism of sediment deposition from debris flow (part 2), *Journal of the Japan Society of Erosion Control Engineering*, Vol. 46, No. 2, ser. 187, pp.51-56, 1993b (in Japanese).

Egashira, S.: Review of research related to sediment disaster mitigation, *Journal of Disaster Research* Vol. 2, No. 1, pp.11-18, 2007.

Egashira, S. and Ashida, K.: Unified view of the mechanics of debris flow and bed-load, *Advances in Micromechanics of Granular Materials*, Elsevier, pp.391-400, 1992.

Egashira, S., Ashida, K., Yajima, H. and Takahama, J.: Constitutive equation of debris flow, *Annuals of the Disaster Prevention Research Institute*, Kyoto University, No. 32 B2, pp.487-501, 1989 (in Japanese).

Egashira, S., Honda, N. and Itoh, T.: Experimental study on the entrainment of bed material into debris flow, *Physics and Chemistry of the Earth (C)*, Vol. 26, No. 9, pp.645-650, 2001.

Egashira, S., Miyamoto, K. and Itoh, T.: Constitutive equations of debris flow and their applicability, *Proceedings of First Conference on Debris-Flow Hazards Mitigation: Mechanics, Prediction, and Assessment*, California, ASCE, pp.340-349, 1997.

Fisher, R. V.: Features of coarse-grained, high-concentration fluids and their deposits, *Journal of Sedimentary Petrology*, Vol. 41, pp.916−927, 1971.

Fujita, M., Mizuyama, T. and Musashi, Y.: Functions of sabo dams with horizontal slit, *Annual Journal of Hydraulic Engineering*, JSCE, Vol. 42, pp.931-936, 1998 (in Japanese).

Fujita, M., Mizuyama, T. and Musashi, Y.: Sediment runoff control by a series of sabo dams, *Annual Journal of Hydraulic Engineering*, JSCE, Vol. 45, pp.697-702, 2001 (in Japanese).

Ghilardi, P., Natale, L. and Savi, F.: Modeling debris flow propagation and deposition, *Physics and Chemistry of the Earth (C)*, Vol. 26, No. 9, pp.651-656, 2001.

Gotoh, T.: Spread of debouching materials, *Research Report on Natural Disasters*, Supported by the Japanese Ministry of Education, Science and Culture, pp.93-97, 1983 (in Japanese).

Gotoh, H., Harada, E., Sakai, T. and Goda, K.: Numerical simulation of blocking process of grid-type dam by debris flow, *Annual Journal of Hydraulic Engineering*, JSCE, Vol. 50, pp.739-744, 2006 (in Japanese).

Gotoh, H., Sakai, T. and Hayashi, M.: Lagrangian model of drift-timbers induced flood by using moving particle semi-implicit model, *Journal of Hydroscience and Hydraulic Engineering*, JSCE, Vol. 20, No.1, pp.95-102, 2002.

Hirano, M., Harada, T., Banihabib, M. B. and Kawahara, K.: Estimation of hazard area due to debris flow, *Proceedings of First Conference on Debris-Flow Hazards Mitigation: Mechanics, Prediction, and Assessment*, California, ASCE, pp.697-706, 1997.

Honda, N. and Egashira, S.: Prediction of debris flow characteristics in mountainous torrents, *Proceedings of First Conference on Debris-Flow Hazards Mitigation: Mechanics, Prediction, and Assessment*, California, ASCE, pp.707-716, 1997.

Huang, X. and Garcia, M. H.: A perturbation solution for Bingham-plastic mudflows, *Journal of Hydraulic Engineering,* ASCE, Vol. 123, No. 11, pp.986-994, 1997.

Hunt, B.: Newtonian fluid mechanics treatment of debris flows and avalanches, *Journal of Hydraulic Engineering,* ASCE, Vol. 120, No. 12, pp.1350-1363, 1994.

Ikari, H., Gotoh, H. and Sumi, T.: Computational mechanics of a blocking of gateless bottom outlet by drift woods, *Annual Journal of Hydraulic Engineering*, JSCE, Vol. 50, pp.793-798, 2006 (in Japanese).

Ikeya, H.: Debris flow and its countermeasures in Japan, *Bulletin of the International Association of Engineering Geology*, pp.15-33, 1989.

Iverson, R. M.: The debris-flow rheology myth, *Proceedings of the Third Conference on Debris-Flow Hazards Mitigation: Mechanics, Prediction, and Assessment*, Switzerland, Rotterdam, pp.303-314, 2003.

Iverson, R. M. and Denlinger, R. P.: Flow of variably fluidized granular masses across three-dimensional terrain, 1. Coulomb mixture theory, *Journal of Geophysical Research*, Vol. 106, No. B1, pp.537-552, 2001.

Jan, C. D.: A study on the numerical modeling of debris flow, *Proceedings of First Conference on Debris-Flow Hazards Mitigation: Mechanics, Prediction, and Assessment*, California, ASCE, pp.717-726, 1997.

Jan, C. D.: Debris flow hazards mitigation in Taiwan, *Proceedings of the International Symposium on Utilization of Disaster Information*, Organizing and Sharing Disaster Information in Asian Countries, Hiroshima, Japan, 2005.

Jin, M. and Fread, D. L.: 1D routing of mud/debris flow using NWS FLDWAV model, *Proceedings of First Conference on Debris-Flow Hazards Mitigation: Mechanics, Prediction, and Assessment*, California, ASCE, pp.687-696, 1997.

Johnson, A. M. and Rodine, J. R.: Debris flow, Slope Instability, *Wiley: Chichester*, pp.257-361, 1984.

Julien, A. M. and Lan, Y.: Rheology of hyperconcentrations, *Journal of Hydraulic Engineering*, ASCE Vol. 117, No. 3, pp.346-353, 1991.

Katatani, M. and Yamada, T.: Study on new type slit sabo dam development for reduction of slit blockade by drift woods, *Journal of the Japan Society of Erosion Control Engineering*, Vol. 59, No. 36, pp.23-31, 2006 (in Japanese).

Koshizuka, S., Nobe, A. and Oka, Y.: Numerical analysis of breaking waves using the moving particle semi-implicit method, *International Journal for Numerical Methods in Fluids*, Vol. 26, pp. 751-769, 1998.

Laigle, D. and Coussot, P.: Numerical modeling of mudflows, *Journal of Hydraulic Engineering*, ASCE, Vol. 123, pp.617-623, 1997.

Liu, K. F. and Lai, K. W.: Numerical simulation of two-dimensional debris-flows, *Proceedings of the Second Conference on Debris-Flow Hazards Mitigation: Mechanics, Prediction, and Assessment*, Taiwan, Balkema, Rotterdam, pp.531-535, 2000.

Locat, J.: Normalized rheological behavior of fine muds and their flow properties in a pseudoplastic regime, *Proceedings of First Conference on Debris-Flow Hazards Mitigation: Mechanics, Prediction, and Assessment*, California, ASCE, pp.260-269, 1997.

Mainali, A. P. and Rajaratnam, N.: Hydraulics of debris flows, a review, *Water Resources Engineering Report (WRE 91-2)*, Department of Civil Engineering, University of Alberta, Edmonton, Alberta, Canada, 1991.

Masuda, S., Mizuyama, T., Fujita, M., Abe, H., Oda, A. and Otsuki, H.: Fundamental study about sediment runoff control by a series of slit sabo dams, *Journal of the Japan Society of Erosion Control Engineering*, Vol. 54, No. 6, pp.39-41, 2002 (in Japanese).

Ministry of Land, Infrastructure and Transport (MLIT) and Infrastructure Development Institute-Japan: development of warning and evacuation system against sediment disasters in developing countries, *Guidelines for construction technology transfer*, Japan, 2004.

Miyamoto, K.: Mechanics of grain flows in Newtonian fluid, *Ph.D. Thesis,* Ritsumeikan University, 1985 (in Japanese).

Miyazawa, N., Tanishima, T., Sunada, K. and Oishi, S.: Debris-flow capturing effect of grid type steel-made sabo dam using 3D distinct element method, *Proceedings of the Third Conference on Debris-Flow Hazards Mitigation: Mechanics, Prediction, and Assessment*, Switzerland, Rotterdam, pp.527-538, 2003.

Mizuno, H., Bovolin, V. and Minami, N.: Study on effectiveness of reducing peak discharge of muddy debris flow with open type dams, *Journal of the Japan Society of Erosion Control Engineering*, Vol. 53, No. 6, pp.45-54, 2001 (in Japanese).

Mizuno, H., Mizuyama, T., Minami, N. and Kuraoka, S.: Analysis of simulating debris flow captured by permeable type dam using distinct element method, *Journal of the Japan Society of Erosion Control Engineering*, Vol. 52, No. 6, pp.4-11, 2000 (in Japanese).

Mizuyama, T.: Structural countermeasures for debris flow disasters, *International Journal of Erosion Control Engineering*, Japan Society of Erosion Control Engineering, Vol. 1, No. 2, pp. 38-43, 2008.

Mizuyama, T., Abe, S., Yajima, S. and Ido, K.: Application of a two-dimensional river bed routing method to slit sabo dams, *Journal of the Japan Society of Erosion Control Engineering,* Vol. 42, No. 5, pp.21-28, 1990 (in Japanese).

Mizuyama, T., Kobashi, S. and Mizuno, H.: Control of passing sediment with grid-type dams, *Journal of the Japan Society of Erosion Control Engineering*, Vol. 47, No. 5, pp.8-13, 1995 (in Japanese).

Mizuyama, T. and Mizuno, H.: Prediction of debris flow hydrographs passing through grid type control structures, *Proceedings of First Conference on Debris-Flow Hazards Mitigation: Mechanics, Prediction, and Assessment*, California, ASCE, pp.74-82, 1997.

Mizuyama, T., Nakano, M. and Nanba, A.: Case study on debris flow control, *Journal of the Japan Society of Erosion Control Engineering*, Vol. 51, No. 4, pp.36-39, 1998 (in Japanese).

Mizuyama, T., Shimohigashi, H., Shimoda, Y. and Ido, K.: Experimental study of a sabo dam with slit, *Proceedings of 28th Japanese Conference on Hydraulics*, JSCE, pp.723-728, 1984 (in Japanese).

Nakagawa, H.: Study on risk evaluation of flood and sediment inundation disaster, *Doctoral Thesis*, Kyoto University, 1989 (in Japanese).

Nakagawa, H., Inoue, K., Ikeguchi, M. and Tsubono, T.: Numerical simulation of driftwood behavior (2) – dam up of drift wood -, *Annuals of the Disaster Prevention Research Institute*, Kyoto University, No. 36 B-2, pp.487-498, 1993 (in Japanese).

Nakagawa, H., Inoue, K., Ikeguchi, M. and Tsubono, T.: Behavior of driftwood and the process of its damming up, *Journal of Hydroscience and Hydraulic Engineering*, JSCE, Vol. 13, No. 2, pp.55-67, 1995.

Nakagawa, H., Satofuka, Y. and Takahama, J.: Water Induced Hazard – I, *Sub Text Book, M. Sc. in Water Resources Engineering*, Institute of Engineering, Nepal, 2002a.

Nakagawa, H. and Takahashi, T.: Estimation of a debris flow hydrograph and hazard area, *Proceedings of First Conference on Debris-Flow Hazards Mitigation: Mechanics, Prediction, and Assessment*, California, ASCE, pp.64-73, 1997.

Nakagawa, H., Takahashi, T. and Adachi, K.: Behavior of drift wood with overland flood flow, *Annuals of the Disaster Prevention Research Institute*, Kyoto University, No. 34 B-2, pp.373-386, 1991 (in Japanese).

Nakagawa, H., Takahashi, T. and Ikeguchi, M.: Numerical simulation of drift wood behavior, *Annuals of the Disaster Prevention Research Institute*, Kyoto University, No. 35 B-2, pp.249-266, 1992 (in Japanese).

Nakagawa, H., Takahashi, T. and Ikeguchi, M.: Driftwood behavior by overland flood flows, J*ournal of Hydroscience and Hydraulic Engineering*, JSCE, Vol. 12, No. 2, pp.31-39, 1994.

Nakagawa, H., Takahashi, T. and Satofuka, Y.: A debris-flow disaster on the fan of the Harihara River, Japan, *Proceedings of the Second International Conference on Debris-Flow Hazards Mitigation: Mechanics, Prediction, and Assessment*, Taiwan, Balkema, Rotterdam, pp.193-201, 2000.

Nakagawa, H., Takahashi, T., Satofuka, Y. and Kawaike, K.: Evaluation of efficiency of sabo facilities by means of numerical simulation methods, *Annual Journal of Hydraulic Engineering*, JSCE, Vol. 46, pp.665-670, 2002b (in Japanese).

Nakagawa, H., Takahashi, T., Satofuka, Y. and Kawaike, K.: Numerical simulation of sediment disasters caused by heavy rainfall in Camuri Grande basin, Venezuela 1999, *Proceedings of the Third Conference on Debris-Flow Hazards Mitigation: Mechanics, Prediction, and Assessment,* Switzerland, Rotterdam, pp.671-682, 2003.

Nakagawa, H., Takahashi, T., Sawada, T. and Satofuka, Y.: Design hydrograph and evacuation planning for debris flow, *Annuals of the Disaster Prevention Research Institute*, Kyoto University, No. 39 B-2, pp.347-371, 1996 (in Japanese).

Nakatani, K., Wada, T., Satofuka, Y. and Mizuyama, T.: Development of "Kanko 2D (Ver.2.00)," a user-friendly one- and two-dimensional debris flow simulator equipped with a graphical user interface, *International Journal of Erosion Control Engineering,* Vol. 1, No. 2, pp. 62-72, 2008.

Naylor, M. A.: The origin of inverse grading in muddy debris flow deposits - a review, *Journal of Sedimentary Petrology*, Vol. 50, pp.1111−1116, 1980.

O'Brien, J. S. and Julien, P. Y.: Laboratory analysis of mudflow properties, *Journal of Hydraulic Engineering*, ASCE, Vol. 114, No. 8, pp.877-887, 1988.

O'Brien, J. S., Julien, P. Y. and Fullerton, W. T.: Two-dimensional water flood and mudflow simulation, *Journal of Hydraulic Engineering*, Vol. 119, No. 2, pp.244-266, 1993.

Okubo, S., Mizuyama, T., Kaba, M. and Ido, K.: Sediment control by a series of slit-sabo dams, *Journal of the Japan Society of Erosion Control Engineering*, Vol. 50, No. 2, pp.14-19, 1997 (in Japanese).

Osti, R. and Egashira, S.: Method to improve the mitigative effectiveness of a series of check dams against debris flows, *Hydrological Processes*, Wiley InterScience, Vol. 22, pp.4986-4996, 2008.

Ozaki, Y., Kamogawa, Y., Mizuyama, T., Kasai, S. and Shima, J.: A debris flow with woody debris trapped by a steel-pipe gridded sabo dam, *Journal of the Japan Society of Erosion Control Engineering*, Vol. 51, No. 2, pp.39-44, 1998 (in Japanese).

Parise, M. and Calcaterra, D.: Debris-flow-related fans in weathered crystalline rocks, and the potential hazard in Calabria, Italy, *Proceedings of the Second International Conference on Debris-Flow Hazards Mitigation: Mechanics, Prediction, and Assessment*, Taiwan, Balkema, Rotterdam, pp.203-211, 2000.

Pierson, T. C.: Dominant particle support mechanisms in debris flows at Mt. Thomas, New Zealand, and implications for flow mobility, *Sedimentology*, Vol. 28, pp.49−60, 1981.

Pudasaini, S. P., Wang, Y. and Hutter, K.: Modelling debris flows down general channels, *Natural Hazards and Earth System Sciences,* Vol. 5, pp.799-819, 2005.

Rickenmann, D., Laigle, D., McArdell, B. W. and Hubl, J.: Comparison of 2D debris-flow simulation models with field events, *Computational Geosciences,* Vol. 10, pp.241-264, 2006.

Sabo Department, Ministry of Construction, Japan: Guideline for driftwood countermeasures, *Guideline of Ministry of Construction,* Japan, 2000.

Satofuka, Y. and Mizuyama, T.: Numerical simulation on a debris flow in a mountainous river with a sabo dam, *Journal of the Japan Society of Erosion Control Engineering*, Vol. 58, No. 1, pp.14-19, 2005 (in Japanese).

Satofuka, Y. and Mizuyama, T.: Numerical simulation on debris flow control by a grid dam, *The 6th Japan-Taiwan Joint Seminar on Natural Hazard Mitigation*, 2006 (in CD-ROM).

Savage, S. B. and Hutter, K.: The dynamics of avalanches of granular materials from initiation to runout. Part I: Analysis, *Acta Mechanica*, Vol. 86, pp.201-223, 1991.

Sharma, R. H.: Study on integrated modeling of rainfall induced sediment hazards, *Ph.D. Dissertation*, Department of Civil and Earth Resources Engineering, Kyoto University, 2006.

Sharp, R. P. and Nobles, L. H.: Mudflow of 1941 at Wrightwood, Southern California, *Bulletin of the Geological Society of America*, Vol. 64, pp.547-560, 1953.

Shieh, C. L., Jan, C. D. and Tsai, Y. F.: A numerical simulation of debris flow and its application, *Natural Hazard*, Vol. 13, pp.39-54, 1996.

Shimizu, Y. and Osada, K.: Numerical simulation on the driftwood behavior in open-channel flows by using distinct element method, *The Eighth International Conference on Hydro-Science and Engineering*, Nagoya, Japan, 2008.

Shrestha, B. B.: Numerical modeling on debris flows and its structural counter measure by sabo dam, *Master Thesis*, Institute of Engineering, Tribhuvan University, Nepal, 2004.

Shrestha, B. B., Nakagawa, H., Kawaike, K. and Baba, Y.: Study on debris-flow deposition and erosion process upstream of a check dam, *Proceedings of the First NEA-JC Seminar on "Current and Future Technologies"*, 2007.

Shrestha, B. B., Nakagawa, H., Kawaike, K. and Baba, Y.: Numerical and experimental study on debris-flow deposition and erosion upstream of a check dam, *Annual Journal of Hydraulic Engineering*, JSCE, Vol. 52, pp.139-144, 2008a.

Shrestha, B. B., Nakagawa, H., Kawaike, K. and Baba, Y.: Numerical simulation on debris-flow deposition and erosion processes upstream of a check dam with experimental verification, *Annuals of the Disaster Prevention Research Institute*, Kyoto University, No. 51 B, pp.613-624, 2008b.

Shrestha, B. B., Nakagawa, H., Kawaike, K. and Baba, Y.: Numerical simulation on prediction of debris-flow hydrograph of heterogeneous bed material and sediment transport in a mountainous river, *Fourth International Conference on Scour and Erosion (ICSE-4)*, pp.672-677, 2008c.

Shrestha, B. B., Nakagawa, H., Kawaike, K., Baba, Y. and Zhang, H.: Numerical simulation on debris-flow with driftwood and its capturing due to jamming of driftwood on a grid dam, *Annual Journal of Hydraulic Engineering*, JSCE, Vol. 53, pp.169-174, 2009.

Takahashi, T.: A mechanism of occurrence of mud-debris flows and their characteristics in motion, *Annuals of the Disaster Prevention Research Institute*, No. 20 B2, pp.405-435, 1977 (in Japanese).

Takahashi, T.: Debris flow on prismatic open channel, *Journal of the Hydraulics Division*, ASCE, Vol. 106, No. 3, pp.381-396, 1980.

Takahashi, T.: Debris flow, Monograph Series of IAHR, *Balkema*, pp.1-165, 1991.

Takahashi, T.: Initiation of debris flow of various types of debris flow, *Proceedings of the Second International Conference on Debris-Flow Hazards Mitigation: Mechanics, Prediction, and Assessment*, Taiwan, Balkema, Rotterdam, pp.15-25, 2000.

Takahashi, T.: Debris flow: Mechanics, Prediction and Countermeasures, *Taylor & Francis/Balkema*, pp.1-448, 2007.

Takahashi, T. and Kuang, S. F.: Formation of debris flow on varied slope bed, *Annuals of the Disaster Prevention Research Institute*, Kyoto University, No. 29 B2, pp.343-359, 1986 (in Japanese).

Takahashi, T. and Nakagawa, H.: Flood/debris flow hydrograph due to collapse of a natural dam by overtopping, *Journal of Hydroscience and Hydraulic Engineering*, JSCE, Vol. 12, No. 2, pp.41-49, 1994.

Takahashi, T., Nakagawa, H., Harada, T. and Yamashiki, Y.: Routing debris flows with particle segregation, *Journal of Hydraulic Engineering*, ASCE, Vol. 118, No. 11, pp.1490-1507, 1992.

Takahashi, T., Nakagawa, H., Satofuka, Y. and Kawaike, K.: Flood and sediment disasters triggered by 1999 rainfall in Venezuela; A river restoration plan for an alluvial fan, *Journal of Natural Disaster Science*, Vol. 23, No. 2, pp.65-82, 2001a.

Takahashi, T., Nakagawa, H., Satofuka, Y. and Wang, H.: Stochastic model of blocking for a grid-type dam by large boulders in a debris flow, *Annual Journal of Hydraulic Engineering*, JSCE, Vol. 45, pp.703-708, 2001b (in Japanese).

Takahashi, T., Nakagawa, H., Satofuka, Y. and Wang, H.: Simulation of debris flow control by a grid-type sabo dam, *Annual Journal of Hydraulic Engineering*, JSCE, Vol. 46, pp.689-694, 2002 (in Japanese).

Takahashi, T., Nakagawa, H. and Satoh, H.: Fan formation due to the runoff of the debris and immature debris flows, *Proceedings of the 32nd Japanese Conference on Hydraulics*, JSCE, pp.497-502, 1988 (in Japanese).

Takahashi, T., Satofuka, Y. and Chishiro, K.: Dynamics of debris flows in the inertial regime, *Proceedings of First Conference on Debris-Flow Hazards Mitigation: Mechanics, Prediction, and Assessment*, California, ASCE, pp.239-248, 1997.

Takahashi, T. and Tsujimoto, H.: Numerical simulation of flooding and deposition of a debris flow, *Annuals of the Disaster Prevention Research Institute*, Kyoto University, No. 27 B-2, pp.467-485, 1984 (in Japanese).

Tsai, Y. F.: Three-dimensional topography of debris-flow fan, *Journal of Hydraulic Engineering*, ASCE, Vol. 132, No. 3, pp.307-318, 2006.

Tsai, Y. F.: A debris-flow simulation model for the evaluation of protection structures, *Journal of Mountain Science*, Vol. 4, No. 3, pp.193-202, 2007.

Tsubaki, T. H., Hashimoto, H. and Suetsugi, T.: Grain stresses and flow properties of debris flow, *Proceedings of 38th Annual Conference of JSCE*, No. 317, pp.79-91, 1982 (in Japanese).

VanDine, D. F.: Debris flow control structures for forest engineering, *Research Branch*, British Columbia, Ministry of Forests, Victoria, Working Paper, 1996.

Varnes, D. J.: Slope movement types and processes. *In: Schuster, R. L. and Krizek, R. J. (eds.), Landslide-analysis and control*, National Research Council, Washington, D. C., Transportation Research Board, Special Report 176, pp.11–33, 1978.

Wada, T., Satofuka, Y. and Mizuyama, T.: Integration of 1- and 2- dimensional models for debris flow simulation, *Journal of the Japan Society of Erosion Control Engineering*, Vol. 61, No. 2, pp.36-40, 2008 (in Japanese).

Wang, C., Li, S. and Esaki, T.: GIS-based two-dimensional numerical simulation of rainfall-induced debris flow, *Natural Hazards and Earth System Sciences*, Vol. 8, pp.47-58, 2008.

Wang, H.: Study of function and performance designing of grid type sabo-dam, *Ph.D. Dissertation*, Department of Civil and Earth Resources Engineering, Kyoto University, 2001 (in Japanese).

Yabe, H. and Watanabe, Y.: Analysis of driftwood behavior and accumulations on sandbar considering flood flow and discharge, *Annual Journal of Hydraulic Engineering*, JSCE, Vol. 52, pp.661-666, 2008 (in Japanese).

Yamada, T., Doi, Y., Minami, N. and Amada, T.: Woody debris trapping by impermeable type sabo dam, *Journal of the Japan Society of Erosion Control Engineering*, Vol. 52, No. 6, pp.49-55, 1999 (in Japanese).

List of Figures

List of Tables

Curriculum Vitae

Name SHRESTHA Badri Bhakta

Citizenship Nepal

Birth 1975 July 27, Dolakha, Nepal

.

Ph.D. Student (2006 - 2009)
Department of Civil and Earth Resources Engineering
Kyoto University, Kyoto, Japan

M. Sc. in Water Resources Engineering (2003 - 2004)
Department of Civil Engineering, Institute of Engineering
Tribhuvan University, Kathmandu, Nepal

B. E. in Civil Engineering (1997 - 2001)
Department of Civil Engineering, Institute of Engineering
Tribhuvan University, Kathmandu, Nepal

Papers based on the Thesis

Shrestha, B. B., Nakagawa, H., Kawaike, K., Baba, Y. and Zhang, H.: Numerical simulation on debris flow with driftwood fan deposition, *Proceedings of the 28th Annual Meeting of the Japan Society for Natural Disaster Science*, September 2009. (to appear)

Shrestha, B. B., Nakagawa, H., Kawaike, K., Baba, Y. and Zhang, H.: Debris flow with driftwood control function of slit-type check dam, *10th Annual Association of Pacific Rim Universities Doctoral Students Conference*, July 2009.

Shrestha, B. B., Nakagawa, H., Kawaike, K., Baba, Y. and Zhang, H.: Capturing process of debris flow with driftwood by an open type check dam, *Annuals of the Disaster Prevention Research Institute*, Kyoto University, No. 52B, June 2009. (in print)

Shrestha, B. B., Nakagawa, H., Kawaike, K., Baba, Y. and Zhang, H.: Numerical simulation on debris-flow with driftwood and its capturing due to jamming of driftwood on a grid dam, *Annual Journal of Hydraulic Engineering*, JSCE, Vol. 53, pp.169-174, February 2009.

Shrestha, B. B., Nakagawa, H., Kawaike, K. and Baba, Y.: Numerical simulation on prediction of debris-flow hydrograph of heterogeneous bed material and sediment transport in a mountainous river, *Proceedings of the Fourth International Conference on Scour and Erosion (ICSE-4)*, pp.672-677, November 2008.

Shrestha, B. B., Nakagawa, H., Kawaike, K. and Baba, Y.: Prediction of debris-flow characteristics with driftwood and process of its capturing due to jamming of driftwood on a grid dam, *Proceedings of the 27th Annual Meeting of the Japan Society for Natural Disaster Science*, pp.25-26, September 2008.

Shrestha, B. B., Nakagawa, H., Kawaike, K. and Baba, Y.: Debris-flow deposition and erosion processes of the sediment deposit upstream of a check dam, *The Eighth International Conference on Hydro-Science and Engineering (ICHE-8)*, September 2008.

Shrestha, B. B., Nakagawa, H., Kawaike, K. and Baba, Y.: Numerical simulation on debris-flow deposition and erosion processes upstream of a check dam with experimental verification, *Annuals of the Disaster Prevention Research Institute*, Kyoto University, No. 51B, pp.613-624, June 2008.

Shrestha, B. B., Nakagawa, H., Kawaike, K. and Baba, Y.: Numerical and experimental study on debris-flow deposition and erosion upstream of a check dam, *Annual Journal of Hydraulic Engineering*, JSCE, Vol. 52, pp.139-144, February 2008.

Shrestha, B. B., Nakagawa, H., Kawaike, K. and Baba, Y.: Study on debris-flow deposition and erosion process upstream of a check dam, *Proceedings of the First NEA-JC Seminar on "Current and Future Technologies"*, October 2007 (in CD ROM).